

UC San Diego

Other Scholarly Work

Title

Offshore Application of Self-potential Prospecting

Permalink

<https://escholarship.org/uc/item/30z508jt>

Author

Corwin, Robert Frederic

Publication Date

1973-06-16

Offshore Application of Self-Potential Prospecting

By

Robert Frederic Corwin

B.S. (University of Missouri at Rolla) 1964

M.S. (University of California) 1969

DISSERTATION

Submitted in partial satisfaction of the requirements for the degree of

DOCTOR OF PHILOSOPHY

in

Engineering

in the

GRADUATE DIVISION

of the

UNIVERSITY OF CALIFORNIA, BERKELEY

Approved:

Pat Wild
.....
J. J. Morrison
.....
Israel Cornet
.....

Committee in Charge

DEGREE CONFERRED JUNE 16, 1973

.....

T7
.6
C 8327
ENGIN.
LIBRARY


OFFSHORE APPLICATION OF SELF-POTENTIAL PROSPECTING

ABSTRACT

Robert Frederic Corwin

Degree: Ph.D.

Engineering Geoscience
Ocean Engineering


Chairman, Thesis Committee

An offshore self-potential prospecting system, consisting of a portable chart recorder and a pair of towed electrodes, is shown to be capable of locating both onshore and submerged offshore deposits of conductive minerals. The silver - silver chloride electrodes, specially designed for this work, are shown to have a small and predictable response to changes in environmental parameters.

The background noise level is generally less than a few tenths of a millivolt, allowing visual recognition of offshore self-potential anomalies with a gradient in excess of one millivolt over the electrode separation. However, some man-made structures, or areas of geothermal activity, may generate fields large enough to interfere with self-potential profiling.

Laboratory and field experiments show that a conductive body, extending from a reducing sea floor into oxidizing sea water, generates a potential field consistent in magnitude and polarity with those seen over sulfide ore bodies on land. As an oxidation - reduction mechanism appears to offer the best explanation for the self-potential phenomenon on land, conductive mineral deposits in the sea floor also should be capable of generating self-potential fields.

The self-potential field generated by a submerged ore body may be simulated by a point current sink or dipole buried in the sea floor, and the potential field at the water surface studied as a function of depth of burial, sea-floor resistivity, water depth, and dipole angle and separation. It is seen in most cases that an ore body of economic size will generate an easily detectable potential field at the water surface.

Field work was conducted in areas of known sulfide mineralization (southeastern Alaska and Penobscot Bay, Maine) and onshore and offshore geothermal activity (California, Nevada, and Ensenada, Mexico). Increased self-potential background noise levels were seen in the geothermal areas, along with some large anomalies. In Maine, large offshore self-potential fields were found to be generated by onshore sulfide and graphite deposits, and submerged mineral deposits are thought to be responsible for other observed offshore anomalies.

ACKNOWLEDGEMENTS

This thesis was made possible by the assistance and advice of many people. I would particularly like to thank those mentioned below for their help.

At the University of California, the help given me by Professor Pat Wilde, in every phase of this work, went far beyond the call of duty. Dr. Ugo Conti assisted with the field work in Baja California and collaborated in the development of the "CoCo" electrodes. Professors I. Cornet and H.F. Morrison contributed valuable advice and criticism, and Mrs. Antoinette Friedman and Mrs. Ann Van Dorn cheerfully handled the unenviable typing job.

While researching and writing this thesis, I was employed by the Marine Minerals Technology Center, a former agency of the National Oceanic and Atmospheric Administration (the Center was closed in March, 1973, in a Federal "economy" move). Mr. Burton B. Barnes, my supervisor, supported the project, untangled red tape, and assisted with the field work in Alaska and Maine. Mrs. Carol Backhus, librarian, unearthed many of the more arcane references. Mr. William Ebersole planned the Alaska field trip, and he and Mr. Clyde Davis assisted with the work.

The traditional last-but-not-least acknowledgement: my wife, Janice. She knows why.

CONTENTS

Abstract	i
Acknowledgements.....	iii
Contents.....	iv
Figures.....	ix
Chapter 1. Introduction.....	1
Definition and description of self-potential.....	2
History and present use.....	6
Equipment and field procedure.....	6
Offshore application.....	7
Chapter 2. Mechanisms.....	10
Introduction.....	11
Early theories.....	11
Oxygen cell mechanism.....	11
pH.....	18
pH mechanism.....	18
Oxidation-reduction mechanism.....	19
Eh.....	19
Eh and pH of natural environments.....	22
Eh-pH, mineral stability, and immunity domains.....	30
Self-potential mechanism.....	32
Alunite.....	38
Offshore ore bodies.....	41
Eh and pH of sea water and marine sediments.....	41
Self-potential generation by offshore ore bodies.....	55
Fresh-water deposits.....	56

Shoreline and near-shore deposits.....	56
Experiments.....	58
Laboratory work.....	60
Field experiment.....	62
Chapter 3. Potential fields.....	71
Introduction.....	72
Sea-floor and sea water resistivity.....	72
Models.....	74
Conformal mapping and downward continuation.....	74
Spherical ore body.....	75
Polarized sheet.....	75
Point and point dipole.....	78
Point source of current buried in the sea floor.....	82
Model studies.....	83
Standard case.....	83
Gradient and detectability.....	85
Survey depth.....	89
Effect of sediment resistivity.....	89
Effect of water depth.....	94
Effect of burial depth.....	98
Uniqueness.....	98
Dipole.....	102
Shoreline.....	107
Chapter 4. Equipment.....	111
Introduction.....	112

Electrodes.....	112
Electrode reversibility.....	113
Electrodes of the first kind.....	114
Electrodes of the second kind.....	117
Lead electrodes.....	119
Coated electrodes.....	120
Lead-lead chloride electrodes.....	122
Calomel electrodes.....	122
Silver-silver chloride electrodes.....	123
Electrode isolation.....	124
"CoCo" electrodes.....	128
Standard potential.....	133
Response to salinity changes.....	135
Response to simultaneous salinity change.....	136
Differential salinity changes.....	136
Response to temperature changes.....	145
Simultaneous temperature change.....	149
Differential temperature changes.....	149
Response to Eh changes.....	157
Response to agitation and mechanical shock.....	158
Response to applied electric fields.....	158
Chart recorder.....	161
Cable and connectors.....	166
Complete system.....	167
Summary of "CoCo" electrode characteristics.....	167

Chapter 5. Noise.....	170
Instrumental noise.....	171
Electrodes.....	172
Cables.....	172
Connections.....	175
Chart recorder.....	179
Environmental noise.....	181
Currents.....	181
Waves.....	184
Wake turbulence.....	184
Magnetic field variations (telluric noise).....	186
Geologic background noise.....	186
Streaming potentials.....	189
Geologic contacts.....	191
Corrosion.....	194
Corrosion control systems.....	195
Stray currents.....	197
Geothermal activity.....	200
Offshore oil and gas fields.....	205
Summary.....	206
Chapter 6. Field Work.....	209
Introduction.....	210
Alaska.....	210
Hump Island.....	212
Roe Point.....	218
Niblack Anchorage.....	226
McLean Arm.....	229

Maine.....	233
Area #1 (North end of Holbrook Island).....	241
Area # 2 (Middle Ground to Trott Ledge).....	245
Area # 3 (Opposite Negro Island).....	248
Area # 4 (Jones Point).....	256
Summary.....	256
Geothermal field work.....	259
Byron Hot Springs, California.....	259
Rocky Point, California.....	261
Spencer Hot Springs, Nevada.....	261
Punta Banda, Baja California, Mexico.....	270
Discussion of geothermal data.....	274
Costs.....	280
Appendix 2-1. Current flow.....	282
Appendix 3-1. The potential field generated by a point source of current buried in the sea floor....	284
Appendix 3-2. Computer program.....	288
Appendix 4-1. Computation of potential between "bare" or "packed" electrodes in a NaCl concentration cell.....	291
Appendix 4-2. Calculation of the potential across KCl:NaCl liquid junctions	293
References.....	295

FIGURES

1-1	Self-Potential Anomalies.....	3
1-2	Self-Potential Profiles.....	4
1-3	Self-Potential Measuring System.....	8
2-1	Electrolysis Cell.....	13
2-2	Differential Aeration Cell.....	15
2-3	Model Experiment of Poldini.....	17
2-4	Eh-pH Measurements of Natural Aqueous Environments.....	24
2-5	Eh-pH "Areas" for Natural Environments.....	25
2-6	Eh-pH "Areas" for Natural Environments.....	26
2-7	Eh and pH Conditions in the Weathering and Depth Zones.....	27
2-8	Natural Environments as Characterized by Eh and pH.....	28
2-9	Eh Values of Natural Waters in Mining Districts.....	29
2-10	Immunity Domain of Substance A.....	33
2-11	Immunity Domains for Sulfide Minerals.....	34
2-12	Oxidation-Reduction Mechanism of Self-Potential Generation.....	36
2-13	Eh vs. Depth -- San Francisco Bay, California.....	43
2-14	Eh. vs. Depth -- Penobscot Bay, Maine.....	44
2-15	Eh, pH, Temperature, and H ₂ S in a Stagnant Bay.....	45
2-16	Eh and Dissolved Oxygen vs. Depth.....	46
2-17	Eh, pH, and Dissolved O ₂ in the Open Ocean.....	47
2-18	Eh and pH for a Marine Core.....	49
2-19	Eh and pH for Marine Cores.....	50
2-20	Temperature and Dissolved Oxygen Profiles.....	51

2-21	Eh-pH Profile for Mud Core.....	52
2-22	Eh and pH of Bottom Sediments.....	53
2-23	Eh Profiles in Marine Cores.....	54
2-24	Eh Profiles in Lakes.....	57
2-25	Tray Model of Becker and Telford.....	59
2-26	Laboratory Model.....	61
2-27	Field Experiment.....	63
2-28	V vs. r	65
2-29	V vs. z	66
2-30	V vs. z (inside pipe).....	67
2-31	Current Flow Lines.....	68
3-1	Electrical Resistivity of Sea Water.....	73
3-2	Spherical Model.....	76
3-3	Model for Tabular Ore Body.....	77
3-4	Dipole Field on Spherical Surface.....	80
3-5	Relative Depth vs. Relative Eh.....	81
3-6	Standard Case.....	84
3-7	Field for Standard Case.....	86
3-8	Effect of Electrode Separation.....	88
3-9a	Symmetrical Monopole Anomaly.....	90
3-9b	Asymmetrical Monopole Anomaly.....	91
3-9c	Symmetrical Dipole Anomaly.....	92
3-9d	Asymmetrical Dipole Anomaly.....	93
3-10	Effect of Sediment Resistivity.....	95
3-11	Maximum Voltage vs. Sediment Resistivity.....	96
3-12	Effect of Water Depth.....	97

3-13	Effect of Burial Depth.....	99
3-14	Effect of Burial Depth and Sediment Resistivity on Curve Shape.....	101
3-15	Dipole Arrangement.....	103
3-16	Effect of Dipole Angle.....	104
3-17	Effect of Varying Dipole Separation D ($\theta=30^\circ$).....	105
3-18	Effect of Varying Dipole Separation D ($\theta=60^\circ$).....	105
3-19	Potential at Water Surface for Shoreline Case.....	108
3-20	Value of z for $\partial V / \partial z = 0.05$ mv/meter.....	110
4-1	Copper-Copper Sulfate "Porous Pot" Electrode.....	116
4-2	Silver-Silver-Chloride Electrode Element.....	118
4-3	Lead Electrode.....	121
4-4	"Packed" Silver-Silver Chloride Electrode.....	126
4-5	Salt Bridge System.....	127
4-6	Salt Bridge System Background Noise.....	129
4-7	Salt Bridge System Handling Noise.....	130
4-8	"CoCo" Electrode.....	131
4-9	Time Response to Simultaneous Salinity Change at Both Electrodes.....	137
4-10	Potential Difference Due to Simultaneous Salinity Change at Both Electrodes.....	138
4-11	Concentration Cell Response for "Packed" Electrodes.....	141
4-12	Concentration Cell Test Arrangement.....	143
4-13	Long-Term Response to Differential Concentration Change.....	144
4-14	Long-Term Potential Difference vs. Differential Salinity Change.....	146
4-15	Short-Term Response to Differential Salinity Change.....	147

4-16	Short-Term Potential Difference vs. Differential Salinity Change.....	148
4-17	Long-Term Drift Test.....	150
4-18	Temperature Step Response for "Packed" Electrodes.....	152
4-19	Temperature Step Response for 2.7 M "CoCo" Electrodes.....	154
4-20	Temperature Step Response for Saturated "CoCo" Electrodes.....	157
4-21	Test Arrangement for Eh Response.....	159
4-22	Response to Shock and Agitation.....	160
4-23	Response to Electric Field Step Input.....	162
4-24	Dock Test Arrangement.....	163
4-25	Dock Test Results.....	164
4-26	Peak Amplitude vs. Distance DB	165
4-27	Complete System.....	168
5-1	Potential Generated by Turn.....	174
5-2	Signals Due to Turns.....	176
5-3	Noise Due to Waves.....	177
5-4	Noise Due to Poor Connection.....	178
5-5	Noise Due to Pounding of Boat.....	180
5-6	Potential Due to Water Current.....	183
5-7	Signal Due to Water Current.....	185
5-8	Noise Due to Increased Boat Speed.....	187
5-9	Potentials Due to Magnetic Storm.....	188
5-10	Geologic Noise.....	193
5-11a	Potential Field Due to BART Transbay Tube Protective Anode.....	196
5-11b	Total Field and Ship's Course.....	198

5-12	Potential Field Due to Ship's Impressed Current System.....	199
5-13	Geothermal Systems.....	201
5-14	Thermoelectric Potential Generation.....	204
5-15	Typical Noise Level.....	207
6-1	Location of Ketchikan, Alaska.....	211
6-2	Test Sites in Ketchikan area.....	213
6-3	Hump Island.....	214
6-4	Self-Potential Surveys, Hump Island.....	215
6-5	Signal from Lead Electrodes.....	217
6-6	Roe Point.....	219
6-7	Mineralized Vein at Shoreline.....	220
6-8	Onshore Self-Potential Survey.....	221
6-9	Horizontal Array Survey.....	223
6-10	Vertical Array Survey.....	224
6-11	Skiff Survey Results.....	225
6-12	Niblack Anchorage.....	227
6-13	Onshore Self-Potential Surveys.....	228
6-14	Mc Lean Arm.....	230
6-15	Skiff Survey.....	231
6-16	Onshore Self-Potential Survey.....	232
6-17	Spurious Offshore Self-Potential Signal.....	234
6-18	Location Map, Maine.....	235
6-19	Survey Lines, Maine.....	236
6-20	Prospect Locations, Maine.....	237
6-21	Onshore Self-Potential Survey.....	238

6-22	Ram Island Self-Potential Surveys.....	240
6-23	Anomaly Locations.....	242
6-24	Anomaly #1.....	243
6-25	Integration of Anomaly #1.....	244
6-26	Anomaly #2.....	246
6-27	Integration of Anomaly #2.....	247
6-28	Anomaly #3a.....	249
6-29	Integration of Anomaly #3a.....	250
6-30	Anomaly #3b.....	251
6-31	Integration of Anomaly #3b.....	252
6-32	Anomaly #3c.....	253
6-33	Integration of Anomaly #3c.....	254
6-34	Anomaly #4.....	257
6-35	Integration of Anomaly #4.....	258
6-36	Byron Hot Springs.....	260
6-37	Self-Potential Survey, Byron Hot Springs.....	262
6-38	Rocky Point, California.....	263
6-39	Self-Potential Survey, Rocky Point.....	264
6-40	Spencer Hot Springs, Nevada.....	265
6-41	Self-Potential Survey Lines, Spencer Hot Springs.....	266
6-42	Self-Potential Data - Spencer Hot Springs.....	267
6-43	Self-Potential on Tie Lines A & B.....	268
6-44	Self-Potential on Line C.....	269
6-45	Bahia Todos Santos.....	271
6-46	Punta Banda.....	272
6-47	Shoreline Self-Potential Survey.....	273

6-48	Offshore Self - Potential.....	275
6-49	Anomaly at Point J.....	276
6-50	Integration of Gradient Anomaly at Point J.....	277

CHAPTER I

INTRODUCTION

..."Hence it seems likely that electro-magnetism may become useful to the practical miner in determining with some degree of probability at least, the relative quantity of ore in veins, and the directions in which it most abounds."

R.W. Fox, 1830

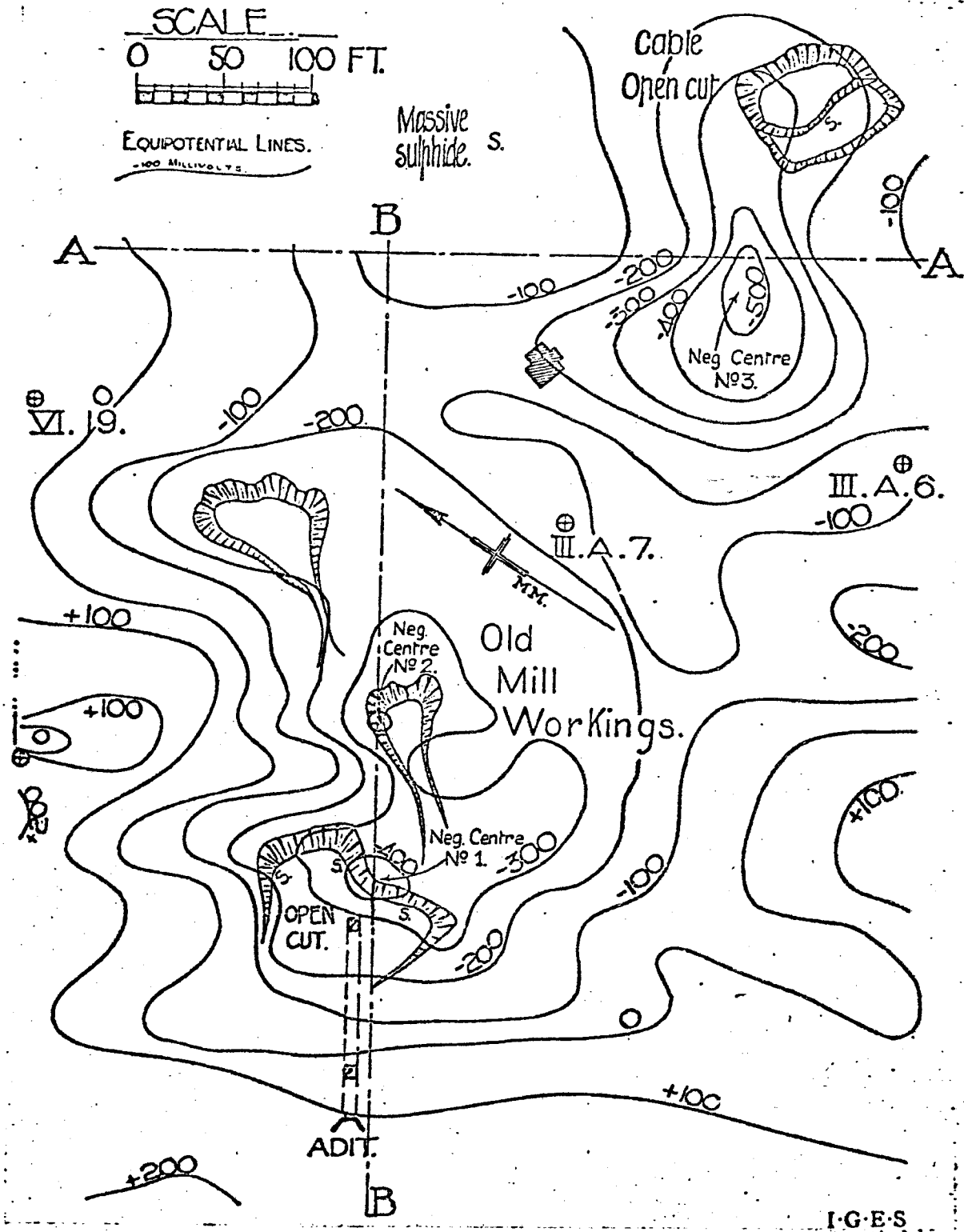
Definition and description of self-potential

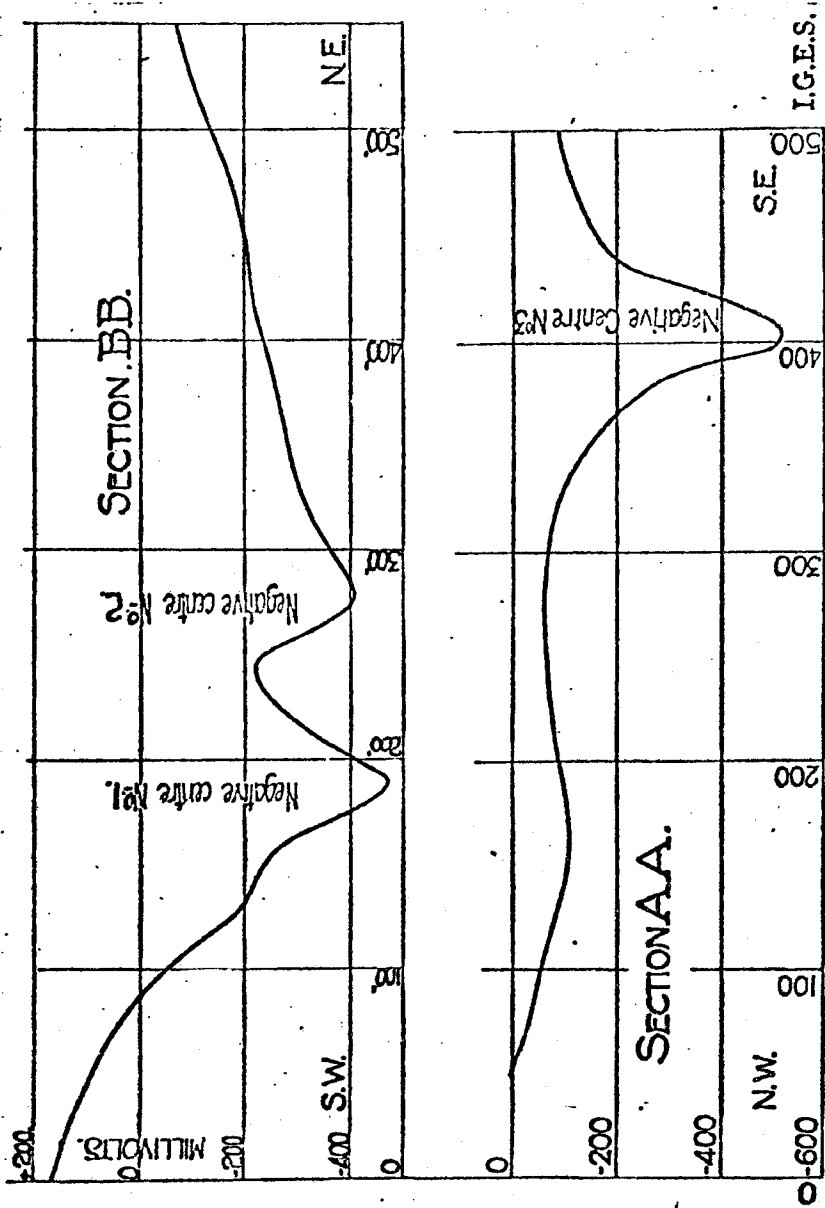
Under certain geologic conditions, an electric potential field may be developed naturally in the soil and rocks surrounding an electrically conductive ore body. This phenomenon is known as self-potential (or spontaneous polarization), often abbreviated "S-P". Self-potential surveying, in which these potential fields are measured along the surface of the earth, has been used for many years as a geophysical tool in the search for ore. (Self-potential well logging is the measurement of electric potential fields in boreholes, developed by differences in dissolved ion concentrations in the pore waters of adjacent formations (Schlumberger Well Surveying Corp., 1958). This definition of self-potential will not be used in this thesis.) The history of self-potential prospecting will be described briefly later in this chapter, and the electrochemical theory of self-potential generation will be discussed in Chapter 2.

Some self-potential anomalies generated by sulfide ore bodies are illustrated in Figures 1-1 and 1-2. The zero reference voltage is theoretically at a point infinitely far from the ore body. In practice, the voltage is assumed to be zero at a point

Figure 1-1
Self-Potential Anomalies
Renison Bell, Tasmania

From Edge and Laby (1931, p. 99)





(From Figure 1-1; Edge and Laby, 1931, p. 100)

Self-Potential Profiles

Figure 1-2

where it ceases to change significantly as the distance from the center of the anomaly is increased.

The anomaly is almost always negative in polarity, and is typically about one hundred to a few hundred millivolts (mv.) at its point of maximum amplitude, called the "negative center". The negative center usually is located above or nearly above the area of richest mineralization. A large anomaly is of the order of -500 millivolts (Sato and Mooney, 1960). The largest recorded anomaly is -1842 millivolts, over alunite $[KAl_3(OH)_6(SO_4)_2]$ near Hualgayoc, Peru (Gay, 1967). Canadian Institute of Mining and Metallurgy (1957) and Edge and Laby (1931) present discussions of several self-potential case histories.

The minerals which most consistently produce strong self-potential anomalies are pyrite (FeS_2) and pyrrhotite ($Fe_{1-x}S$). Chalcopyrite ($CuFeS_2$), chalcocite (Cu_2S), covellite (CuS), graphite (C), and anthracite (C) also produce anomalies (Sato and Mooney, 1960). Many other natural and artificial phenomena also may produce electric potential fields in the earth (and in sea water). These noise sources (for self-potential prospecting) are discussed in Chapter 5.

The anomalies produced by sulfide ore bodies seem to change little with time (Sato and Mooney, 1960). Parasnis (1970) studied a self-potential anomaly in northern Sweden over a period of 8 years, and found that "... in many cases small wiggles having amplitudes of only 10 to 20 mv. can also be followed in the same position from year to year." (The amplitude of the test anomaly

was about 300 millivolts.)

History and present use

The phenomenon of self-potential generation by sulfide ore bodies apparently was discovered by Fox (1830), in the copper mines of Cornwall, England in the early 1800's. The method came into use as a practical prospecting tool early in the 1900's, and has been in continuous use since that time. Van Nostrand and Cook (1966) give an excellent summary of the development of the method.

Although the reported use of self-potential was only 11 crew - months for the year 1969 (Allen, 1971), as compared with 1280 crew - months for induced polarization, 391 for magnetic ground surveys, and 72 for resistivity, the method still is considered useful (see, for example, Sengupta and others, 1969), and Parasnis (1970) feels that better understanding of the nature of self-potential and more care in the interpretation of data may result in increased usage for the method. The comparative cost of self-potential surveying is given in Table 1-1. Costs for offshore self-potential surveying are considerably lower; about \$30 per line mile (Chapter 6).

Equipment and Field Procedure

The only equipment needed to measure self-potential fields on land are a voltmeter, two electrodes to make contact with the earth, and sufficient insulated wire to connect the electrodes to the voltmeter. A supply of salt water may be needed to help reduce the electrical resistance between the electrodes and the

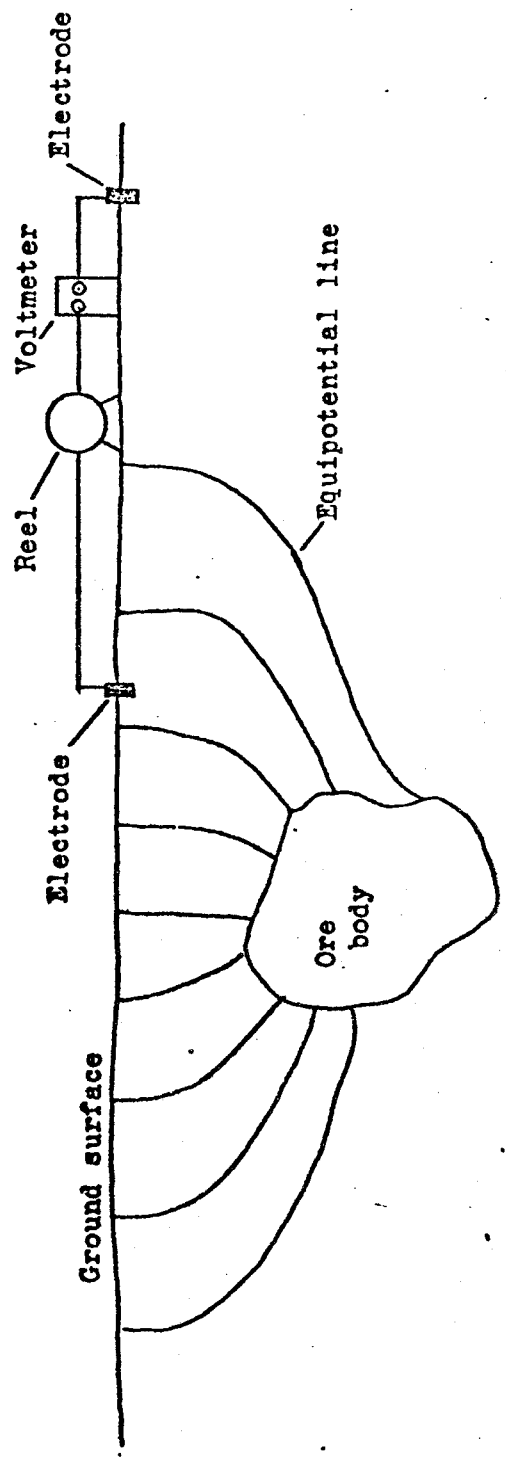
earth. Figure 1-3 shows the components of a self-potential measuring system.

The voltmeter must have high impedance to prevent it from drawing current from the electrodes and polarizing them. Voltmeters have evolved from the wire-wound compass of Fox (1830) to potentiometric and solid-state instruments which can resolve one millivolt and which draw no appreciable current during measurement. The electrodes used are of the non-polarizing type to minimize spurious contact and chemical potential readings. (Electrode theory and operation are discussed in detail in Chapter 4.) A complete self-potential system, including meter, electrodes, reel, and cable may be purchased for about \$600-\$900.

A self-potential survey (on land) may be conducted by total-field or by gradient measurement. In the total-field method, one electrode is held stationary as a reference while the other is moved. In the gradient method, both electrodes are moved together, with constant separation maintained between them. The gradient method allows greater speed and flexibility in surveying, but the signal-to-noise ratio is lower than that for the total-field method. Edge and Laby (1931, p. 241) give a detailed discussion of field procedures for self-potential surveying.

Offshore application

It will be shown in Chapter 2 that the geologic and geochemical conditions which give rise to self-potential anomalies on land also may exist in the vicinity of the sea floor. It is possible, therefore, that a submerged ore body may produce an



Self-Potential Measuring System

Figure 1-3

electric potential field in the sea water and sediments surrounding the body. Detection of this field (potential fields are discussed in Chapter 3; and the equipment used is described in Chapter 4) then could provide a simple method of locating and delineating offshore ore bodies. Work by Marke (1965) provides evidence that offshore sulfide ore bodies do produce measurable anomalies.

The field produced by an ore body located near a shoreline will propagate into the adjacent water. A pair of electrodes towed just offshore may, as discussed in Chapter 3, be used to detect the presence of an onshore ore body. The results of such surveys, described in Chapter 6, indicate that this is a practical and economical prospecting technique.

CHAPTER 2

MECHANISMS

"Curiouser and curiouser!"

Lewis Carroll
Alice's Adventures in Wonderland

Introduction

The electric potential field which constitutes a self-potential anomaly is generated by a flow of electric current through the earth. The mechanism of self-potential, therefore, must be one which is capable of generating and sustaining a flow of electric current through the ore body and its surrounding environment. Many mechanisms have been proposed, but that of Sato and Mooney (1960) appears to fit best the observed data related to the self-potential phenomenon.

In this chapter, two of the earlier theories of self-potential generation are discussed briefly, followed by a more detailed presentation of the mechanism proposed by Sato and Mooney (1960). It is then shown that this mechanism can be extended to offshore ore bodies which may, under the proper geological and geochemical conditions, generate self-potential anomalies in the surrounding sediments and sea water. Finally, the results of laboratory and field experiments which appear to confirm the feasibility of self-potential generation by offshore ore bodies are presented.

Early theories

Sato and Mooney (1960) present an extensive review of previous theories of the origin of self-potential anomalies over conductive ore bodies. Of these, only two are supported by experimental work: the oxygen cell theory of Schlumberger, as discussed by Poldini (1938, 1939), and the pH gradient mechanism of Kelly (1945).

Oxygen cell mechanism

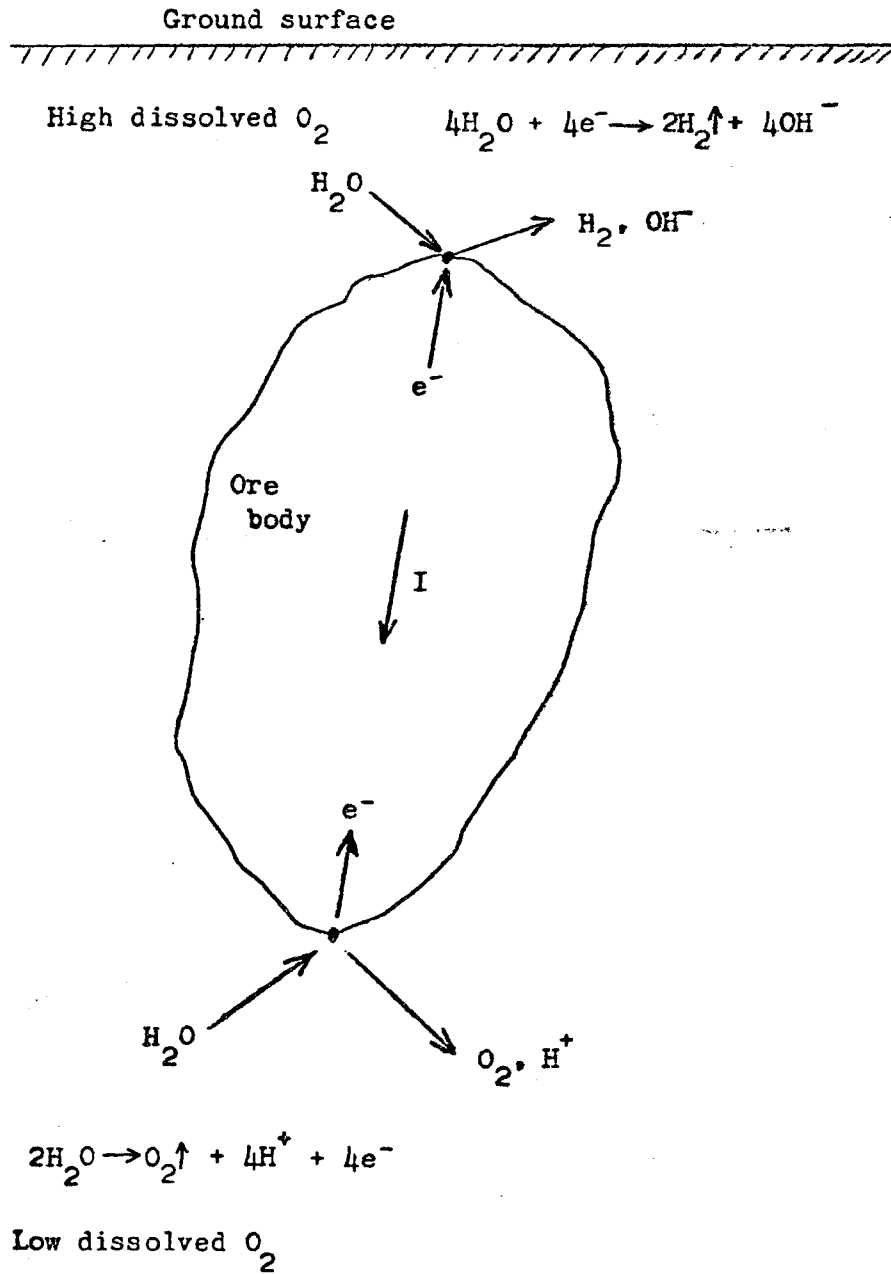
Schlumberger, as quoted in Poldini (1938, 1939), states that the current flow through the ore body is due to the dissolved oxygen (O_2) concentration gradient in the groundwater; the shallow

groundwater containing more dissolved O_2 than that at depth. The O_2 concentration gradient creates a "gas battery" which results in "electrolysis" of the water surrounding the ore body, with hydrogen (H_2) gas evolved at the upper end (cathode) and O_2 at the lower end (anode). The H_2 gas combines with dissolved O_2 to form water at the top of the ore body, and the O_2 generated at the bottom of the ore body dissolves into the groundwater, which is initially low in dissolved O_2 . This process provides a mechanism for the diffusion of dissolved O_2 from the near-surface groundwater, where its concentration is high, to the deep groundwater, where its concentration is low.

Unfortunately, Schlumberger (and Poldini) do not give the chemical reactions for this proposed mechanism, nor do they explain how the flow of electric current through the ore body is generated. The generation of H_2 at the top of the ore body and O_2 at the bottom would seem to require a spontaneous water electrolysis process (see Figure 2-1), with water combining with electrons and being broken down into H_2 and OH^- at the top of the ore body, and water breaking down into O_2 and H^+ at the bottom of the ore body, with the release of electrons. Electrons flow upward through the ore body, so conventional current flows downward, as required by field observation.

As these reactions are not spontaneous under standard conditions, the energy to drive them would presumably be provided by the difference in O_2 partial pressure between the top and bottom of the ore body. Therefore, the dissolved oxygen would have to be removed rapidly from the bottom of the ore body to prevent polarization of the cell. It should be noted that this mechanism

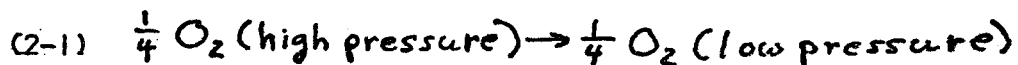
Figure 2-1
Electrolysis Cell



requires the consumption, not the production of water, at the top of the ore body. (Schlumberger states that "the nascent hydrogen combines with the dissolved oxygen so as to form water".)

Another possible oxygen mechanism is the differential aeration cell (Uhlig, 1963, p. 11; 26). This mechanism (Figure 2-2) provides for the consumption of water, O_2 , and electrons at the top of the ore body, with the release of OH^- ions; and for the consumption of OH^- ions at the bottom of the ore body, with the production of water, O_2 , and electrons. As with the electrolysis mechanism, electrons are released at the bottom of the ore body and consumed at the top, creating a downward flow of conventional current.

The driving force for this process is again the difference in the partial pressure of dissolved O_2 , P_{O_2} , in the groundwater at the top and bottom of the ore body. The potential for the overall reaction,



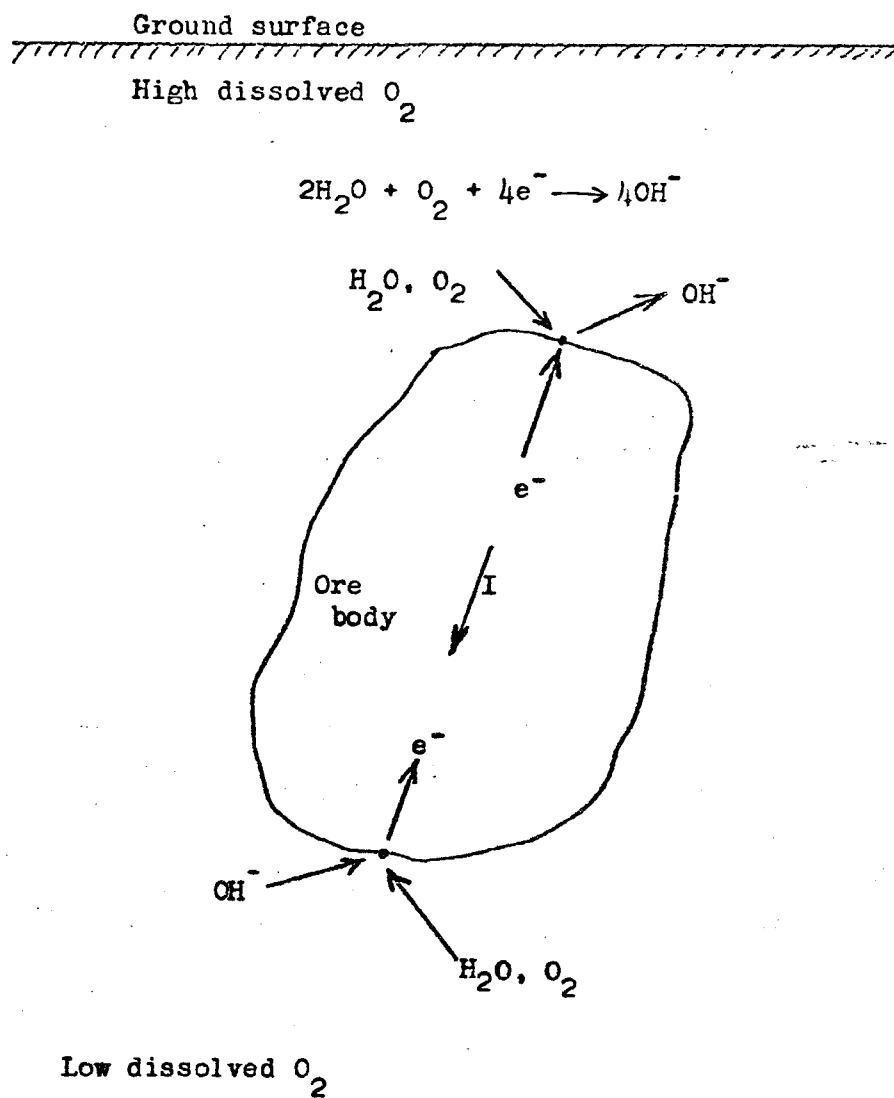
is

$$(2-2) \quad E = \frac{.059}{4} \log \frac{P_{O_2} (\text{high})}{P_{O_2} (\text{low})} \quad (\text{volts}).$$

For a "typical" self-potential anomaly of 200 mv, $P_{O_2} (\text{high})/P_{O_2} (\text{low})$ would have to be $10^{-13.5}$, a ratio which could be maintained only if $P_{O_2} (\text{low})$ is kept at a very small value. This implies that the O_2 generated at the bottom of the ore body must be removed very rapidly to prevent polarization of the cell.

Although various side reactions between the ore body and the groundwater may serve as depolarizers for the two mechanisms described above, Sato (1960a, 1960b) has shown that many minerals which produce strong self-potential anomalies do not react significantly

Figure 2-2
Differential Aeration Cell



within the usual Eh-pH constraints of oxidizing or reducing groundwater (the definitions of Eh and pH are given later in this chapter). Thus, it is difficult to see how the self-potential current flow could be maintained over long periods of time.

Poldini (1938, 1939) constructed a model (Figure 2-3) using an ore mineral in a layered medium consisting of a layer of sand and clay overlaid by a layer of washed sand. The electric field was measured on the surface of the sand, and among the conclusions were the following:

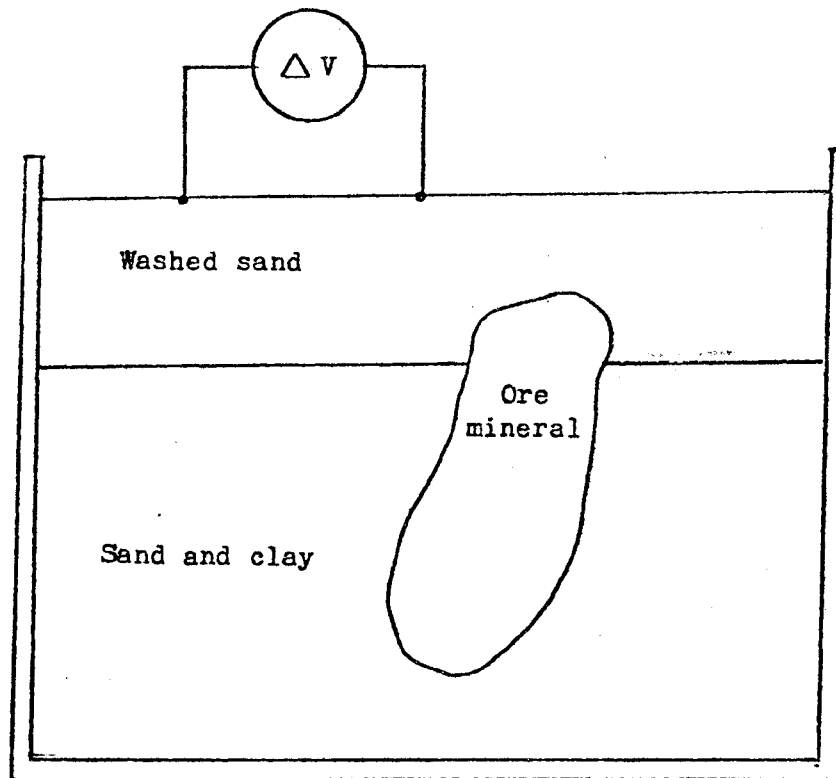
1. "A negative centre exists above the apex of the ore body."
2. "The phenomenon appears to remain permanent as long as care is taken to renew the moisture."
3. Continuity of electrical conductivity in the ore mineral is required for the field to be generated.
4. "It is probable that the battery constituted by the ore-body becomes largely polarized." Rubbing the apex of the ore body with damp sand mechanically removes the "hydrogen" and causes the potential to increase.

Unfortunately, Poldini does not state whether the presence of H_2 at the top of the ore was verified chemically, or whether pH was monitored to detect the formation of OH^- , as required by either the electrolysis cell or the differential aeration cell. Thus, his experiment appears to leave open the question of whether an oxygen cell mechanism could cause some or all of the observed self-potential anomalies. As Sato and Mooney (1960) point out, Eh-pH conditions in the natural environment are not favorable for the reactions shown in Figures 2-1 and 2-2.

Figure 2-3

Model Experiment of Poldini

After Poldini (1938, 1939)



Ore, sand, and clay are boiled to remove air before assembly. The system is watered from time to time to maintain moisture in the formation.

pH

The pH of a solution is related to the activity of H^+ ions in the solution:

$$(2-3) \quad pH = -\log a_{H^+}$$

where a_{H^+} is the activity of H^+ :

$$(2-4) \quad a_{H^+} = \gamma_{H^+} m_{H^+} ,$$

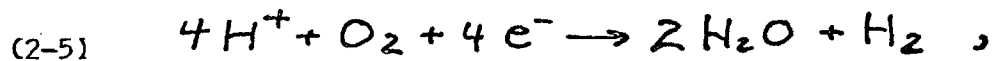
γ_{H^+} is the "practical activity coefficient", and the molality m_{H^+} is the concentration of H^+ , in moles of H^+ per 1000 grams of water (Garrels and Christ, 1965, p. 3, 13, 42). The measurement of pH may be done electrometrically by using a glass pH electrode together with a reference electrode (Bates, 1954; Garrels and Christ, 1965). The techniques are well known and will not be discussed here.

pH mechanism

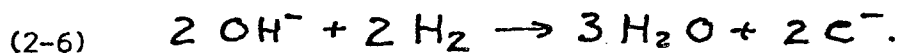
Kelly (1945) states: "My own laboratory and field investigations, however, lead me to ascribe the principal, but not the sole role in this electrochemical phenomenon [self-potential] to the difference in acidity between the waters bathing the apical portions of the sulphide deposit, and those waters in contact with the lower reaches of the mineral body." As Sato and Mooney (1960) point out, however, a pH gradient (in itself) does not provide a mechanism for the transfer of electrons. For an electronic current flow to take place in an ore body, some chemical species must be reduced (gain electrons) at the top of the ore body, and some species must be oxidized (lose electrons) at the bottom.

These oxidation and reduction reactions must increase the pH (decrease the relative H^+ ion concentration) near the surface;

for example,



and to decrease the pH (decrease the relative OH^- ion concentration) at depth; for example,



Such reactions are improbable at the Eh (see below) and pH values actually measured in the earth. Therefore, although the pH gradient may contribute to the self-potential mechanism, it seems unlikely as a primary explanation except, possibly, in the case of alunite deposits (see section of this chapter on alunite).

Oxidation-reduction mechanism

Sato and Mooney (1960) propose a self-potential mechanism in which the difference in oxidation-reduction potential (also called redox potential or Eh) of the groundwater in contact with the upper and lower parts of the ore body provides the driving force for the transfer of electrons from the bottom to the top of the ore body, thus generating a conventional current flow from the top toward the bottom of the body. The mechanism depends upon the Eh gradient in the soil, and upon the concept of immunity domains of minerals. The definition of Eh, its distribution in the earth, and the concept of immunity domains will be discussed in the following sections.

Eh

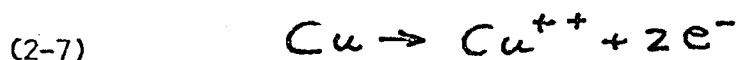
The Eh of a solution indicates the tendency of the ions in the solution to give up or to accept electrons. Eh is a function of ionization energy (for an element which loses electrons when ionized) or electron affinity (for an element which gains electrons when ionized),

as well as the sublimation, dissociation, lattice, and hydration energy of the substance (Latimer, 1952, p. 14). The Eh of a solution also will depend upon the pH, if H^+ or OH^- enters the Eh-establishing reaction. Eh measures the intensity of the tendency to lose or gain electrons, but not the capacity of a solution to supply or take up electrons (ZoBell, 1946). The Eh of a system is "well-poised" if the system has a large electron exchange capacity (i.e. if the Eh tends to remain constant during an oxidation-reduction reaction). The Eh of a "poorly poised" system will change rapidly during an oxidation-reduction reaction. The following discussion of Eh will be brief and qualitative; for a more detailed discussion see Latimer (1952), Pourbaix (1949), Garrels and Christ (1965), Krauskopf (1967, p. 243), or ZoBell (1946).

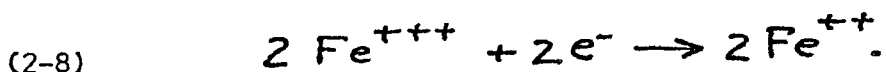
The Eh of a solution is measured in volts (or millivolts) referred to a standard hydrogen electrode (see Chapter 4). An Eh value of zero is sometimes arbitrarily set as the "redox boundary", although Eh is a relative value in that any solution will tend to oxidize another solution with a lower Eh value. The Eh of a solution is high (algebraically more positive) if it has a strong tendency to remove electrons from ions added to the solution. As oxidation is defined as the loss of electrons by an ion, a solution with a high Eh value is known as an oxidizing solution.

An example of an oxidizing solution is one containing a high concentration of Fe^{+++} (ferric) ions. Fe^{+++} has a strong tendency to add an electron to itself, so that if, for example, metallic copper is added to a solution containing Fe^{+++} ions, the copper will be

oxidized and will lose electrons:



which are taken up by the ferric ions:



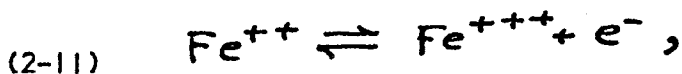
A reducing solution (one with an algebraically more negative Eh) contains ions which have a strong tendency to give up electrons to ions added to the solution. A solution containing a high concentration of chromous (Cr^{++}) ions is strongly reducing, as the chromous ions have a strong tendency to give up an electron and change to the chromic (Cr^{+++}) valence state:



As mentioned above, the Eh of a solution is measured in volts, and depends upon the concentration of the oxidized and reduced ions in the solution. The general expression for the Eh of a solution is

$$(2-10) \quad \text{Eh} = \text{Eh}^{\circ} - \frac{.059\text{m}}{n} \text{pH} + \frac{.059}{n} \log \frac{(\text{B})^b}{(\text{A})^a} \quad (\text{volts})$$

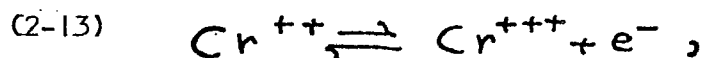
where the parenthesis signify the activity of the species (see formulas (2-13) and (2-14) of this chapter). For the reaction



$$(2-12) \quad \text{Eh} = 0.746 + .059 \log \frac{(\text{Fe}^{+++})}{(\text{Fe}^{++})} \quad (\text{volts}).$$

A solution in which (Fe^{+++}) is 1.0 and (Fe^{++}) is 0.001 will have an Eh of + 0.923 volts (strongly oxidizing), and a solution in which (Fe^{+++}) is 0.001 and (Fe^{++}) is 1.0 will have

an Eh of + 0.569 volts (less strongly oxidizing). For the reaction



$$(2-14) \quad \text{Eh} = -0.41 + .059 \log \frac{(\text{Cr}^{+++})}{(\text{Cr}^{++})} \text{ (volts)},$$

so a solution in which (Cr^{++}) is 1.0 and (Cr^{+++}) is 0.001 will have an Eh of -0.23 volts (strongly reducing) and will have a strong tendency to give up electrons.

As discussed in Chapter 4, Eh is measured using an unattackable (inert) electrode together with a reference electrode (Glasstone and Lewis, 1960, p. 456; Garrels and Christ, 1965, p. 132). The inert electrode (usually platinum, although gold is used also) functions only as a conductor to make electrical contact with the solution and allow electrons to be transferred freely to and from the solution. The reference electrode serves as a "stand-in" for the standard hydrogen electrode, to which all Eh readings are referenced. The measurement of Eh is a tricky business and, even when carefully done, there is considerable doubt as to what quantity truly is being measured. Starkey and Wight (1945), Garrels and Christ (1965, p. 136), ZoBell (1946), and Morris and Stumm (1967) discuss the techniques and pitfalls of Eh measurements in natural environments.

Eh and pH of natural environments

The Eh and pH of natural environments are described extensively by Baas Becking and others (1960), and also are discussed by Sato (1960a), Garrels and Christ (1965, p. 379), Krauskopf (1967, p. 245), Starkey and Wight (1945), Merkle (1955) and Sato and Mooney (1960).

The following discussion is based on these references unless otherwise stated.

The Eh and pH of a natural environment are determined by a combination of many factors, including the nature and amount of dissolved ions, the availability of oxygen, the amount and type of organic material, the mineral assemblages present, and the temperature and pressure of the environment. All of these factors (and possibly others) interact to establish the tendency and ability of the environment to remove or supply electrons. The Eh of most natural environments is poorly posed, which compounds the difficulty of measurement and interpretation. The Eh-pH data compiled by Baas Becking and others (1960) is summarized in Figures 2-4, 2-5, and 2-6; the "weathering" and "depth" environments of Sato and Mooney (1960) are shown in Figure 2-7; and a "summary of summaries" by Garrels and Christ (1965, p. 381) is shown in Figure 2-8.

The distribution of Eh and pH with depth is of prime importance in the self-potential mechanism discussed later in this chapter. A trend of decreasing Eh with increasing depth of environment may be seen in Figures 2-5 through 2-8. Figure 2-9 is a plot of the data of Sato (1960a), showing the decrease of Eh with increasing depth of the natural waters of four different mining districts. The decrease is far from monotonic, but the trend is evident. The depth distribution of the Eh and pH of sea water and marine sediments will be discussed in more detail in the section of this chapter on the extension of the self-potential mechanism to the marine environment.

Figure 2-4

Eh-pH Measurements of Natural Aqueous Environments

From Garrels and Christ (1965, p.380)

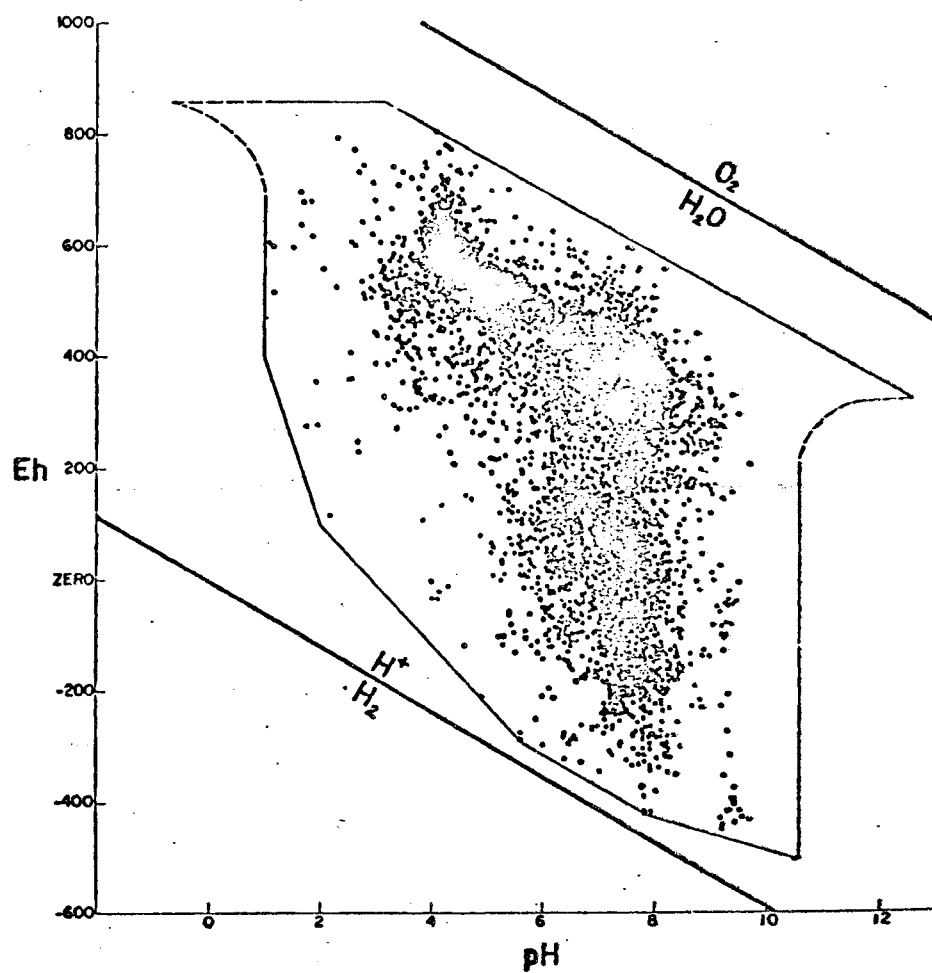


Figure 2-5

Eh-pH "Areas" for Natural Environments

From Baas-Becking and others (1960, p. 278)

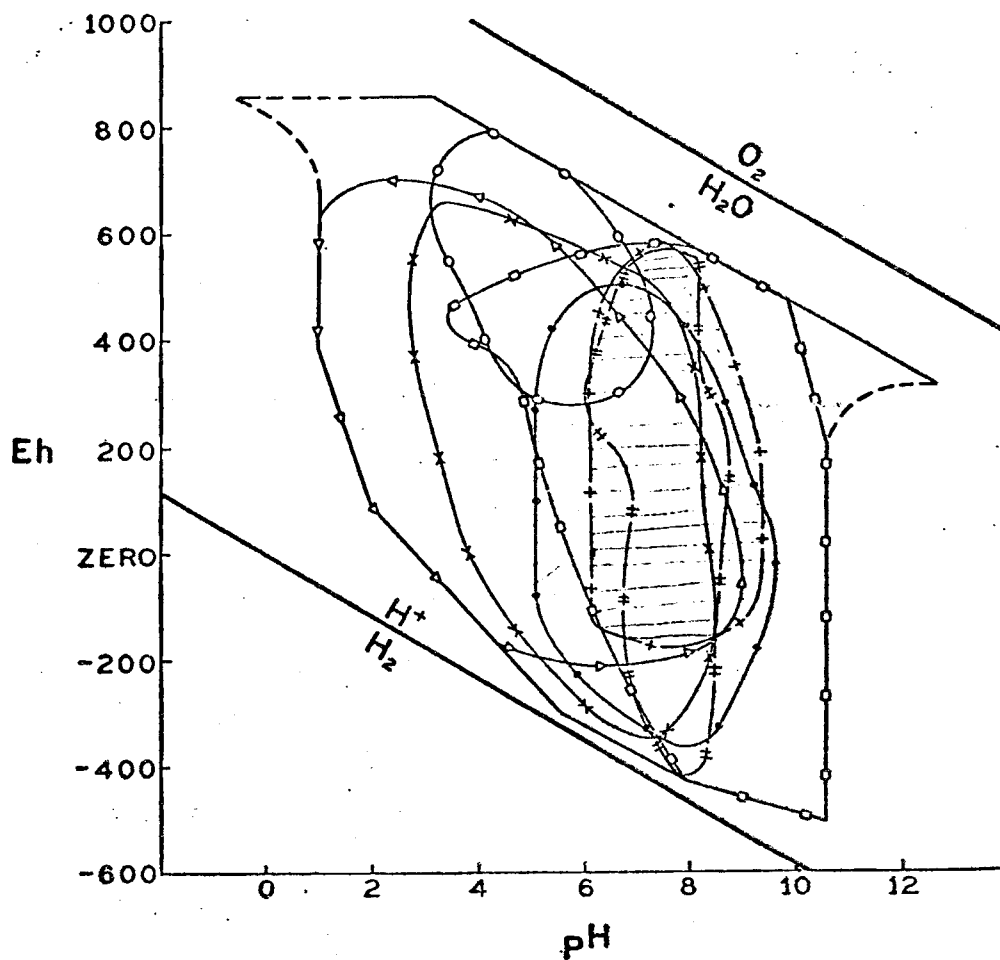


FIG. 33a.—Approximate "areas" of Eh and pH for some natural environments studied in this work. The "area" for each environment is bounded by a different symbol: $\circ\circ\circ$ = meteoric water; $\times\times\times$ = peat bogs; $\circ\circ\circ$ (with horizontal lines) = marginal marine sediments; $\times\times\times$ (with vertical lines) = sea water; $\times\times\times$ (with diagonal lines) = open-sea sediments; $\square\square\square$ = evaporites; $\triangle\triangle\triangle$ = geothermal environment.

Figure 2-6

Eh-pH "Areas" for Natural Environments

From Baas-Becking and others (1960, p. 279)

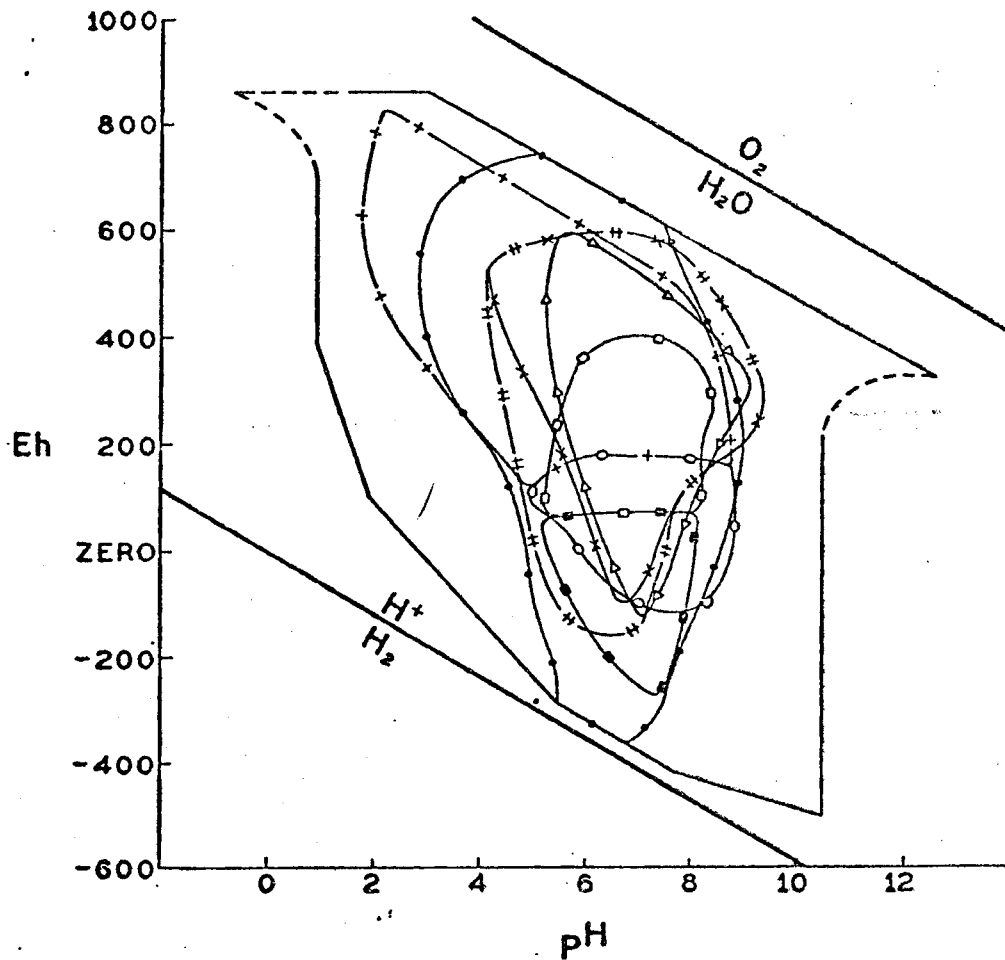


FIG. 33b.—Approximate "areas" of Eh and pH for some natural environments studied in this work. The "area" for each environment is bounded by a different symbol: $\odot\odot\odot$ = soils; $\triangle\triangle\triangle$ = shallow ground water; $+++$ = oxidized mine water; $\circ\circ\circ$ = primary mine water; $\times\times\times$ = fresh water; $\# \# \#$ = fresh-water sediments; $\square\square\square$ = oxidized connate water; $\square\square\square$ = uncontaminated connate water.

Figure 2-7

Eh and pH Conditions in the Weathering and Depth Zones

From Sato and Mooney (1960, p. 238)

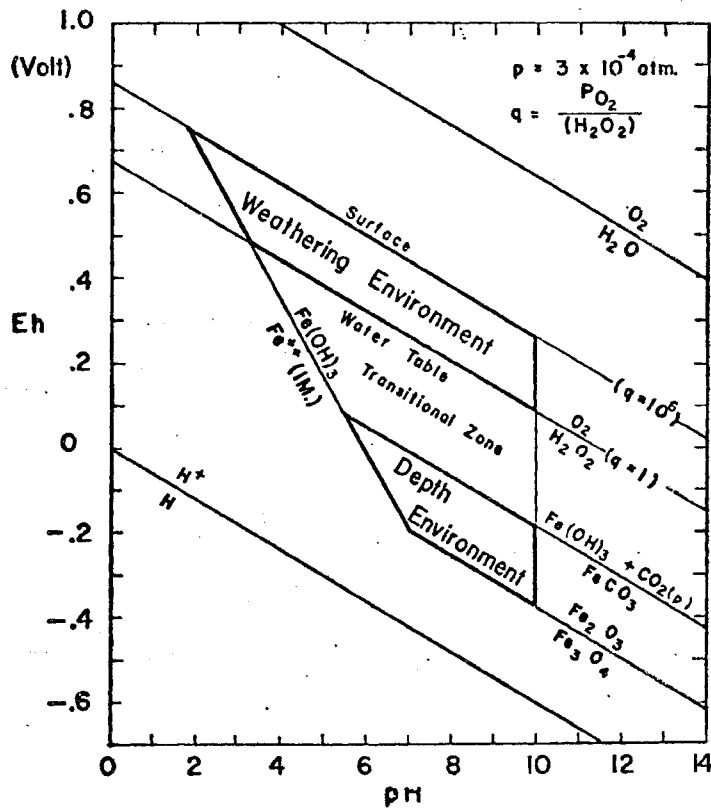


Figure 2-8

Natural Environments as Characterized by Eh and pH

From Garrels and Christ (1965, p.381)

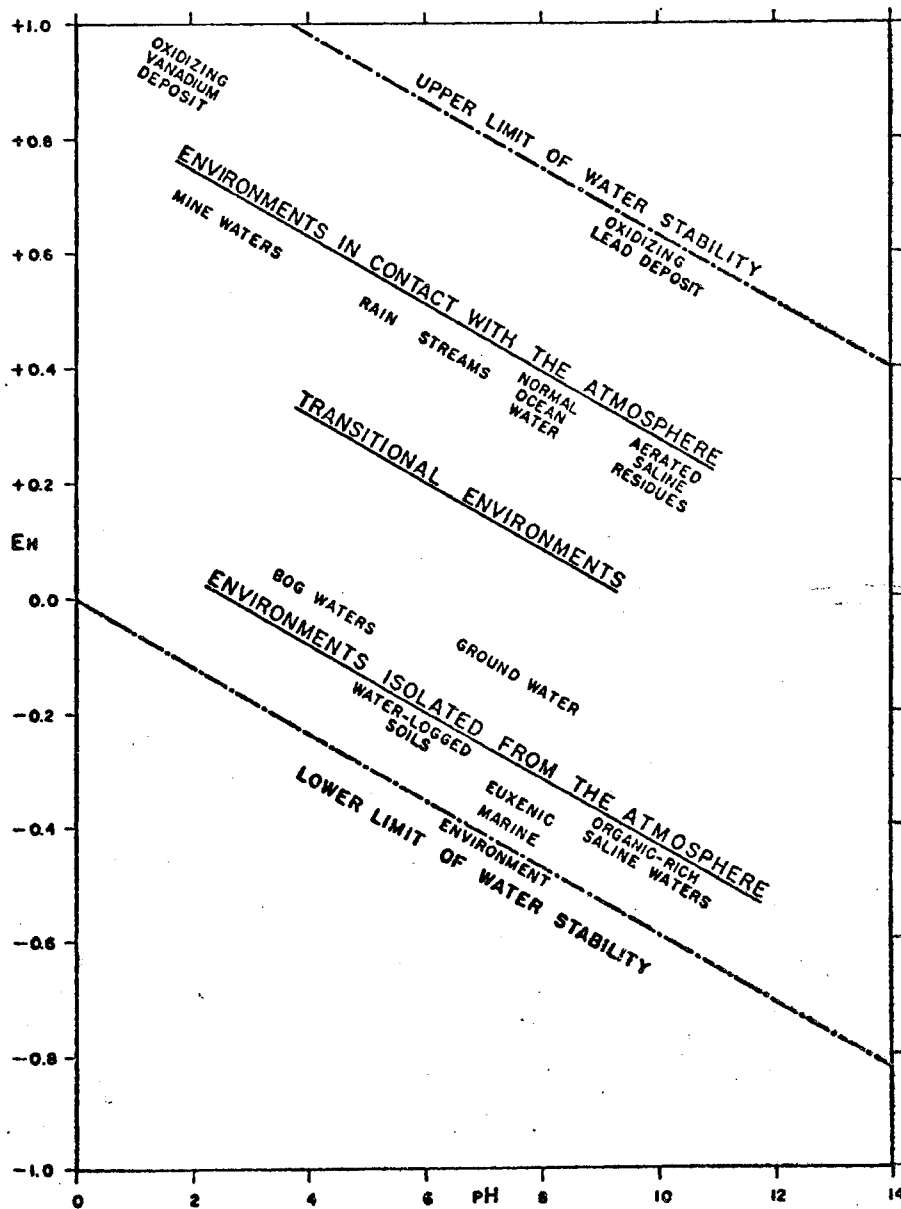
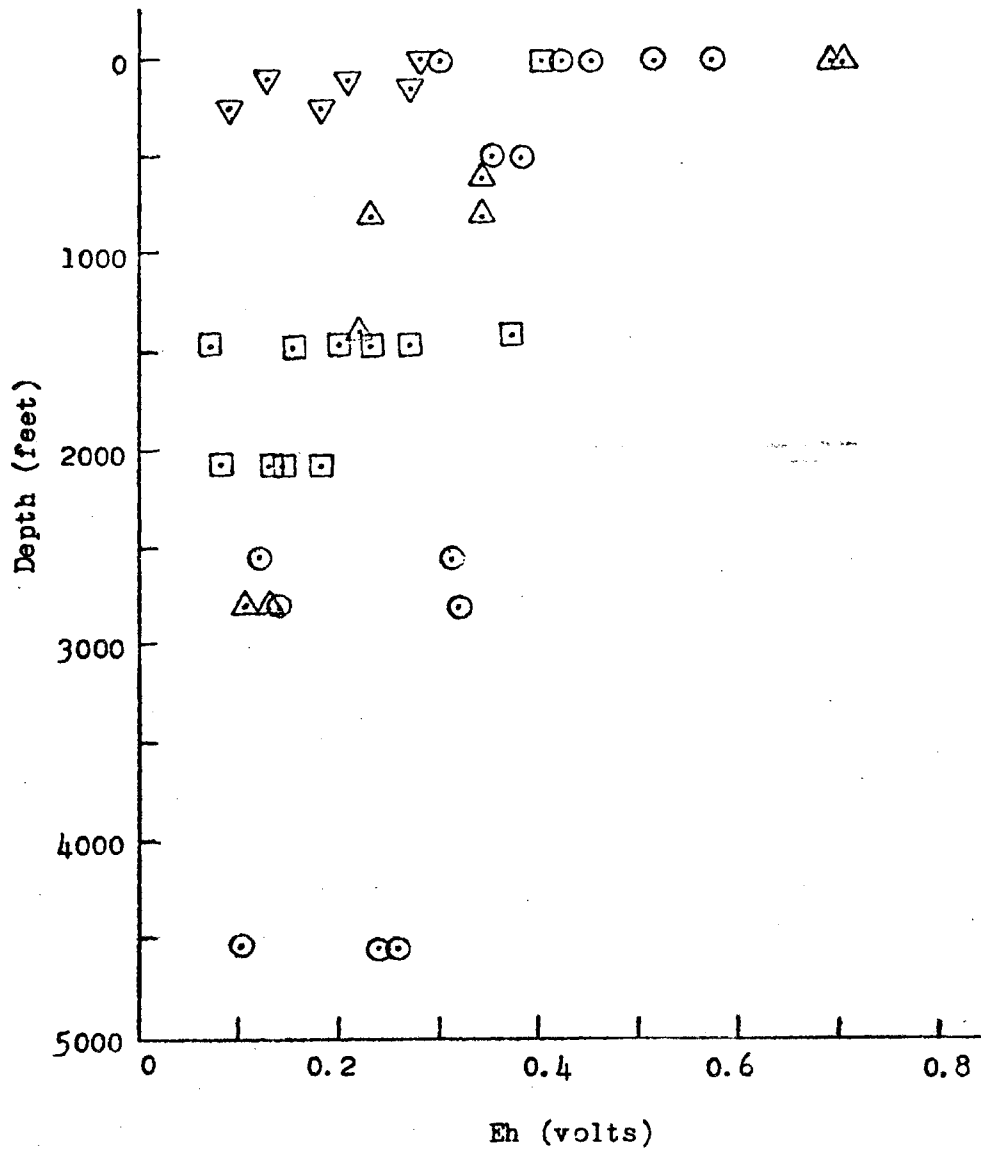


Figure 2-9

Eh Values of Natural Waters in Mining Districts

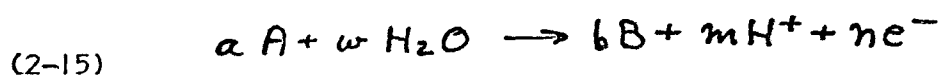
Data from Sato (1960a)



Eh-pH, mineral stability, and immunity domains

The concept of representing the stability field of materials as a function of Eh and pH was developed by Pourbaix (1949, p. 50) for studies of metallic corrosion, and has proven extremely useful in studies of mineral equilibrium in natural environments (Garrels and Christ, 1965, p. 172). Eh-pH diagrams and mineral immunity domains will be discussed briefly below; for a more complete discussion the reader is referred to the references cited above, and to Krauskopf (1967, p. 246) and Sato and Mooney (1960).

An electrochemical reaction in an aqueous medium may be written



where A, B, H₂O, H⁺, and electrons (e⁻) are the reactants, and a, b, w, m, and n are, respectively, their molar concentrations. If water, or H⁺ ions, or electrons do not take part in a given reaction, then w, m, or n, respectively, will be zero for that reaction. The Eh of the above reaction is

$$(2-16) \quad Eh = Eh^\circ - \frac{.059m}{n} pH + \frac{.059}{n} \log \frac{(B)^b}{(A)^a} \quad (\text{volts; } 25^\circ\text{C})$$

where (A) and (B) are the activities of the reactants and Eh^o is the standard oxidation potential for the reaction (the potential existing when (A) and (B) are unity), measured against a standard hydrogen half-cell.

If the Eh and pH of an environment are specified, then the equilibrium ratio of (B) to (A) is determined uniquely. If

$$(2-17) \quad \log \frac{(B)^b}{(A)^a} = \frac{n}{.059} (Eh - Eh^\circ) + m pH,$$

then A will change to B, or B to A, until the equation is satisfied (assuming the Eh, pH, temperature, and pressure of the environment remain constant and are not affected by the reactions $A \rightarrow B$ or $B \rightarrow A$; this may not always be the case).

The oxidation of copper to cuprite (Cu_2O) may be used to illustrate the above discussion. The reaction is



By analogy with (2-15),

$$\begin{array}{ll} A \sim \text{Cu}; a=2 & m=2 \\ B \sim \text{Cu}_2\text{O}; b=1 & h=2 \end{array}$$

From (2-16)

$$(2-19) \quad \text{Eh} = 0.468 - .059 \text{ pH} + \frac{.059}{2} \log \frac{(\text{Cu}_2\text{O})}{(\text{Cu})^2}$$

or,

$$(2-20) \quad \log \frac{(\text{Cu}_2\text{O})}{(\text{Cu})^2} = 33.9 \text{ Eh} + 2 \text{ pH} - 15.9 .$$

For a "typical" surface condition, $\text{Eh} = 0.3$ volts and $\text{pH} = 7$,

$$(2-21) \quad \log \frac{(\text{Cu}_2\text{O})}{(\text{Cu})^2} = 10.2 + 14 - 15.9 = 8.3$$

or, at equilibrium,

$$(2-22) \quad \frac{(\text{Cu}_2\text{O})}{(\text{Cu})^2} = 10^{8.3} .$$

Thus, under these conditions the concentration of cuprite is much greater than the concentration of native copper. Many factors may preclude this condition from existing in nature; among these, the reaction (2-18) may be so slow that equilibrium is never reached, or a coating of some other oxide, hydroxide, or sulfide

may form on the copper and inhibit the reaction. Nevertheless, the technique does provide a quantitative approach to the study of the stability of mineral assemblages in natural environments.

For reaction (2-15) Pourbaix (1949) defines the "immunity domain" of A as the boundaries of the Eh-pH region within which the concentration of any reaction product such as B is less than the arbitrary value of 10^{-6} M; in other words, the Eh-pH region in which the tendency of A to transform into any other substance is negligible (see Figure 2-10). Outside the immunity domain, the concentrations of the reaction products may be greater than 10^{-6} M, subject to the constraints mentioned above.

The behavior of minerals in natural environments may be predicted using the immunity domain concept. If a metallicly conducting mineral is immune from any conceivable reaction at a given Eh-pH locus, the mineral assumes the potential (Eh) of the environment, and functions as an inert conductor of electrons; if it is not immune, it will be oxidized or reduced by the environment. The fact, established by Sato (1960b), that many conductive ore minerals are immune within a large portion of the natural Eh-pH environment (see Figure 2-11) forms the basis of the self-potential mechanism discussed below.

Self-potential mechanism

The self-potential mechanism proposed by Sato and Mooney (1960) utilizes the observations that the Eh in the earth generally becomes more negative (reducing) with increasing depth, and that most of the ore minerals which are known to produce self-potential anomalies are largely immune from oxidation or reduction within the Eh-pH

Figure 2-10

Immunity Domain of Substance A
(with respect to substances B, C, D, and F)

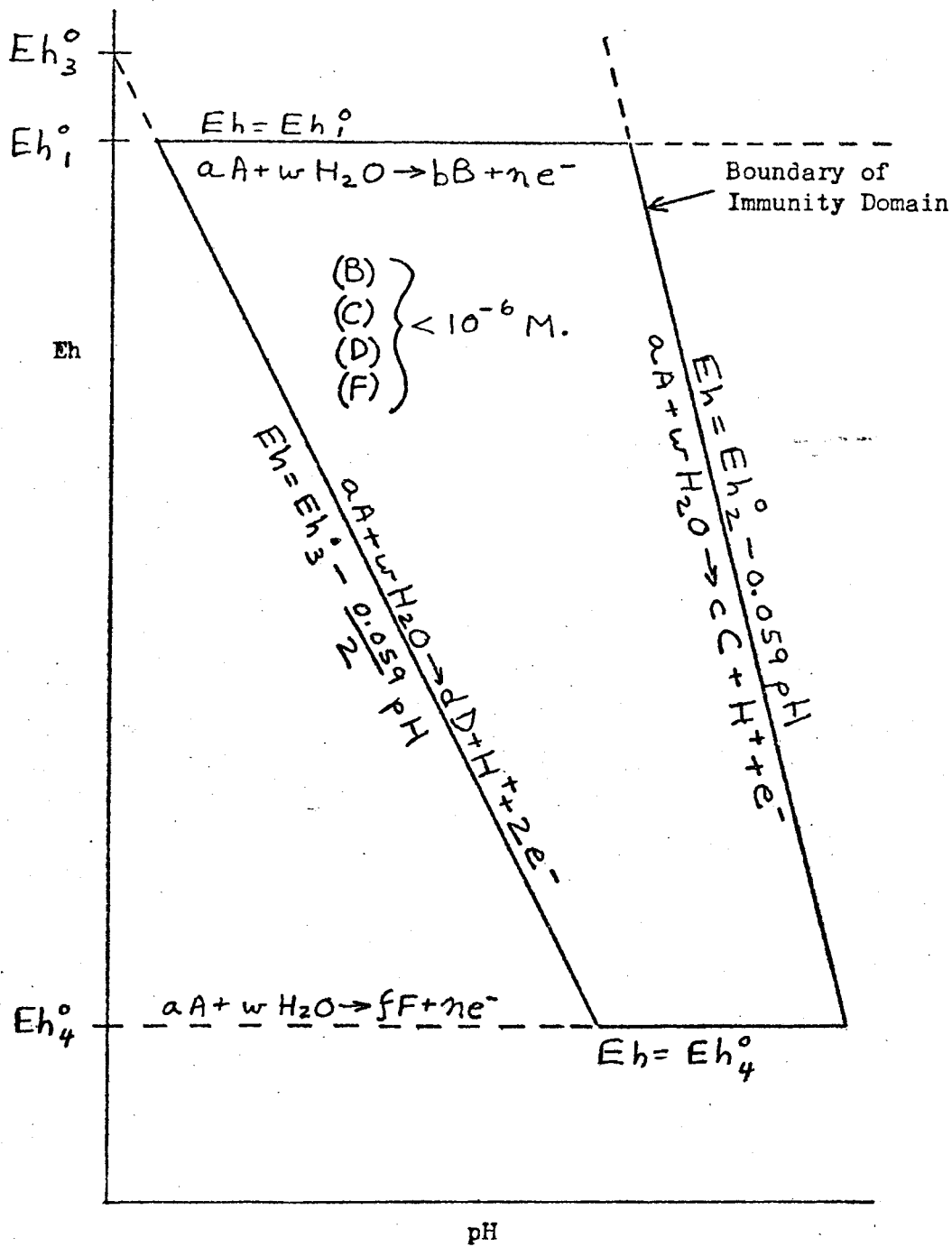
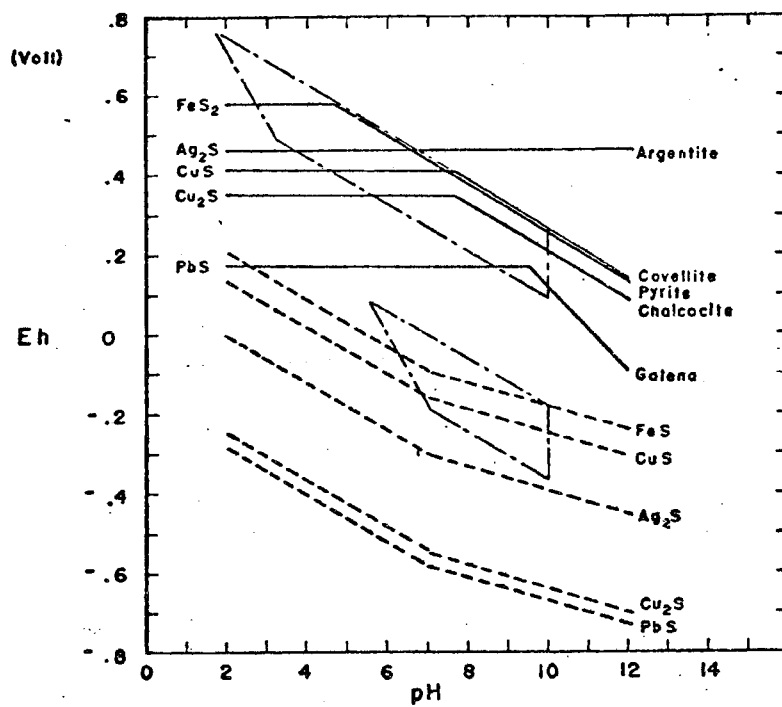


Figure 2-11

Immunity Domains for Sulfide Minerals

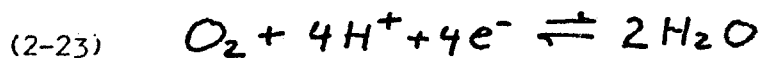
From Sato and Mooney (1960, p. 241)



constraints of the natural environment, and so are able to function as inert conductors of electrons. The ore body thus serves as the "bridge" which allows electrons to be transferred from the reducing environment in the primary zone at depth to the oxidizing environment in the weathering zone near the surface, thus generating a flow of conventional current from the top to the bottom of the ore body.

The oxidizing and reducing regions exist independently of the ore body, but no transfer of electrons between the two environments, and thus no current flow, is possible without the presence of the metallicly conducting ore body. This is because electrical current flow through the aqueous media of the natural environment is accomplished through the movement of charged ions, not electrons, and because the Eh gradient creates a potential only for the flow of electrons. The return current through the earth surrounding the ore body is ionic and the transfer from electronic to ionic current flow is accomplished by chemical reactions at the surface of the ore mineral, with reduced species at the lower end of the ore body being oxidized by their loss of electrons to the body, while oxidized species at the upper end of the body are reduced by the electrons they pick up from the body (Figure 2-12).

Obviously, some mechanism must be provided to re-oxidize the reduced species, and to re-reduce the oxidized species, or the current flow would soon cease. Sato and Mooney propose that in the weathering zone, the conversion of oxygen to hydrogen peroxide:



aids in the removal of electrons from reduced species, e.g.

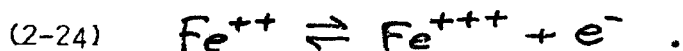
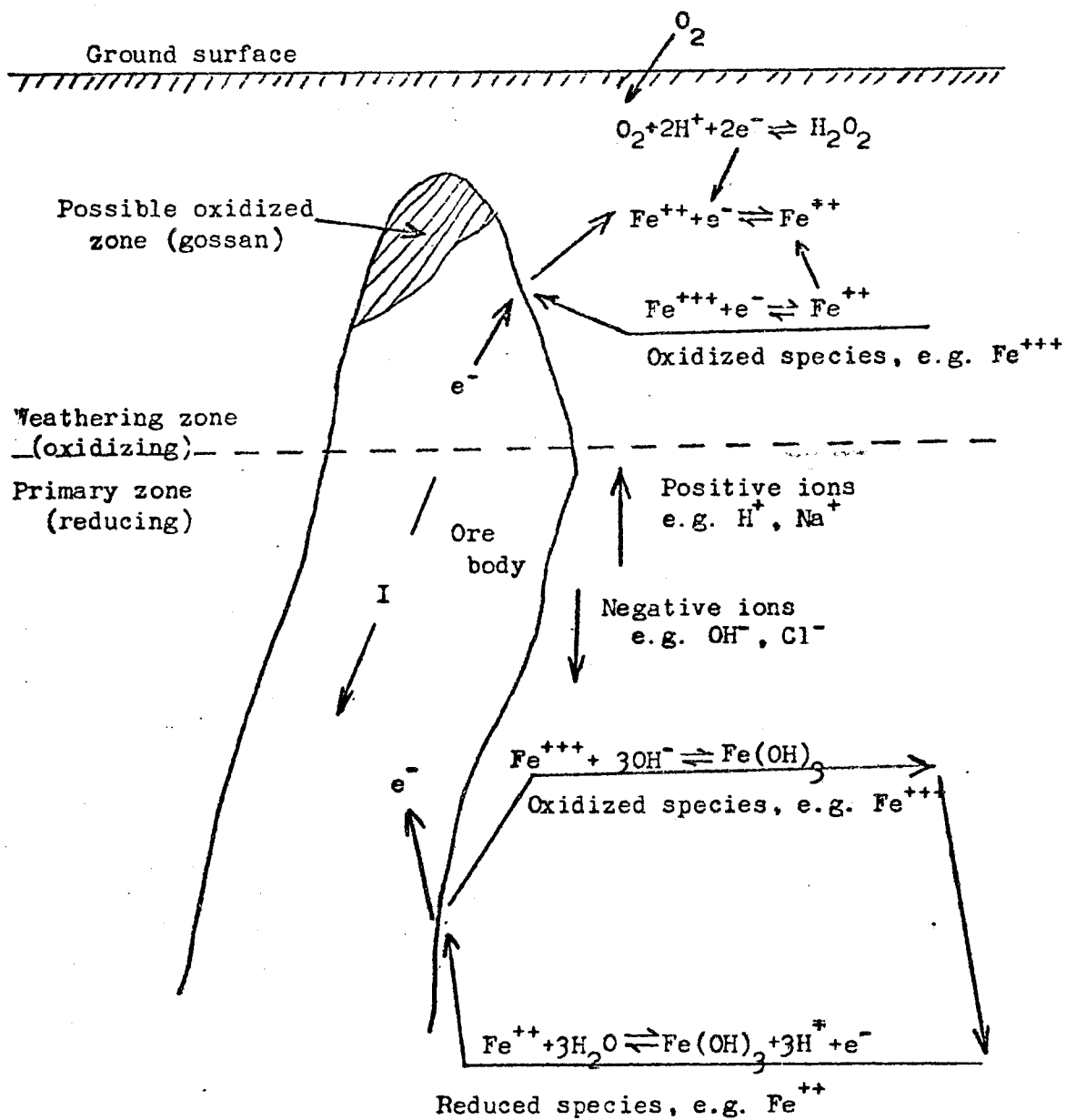


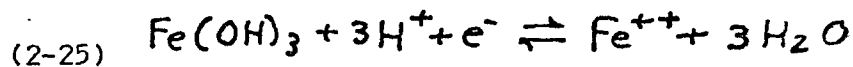
Figure 2-12

Oxidation-Reduction Mechanism of Self-Potential Generation

After Sato and Mooney (1960, p. 246)



In the primary zone, reactions of ferrous and ferric hydroxide provide a means for the addition of electrons to ferric ions, to return them to the reduced ferrous state:



The action of anaerobic bacteria also may play a role in maintaining low Eh values at depth.

It is not necessary that the ore mineral be entirely immune from oxidation in the weathering zone, nor entirely immune from reduction in the primary zone. If the Eh-pH environment in the weathering zone is out of the immunity domain of the ore mineral, the top of the ore body will be oxidized to a depth where the Eh-pH value is within the immunity domain, at which point the body begins to function as an inert electron carrier. An analogous reduction process will occur in the primary zone if the ore mineral is subject to reduction at depth.

The nature of the ore mineral and the geologic environment of the ore body must be favorable in order for the self-potential phenomenon to occur. Sato and Mooney discuss the following requirements:

1. The ore mineral must be a good electronic conductor (or semiconductor).
2. The ore body must connect continuously environments of different Eh.
3. The ore mineral must be immune from oxidation or reduction at some point within the Eh-pH environment.

4. No permanent insulating films may form on the surface of the ore.
5. There must not be a continuous layer of high-resistivity material surrounding the ore body at any depth. Such a layer would block the flow of ionic return current. A layer of low-resistivity, anisotropically conducting material such as montmorillonite clay might tend to "short-circuit" the mechanism by diverting the ionic return flow.

Nourbehecht (1963) examined this mechanism from the point of view of irreversible thermodynamics, and concluded that the explanation seems plausible.

Alunite

No discussion of the mechanism of self-potential would be complete without mention of the alunite problem. Two very large self-potential anomalies have been measured over alunite $[KAl_3(OH)_6(SO_4)_2]$ deposits: Kruger and Lacy (1949) recorded potentials of more than 700 millivolts over a deposit near Cerro de Pasco, Peru, and Gay (1967) measured a self-potential anomaly with a maximum amplitude of -1,842 millivolts at Tantahuatay, near Hualgayoc, Peru. The latter is believed to be the largest self-potential anomaly ever measured.

The problem is that alunite is not a metallic conductor of electricity, so there is no way for the current flow necessary for a self-potential field to be generated in an alunite deposit. There appears to be no data in the literature regarding the electrical conductivity of alunite, so I measured the resistance of a specimen from Tonopah, Nevada measuring about 4 by 2 by 2 cm, using a Triplett Model 801 V-O-M. Resistance of the specimen was greater

than 10^9 ohms, implying that resistivity exceeded 10^7 ohm-m; well above the resistivity range of other minerals known to produce self-potential anomalies. It thus appears highly unlikely that alunite could support a current flow which could produce a detectable self-potential anomaly, let alone an anomaly exceeding one volt.

Kruger and Lacy noted that the self-potential equipotential lines appeared to correlate with contours of alunite percentage, and that high alunite concentrations (20%) implied low pH values (about 4.5), corresponding to high sulfuric acid content, for the interstitial water of the rocks. They propose that this "pH anomaly" is responsible for the self-potential anomaly, as the pH of the non-alunite bearing rocks surrounding the deposit is about 7.8.

The non-polarizing electrodes used for self-potential surveys (Chapter 4) show little or no response to concentration differences of any type, including concentration of H^+ ion, which defines pH, so assuming that Kruger and Lacy (and Gay) used non-polarizing electrodes, anomalies of the amplitude they report could have been caused only by a flow of electric current in the earth. (Even if the survey was made with a pH electrode, the maximum possible anomaly for a pH difference of (7.8-4.5) is about 200 mv). It is possible that, as argued by Kelly (1945), a strong pH concentration cell could produce a flow of ionic current of the proper (observed) polarity in the earth. The excess of H^+ ions near the surface, flowing downward, would result in a flow of conventional (positive) current away from the surface, producing a negative potential at the surface. The high mobility of the

H^+ ion would facilitate this flow, although it is not clear whether anomalies of the observed magnitude could be generated. Although the pH cell mechanism may be responsible for all or part of the self-potential anomalies observed over alunite deposits, it seems unlikely, as discussed previously in this chapter, that it is the primary cause of self-potential anomalies over sulfide bodies, as little or no pH gradient seems to be necessary for the generation of sulfide self-potentials.

As both of these surveys were made in mining districts containing many rich sulfide ore bodies, it is not inconceivable that the anomalies were caused, at least in part, by an undetected sulfide ore body in the vicinity of the alunite deposit. Kruger and Lacy state that "only sparse sulphides were encountered by drilling beneath the area", but that "the geological situation... does not exclude the possibility of the existence of a sulphide mass." The anomaly described by Gay was not drilled. It is possible, then, that these anomalies were partially due to sulfide bodies located beneath the alunite deposits. The high sulfuric acid content of the alunite, percolating downward, may contribute to the strength of the anomaly by reaction with the sulfide, as postulated by Kelly (1945). This possibility is highly speculative, but at least it offers an additional explanation for the observed data. Gay states "The writer commends the Tantauatay anomalies to future students of the self-potential process". The present student passes on the commendation.

Offshore ore bodies

There are many areas of the world where sulfide ore bodies occur near or at marine shorelines. These include Cornwall, England (Tooms and others, 1965; Marke, 1965), Penobscot Bay, Maine (Beck, 1970; Young, 1962), southeastern Alaska (Banister, 1962; Wright and Wright, 1908; Buddington and Chapin, 1929), and Santa Rosalia, Baja California, Mexico (Wilson and Rocher, 1955).

In many of these areas, the ore-bearing geologic structures extend, or appear to extend, offshore, implying that mineral deposits also may occur offshore.

If such deposits generate self-potential anomalies, offshore use of the self-potential method could provide a valuable exploration and delineation tool. The remainder of this chapter will be devoted to the question of whether offshore and nearshore ore bodies can generate self-potential fields in the surrounding or nearby sea floor and water.

It will be assumed for the following discussion that the oxidation-reduction mechanism of Sato and Mooney is the primary mechanism for the self-potential phenomenon. Although it is difficult to demonstrate this conclusively, this mechanism does seem to provide the most complete explanation, and the experiments described later in this chapter seem to reinforce this conclusion. Accordingly, the following paragraphs will discuss the Eh-pH values of the marine environment.

Eh and pH of sea water and marine sediments

The pH of reasonably pure surface sea water is about 8.1 to 8.3 (Sverdrup and others, 1942, p. 195). At this pH value, the

Eh of surface sea water, measured with a platinum electrode, is generally about +0.4 volts (Baas Beeking and others, 1960; Cooper, 1937; Breck, 1972). Manheim (1961) measured an Eh of +0.2 volts on the surface of a stagnant, brackish bay. I made measurements of Eh in San Francisco Bay, California and Penebscot Bay, Maine, both of which showed Eh values close to +0.4 volts at the surface (Figures 2-13 and 2-14).

Few measurements appear to have been made of Eh as a function of depth in the water column. The results of Manheim (1961) and Skopintskov (given in Riley and Skirrow, 1965, vol. 1, p. 635) are shown in Figures 2-15 and 2-16. Both of these measurements were done in areas where the bottom water was stagnant; while the readings shown in Figures 2-13 and 2-14 were in areas of strong bottom current flow. Ben-Yaakov (1970, p. 328) measured the variation of Eh, pH, and dissolved oxygen with depth in the open ocean off Hawaii (Figure 2-17).

In all the above studies, Eh was found at first to become more negative with depth. In Ben-Yaakov's data, the Eh increased again as the oxygen minimum zone was passed. From Figures 2-15 and 2-16, it appears that Eh is related to the dissolved oxygen content of the water. Baas Beeking and others (1960), Cooper (1937), Breck (1972), and Morris and Stumm (1967) argue that Eh is not controlled by the level of dissolved oxygen, so the relationship may not be causal. Nevertheless, the dissolved oxygen content of sea water seems to be a good indicator of Eh; dissolved oxygen implying high Eh.

Eh-pH values in marine sediments have been reported widely: Baas Becking and others (1960) summarize much of the available data,

Figure 2-13

Eh vs. Depth--San Francisco Bay, California

29 August 1971

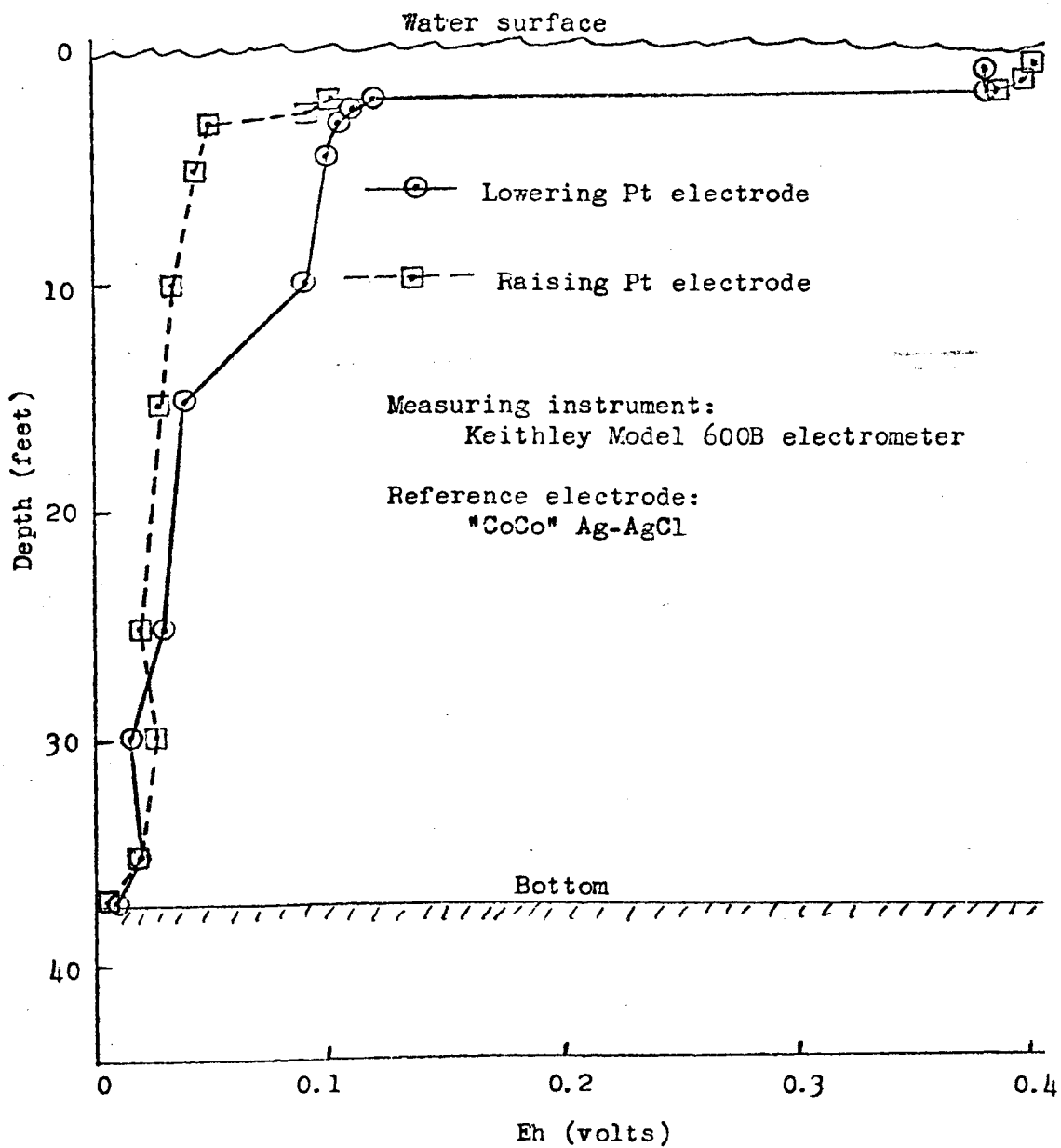


Figure 2-14

Eh vs. Depth--Penobscot Bay, Maine

8 Sept. 1971

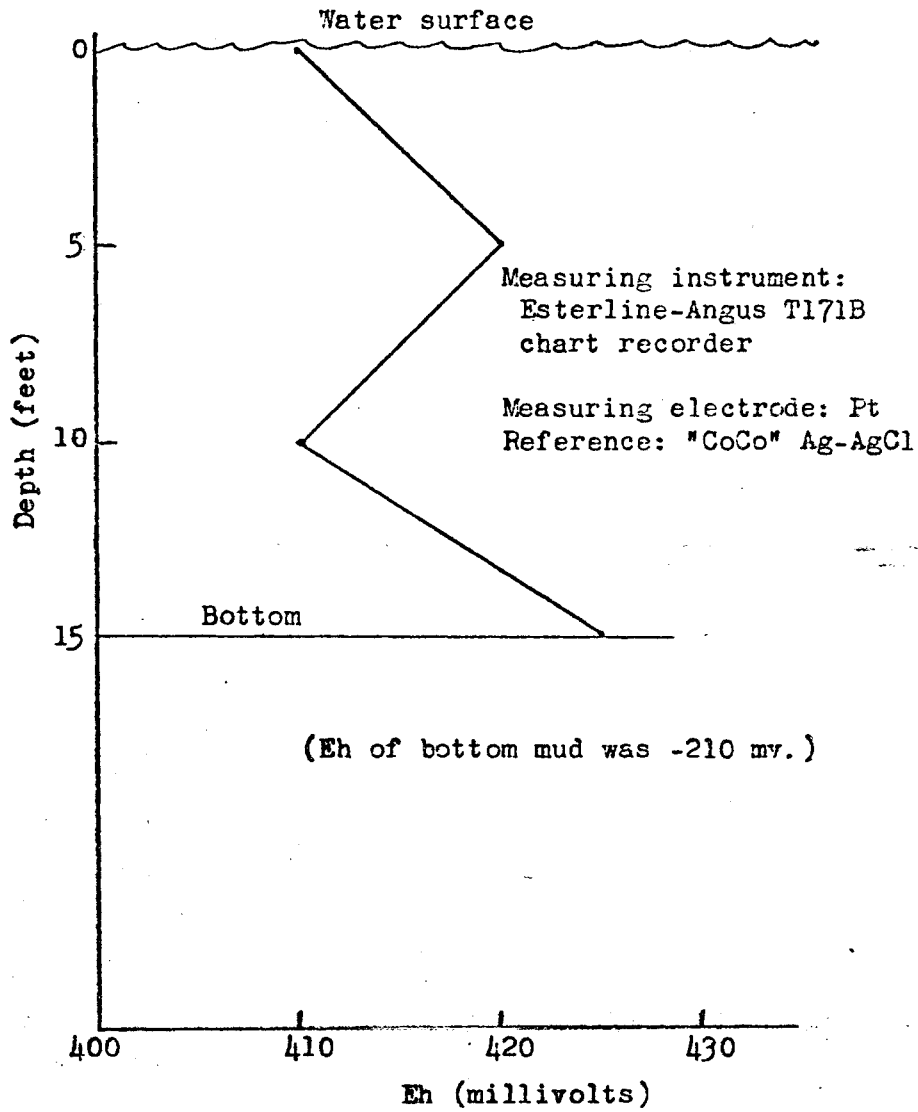


Figure 2-15

Eh, pH, Temperature, and H₂S in a Stagnant Bay

From Manheim (1961)

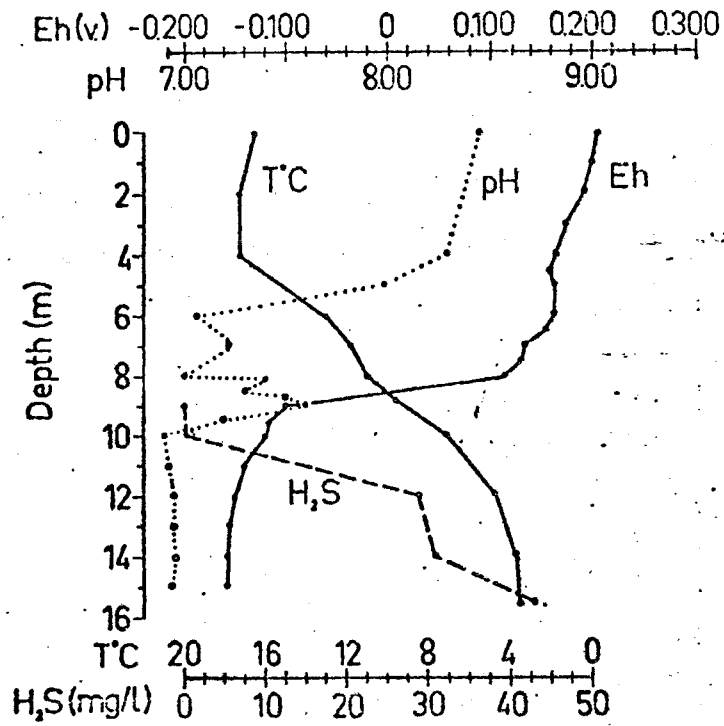


Figure 2-16

Eh and Dissolved Oxygen vs. Depth

From Skopintsev, in Riley and Skirrow (1965, p.635)

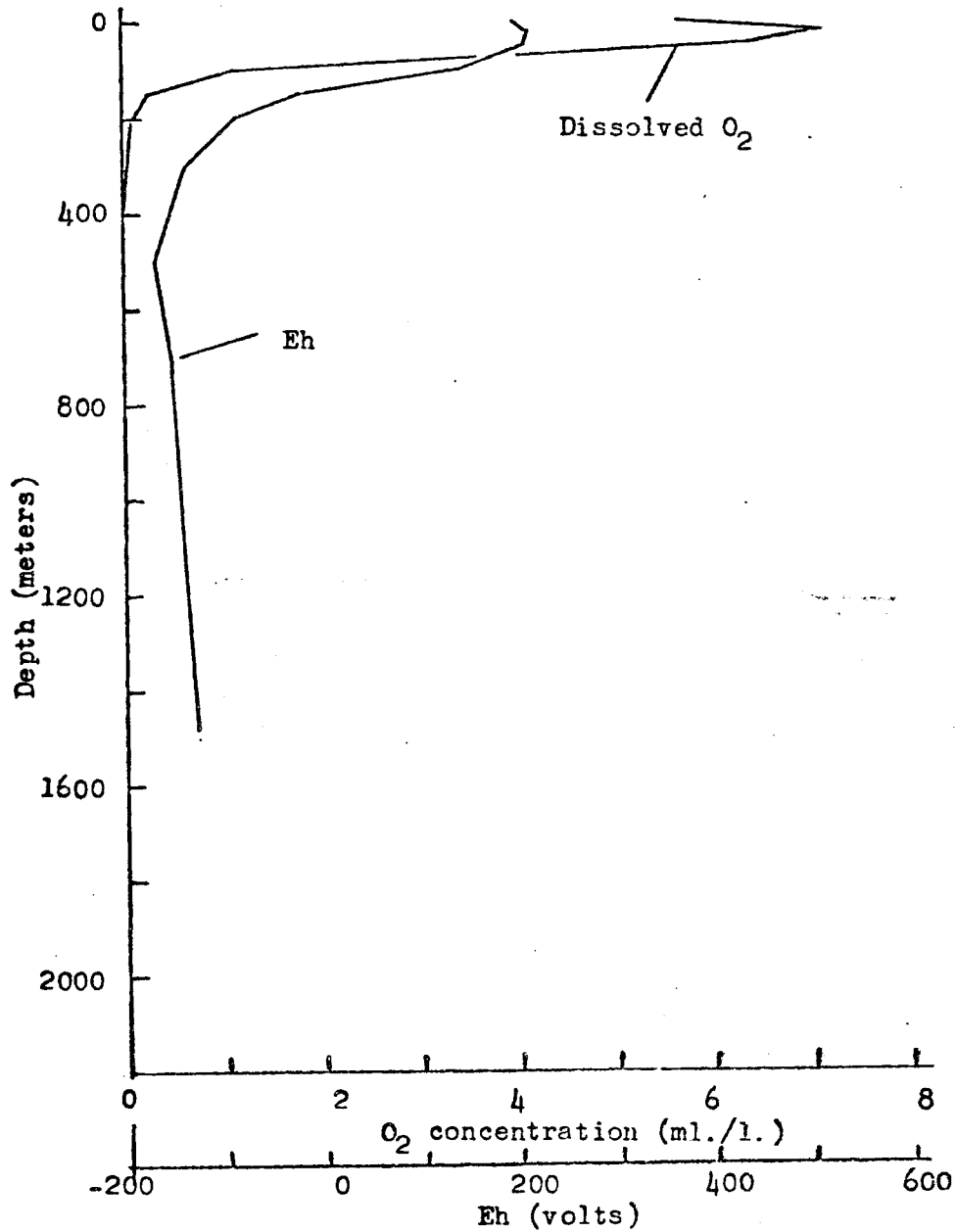
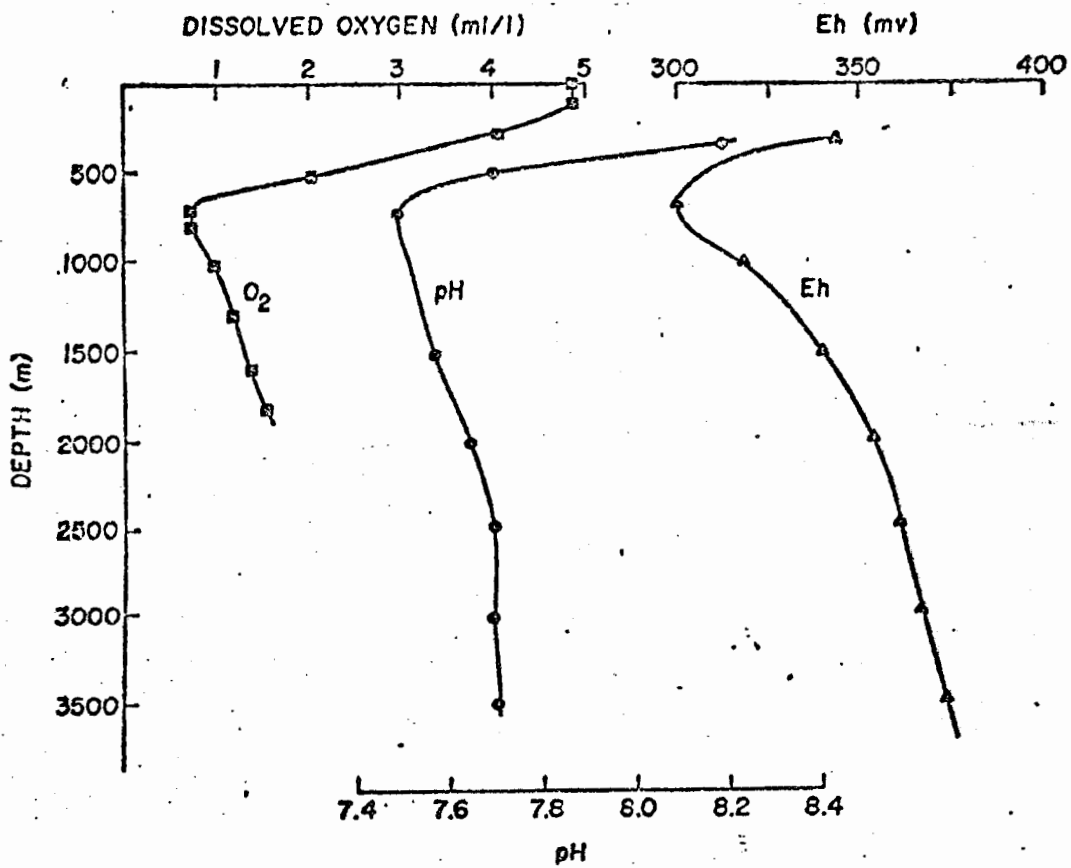


Figure 2-17

Eh, pH, and Dissolved O₂ in the Open Ocean

From Ben-Yaakov (1970, p. 335)



and some profiles from the literature are shown in Figures 2-18, 2-19, and 2-21 through 2-23. Figure 2-20 shows the temperature and dissolved oxygen profiles of the water overlying the sediments analyzed in Figures 2-18 and 2-19. Except in areas such as the Santa Barbara Basin, where the bottom waters are stagnant and anoxic, Eh values range from just above zero to +0.2 volts at the surface of the sediment and decrease with increasing depth. An Eh value of zero (the "redox boundary") is reached within the first meter or so of sediment, and maximum negative values of about -0.2 volts are seen in the upper few meters of sediment. pH values show less change than those for Eh, ranging from about 7.5 to 8.5, except for a somewhat wider range described by Trofimov (in Riley and Skirrow, 1965, vol. 2, p. 181). In the "hot brine" areas of the Red Sea, Eh values in the upper 4 to 8 meters of sediment range from +0.220 to +0.575 volts (Brooks and others, 1969, p. 200). Such areas are far from typical, but are of great geologic interest. The chemical and biological factors controlling the Eh and pH in marine sediments are many and complex, and will not be discussed here. ZoBell (1946), Baas Becking and others (1960), and Emery and Rillenberg (1952) discuss these factors in detail.

To summarize, a typical offshore Eh profile in areas of active bottom water circulation would show values of about +0.4 near the water surface, decreasing or remaining constant with increasing depth, and values at the bottom ranging from about zero to +0.4 volts. In the sediment, the Eh usually will decrease to zero within the first few tens of centimeters, and reach maximum negative values of about -0.1 to -0.3 volts in the first few meters. The redox boundary will tend to be higher in impermeable, fine-grained

Figure 2-18

Eh and pH for a Marine Core

From Emery and Rittenberg (1952)

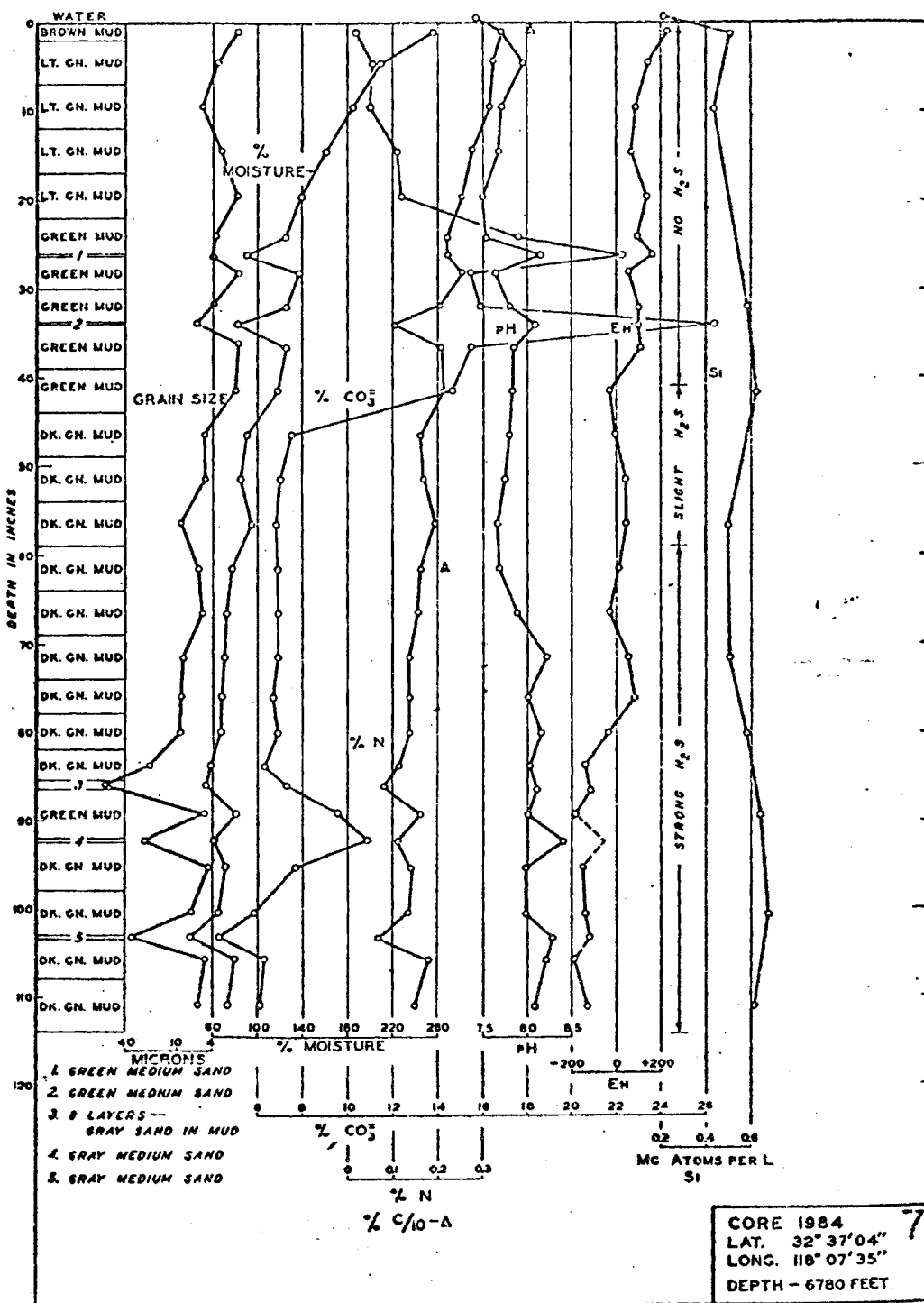


Figure 2-19

Eh and pH for Marine Cores

From Emery and Rittenberg (1952)

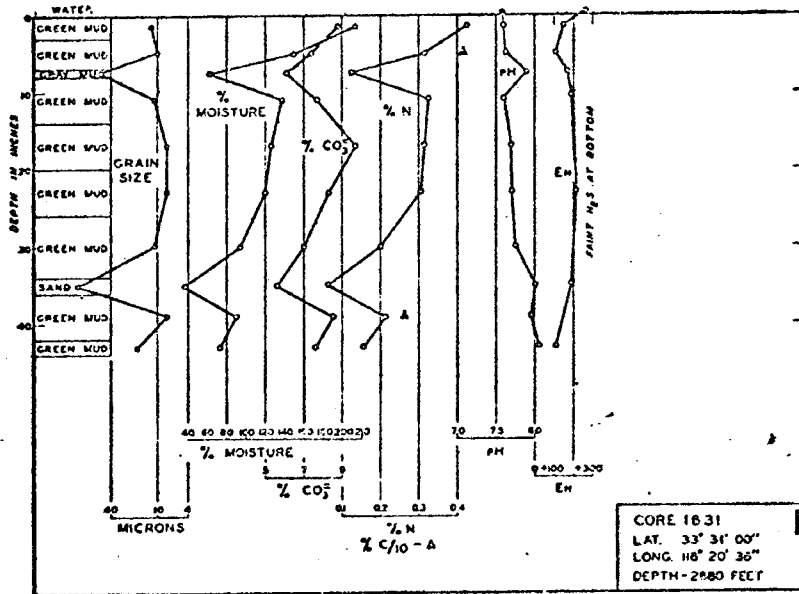


FIG. 6.—Analytical data for Core 1, San Pedro Basin.

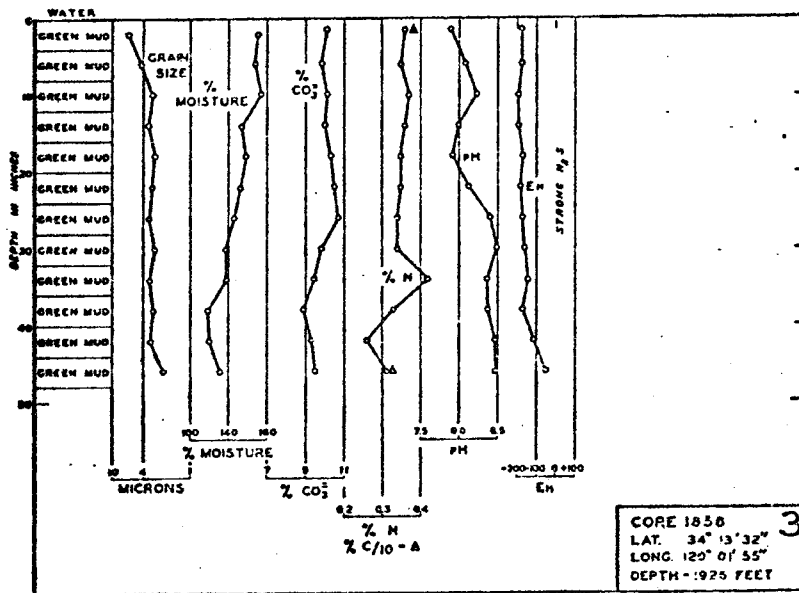


Figure 2-20

Temperature and Dissolved Oxygen Profiles

From Emery and Rittenberg (1952)

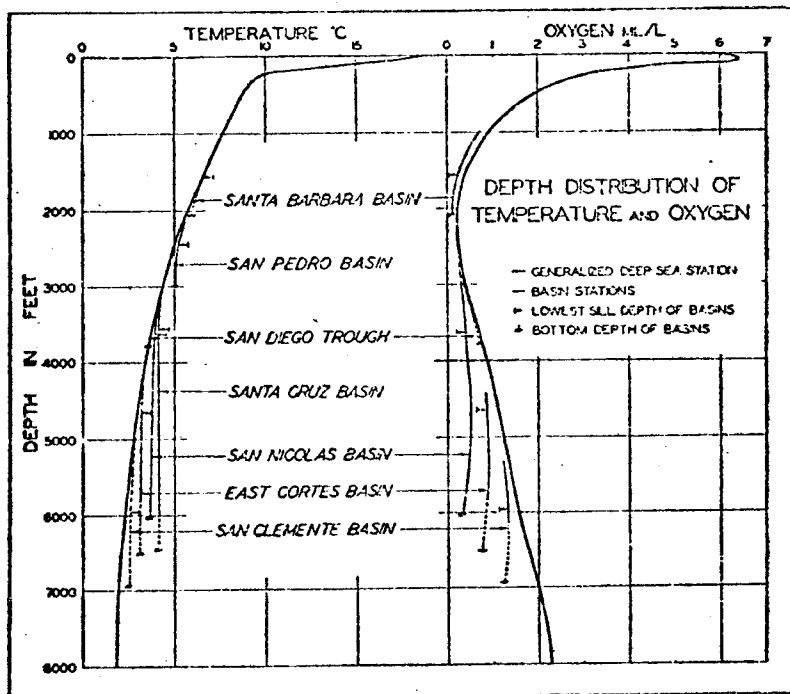


Figure 2-21

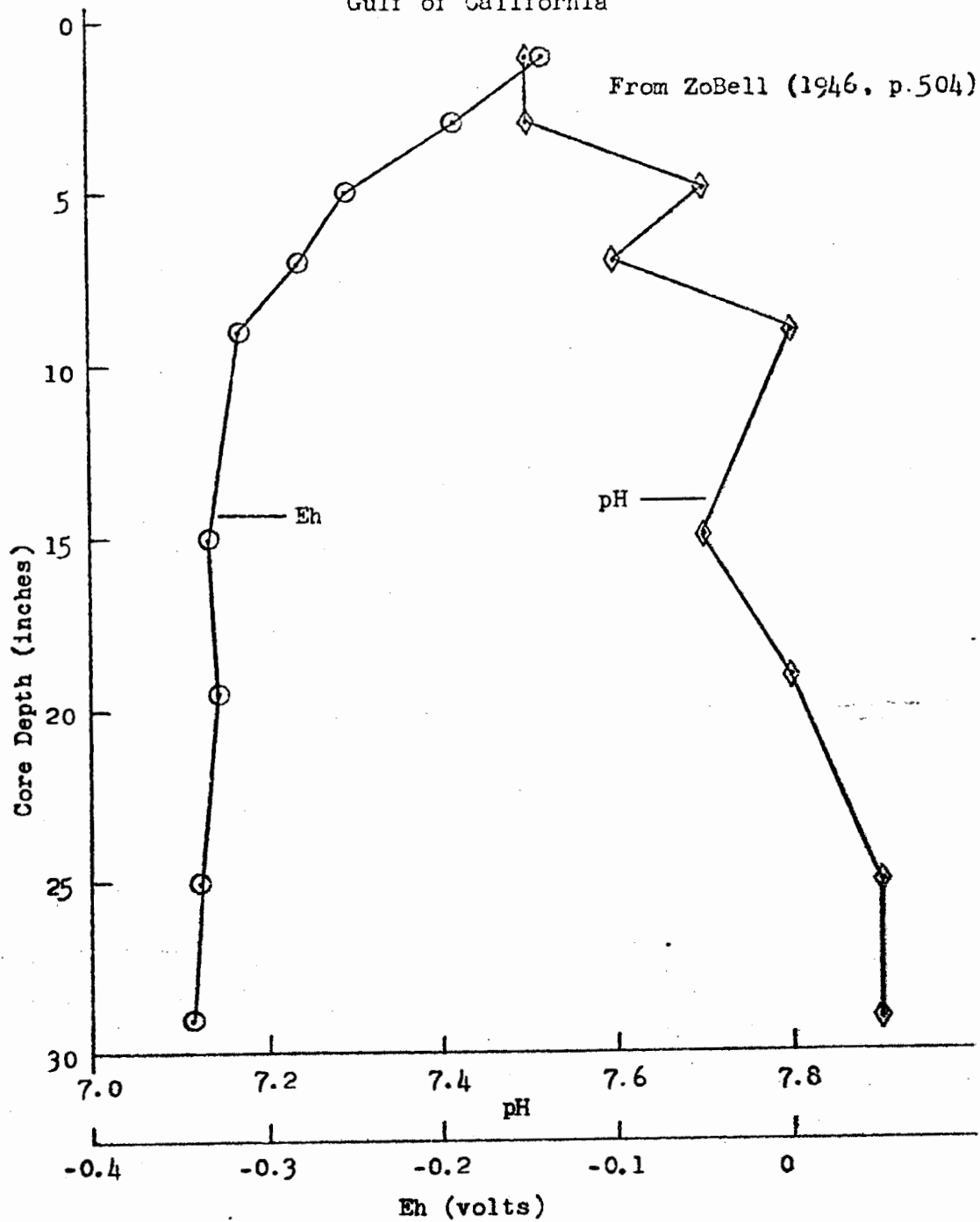
Eh-pH Profile for Mud Core
Gulf of California

Figure 2-22

Eh and pH of Bottom Sediments

From Riley and Skirrow (1965, p.181)

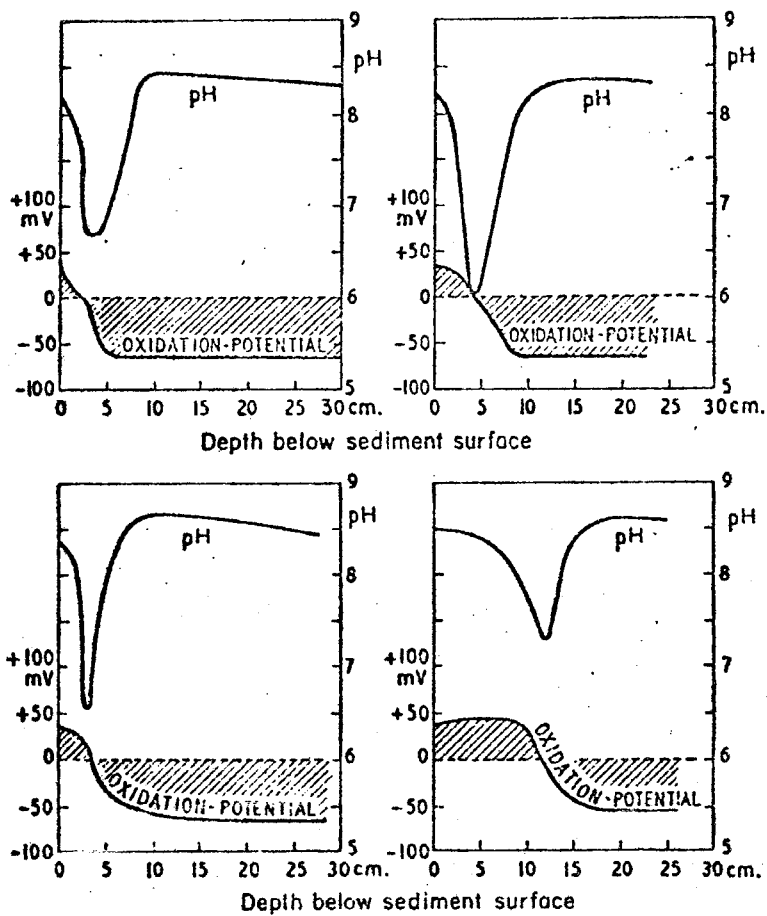
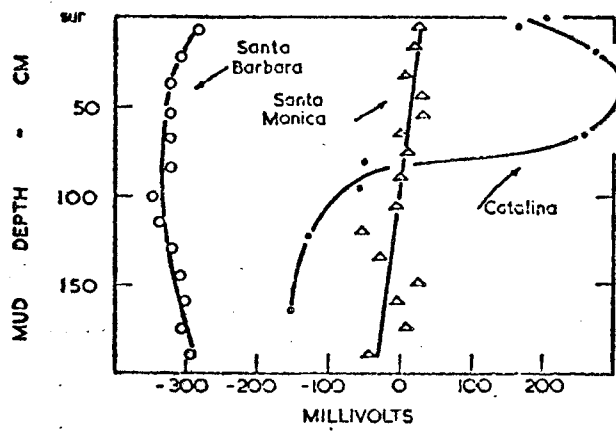


Figure 2-23

Eh Profiles in Marine Cores

From Hayes (1964)



sediments with high organic content than in loosely packed, coarse-grained sediments of low organic content. In areas where the bottom water is stagnant and anoxic, the redox boundary may occur in the water column instead of in the bottom sediments. The offshore pH profile shows relatively little change throughout the water column and sediments, with pH values generally remaining between 7.8 and 8.3 in the water column, and 6.8 to 8.3 in the sediments (Wilde, 1966). Eh-pH boundaries for the aerated and anoxic marine situations are shown in Figures 2-4, 2-5, 2-7 and 2-8.

Self-potential generation by offshore ore bodies

The offshore Eh gradient, as described above, is similar to that on land, with oxidizing values near the surface and reducing values at depth. An offshore ore body, then, which spanned all or part of this Eh gradient should be capable of generating a self-potential field similar to those found on shore. It should not be necessary for the body to extend from an oxidizing to a reducing area, as long as some portion of an Eh gradient is spanned.

In areas with well-oxygenated bottom waters, an ore body which extended out of the sediments and into the water usually would traverse an Eh gradient of at least a few hundred millivolts. A body buried more than a few meters deep in the sediments may be subjected to more reducing values at depth than near the surface, thus enabling a self-potential field to be generated, although there appears to be no information available about the Eh of sediments at depths greater than a few meters. In areas of anoxic bottom waters, an ore body which penetrated the redox boundary would be subjected to an Eh gradient of a few hundred millivolts, and

should be capable of generating a self-potential field. An ore body located entirely below the redox boundary may be subjected to slightly more reducing conditions at depth, especially below the sediment surface. The total Eh change, though, probably would be small.

Summarizing, an offshore ore body which penetrates the redox boundary, located just below the sea floor in areas of well-aerated bottom water, or in the water column for anoxic bottom water, should be capable of generating a self-potential field. An ore body which does not penetrate the redox boundary may generate a small self-potential field, or none at all, unless current is supplied from an onshore extension of the body (see below).

Fresh-water ore bodies

Eh-pH conditions for lakes and rivers are generally similar to those for the marine environment (Hayes, 1964; Baas Becking and others, 1960) with oxidizing conditions existing near the surface and reducing conditions at depth (Figure 2-24). Fresh water is, of course, less conductive than sea water, so the ionic return current necessary for self-potential generation might be inhibited in fresh-water environments. Even so, an ore body submerged in fresh water should, if it penetrates the redox boundary or spans part of an Eh gradient, be capable of generating a self-potential field.

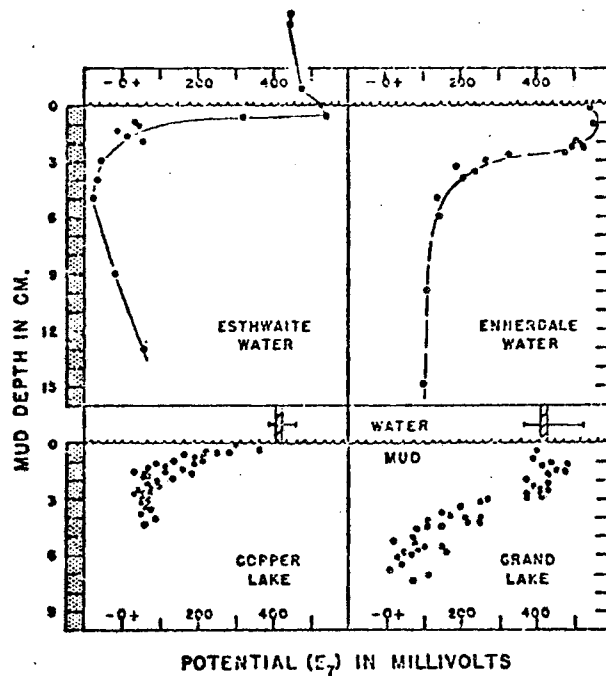
Shoreline and near-shore deposits

An onshore body located at or near a shoreline is, of course, subjected to onshore Eh-pH conditions. A self-potential field generated by such an ore body will propagate into the offshore water and sediments, as described in Chapter 3. An ore body which continuously

Figure 2-24

Eh Profiles in Lakes

From Hayes (1964)



The potential in millivolts at various mud depths in four lakes. All measurements were made with Mortimer's multiple electrode. Upper pair, English lakes measured in winter by Mortimer (1941, 1942), Lower pair, Canadian east coast, measured in summer by Hayes, Reid and Cameron (1958); the mean water potential $\pm \sigma_M$ is shown as a hatched strip, and a horizontal bar defines the range.

extends from land to offshore may have current flow generated in it by the onshore conditions, and this current flow will extend to the offshore portion of the body. Thus, even though the offshore portion of the body may be buried deep beneath the sea floor, it could still generate a considerable self-potential anomaly in the overlying sediments and water. Such shoreline and near-shore deposits will probably provide more good self-potential targets than the relatively few isolated offshore ore bodies which meet the necessary geologic and geochemical conditions. Examples of onshore deposits which generate offshore self-potential fields are discussed in Chapter 6.

Experiments

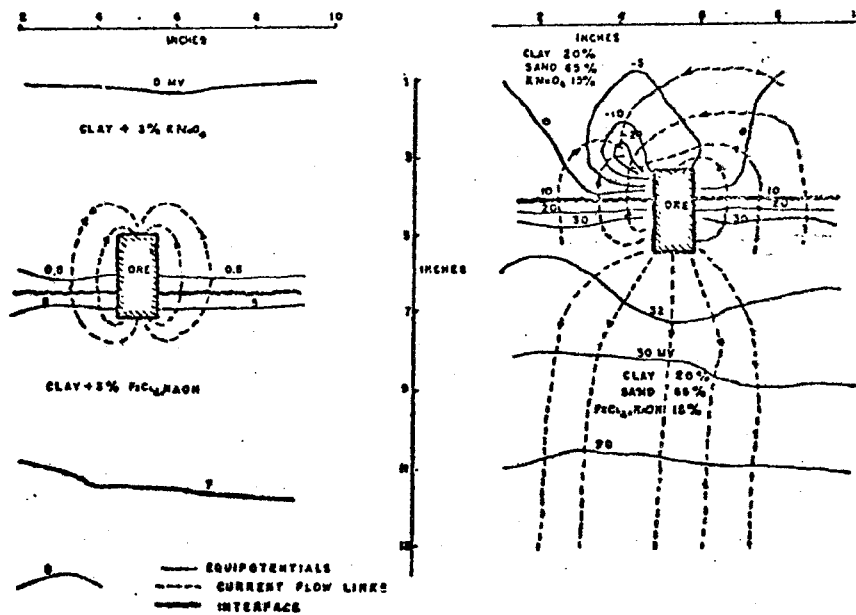
In addition to the model study done by Poldini (Figure 2-3) and the "laboratory investigations" mentioned by Kelly (1945), only one other model study of self-potential has been described in the literature -- that of Becker and Telford (1965). Their model was a rectangular piece of iron placed in a tray (Figure 2-25). The oxidizing zone consisted of sand, or sand plus clay, mixed with a KMnO_4 solution, and the reducing zone was sand and clay mixed with FeCl_2 and NaOH . This arrangement was found to produce a potential field of the proper polarity, lending support to the oxidation-reduction mechanism proposed by Sato and Mooney (1960).

Although the results of this experiment were encouraging, the conditions were artificial, in that chemicals were used to create the oxidizing and reducing zones. Therefore, I decided to try to generate a self-potential field using only natural media; specifically, sea water and marine sediments. The results of these experiments are described below.

Figure 2-25

Tray Model of Becker and Telford

From Becker and Telford (1965)

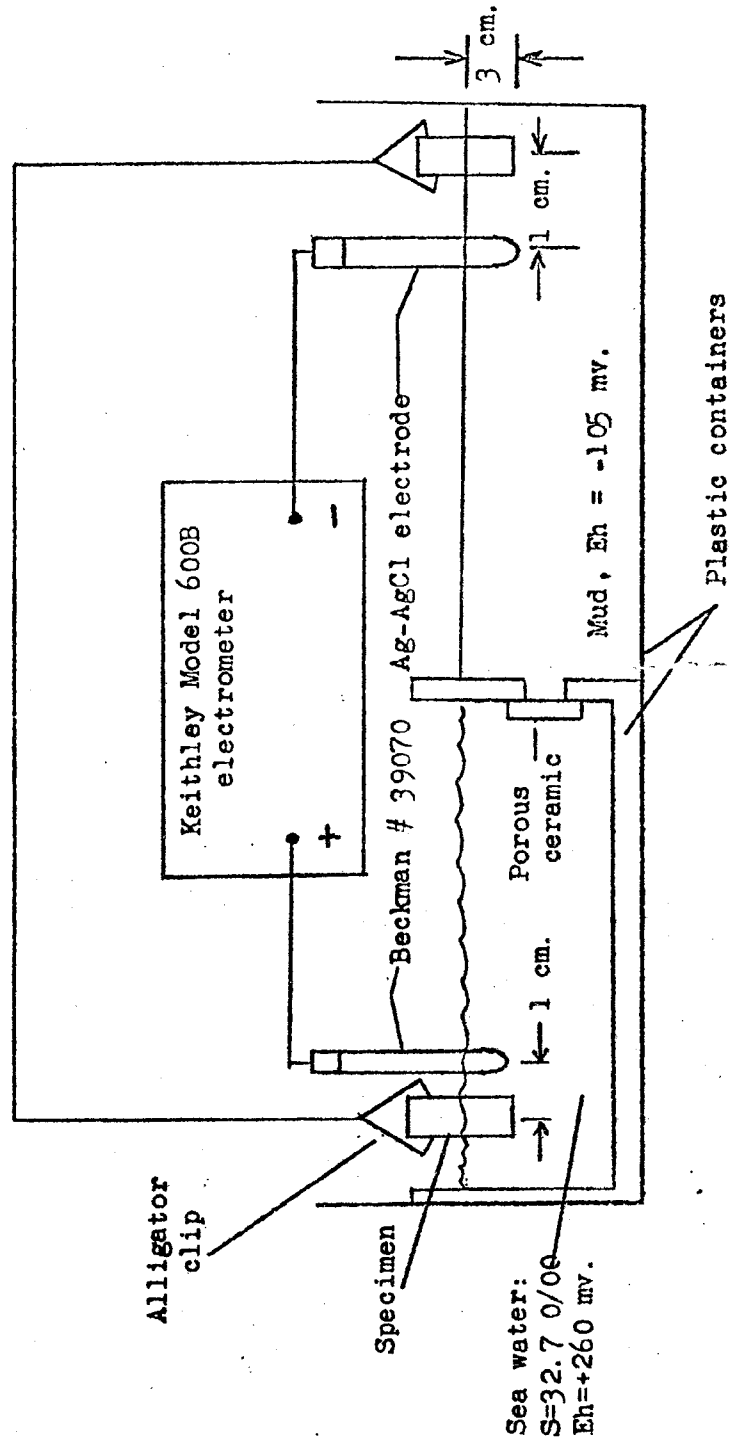


Laboratory work

The experimental arrangement used is shown in Figure 2-26. The procedure was to zero the voltmeter with the jumper wire disconnected, then to clamp the alligator clips to the specimens. Any current flowing in the system would then be detectable as a change in potential between the electrodes; a negative reading indicating that conventional current was flowing through the jumper wire from the specimen in the water to the specimen in the mud, with a return current from the mud to the water, as predicted by the oxidation-reduction mechanism. Twenty-four hours were allowed for equilibrium to be reached before final readings were recorded.

Two pairs of specimens were used, each measuring roughly 3 by 3 by 1 cm. The first pair were samples of ore containing 5% pyrite, chalcopyrite, and chalcocite from Blue Hill, Maine. The second pair were fragments from a pipe composed of "Duriron" (the Duriron Co., Dayton, Ohio). This material is an alloy of iron (84%), silicon (14.5%), carbon (0.85%) and manganese (0.65%) which is extremely corrosion-resistant (Duriron Company Bulletin A/26; Uhlig, 1948, p. 201) and could be expected to function as an inert electron conductor in any natural environment. The electrical resistivity of Duriron is 72×10^{-6} ohm-cm at 20° C, comparable to most metals.

The Duriron samples gave an equilibrium potential of -15 mv in the test cell; the ore samples, with the same surface area, a potential of -1 mv. Increasing the surface areas of the samples increased the potential; the potential increase appearing to be linearly related to increased surface area. These results indicate that both actual ore samples and "ideal" materials like Duriron



Laboratory Model

Figure 2-26

SECRET

are capable of generating current in the direction predicted by theory when subjected to an Eh gradient, with the current generated by the Duriron about an order of magnitude greater than that for the ore sample.

Field Experiment

The field experiment was conducted in a polluted, but convenient lagoon (Corwin, 1970) at Aquatic Park, Berkeley, California. Two lengths of Duriron pipe were used. The first, measuring 48 inches (122 cm) long, with an outside diameter of 3 1/8 inches (7.9 cm) and an inside diameter of 2 5/8 inches (6.7 cm) was driven 30 cm into the bottom mud, in water 50 cm deep. (Figure 2-27). It would have been preferable to use a sample of actual ore mineral as the specimen, but it would have been difficult to locate a sample of suitable size and shape. Also, from the results of the laboratory work described above, the external generated field probably would be an order of magnitude less for an ore sample than for the Duriron, making measurement difficult.

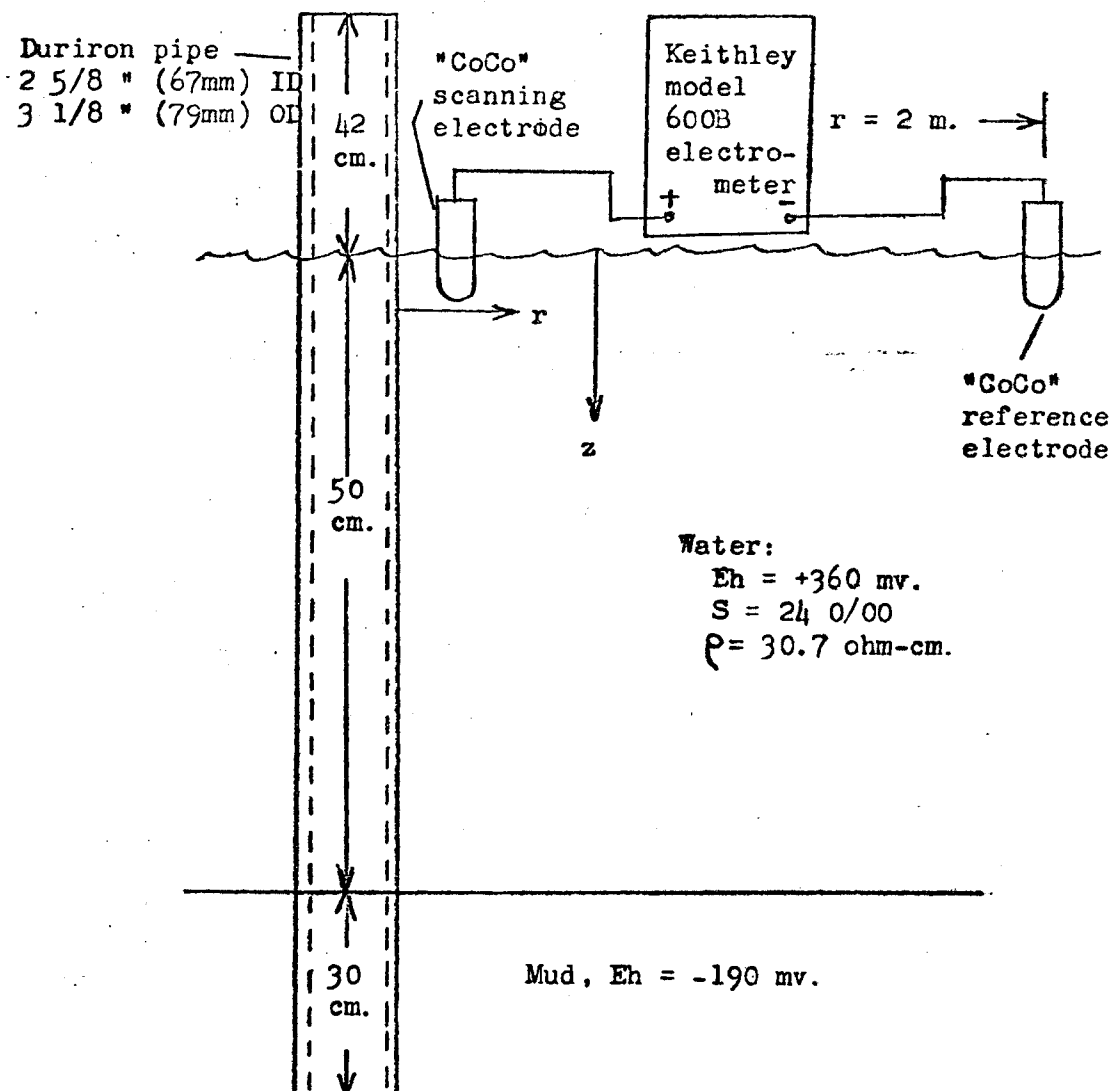
The potential field was measured both inside and outside the pipe, and the Eh of the water and of the mud was measured with a platinum electrode. "CoCo" Ag-AgCl electrodes (Chapter 4) were used for both potential and Eh measurements. The reference electrode was located 2 meters from the pipe, at the water surface. The potential field generated by the pipe was undetectable at this distance, so the reference electrode was effectively at zero potential.

The field measured at the water surface ($z=0$) is shown function of distance r from the outer surface of the pipe

Figure 2-27

Field Experiment

28 Oct. 1972
 Aquatic Park, Berkeley, Calif.



in Figure 2-28 (the field was radially symmetrical around the pipe). Figure 2-29 shows the vertical potential profile at a distance, $r = 1.3$ cm (the radius of the "CoCo" electrode; see Chapter 4) from the surface of the pipe, and Figure 2-30 shows the vertical potential distribution inside the pipe. From these potential plots, it is apparent that conventional (positive) current flowed downward through the walls of the pipe, returning upward through the mud and water (Figure 2-31), as predicted by the oxidation-reduction mechanism.

The break in the slope of the vertical profiles (Figures 2-29 and 2-30) indicates that the current flow in the upper 15 cm of the pipe is greater than in the section from $z = 15$ cm to $z = 50$ cm. A rough calculation (Appendix 2-1) shows that the current flowing through the water inside the pipe is about 41 ma in the upper 15 cm and 2 ma in the lower 35 cm. This difference may have been due to reducing mud stirred up when the pipe was inserted in the bottom, and suspended in the water trapped inside the pipe. The Eh of the water was poorly poised, as evidenced by the long stabilization time of the Eh readings, so relatively little reducing mud suspended in the water could reduce the Eh of the water considerably.

A second Duriron pipe, 68 cm long, with an outside diameter of $3 \frac{11}{16}$ inches (9.4 cm) and an inside diameter of 3 inches (7.6 cm) was driven 59 cm into the bottom mud, so that the top of the pipe was 9 cm above the bottom and 41 cm below the water surface. The potential at a point on the water surface directly above the center of the pipe was -3.2 mv.

If the top of the pipe is considered to be a point sink of

Figure 2-28

V vs. r

(z = 0)

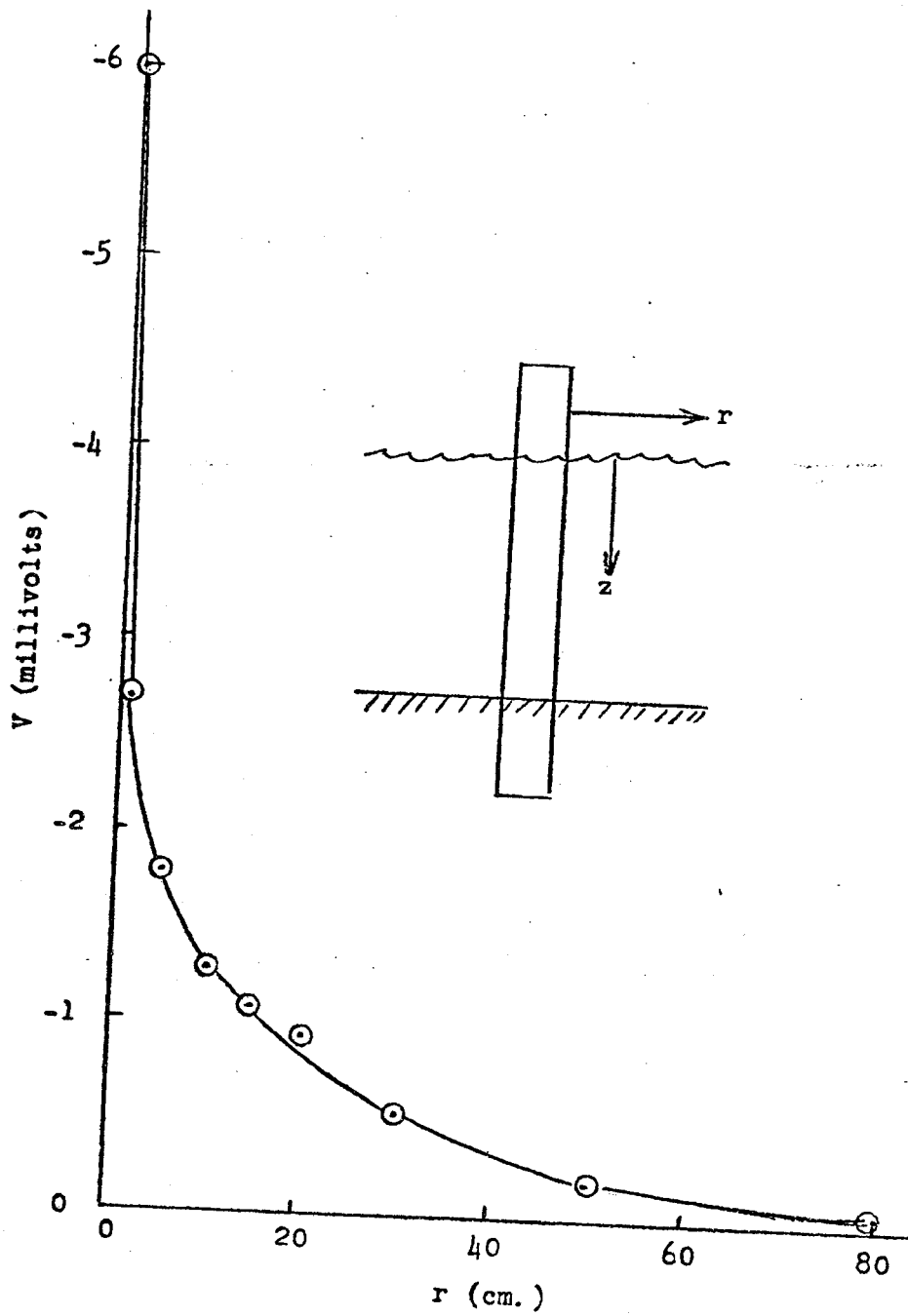


Figure 2-29

V vs. z

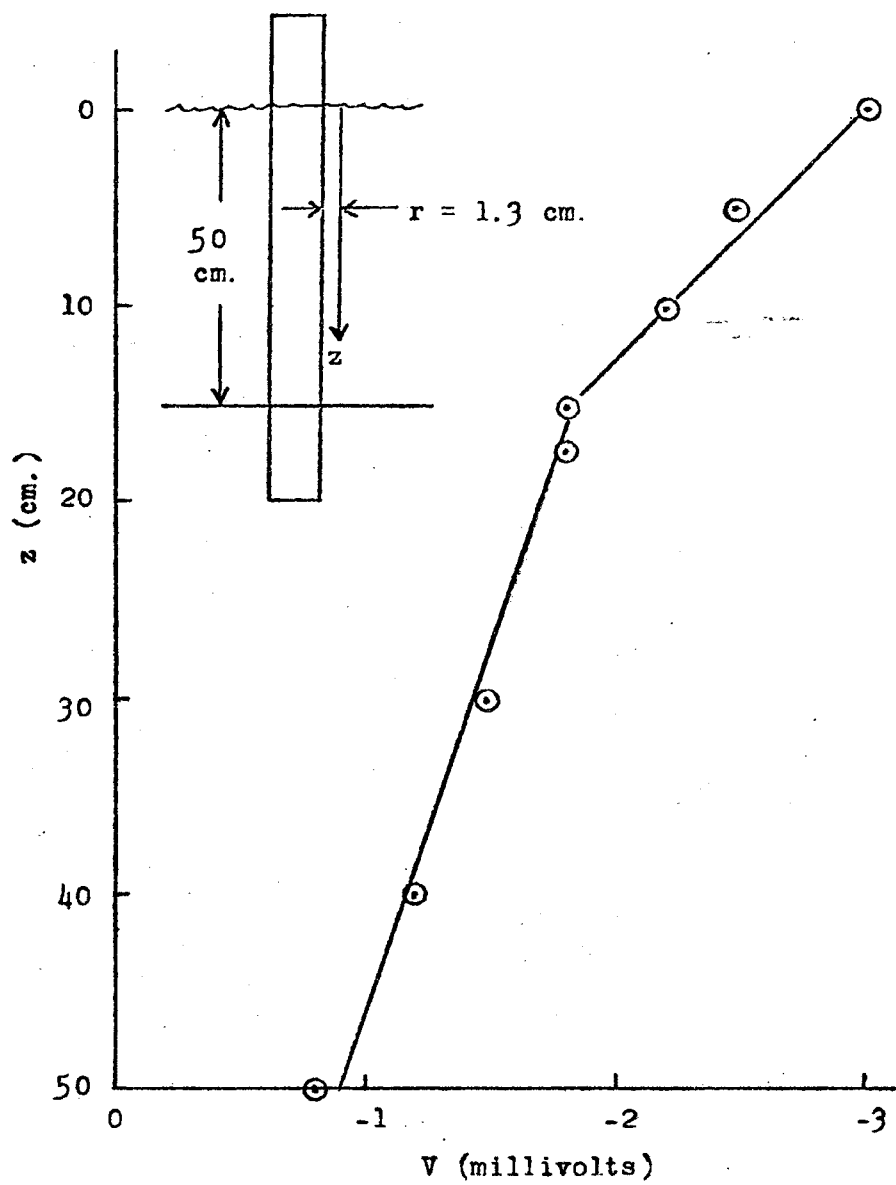
 $(r = 1.3 \text{ cm.})$ 

Figure 2-30

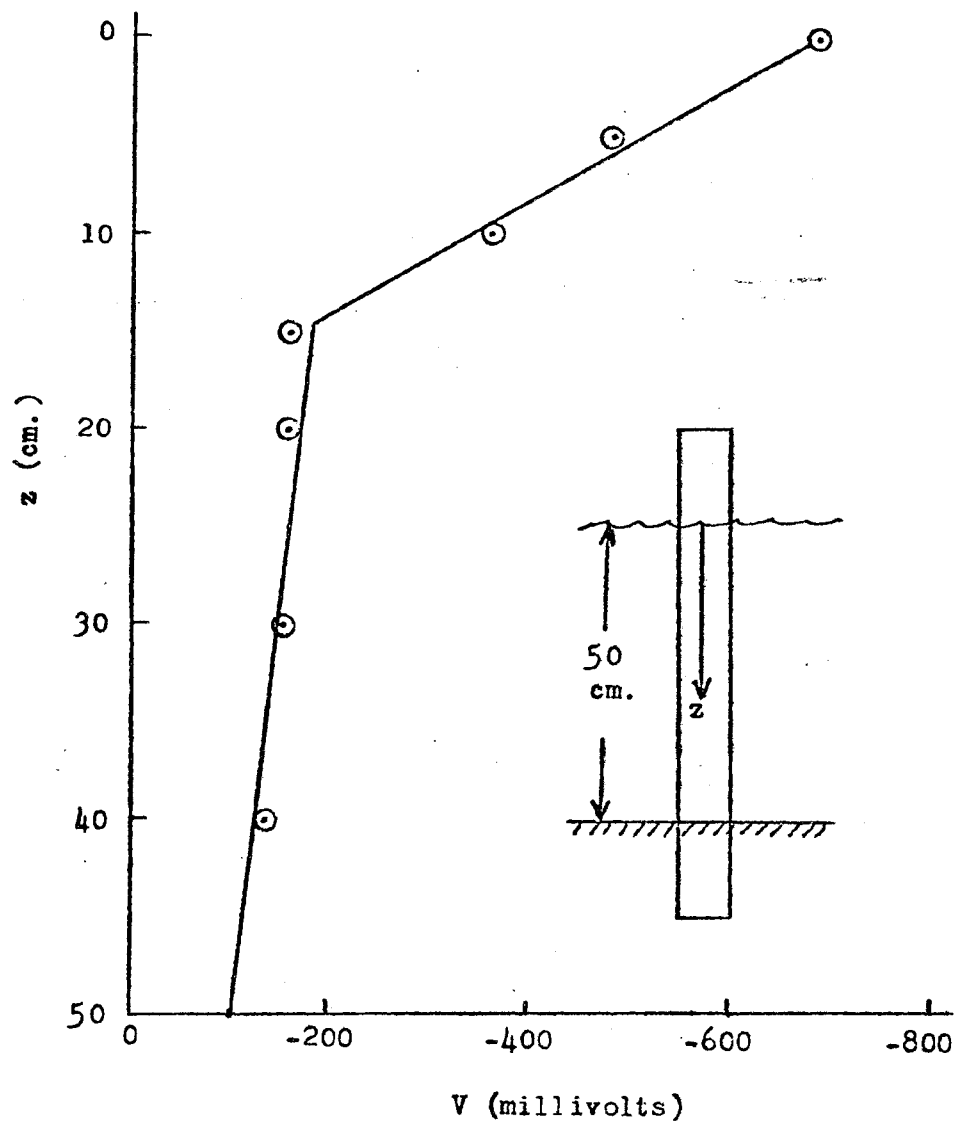
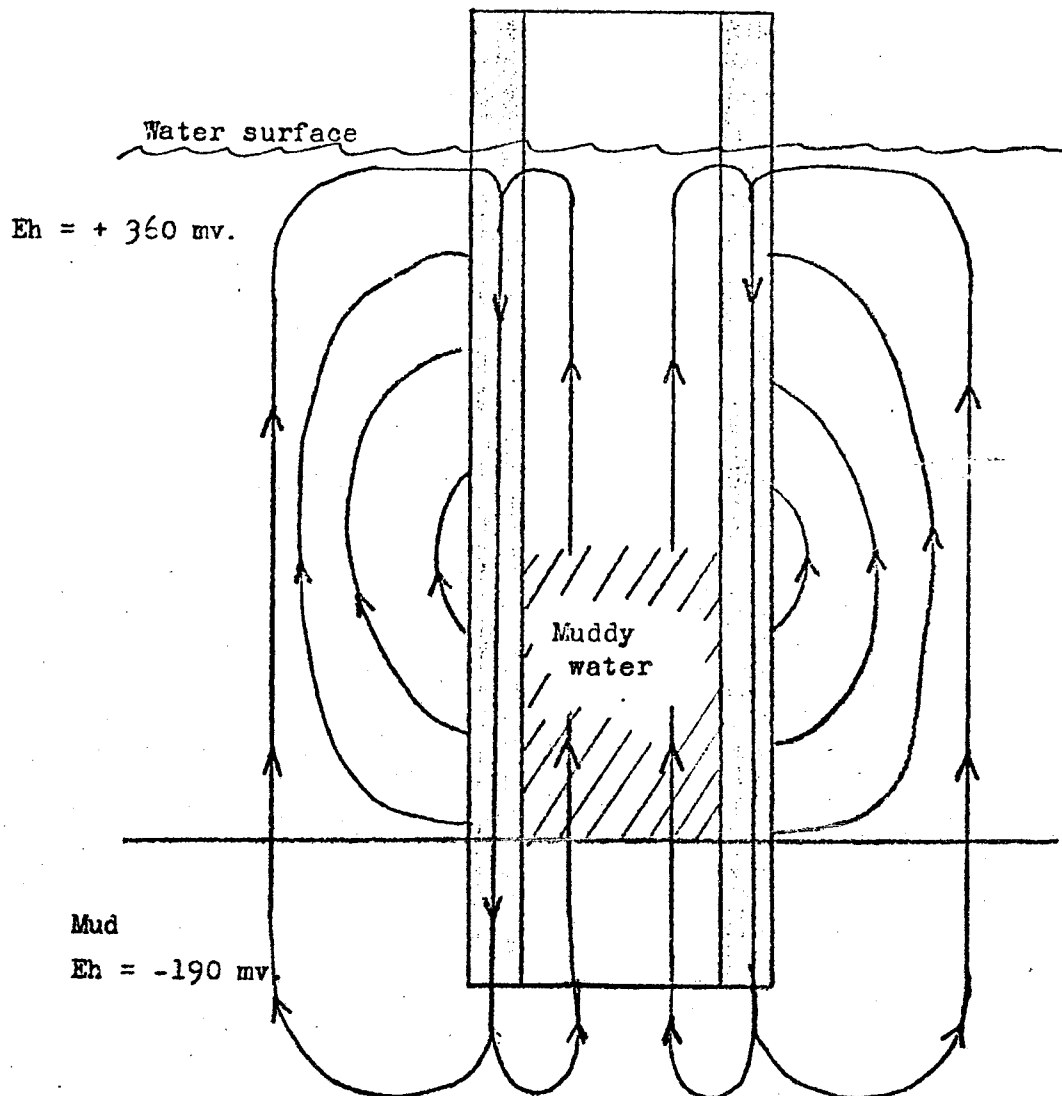
V vs. z
(inside pipe)

Figure 2-31
Current Flow Lines

(Not to Scale)



current, the potential V at the measured point is

$$(2-27) \quad V = \frac{I \rho}{2\pi r}$$

where: I = current

ρ = water resistivity (30.7 ohm-cm)

r = depth to top of pipe.

For $V = -3.2$ mv, I is -26.9 ma. As the surface area of the pipe is 0.36 m^2 , the current density is 74.7 ma/m^2 , close to the 100 ma/m^2 value calculated for the first pipe (Appendix 2-1). The pipe was left buried for 17 days, after which time the voltage was re-measured and found to be close to the original value.

The results of these experiments were encouraging:

- (1) An inert, conducting body extending from the reducing zone in the bottom into oxidizing sea water was seen to generate a detectable self-potential field.
- (2) No decrease in the magnitude of the field was observed in 17 days.
- (3) The magnitude of the current generated in the pipes was reasonable (see calculation for first pipe in Appendix 2-1). The current density of about 75 to 100 ma/m^2 generated by the pipes implies that currents of the order of 10 to 100 amps are generated by sulfide ore bodies, in agreement with field observations (Chapter 3).

It would be desirable to repeat this type of experiment, using actual ore samples in place of the Duriron pipe, and instrumenting the ore so that actual current flow could be measured. Although beyond the scope of this work, such experiments could provide

estimates of the current generated in an ore body as a function of surface area. Such estimates could prove useful in gaining some idea of the size of an ore body producing a given self-potential anomaly.

CHAPTER 3
POTENTIAL FIELDS

"Do you realize that it is in
our power to deepen the source
simply by moving toward it?
And then drawing from it?"

Elie Wiesel
"A Beggar in Jerusalem"

Introduction

It is necessary to have some idea of the magnitude and distribution of the electric potential field surrounding an ore body in order to design an efficient search pattern, and to relate self-potential survey results to the location, size, and shape of the ore body.

The mechanism discussed in Chapter 2 maintains a potential distribution on the surface of the ore body. This potential distribution causes electrical current to flow in the body and in the surrounding medium (the sea floor and the overlying water), and the current produces an ohmic potential gradient as it flows through the surrounding medium. This potential gradient, detectable as a voltage difference, generates the observed self-potential anomaly.

Sea-floor and sea water resistivity

In order to carry out potential field calculations, the electrical resistivities of the materials in which the field is generated must be known. Resistivities for soils and rocks have been tabulated extensively by authors such as Jakosky (1950, p. 440-442), Heiland (1940, p. 656-665), and Keller and Frischknecht (1966, p. 39-49). The resistivity of sea water as a function of salinity and temperature has been measured by Cox (1966), and a useful resistivity graph is shown in Figure 3-1.

Electrical resistivity measurements on unconsolidated sea-floor sediments have been made by Boyce (1967), Kermabon and others (1969), Erchul and Nacci (1971), Bouma and others (1971), Marke (1965), Corwin and Conti (in preparation), and Barnes and others (1972). The formation factors of these sediments range from just over

1.0 to about 5 (the formation factor (Archie, 1942) is the resistivity of the sediment divided by the resistivity of the interstitial water).

Models

The potential field generated in the most general case, an ore body of arbitrary size and shape, with an arbitrary potential distribution on its surface and placed in an arbitrary geological setting, cannot be calculated analytically. Such a field could be computed approximately using numerical methods and a high-speed computer, but because it is doubtful that all of the parameters listed above would be known with a reasonable degree of accuracy until after the ore body had been thoroughly drilled, such a computation would rarely be useful.

Conformal mapping and downward continuation

For an ore body of simple geometric shape and of infinite extent in one direction, buried in a homogeneous whole space or half space, the method of conformal mapping (Becker and Telford, 1965) may be used to find the distribution of the equipotential lines around the body. Downward continuation may be performed on the observed field data in an effort to find the depth of burial of the ore body, but interpretation is not easy (Roy, 1963). Application of conformal mapping or downward continuation to the offshore situation, in which the homogeneous half space in which the ore body is placed (the sea floor) is covered by a finite, conducting layer of water, may be possible. However, the use of simple sources, as discussed below, seems to be an easier way to approach the problem.

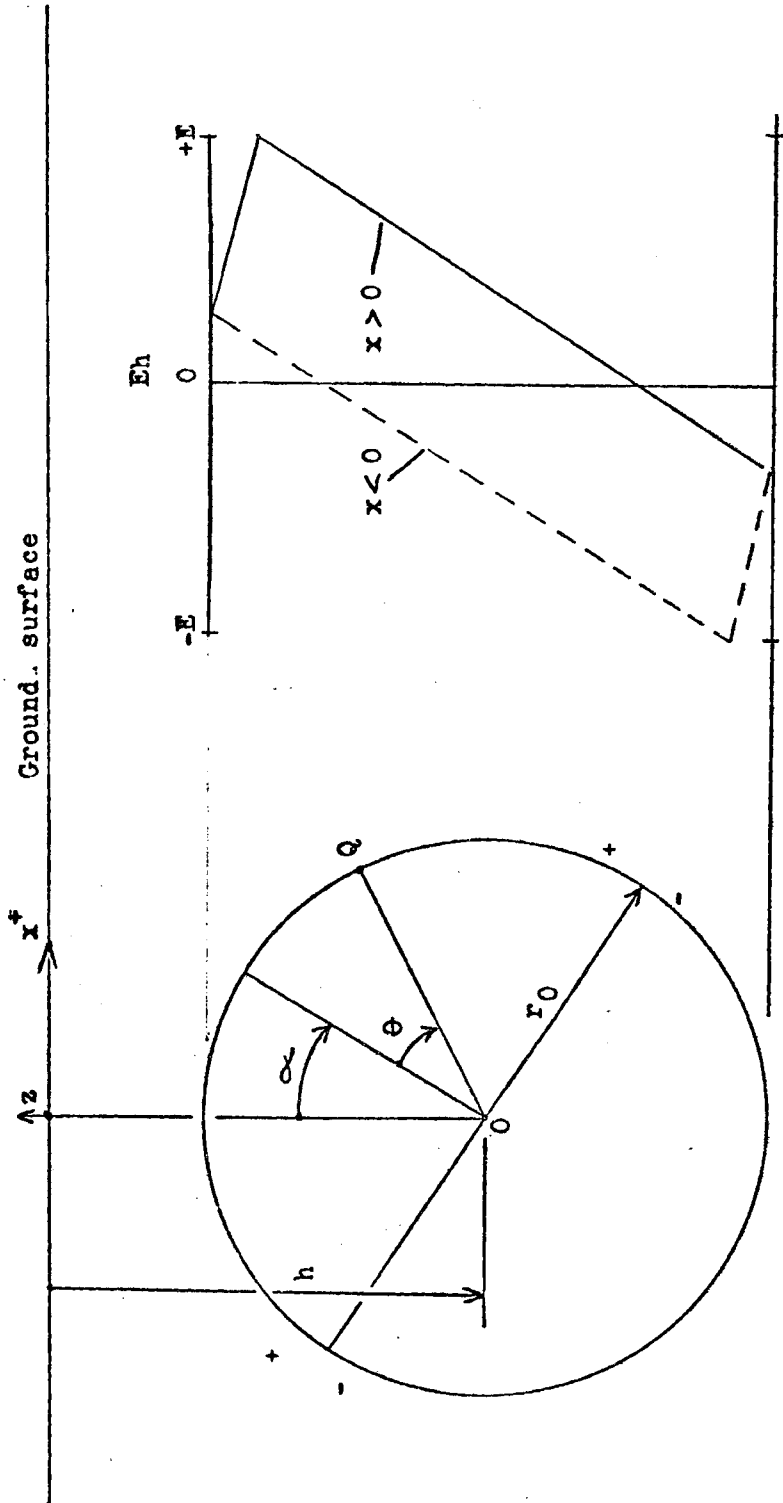
An ore body generating a self-potential field may be simulated by placing a point, point dipole, line, or line dipole current source, or an electrically charged body of simple geometry (such as a sphere or ellipsoid), in the surrounding medium. By manipulation of these simple sources, the potential distribution on a closed surface, which encloses the source or sources and resembles the surface configuration of the ore body, may be made to approximate the desired potential distribution on the surface of the actual body.

Spherical ore body

Petrowsky (1928) calculated the potential distribution on the earth's surface caused by an inclined, sinusoidally polarized sphere buried in a homogeneous earth (Figure 3-2), and presented numerous curves useful for estimating the size, inclination, and depth of the sphere. His work has been discussed and expanded by de Witte (1948), Meiser (1962), Poldini (1938, 1939), Yüngüü (1945, 1950) and Heiland (1940, p. 672). None of these authors have considered a case analagous to the offshore one, in which a water layer must be added above the homogeneous half space. This complicates the problem, and, as a polarized sphere may be closely approximated by a point source and sink of current (discussed later in this chapter), for which computation of the potential field is simpler, no further analysis of Petrowsky's model was done for this work.

Polarized sheet

An inclined polarized sheet (i.e., a line source and sink of current) buried in a homogeneous half space of resistivity ρ may be used to simulate a tabular ore body (Figure 3-3). The potential V at a point P on the surface of the half space is



EMF e at point Q on surface of sphere is $e = E \cos \theta$

Spherical Model

Figure 3-2

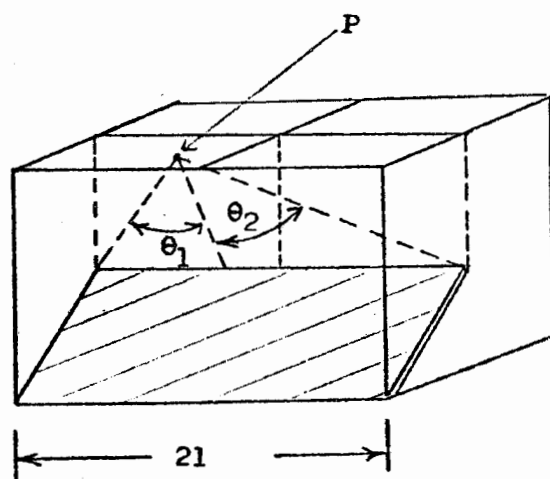
PHS

PHS

Figure 3-3

Model for Tabular Ore Body

After Edge and Laby (1931, p. 244)



θ_1' and θ_2' are the corresponding angles for the lower edge

$$V = \frac{-I\rho}{4\pi l} \left\{ \log \tan\left(\frac{\pi}{4} + \frac{\theta_2}{2}\right) - \log \tan\left(\frac{\pi}{4} + \frac{\theta_1}{2}\right) \right. \\ \left. - \log \tan\left(\frac{\pi}{4} + \frac{\theta_2'}{2}\right) + \log \tan\left(\frac{\pi}{4} + \frac{\theta_1'}{2}\right) \right\} \quad (3-1)$$

(Edge and Laby, 1931, p. 244). Interpretation curves for this model are presented by Meiser (1962), Paul (1965), and Roy and Chowdhury (1959). (The work of Roy and Chowdhury is especially complete, including interpretation curves for finite as well as infinite line dipoles). As is the case for the sphere, adding a layer of water above the half space would complicate considerably the expression for V , if indeed an analytical solution could be found. It appears more efficient for the offshore case to approximate the inclined sheet with a line of point current dipoles, if such an analysis seemed justified for a particular offshore self-potential anomaly.

Point and point dipole

Unless an ore body is strongly tabular in shape (i.e. much longer in one horizontal direction than the other), it often may be simulated adequately by a point source and sink of current (Stern, 1945). If a current dipole can be placed within the boundary of the ore body in a location such that the potential distribution on the boundary is the same as the E_h distribution of the surrounding medium at the boundary, the potential field everywhere outside the boundary will be equivalent to the self-potential field generated by the body. This method has the advantage that the field of a point source or sink of current is not difficult to calculate, and that the field may be extended through a multi-layered medium such as the sea floor and overlying water layer.

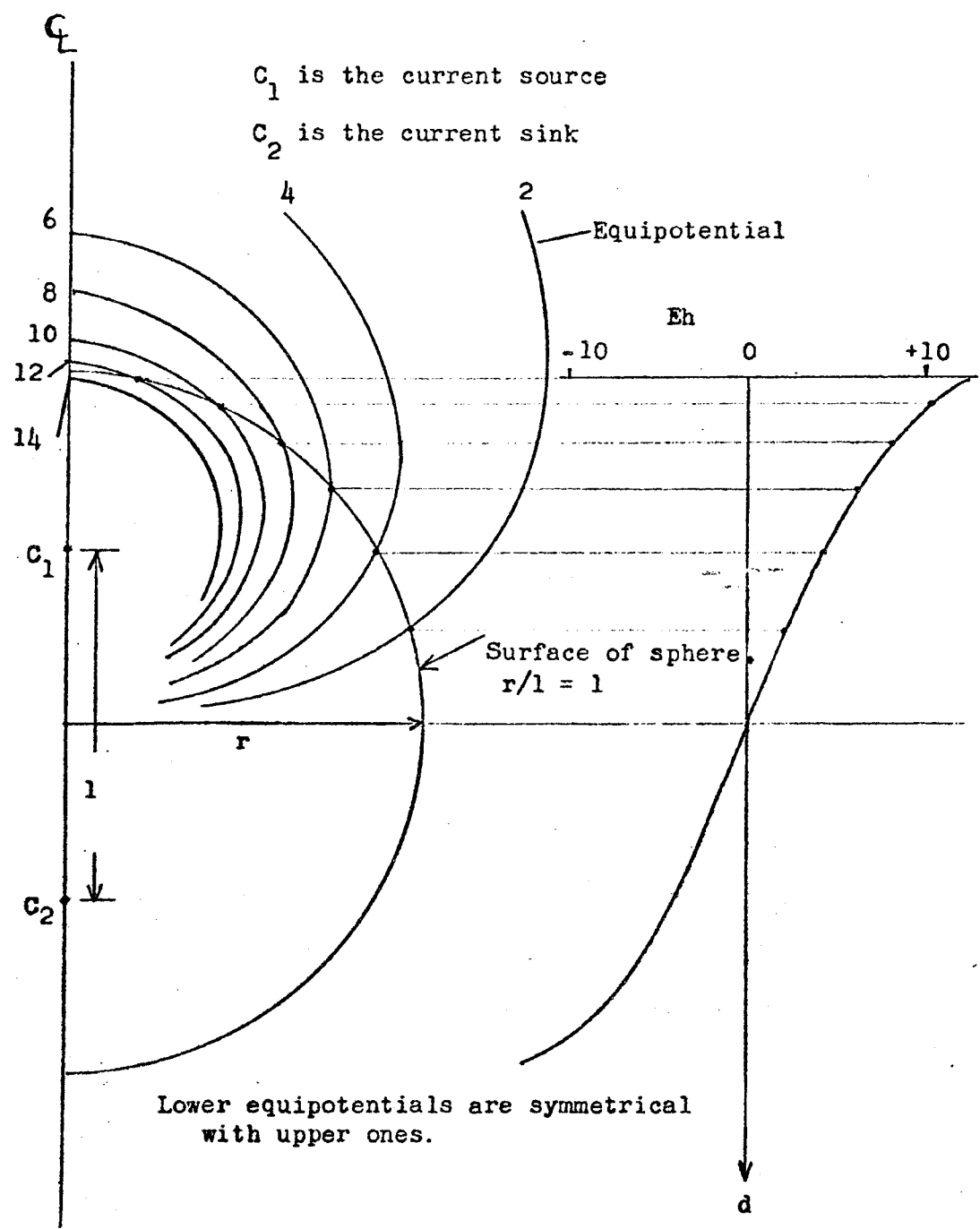
The case of a spherical ore body provides an example of the flexibility of the dipole method. Implicit in the sinusoidal distribution of potential along the surface of the sphere used by Petrowsky and the other authors mentioned above is the assumption that the E_h distribution in the surrounding medium is linear with depth (Figure 3-2). Any other assumption for the E_h -depth relationship would complicate considerably the analytical solution of the problem. However, by constructing a spherical surface around a current dipole, many different E_h -depth distributions may be simulated, depending on the ratio of the radius of the sphere (r) to the length of the dipole (l).

The procedure is done easily by drawing a circle on a map of the potential field surrounding a current dipole (Figure 3-4). For small values of r/l , the E_h in the surrounding medium changes more rapidly at the top and bottom of the sphere than at the center, while for large ratios of r/l the distribution is more nearly linear, approaching that of the Petrowsky model (Figure 3-5). From Figure 3-5, it is apparent that an r/l ratio greater than 2 very closely approximates the linear distribution of the Petrowsky model (the dipole may be inclined to represent an inclined axis of polarization). The dipole model, however, is easier than the sphere to handle analytically, especially in a layered medium.

Other ore body shapes, such as ellipsoids or prisms also may be simulated by this procedure. In fact, the potential produced by any current distribution of finite extent may be simulated, if a sufficient number of dipoles are used (Cowan, 1968, p. 148). It is doubtful, however, that field data would ever be of such

Figure 3-4

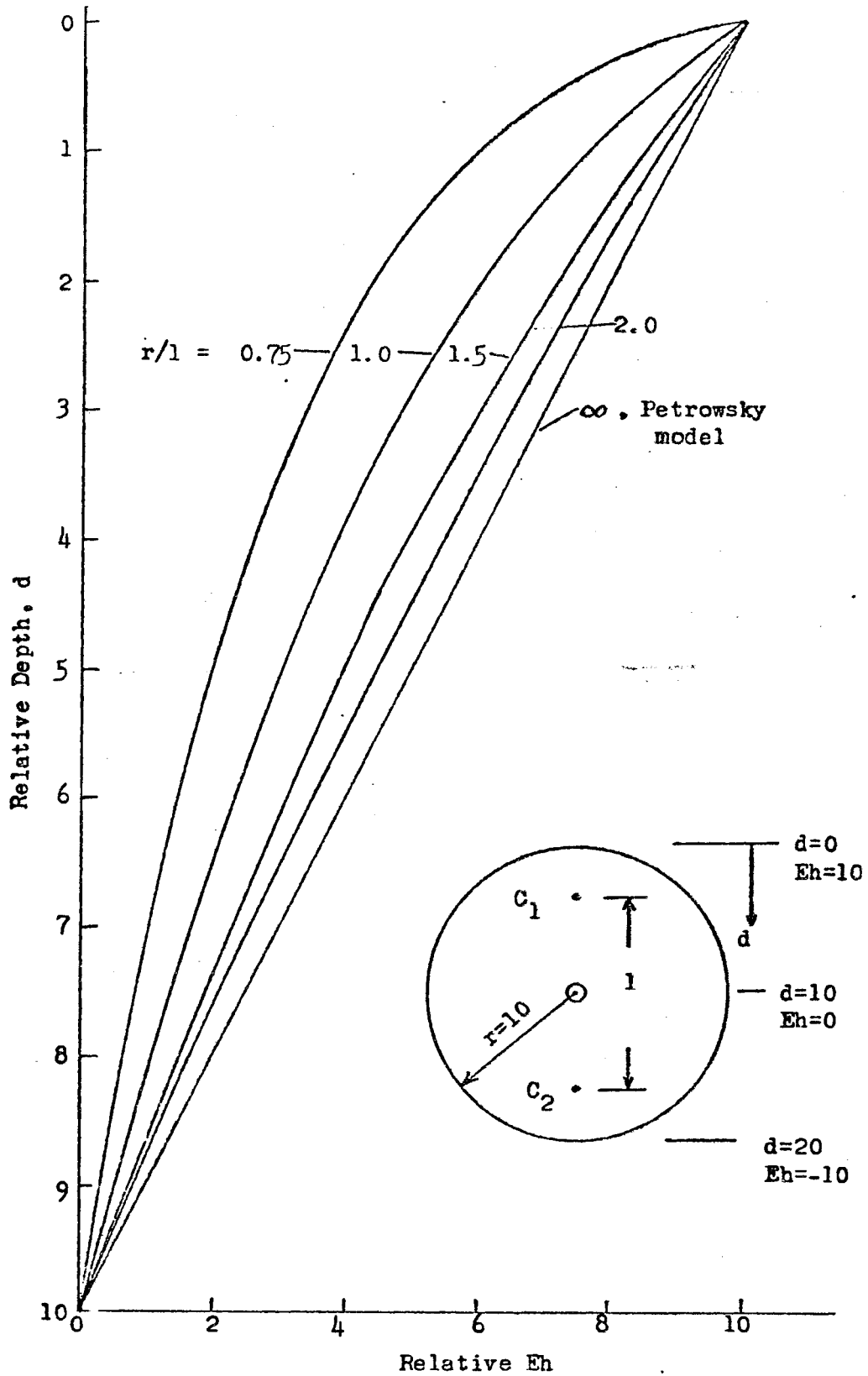
Dipole Field on Spherical Surface



After Van Nostrand and Cook (1966, p. 31)

Figure 3-5.

Relative Depth vs. Relative Eh



precision that realistic distinctions between shapes could be made, even if the E_h -depth distribution were known. If the distribution is not known, the interpretation problem cannot be solved uniquely as a given dipole, corresponding to a given measured field, represents an infinite combination of ore body shapes and E_h -depth distributions.

Although unambiguous interpretation of field data is impossible, the dipole simulation method is useful in answering the question: given an ore body size, shape, and depth, and an E_h distribution along the surface of the body, what is the potential field in the surrounding medium? Such studies, comprising the remainder of this chapter, are useful for determination of the detectability of an ore body, and for optimizing the electrode array and the search pattern.

Point source of current buried in the sea floor

The potential field produced by a point source of current buried in a homogeneous sea floor (Figure A3-1) is discussed in Appendix 3-1. A point sink of current produces the same field with the sign of the potential reversed, and the field of a point current dipole (one source and one sink) at a given point is the algebraic sum of the source and sink fields at the point. Because E_h is usually more positive in an upward direction, and therefore positive current usually flows downward through the ore body (Chapter 2), the current sink usually will be located at a shallower depth than the source.

It is not conceptually difficult to represent the sea floor as composed of a number of layers of arbitrary resistivity, with the source and sink located in any desired layer. The potential

field expression for such a representation is, however, considerably more complex algebraically than that for a homogeneous sea floor, requiring a correspondingly more complicated computer program for solution. Because of the large number of variables studied in this chapter (dipole separation, depth, and inclination; water depth, and sea-floor resistivity) the effect of sea-floor layering is not examined in this thesis. Equations applicable to a two-layered sea floor may be obtained from Alfano (1962).

Model studies

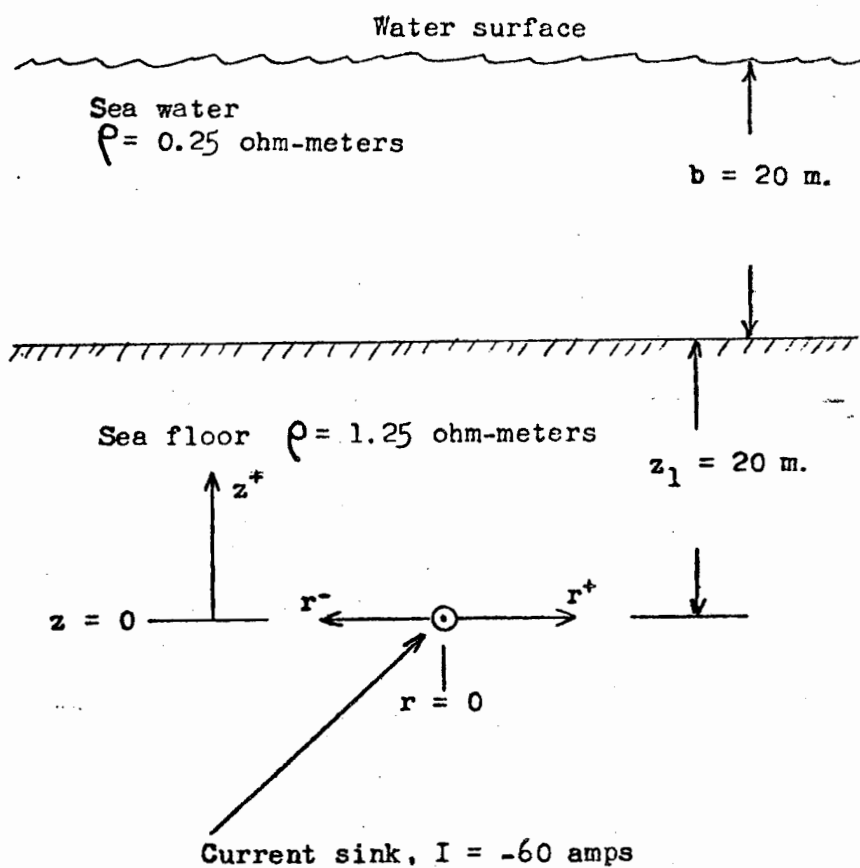
A computer program has been written to calculate the value of V , the potential in the water layer. The program, VSP, calculates the field due to a point sink of current of magnitude I of 60 amps buried in a homogeneous sea floor. The program is written in FORTRAN for the CDC 6400 computer, and a sample run is presented in Appendix 3-2. The value of V is given in millivolts.

The program is reasonably fast and economical. If ρ_s / ρ_w (see Appendix 3-1 for a list of symbols used) is kept under 10, a value of 100 for n in equation (A3-5) assures convergence. Using $n=100$, the value of V at 324 points was computed by VSP in 90 seconds, at a cost of \$7.77, or about \$.02 per point.

Standard case

The remainder of this chapter is devoted to an examination of the potential field produced in the water layer by a point current sink or a dipole current source buried in a homogeneous sea floor. The standard case used for reference (Figure 3-6) is a point current sink buried 20 meters deep in a sea floor having resistivity of 1.25 ohm-meters. The current flow into the sink is 60 amps, and

Figure 3-6
Standard Case

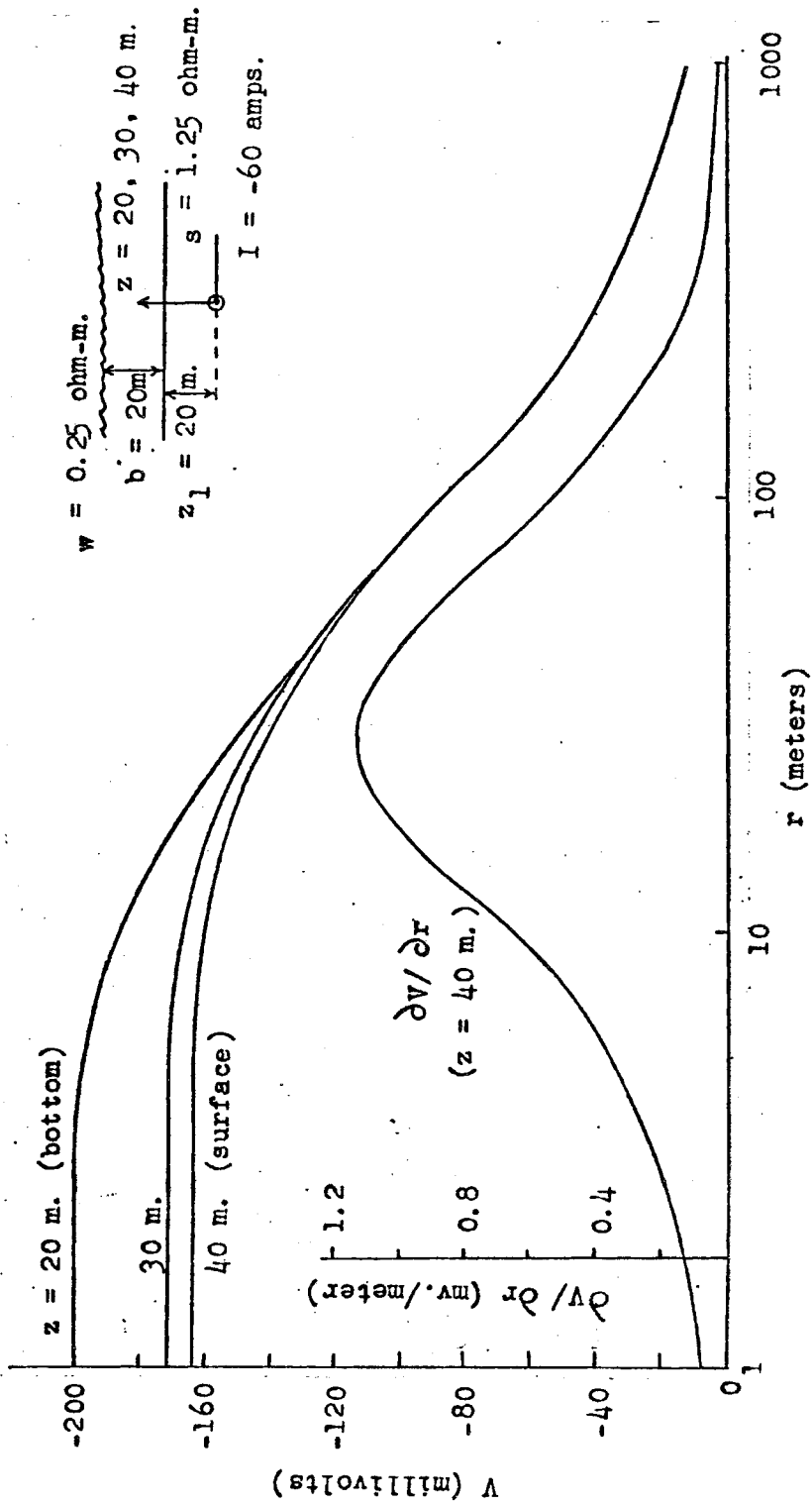


the overlying water has a depth of 20 meters and a resistivity of 0.25 ohm-meters (this resistivity corresponds to a temperature of 15°C and salinity of about 32 ‰).

This arrangement produces a field on the sea floor comparable in magnitude and shape to a "typical" self-potential anomaly found on land. Self potential anomalies, of course, vary considerably in size and shape, but a magnitude of -200 millivolts (mv) and a half-width (the distance from the peak of the anomaly to the point where it has dropped to half of its maximum value) of 75 meters is reasonably representative. The anomalies often show an area of positive potential (Figure 1-2), indicating that the lower end of the ore body is at a finite depth. Just as frequently, however, no positive potential is seen, and because the potential of the positive area usually is small, a point current sink alone, without a source, probably gives as good a representation of a "typical" anomaly as a dipole. The dipole, in this study, will be treated as a variation of the "standard" case. The field of the standard case on the sea floor, at a depth of 10 meters, and at the water surface is shown in Figure 3-7, along with the gradient at the water surface.

Gradient and detectability

The most important question to be answered in this chapter is: what is the maximum distance from the center of the anomaly at which the presence of the anomaly may be detected (i.e., separated from the background noise)? The background noise level in most offshore situations has been found to be on the order of a few tenths of a millivolt (Figures 5-8 and 5-15) with electrode separations of less than 50 meters, and Figure 6-24 indicates



Field for Standard Case

Figure 3-7

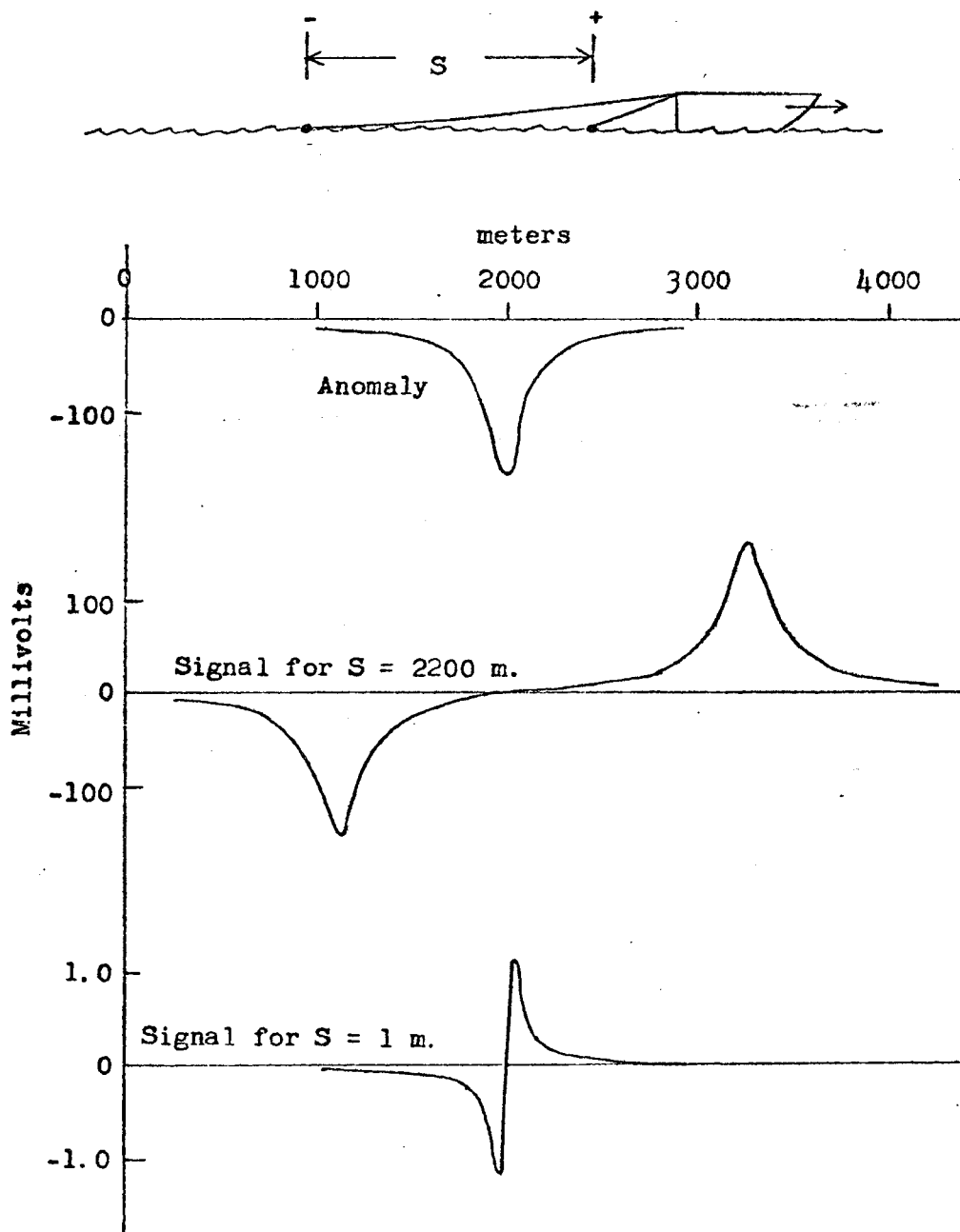
514
 100
 1000

that a signal of one millivolt is readily distinguished by visual inspection. More sophisticated data analysis techniques could, of course, be used to increase the signal-to noise ratio, but for the purposes of this study a signal of one millivolt will be used as the criterion of detectability.

The magnitude of the signal is increased by increasing the electrode separation S (Figure 3-8). If S is very large compared to the lateral extent of the anomaly, the magnitude of the signal will be equal to the magnitude of the anomaly, while for small values of S , the signal will be approximately equal to the gradient of the anomaly ($\partial V / \partial r$) multiplied by S . Noise increases somewhat as S is increased (Chapter 5), but the signal usually increases more rapidly than the noise, so increasing S often will improve the signal-to-noise ratio. A large separation, however, implies a large amount of wire in the water, with increased probability of electrical leaks. Also, maneuverability of the boat is decreased when long wires are being streamed astern, and exploration of indentations in the shoreline is difficult. Field experience has proven that, for shallow water, near-shore work, separations greater than about 50 meters become quite unwieldy. Separation may be increased from this value for open-water work, while about 20 meters is manageable along most shorelines.

As mentioned above, if the electrode spacing S is small relative to the length of the anomaly, the recorded anomaly signal will approximate the product of electrode separation S and the gradient of the total field anomaly. In many instances, when an anomaly is seen on the chart recorder record the boat's course will be

Figure 3-8
Effect of Electrode Separation



reversed and the anomalous area traversed in the opposite direction. If the observed signal was real, it will be repeated as a reversed mirror image of the original anomaly. Figures 3-9a through 3-9d show some simplified total field anomalies together with the associated gradient anomaly and chart recorder output. These simple shapes are useful in forming a first estimate of the total field anomaly shape from the chart recorder output.

Survey depth

Obviously, the magnitude of the field decreases toward the surface of the water. Is it, therefore, worthwhile to tow one or both electrodes at some depth below the water surface? In Figure 3-7, there is a difference of 36 mv between the surface and the bottom over the center of the anomaly. The difference decreases rapidly, and virtually disappears 60 m from the center of the anomaly. A surface-towed horizontal array with $S = 20$ m would show a signal of 14 mv over the center of the anomaly and about 15 mv 60 m from the center. The same array towed along the bottom would show 35 mv at the center of the anomaly and about 18 mv 60 m from the center. Towing one or both electrodes near the bottom in typical rugged offshore topography is difficult to accomplish in practice, unless a bottom-following device such as that described by Conti (1972) is used. Unless the water is very deep, the small increase in signal strength would not be worth the extra effort involved in towing one or both electrodes below the water surface.

Effect of sediment resistivity

Most unconsolidated deep-sea sediments have formation factors of about 1.5 to 3 in the upper 10 m (Kermabon and others, 1969;

Figure 3-9a
Symmetrical Monopole Anomaly

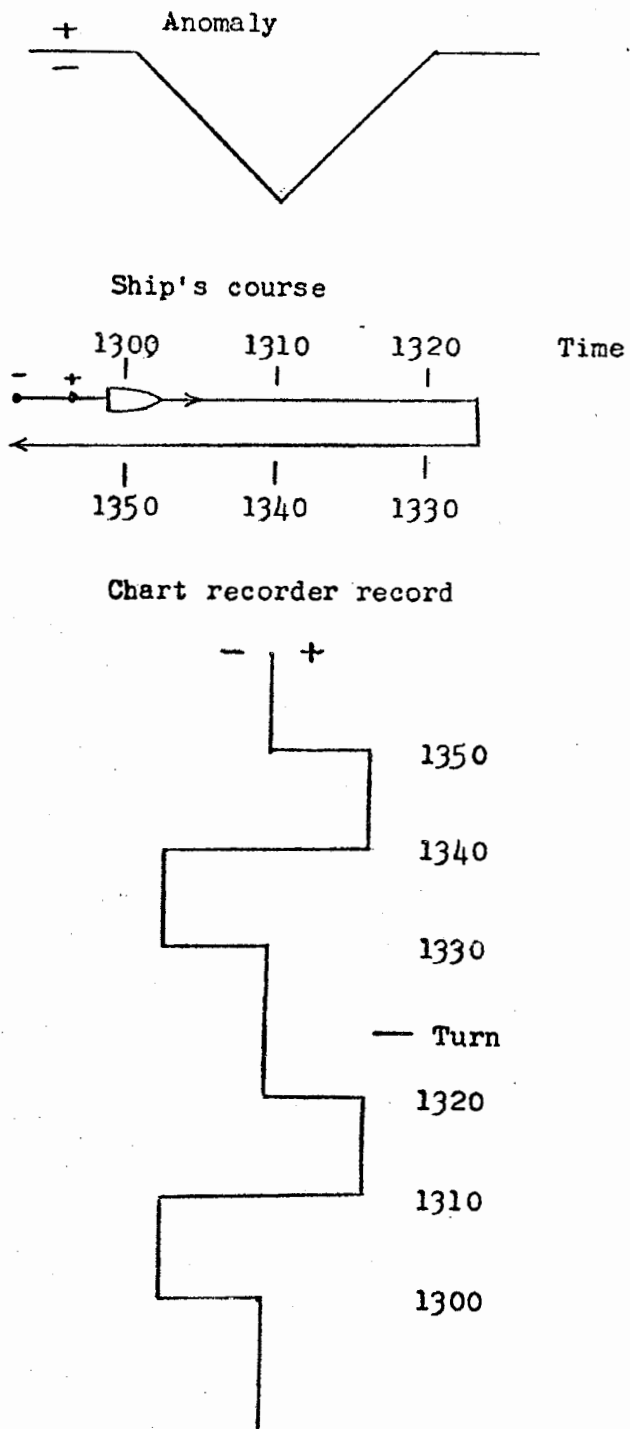


Figure 3-9b

Asymmetrical Monopole Anomaly

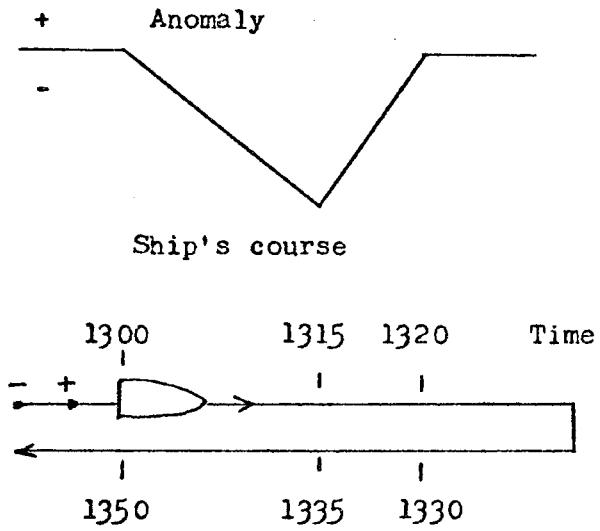


Chart recorder record

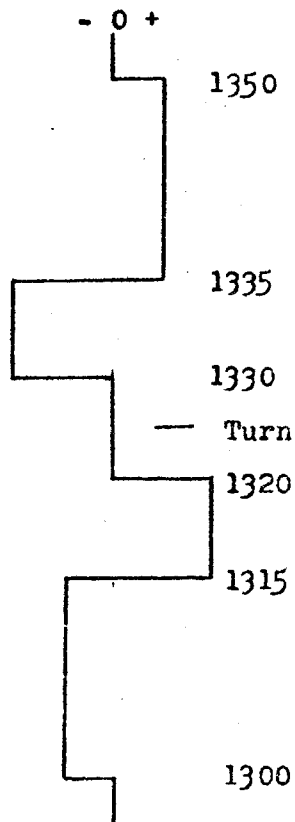


Figure 3-9c
Symmetrical Dipole Anomaly

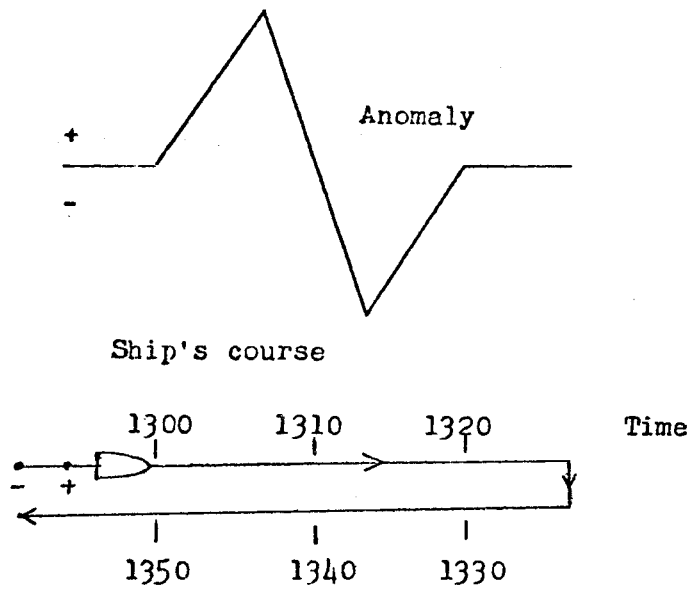


Chart recorder record

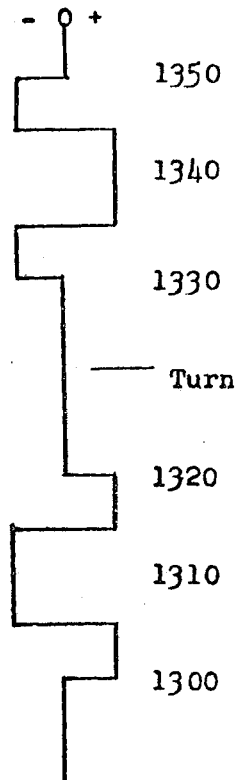


Figure 3-9d

Asymmetrical Dipole Anomaly

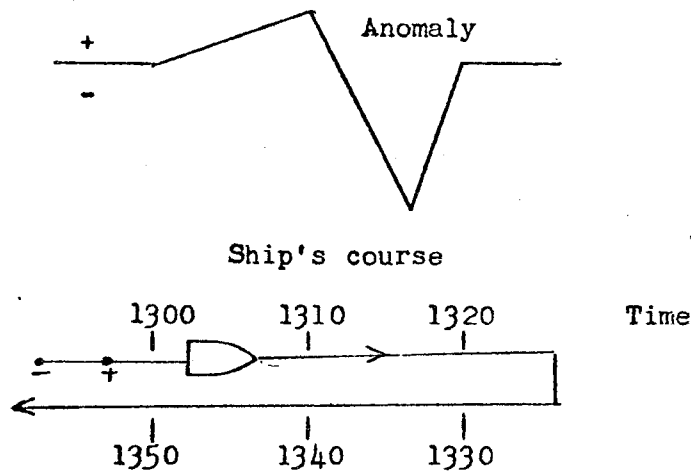
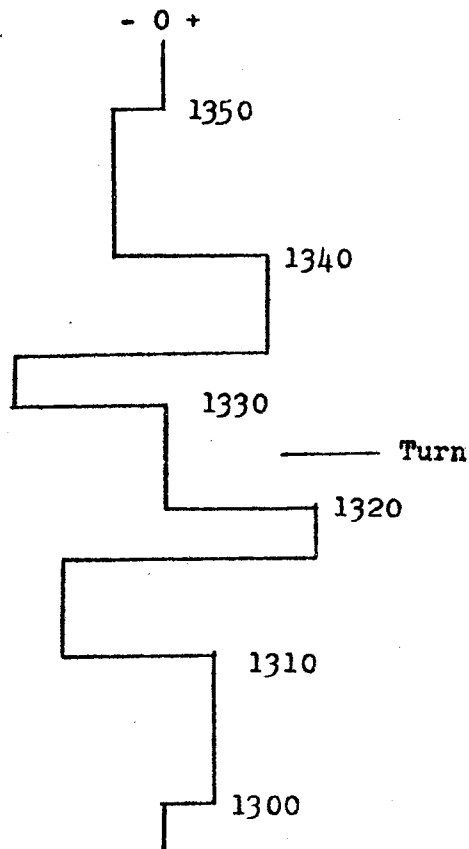


Chart recorder record



Boyce, 1967; Erchul and Nacci, 1971) corresponding to sediment resistivities of about 0.5 to 1.0 ohm-meters. Shallow water sediments show similar resistivity values (Corwin and Conti, in preparation) but are likely to overlie more consolidated material with considerably greater resistivity. The resistivity structure of the sea floor in a particular location may be measured from core samples or by using a well-logging type probe (Erchul and Nacci, 1971) or a horizontal array (Barnes and others, 1972).

The amplitude of the signal at the water surface increases with increasing sea-floor sediment resistivity (Figures 3-10 and 3-11). Doubling the bottom resistivity causes the maximum voltage for the standard case to increase by a factor of 1.38; halving the resistivity decreases the maximum voltage to 0.68 times the standard value. In the extreme situation where the formation factor of the bottom is close to 1, the maximum voltage is 0.58 times the standard value, and for a very resistive bottom the maximum voltage is about 2.75 times the standard value.

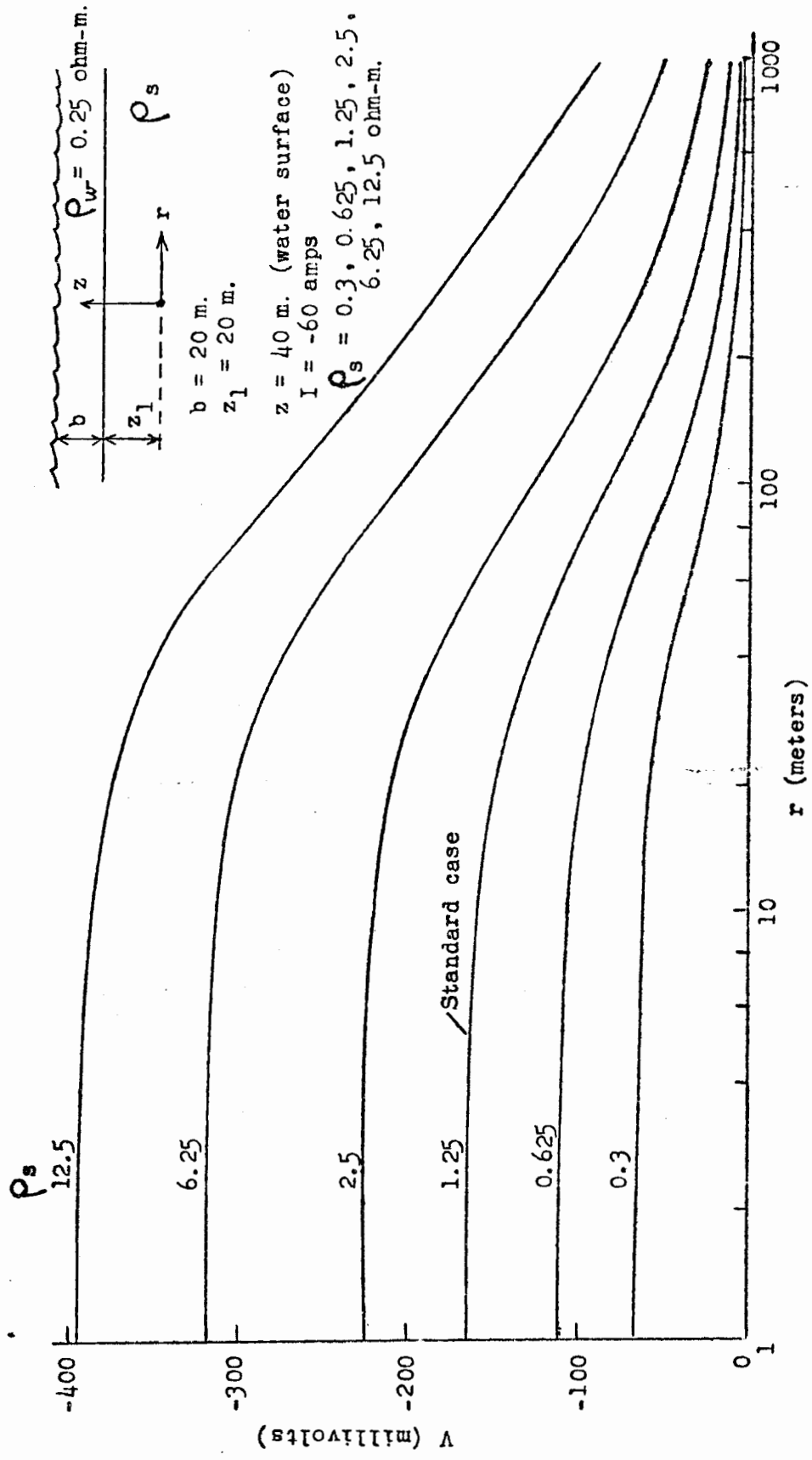
More important, as the bottom resistivity increases the width and gradient of the field also increase. At 100 m from the center of the anomaly, the signal ΔV between two electrodes with a separation S of 20 m is shown below:

ρ_s (ohm-m)	12.5	2.5	1.25	0.3
ΔV (mv)	17.4	13.3	10.4	4.4

Detectability at 100 m is thus about 4.5 times better over the most resistive bottom compared with the least resistive.

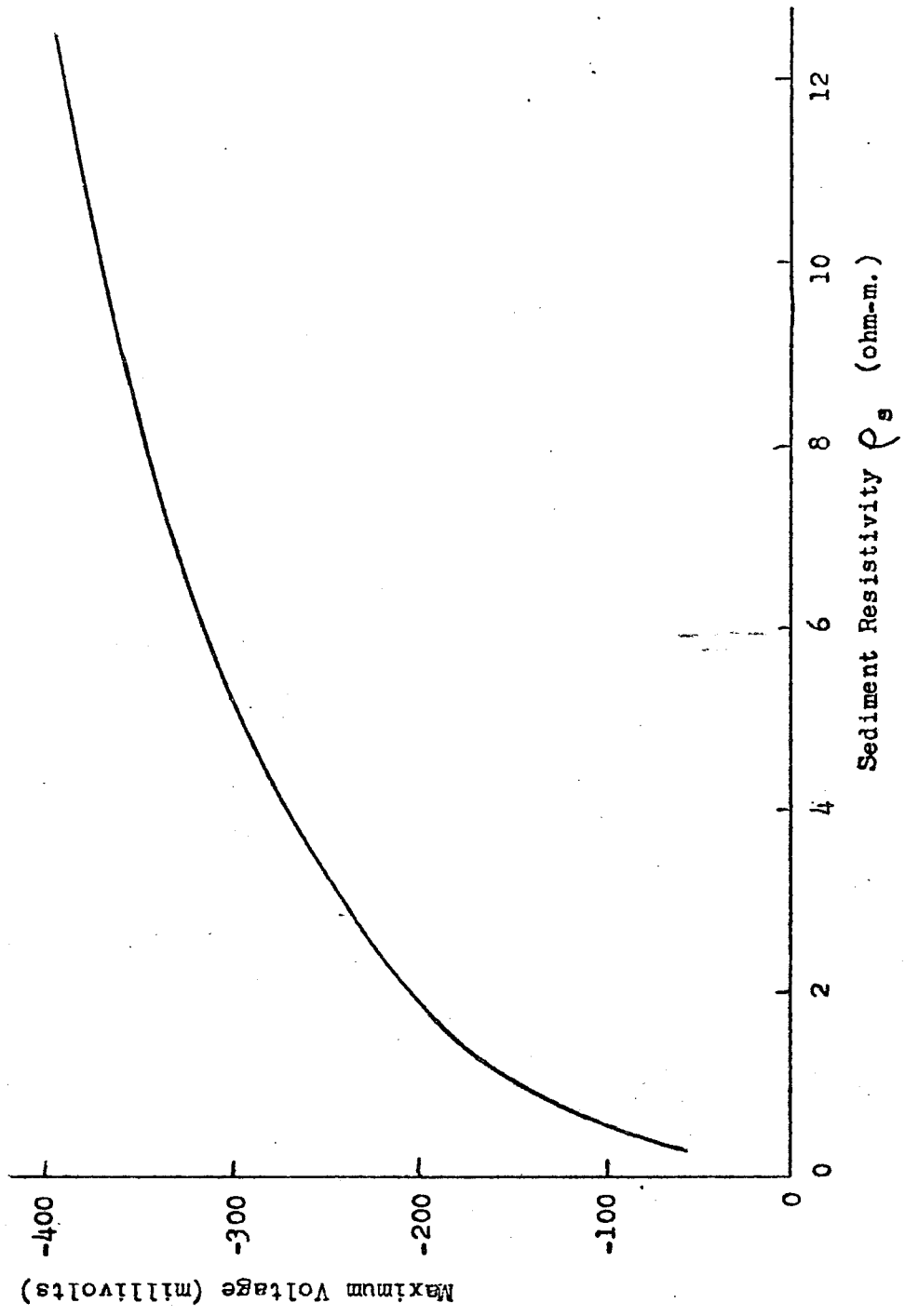
Effect of water depth

Increasing the water depth b decreases the magnitude and gradient of the signal on the surface of the water (Figure 3-12). For a



Effect of Sediment Resistivity

Figure 3-10

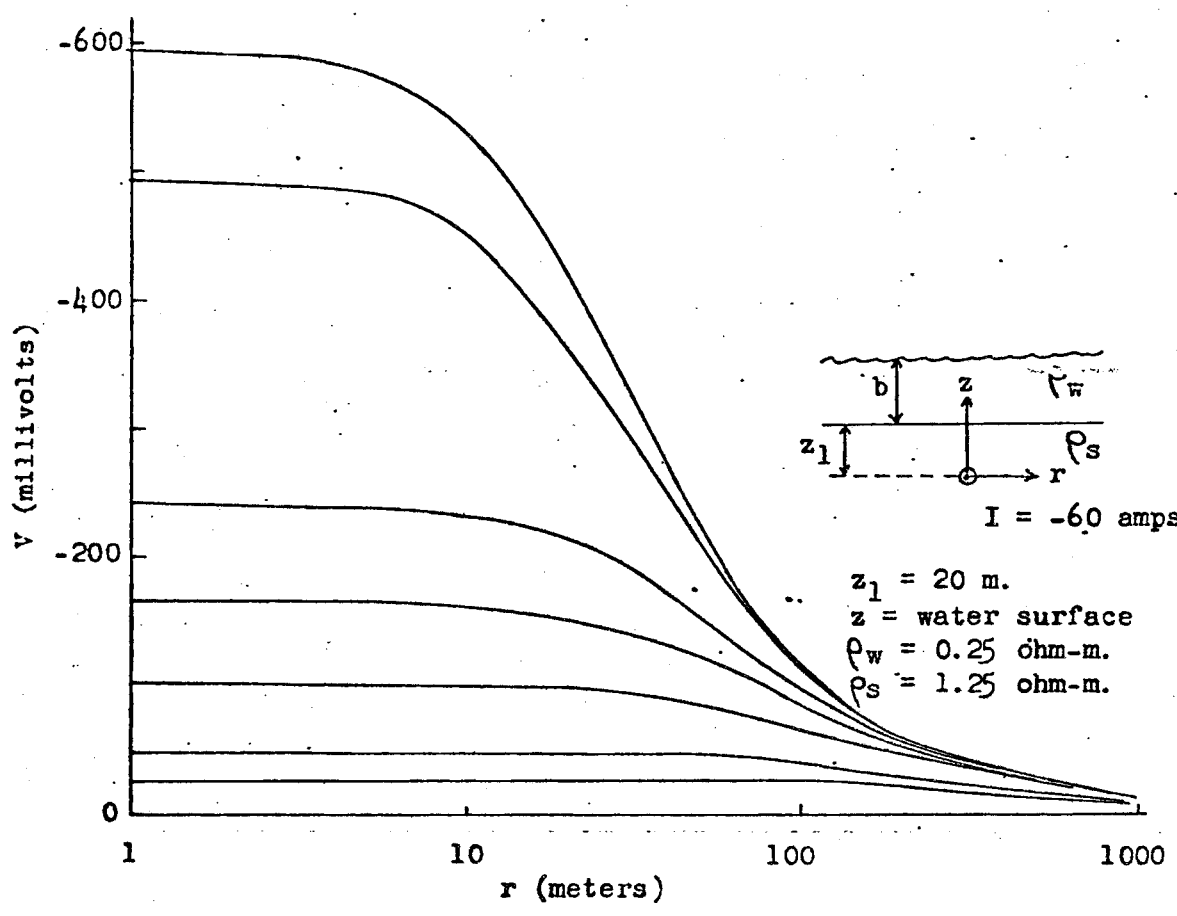


Maximum Voltage vs. Sediment Resistivity

Figure 3-11

W. H. B. 1111

Figure 3-12
Effect of Water Depth



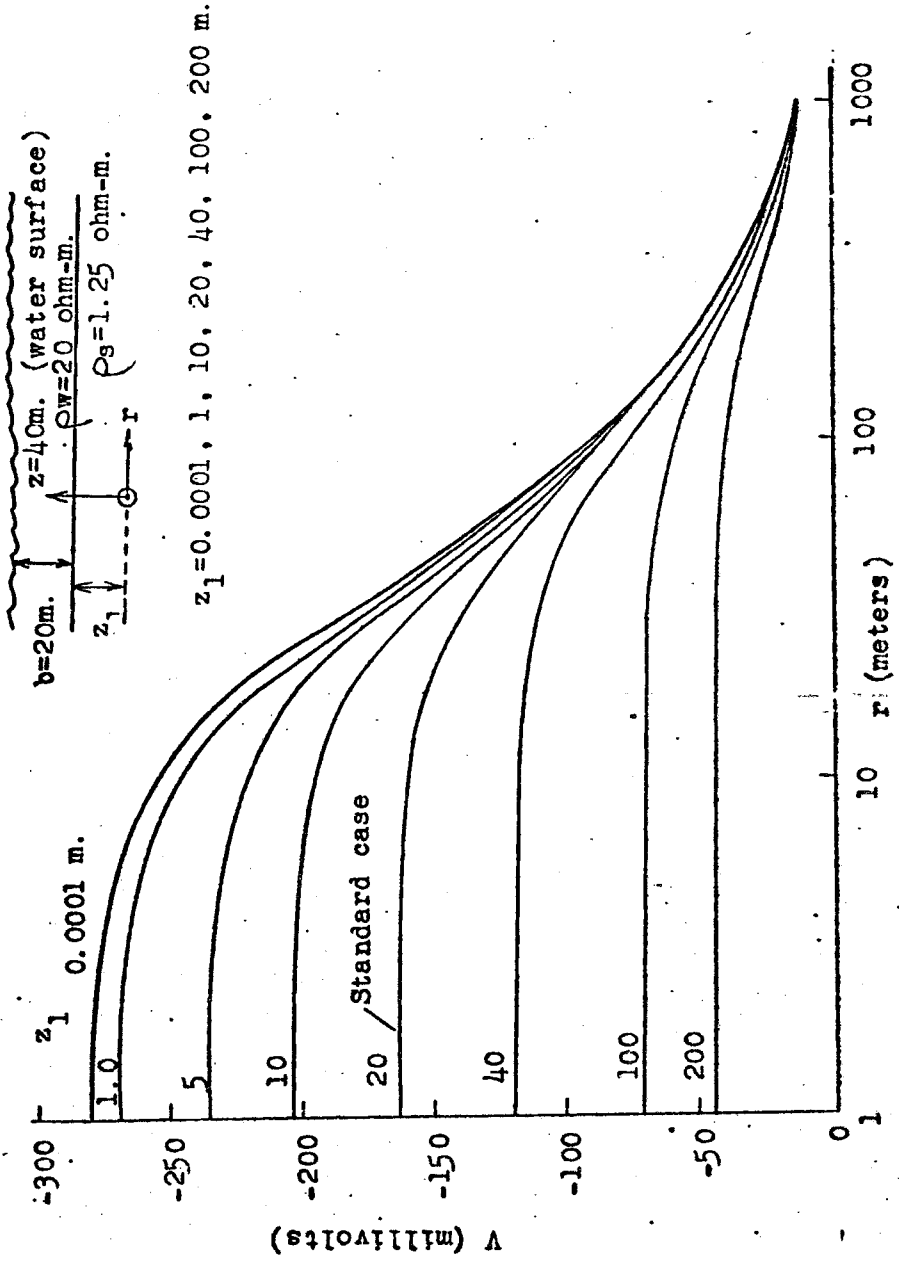
water depth of 200 m (approximately the maximum depth of the continental shelf), an electrode separation S of about 75 m would be required in order to register a signal of 1 mv when towed directly over the center of the anomaly. The maximum voltage at the surface even at this water depth is about 26 mv, and an electrode separation of several hundred meters would produce easily detectable signals as far as 1000 m from the center of the anomaly (the gradient is about .006 mv/m at $r = 1000$ m, so a separation of 167 m would give a 1 mv signal).

Effect of burial depth

The amplitude and gradient of the signal decrease as the depth of burial Z_1 of the point sink increases (Figure 3-13). For a sink located at the interface of the water and sea floor (burial depth $Z_1 = 0$) the maximum signal at the water surface is -279 mv, while for the standard case (burial depth of 20 m) the maximum signal is -164 mv, and for a burial depth Z_1 of 200 m the maximum signal decreases to -43 mv. The gradient $\partial V / \partial r$ at $r = 1000$ m for a burial depth of 200 m is 0.010 mv/m, so an electrode separation S of 100 m would be required for a 1 mv signal. The maximum gradient at the water surface is 1.123 mv/m at $r = 30$ m for the standard case, 3.701 mv/m at $r = 10$ m for $Z_1 = 0$, and 0.061 mv/m at $r = 200$ m for $Z_1 = 200$ m.

Uniqueness

The depth of burial of an ore body is an important economic parameter. It would be desirable, then, to be able to estimate the burial depth (Z_1) by inspection of the self-potential anomaly curve. A deeply buried ore body in a low-resistivity sediment may produce the same anomaly amplitude as a less deeply buried body



Effect of Burial Depth
Figure 3-13

NAVY LIBRARY

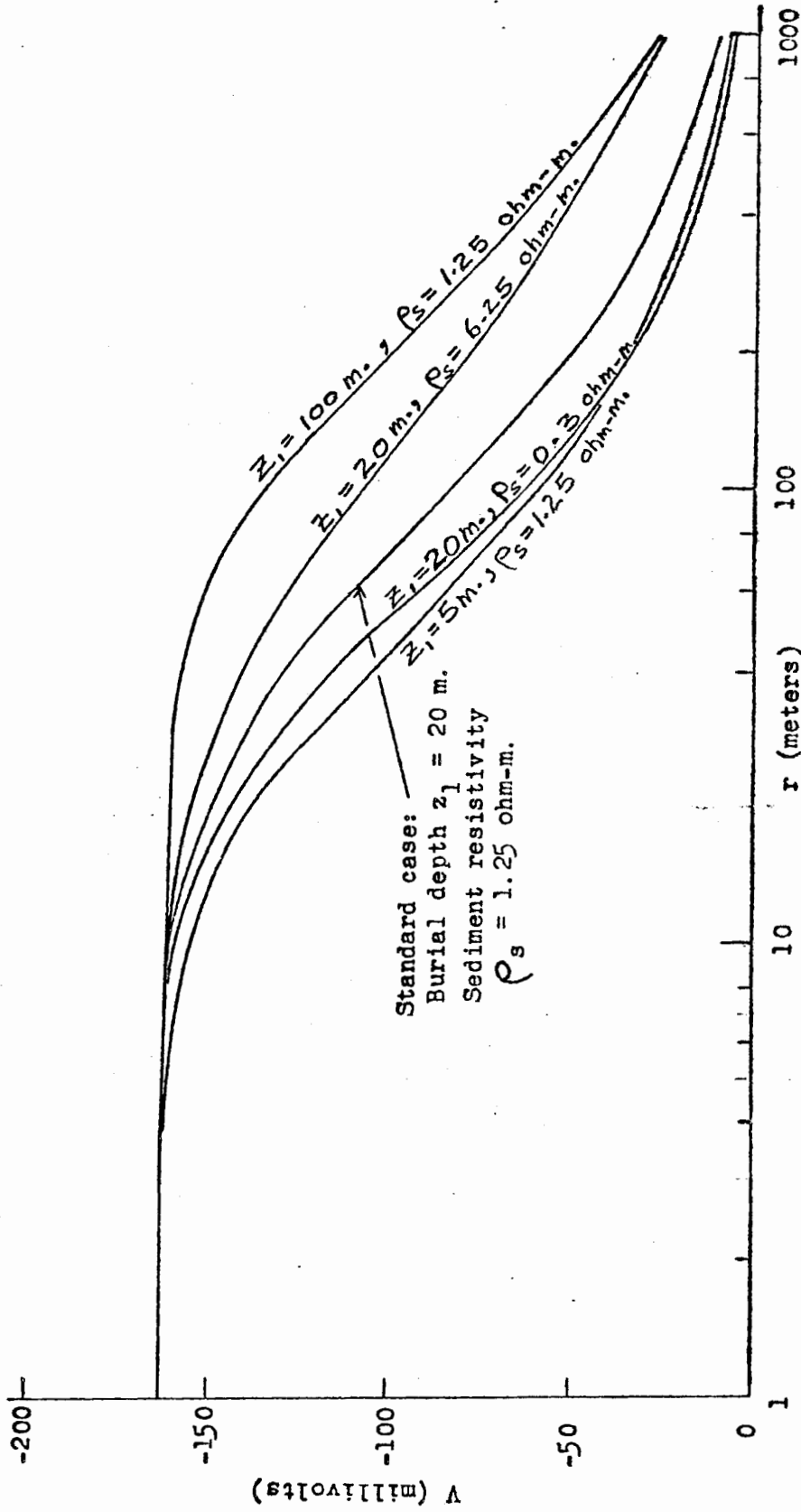
NAVY

in sediments of higher resistivity. In order to distinguish such cases, the shapes of their anomaly curves must differ.

Figure 3-14 shows such a situation, with all anomaly amplitudes normalized to that of the standard case, -164 mv. The curve for a body buried to a depth Z_1 of 20 m in sediments of resistivity ρ_s of 6.25 ohm-m is different from that for a body buried 100 m deep in sediments of 1.25 ohm-m resistivity, the latter being more sharply "peaked". The half-width of the anomaly curve (the distance from the center of the anomaly to the point at which the amplitude is half of its maximum value) is indicative of the sharpness of the peak of the curve. For the body with Z_1 of 100 m and ρ_s of 1.25 ohm-m, the half-width is 280 m; for the body with Z_1 of 20 m and ρ_s of 6.25 ohm-m, the half-width is 188 m.

The half-width decreases when either ρ_s or Z_1 decreases, as shown in Figure 3-14. The relationship of curve shapes changes also, with the more deeply buried body (20 m) in low-resistivity sediments (0.3 ohm-m) showing a greater half-width (72 m) than the 63 m half-width exhibited by the shallower body (5 m) in more resistive sediments (1.25 ohm-m). The curve shapes even for these two sharply peaked cases still should be distinguishable from good field data, as the curves diverge by 11 mv (9%) at $r = 30$ m.

An actual ore body, of course, is only approximated by a perfect point current sink. This approximation becomes better as the depth of burial increases, so the determination of burial depth by curve-matching will be more accurate for the large half-width curves produced by deeply buried bodies. A sharply peaked anomaly is indicative of shallow burial depth and/or low sediment resistivity.



Effect of Burial Depth and Sediment Resistivity on Curve Shape
 Figure 3-14

For such anomalies, it will probably be necessary to measure the sediment resistivity independently in order to obtain a reliable estimate of burial depth.

Dipole

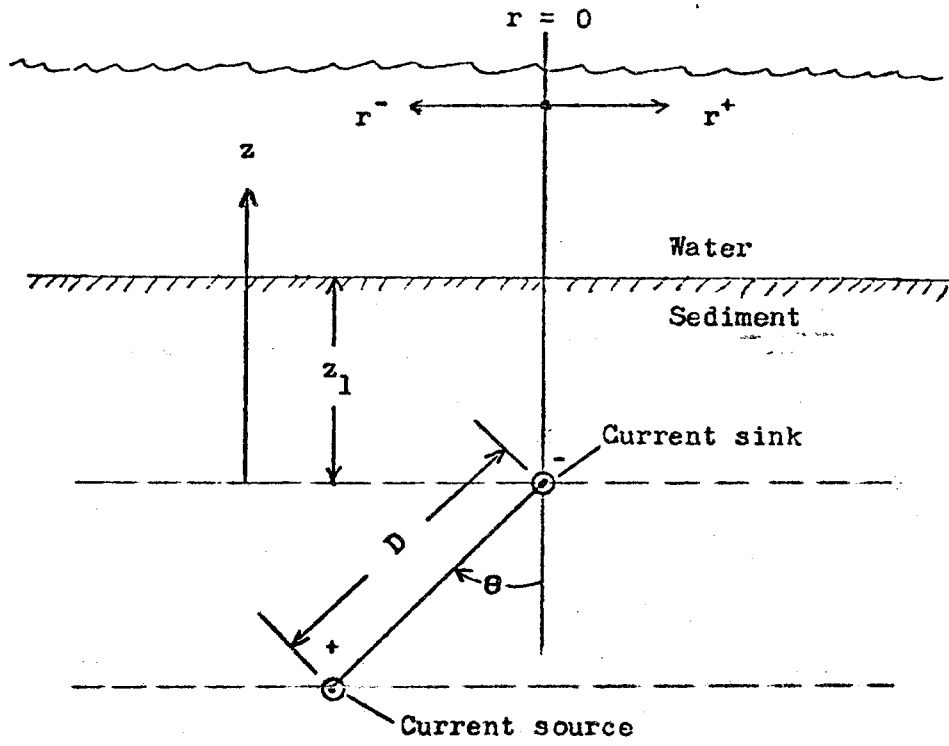
Addition of a current source at a distance D and dipole angle θ from the current sink (Figure 3-15) produces a point current dipole. The magnitude of the dipole field at the water surface will be less than that for the standard case (current sink only), and if θ is not 0° , the field will not be symmetrical about $r = 0$, and will be positive in sign for large negative values of r .

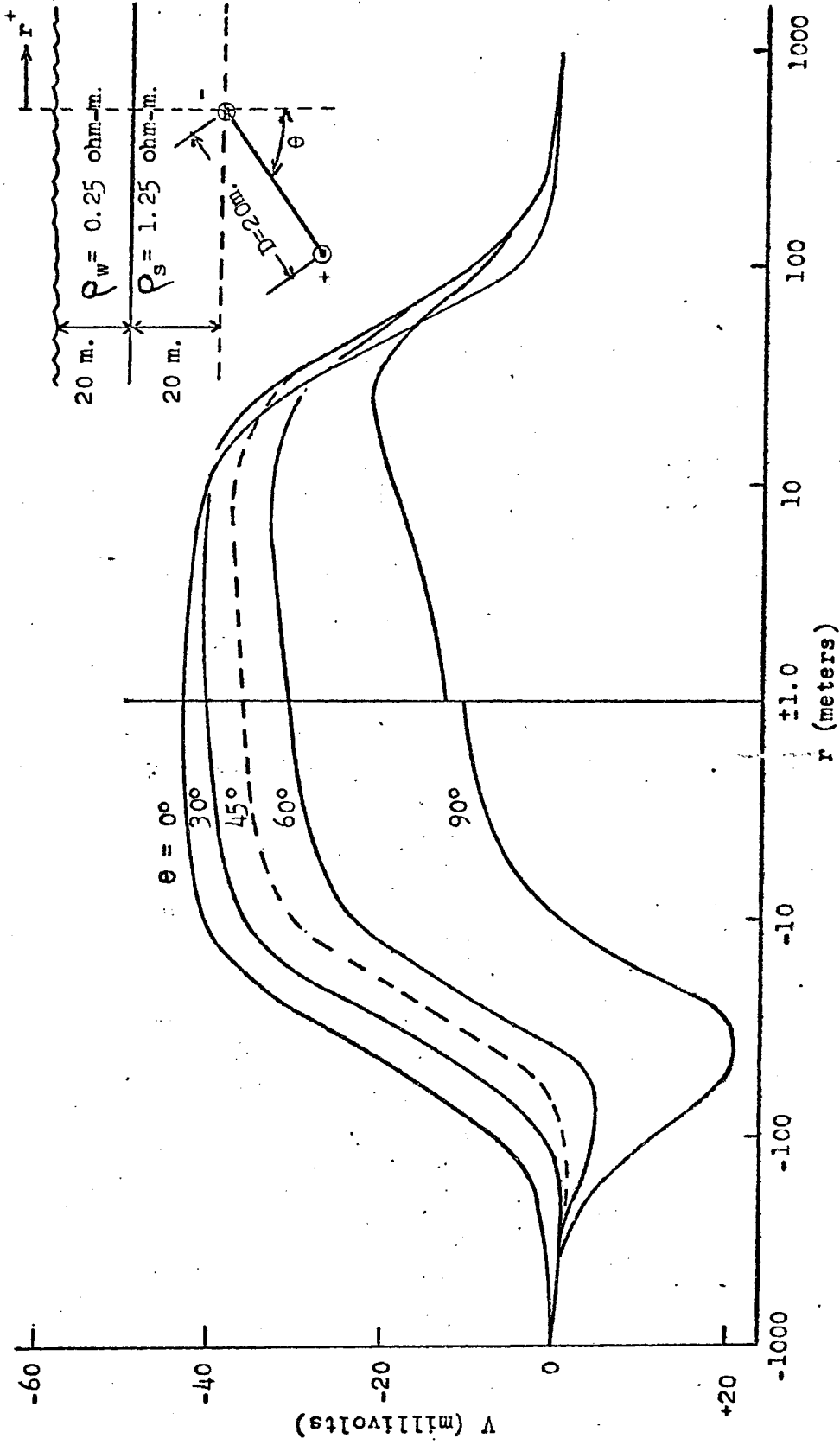
Figure 3-16 shows the effect of varying the dipole angle θ with the separation D remaining fixed at 20 m. For $\theta = 0^\circ$, the field has maximum amplitude (-43 mv) and is symmetrical about $r = 0$. The maximum amplitude is 0.26 times that for the standard case, so the effect of moving the current source from infinity to a point 20 m directly below the sink is to reduce the signal strength by a factor of 4.

As θ is increased, a positive component of the field appears at negative values of r , and the magnitude of the negative portion of the field is reduced. For the limiting case, $\theta = 90^\circ$, the field is skew-symmetric about the center of the dipole (the curve in Figure 3-15 does not appear symmetrical because r is taken as zero at the negative sink, not at the center of the dipole), and the maximum amplitude is about half as large as that of the vertical dipole.

Figures 3-17 and 3-18 show the effect of varying the dipole separation D with θ held constant at 30° or 60° . As the positive

Figure 3-15
Dipole Arrangement

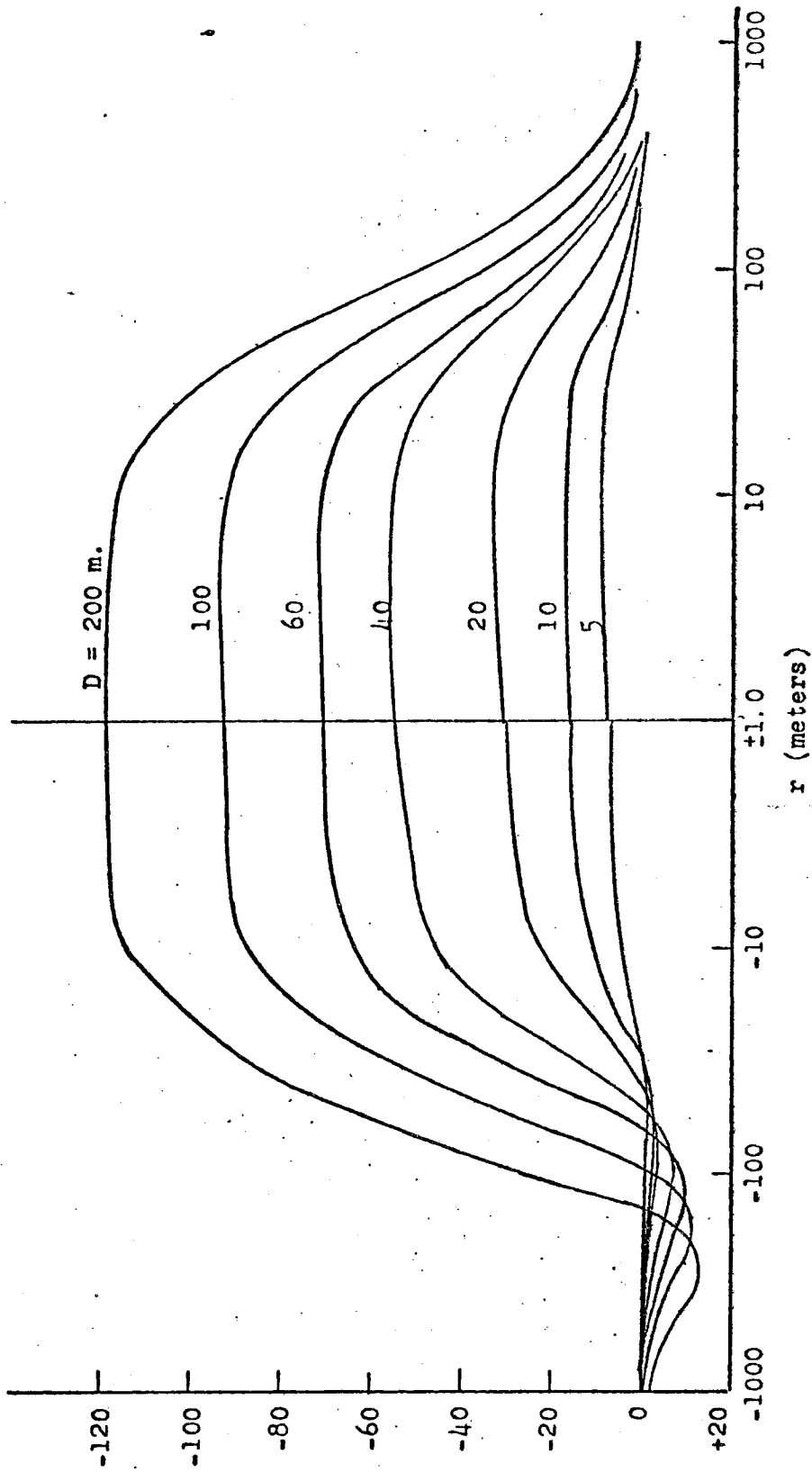




Effect of Dipole Angle ($D = 20$ m.)

Figure 3-16

SAFETY



Effect of Varying Dipole Separation D ($\theta = 60^\circ$)

Figure 3-18

NAVY
OFFICE OF THE
CHIEF OF NAVAL
OPERATIONS
WASHINGTON, D.C.

source is moved further from the negative sink, the amplitude and gradient of the field at the water surface increase.

An ore body of small vertical extent, therefore, will show a smaller anomaly than one which extends deeply into the sea floor. For a dipole angle of 30° , a separation of 20 m gives a maximum anomaly of -41 mv, or 25% of the maximum anomaly for the standard case (which has infinite separation). A separation of 200 m gives a maximum of -123 mv, or 75% of that for the standard case. For the same value of D , there is little difference between the cases for $\theta = 30^\circ$ and $\theta = 60^\circ$ (Figures 3-17 and 3-18).

Shoreline

In an area where onshore bodies producing self-potential fields occur at or near a shoreline, offshore prospecting may be done by following the shoreline as closely as possible. The self-potential field generated in the water by a body on shore may be calculated by the use of a point current sink located on the ground surface at a distance Z_1 from the shoreline (Figure 3-19). Geometrically, this situation is analogous to the field produced at the surface of the earth by a current source located on one side of an infinitely deep vertical fault. The potential field for this case is derived by Van Nostrand and Cook (1966, p. 53). The potentials V_s on shore and V_w at the water surface are:

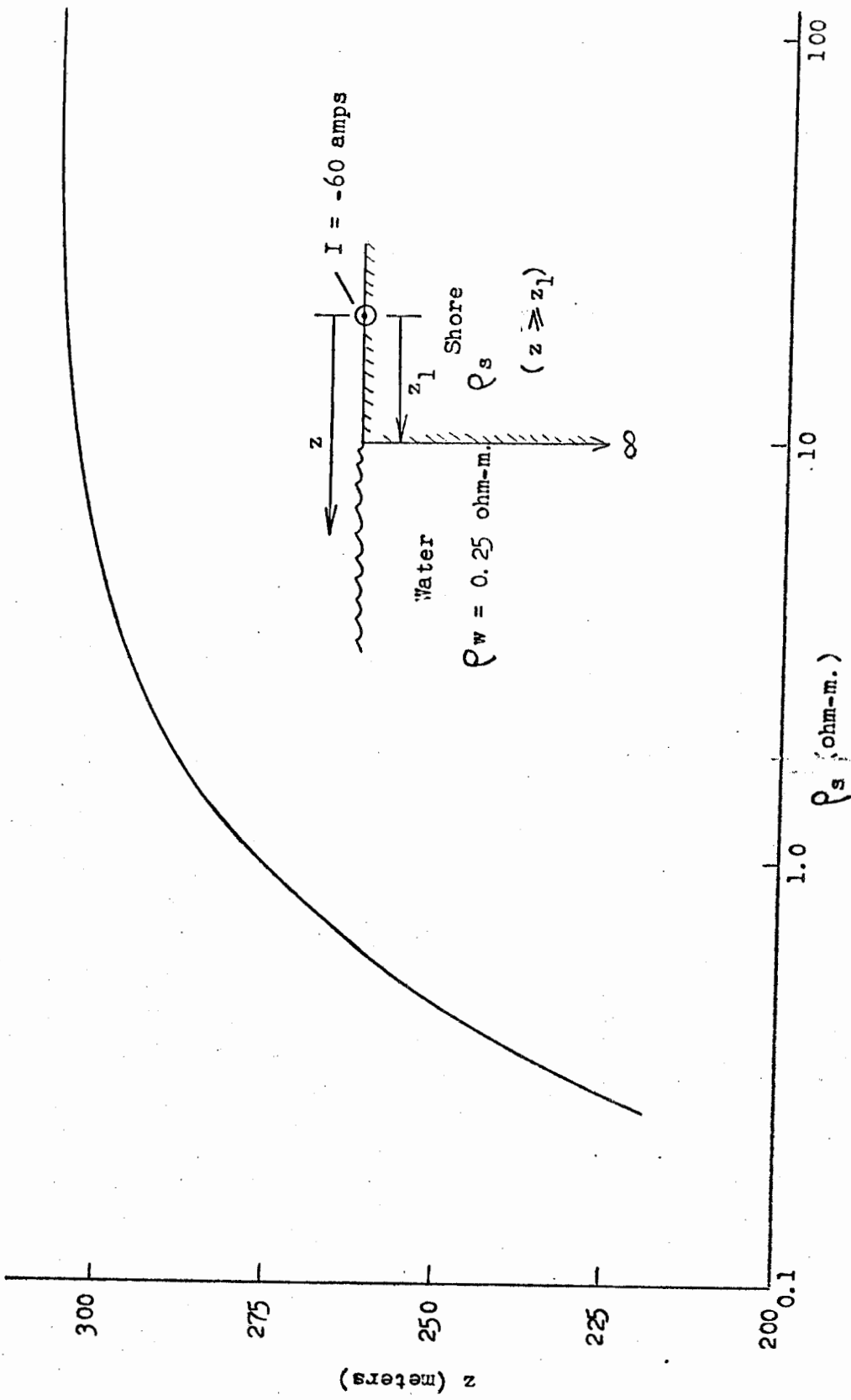
$$(3-2) \quad V_w = \frac{I \rho_s}{2 \pi Z} \frac{\rho_w \rho_s}{\rho_w + \rho_s}$$

$$(3-3) \quad V_s = \frac{I \rho_s}{2 \pi} \left[\frac{\rho_w - \rho_s}{(\rho_w + \rho_s)(2Z_1 - Z)} + \frac{1}{Z} \right]$$

It is interesting to note that the field in the water, V_w , is a

function only of Z , the distance from the current sink to the point at which the field is calculated, and not of Z_1 , the distance from the sink to the shoreline. The equipotential lines on the water surface, therefore, are circles of radius Z centered on the current sink.

The magnitude of the field produced by a current sink of -60 amps is shown as a function of shore resistivity ρ_s and distance Z from the source in Figure 3-19. The field magnitude decreases as ρ_s decreases. In the limiting case where $\rho_s = \rho_w$, $V_w = 2387/Z$ mv; for $\rho_s = \infty$, $V_w = 4665/Z$ mv. The gradient of the field is also a function of ρ_s and Z . The value of Z at which the gradient is 0.05 mv/m is shown as a function of ρ_s in Figure 3-20. This is the distance from the sink at which an electrode separation S of 20 m will produce a signal of 1 mv and may be used as an estimate for the "radius of detectability" for an ore body. This value ranges from 220 m for $\rho_s = \rho_w$ to 310 m for $\rho_s = \infty$.



Value of z for $\partial V / \partial z = 0.05 \text{ mv./meter}$

Figure 3-20

CHAPTER 4

EQUIPMENT

"For the measurement of intensity
I was fortunate in securing a
magnificent instrument... "

Carl Barus
"On the Electrical Activity
of Ore Bodies", 1882

Introduction

A wide variety of systems have been used to measure electric potential fields in natural bodies of fresh and sea water. These systems all consist of a pair of electrodes which make contact with the water, and are connected to an instrument which measures, usually records, and occasionally electronically processes the signal. The system must accurately measure the potential difference between two points in the conducting medium with minimum distortion, noise, drift, and response to environmental factors such as temperature, pressure, and changes in chemical composition.

For use in marine self-potential investigations the additional requirements of portability, ruggedness, and ease of use in the difficult near-shore environment must be met. Finally, reasonable cost is an important design consideration. The system described in this section meets, to a satisfactory degree, all the criteria above, and has given excellent results in actual field use.

Electrodes

The electrodes form the electrical contact between the water and the leads to the potential measuring instrument, i.e., between an ionically conducting and a metallicly conducting medium. It is difficult to transfer an existing potential difference across such an interface without introducing spurious voltages which may mask or distort the signal. By careful design, however, the irreproducible noise and drift of the electrode may be limited to the point where actual signal levels of 0.1 millivolts in the water may be measured with confidence. Furthermore, the response of the electrode to changes in temperature, salinity, or chemical composition of the sea water may be minimized and be made predictable and reproducible.

Electrode reversibility

An electrode must operate in a reversible manner to give meaningful readings. Thermodynamically, for an infinitesimal current flow through the electrode, the equation

$$(4-1) \quad \Delta F = -n \mathcal{F} E$$

where:

ΔF = the free energy change

n = the number of faradays passed

\mathcal{F} = Faraday's constant

E = the potential

governs the relationship between electrical work done and the free energy change of the system (Glasstone and Lewis, 1960, p. 459).

Practically, this means that any chemical change in an electrode brought about by the passage of a small amount of current must be reversed by the flow of an equal amount of current in the opposite direction. This is an important requirement, because in practice a finite amount of current must be drawn from the electrodes in order for the potential between them to be measured. If the passage of this current results in a change in the composition of one electrode relative to the other, a galvanic potential (called polarization) between the electrodes will be added to the actual electric field, giving an incorrect reading of the field potential. Such irreversible electrode polarizations may be minimized by proper electrode design, and by minimizing the current flow through the electrode. For any reversible electrode, the standard oxidation potential E of the electrode measured against a standard hydrogen electrode (S.H.E.) is given by

$$(4-2) \quad E = E^{\circ} - \frac{RT}{nF} \ln \frac{(\text{oxidized state})}{(\text{reduced state})}$$

(Glasstone and Lewis, 1960, p. 464).

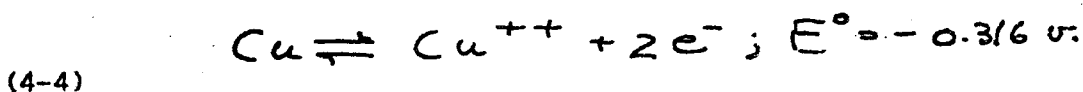
Electrodes of the first kind

The simplest type of reversible electrode is a piece of bare metal placed directly in a conducting solution. It is known as an "electrode of the first kind (or type)" (Glasstone and Lewis, 1960, p. 455) and is reversible with respect to ions of the electrode metal, i.e. the reaction



(4-3)

where M represents the non-ionized metal, M^{+} represents a metal cation and e^{-} represents an electron, is reversible. This condition is met for a metal in contact with a reasonably concentrated solution of its own ions, such as copper in saturated CuSO_4 , where the reversible reaction is



(Uhlig, 1963, p. 35).

Because ions of almost every metal are present in detectable quantity in sea water (Sverdrup and others, 1942, p. 176), it may appear that almost any metal might serve as a reversible electrode in sea water. For kinetic and electrochemical reasons, however, this is not so. First, using kinetic arguments, Ives and Janz (1961, p. 15) show that for a metal electrode to function reversibly, ions of that metal must be contained in the solution at sufficiently

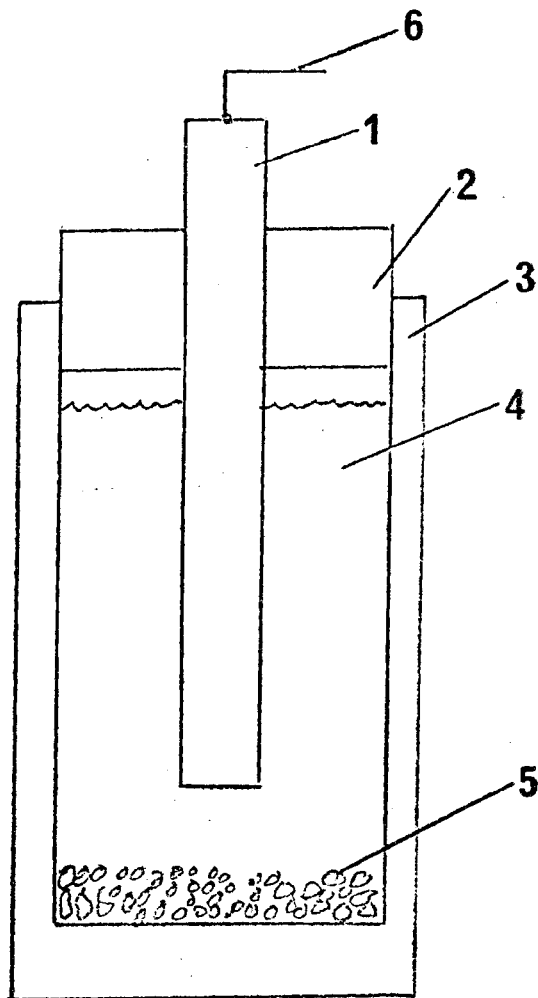
high concentrations for the reversible reaction to work. Sodium, the metal with the highest concentration in sea water, is only about 0.47 M (Sverdrup and others, 1942, p. 176) with the other metal ions present in much lower concentrations.

Of course, due to the extreme reactivity of sodium in water, it would be impossible to use an electrode made of metallic sodium in sea water. In fact, most metals are attacked electrochemically by sea water (Uhlig, 1948), and any attempt to measure external potentials accurately will be frustrated by the addition of the signal of galvanic potentials due to corrosion of the metal. The problem of galvanic potentials was noted by Michael Faraday (1832, p. 174), who attempted to measure electric fields in a reservoir and in the Thames River, using electrode pairs made of copper and of "platina" (platinum). His statement, "I constantly obtained deflections at the galvanometer, but they were very irregular, and were in succession referred to other causes than that sought for", summarizes the results to be expected from the use of bare metal electrodes immersed directly in sea water.

Electrodes of the first kind, however, can be made to function reversibly in geophysical applications. All that is needed is to insert the bare metal in a solution containing ions of the metal in high concentration. Contact with the external medium is made through a liquid junction in the form of a very small opening, a porous membrane, or a wick. An example of this type of electrode is the venerable copper-copper sulfate (Cu-CuSO_4) "pot", which has served geophysicists for many years (Figure 4-1). These electrodes are described by Edge and Laby (1931, p. 232), and

Figure 4-1

Copper-Copper Sulfate "Porous Pot" Electrode



- 1 Copper rod
- 2 Plug
- 3 Cylindrical porous ceramic cup
- 4 CuSO_4 solution (saturated)
- 5 CuSO_4 crystals
- 6 Connecting wire

Jakosky (1950). Ewing (1939) presents a detailed study of the properties of Cu-CuSO₄ electrodes.

Although Cu-CuSO₄ electrodes have been used in borehole self-potential investigations (Becker and Telford, 1965, p. 180) and apparently used with success in salt water by Schlumberger in 1930 (Ocean Industry, 1967, p. 61), they would seem to be unsuitable for long-term, high-precision oceanographic use because of their relatively large response to temperature changes (Ewing, 1939), and because of the possibility of contamination of the internal CuSO₄ solution by sea water. Because sea water is primarily a sodium chloride (NaCl) solution, there is a large difference in the concentrations of Cu⁺⁺, SO₄⁼, Na⁺ and Cl⁻ ions in the internal (CuSO₄) solution and the sea water. The flow of CuSO₄ out of the electrode, and sea water into it, would be rapid unless a junction of very low permeability were to be used. A very low permeability junction implies high electrode impedance and increased susceptibility of the junction to clogging.

Electrodes of the second kind

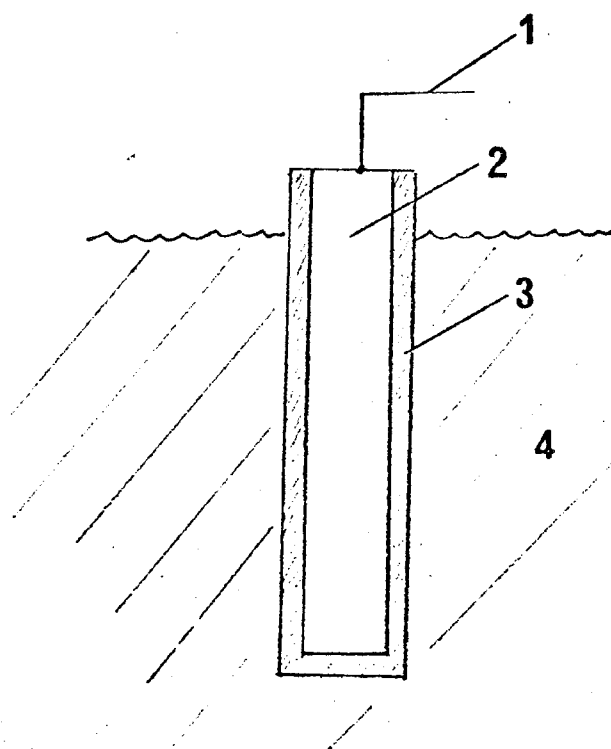
Reversible "electrodes of the second kind" are composed of "a metal and a sparingly soluble salt of this metal in contact with a solution of a soluble salt of the same anion" (Glasstone and Lewis, 1960, p. 456). The electrode may be represented by



where M represents the solid metal, A the anion, C a cation, and MA the sparingly soluble salt coating. An example is the silver-silver chloride (Ag-AgCl) electrode in a potassium chloride (KCl) solution (Figure 4-2):

Figure 4-2

Silver-Silver Chloride Electrode Element



- 1 Connecting wire
- 2 Substrate: Ag or Pt
- 3 Coating: Ag + Cl
- 4 Chloride solution

Ag; AgCl (solid), KCl.

The electrode reaction for an electrode of the second kind is



Lead electrodes

The simplest example of an electrode of the second kind is one made of pure lead. When used in boreholes to obtain self-potential logs, the lead apparently becomes coated with a film of chloride or sulfate and functions in a reversible manner as described in equation 4-6 (Wyllie, 1963, p. 48). Lead electrodes have proven satisfactory in well-logging work, although "porous-pot" electrodes also have been used (Heiland, 1940, p. 827; Becker and Telford, 1965, p. 180). Lead electrodes apparently have been used successfully in sea water to detect electric fields due to corrosion currents. Grice (1968, p. 28) describes a marine self-potential system in which "the electrodes are usually made of lead", although he never explicitly states that lead electrodes were used in his successful attempt to locate the sunken Civil War ironclad "Tecumseh" in Mobile Bay, Alabama (Ocean Industry, 1967).

Snyder (1966, p. 12), in describing the system used in the search for the lost submarine "Thresher", states that "lead is usually used" for electrodes, although, again, it is never explicitly stated that lead electrodes were used in the specific system described. Snyder also discloses some problems encountered in using the (presumed) lead electrodes. First, the observed noise level was ± 2 millivolts. Second, a potential difference of 140 millivolts appeared between an electrode at the surface and one

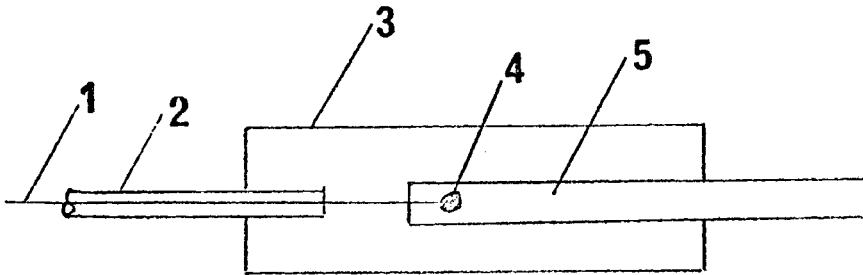
at a depth of 8000 feet. This offset is much too large to be accounted for by any kind of thermodynamic process, or water current velocity or temperature distribution, and, even if reversible, would present a nuisance in any attempt to measure anomalies of a few millivolts.

I have attempted to use lead electrodes (Figure 4-3) to measure offshore potential fields caused by onshore sulfide ore bodies. The electrodes were tested in San Francisco Bay by towing them through an artificial potential field and in an electrically inactive area. Although results of these tests appeared satisfactory, problems were encountered in field tests conducted off known sulfide deposits near Ketchikan, Alaska (see Chapter 6). Even though a very high input impedance electrometer (Keithley model 600A; 10^{14} ohms) was used, large irreversible potentials appeared between the electrodes from time to time. Such potentials could be eliminated only by scraping the electrodes clean. Because of this unreliability, possibly due to the fact that the nature of the coating on the lead may change in a variable environment, the use of lead electrodes was discontinued.

Coated electrodes

If the sparingly soluble salt coating (MA in expression 4-4) is applied to the substrate metal M carefully, under controlled conditions, a satisfactory electrode of the second kind may be produced. Lead-lead chloride, mercury-mercurous chloride, and silver-silver chloride electrodes have been used successfully in marine applications. These three types of coated electrodes are discussed below.

Figure 4-3
Lead Electrode



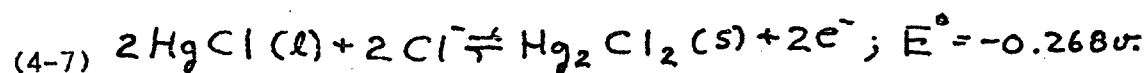
- 1 Connecting wire
- 2 Insulating jacket
- 3 Cast polyester resin cylinder
- 4 Solder joint
- 5 Chemically pure lead cylinder, 1/4" diameter

Lead-lead chloride electrodes

An electrode which uses a lead rod coated with lead chloride as the sensing element has been designed by the Scientific Research Institute of Arctic Geology of the U.S.S.R. (Demenitskaya and others, 1970, p. 96; Ogilvy and others, 1969, p. 52). The element is immersed in jellied agar-agar saturated with potassium chloride and makes contact with the external medium through the end of a ceramic cylinder. The sides of the cylinder are protected by a polyethylene pipe. The electrodes appear to have satisfactory temperature, pressure, and drift characteristics. In particular, the potential between an electrode at the surface and one at 1500 meters changed only about one millivolt due to the increase of pressure on the lower electrode (Demenitskaya and others, 1970, p. 96). Because the use of lead-lead chloride electrodes seems to be infrequent outside the Soviet Union, more extensive information about their preparation and properties is not easily found. For this reason, their use was not considered for the marine self-potential system.

Calomel electrodes

The mercury-mercurous chloride (or "calomel") electrode is one of the workhorses of the experimental physical chemist (Ives and Janz, 1961). Its half-cell reaction is

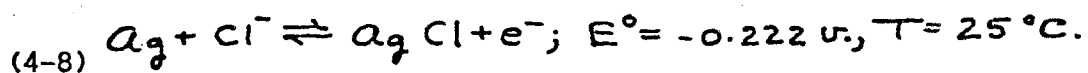


Calomel electrodes have many desirable properties for laboratory reference use, and also have been used in the field. Parasnis (1966) describes a calomel electrode for land use, and Manheim (1961, p. 28) used a calomel reference electrode, at or just

below the surface, as a reference in a study of vertical Eh and pH gradients in the Baltic Sea. Unfortunately, a strong temperature hysteresis effect limits the usefulness of the calomel electrode in an environment where the temperature may change appreciably (Covington, 1969, p. 126). Because substantial temperature changes in both the vertical and the horizontal directions may be expected in the shallow-water marine environment, calomel electrodes were not considered for marine self-potential application.

Silver-silver chloride electrodes

The silver-silver chloride (Ag-AgCl) electrode has found widespread oceanographic application. It consists of a coating of silver chloride applied on a substrate of platinum or silver by a thermal, electrolytic, thermal-electrolytic, or precipitation process (Ives and Janz, 1961, p. 203; von Arx, 1962, p. 275; Covington, 1969, p. 115). The electrode reaction is



Ag-AgCl electrodes are easily prepared, stable, and rugged, and their properties have been extensively tabulated. In the following discussion, the substrate and coating will be referred to as the electrode element, and the assembly which includes the element as the electrode.

Ag-AgCl electrodes in various forms have been used by von Arx (1950, p. 45; 1962, p. 276), Sanford (1967, p. 70), Manglesdorf (1962, p. 173), Drever and Sanford (1970), and Curtin (1970, p. 8) to measure water current velocities; by Marke (1965, p. 231) and Corwin and others (1970) to measure self-potential and resistivity on the sea floor; by Ben-Yaakov and Kaplan (1968) as the reference

electrode for a high-pressure, deep-sea pH measuring system; by Conti (1972) as a reference for pH, Eh, and specific ion electrodes in a towed monitoring system; and by Bomar and Marchand (1970) to measure potential fields generated by a cathodic protection system in San Francisco Bay. They are commercially available in "packed" form (described below) for oceanographic use, and in "filled" form (described below) from a large number of manufacturers for various land-based applications.

Electrode Isolation

Changes in the temperature, pressure and chemical composition of the fluid surrounding an electrode element will produce changes in the potential of the electrode. Because it is impossible to produce perfectly matched pairs of electrodes, even simultaneous changes of these variables at a pair of electrodes will result in a varying potential between the pair. The elements are sensitive to flow past their surfaces, and even a small flow may produce noise levels of several millivolts (Curtin, 1970, p. 89). Additionally, the elements are susceptible to reaction with dissolved oxygen (in acid solutions) and bromide (Covington, 1969, p. 116). It is for these reasons that von Arx (1950) states "In general, it is found that an electrode works best when it is nearly isolated from the sea both physically and chemically."

Various strategies have been used to effect this isolation, although there is no way to completely isolate the electrodes from chemical changes in the sea water. Marke (1965, p. 233) used an electrode in which a coil of silver was surrounded by silver-silver chloride powder, which in turn was enclosed by a porous tube. The design used by von Arx (1950, p. 47; 1962), Ocean

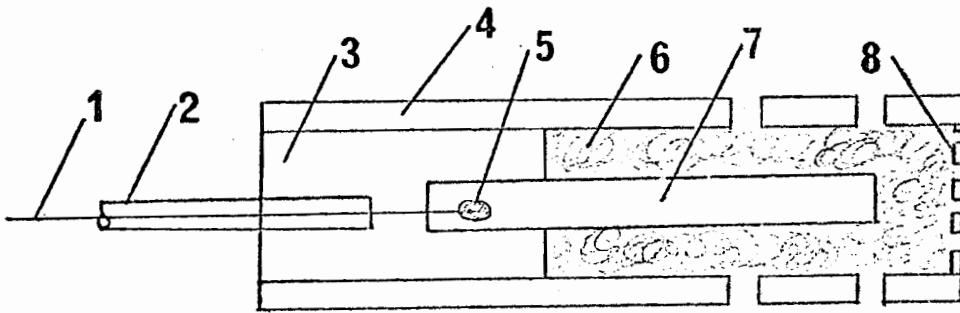
Research Equipment, Sanford (1967), and Curtin (1970) employs a packing of glass wool around the electrode element (see Figure 4-4). This serves to isolate the element hydrodynamically, and, to some extent, chemically and thermally from the sea. (This design will be referred to as the "packed" electrode). The disadvantage of this design is that if the electrode is used in the highly contaminated or reducing waters often found in near-shore, shallow water, or estuarine environments, or in mud, the nature of the solution surrounding the elements may change, leading to electrochemical potential changes, or to "poisoning" of the electrodes.

A greater degree of isolation is provided by the design of Ben-Yaakov and Kaplan (1968), in which the element is immersed in a solution of 2.7 M potassium chloride (KCl) (the reason for the choice of 2.7 M as the KCl concentration is explained later in this section), saturated with silver chloride (AgCl). Electrical connection to the sea water is made through a porous ceramic tip. In this design, the electrode element is completely isolated hydrodynamically and well isolated chemically from the sea water, with thermal insulation (but not full isolation), provided by the electrode housing walls. This type of electrode, in which the Ag-AgCl element is immersed in a filling solution of constant composition, will be referred to as the "filled" electrode. Similar designs are widely used for land-based industrial and research applications and this is the type of electrode design finally chosen for this work.

The greatest degree of isolation is found in the salt-bridge design originated by Manglesdorf (1962) and used in modified form by Drever and Sanford (1970) and Corwin and others (1970) (Figure 4-5).

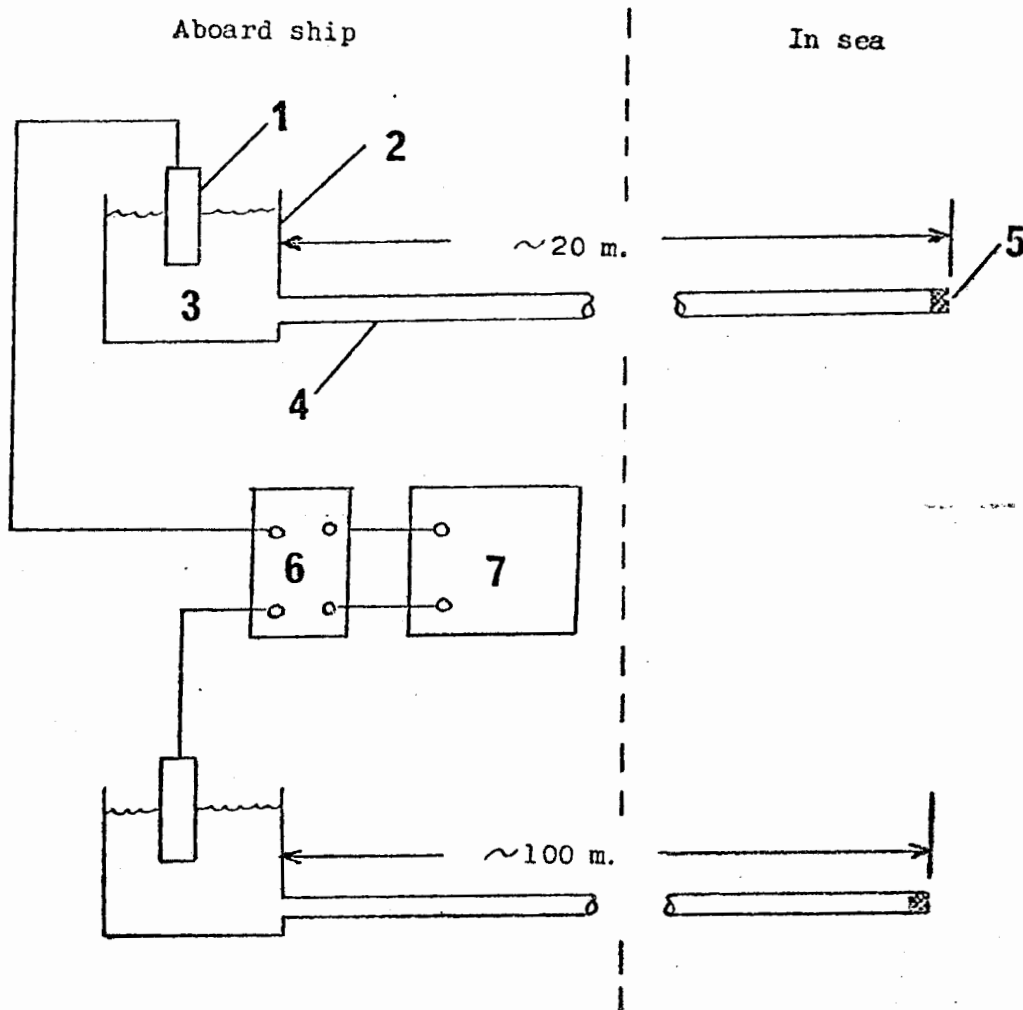
Figure 4-4

"Packed" Silver-Silver Chloride Electrode



- | | | | |
|---|-----------------------------|---|--------------------------------|
| 1 | Connecting wire | 5 | Solder joint |
| 2 | Insulation | 6 | Silver-silver chloride element |
| 3 | Epoxy resin potting | 7 | Glass wool packing |
| 4 | Cylindrical plastic housing | 8 | Plastic screen |

Figure 4-5
Salt Bridge System



- 1 Electrode
- 2 Plastic container
- 3 Sea water
- 4 Plastic tube
- 5 Porous ceramic tip
- 6 Impedance isolation
- 7 Chart recorder

The electrode element in these designs is very well isolated, hydrodynamically, chemically, and thermally, from the sea. The penalty paid for this high degree of isolation is extremely high electrical impedance and increased difficulty in shipboard handling. Manglesdorf (1962) discusses these problems in some detail. The problems are compounded when working from a small boat in the near-shore environment, where frequent handling of the salt-bridge tubes is necessary, and the necessary high-impedance isolation circuitry between the chart recorder and the electrodes is, unless very carefully protected, likely to malfunction in salt water spray.

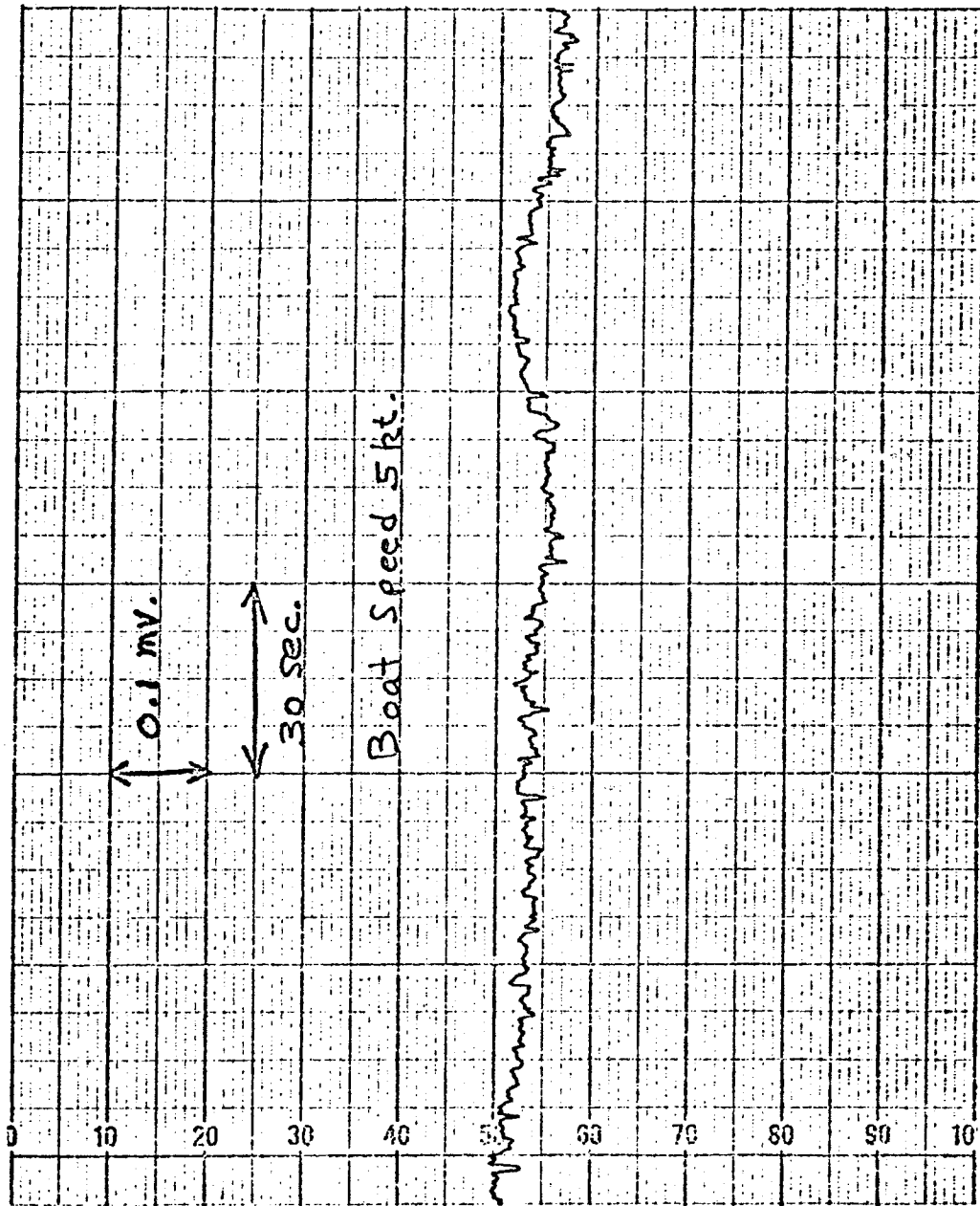
The salt bridge system designed for self-potential measurements (Corwin and others, 1970) proved satisfactory in tests run in San Francisco Bay, showing low noise and drift levels (Figure 4-6). However, in field use in the Ketchikan, Alaska area (see Chapter 6) the salt bridge proved very susceptible to noise during handling (Figure 4-7), and also proved rather difficult to deploy and retrieve, as it is not easy to store the water-filled tubes on reels without disconnecting them and running the risk of introducing bubbles into the system. Finally, the tubes apparently developed a small leak, which was difficult to locate and produced a spurious signal when the section of tubing containing the leak entered and left the water. Due to these operational difficulties, further use of the salt bridge system was abandoned.

"CoCo" electrodes

The electrodes finally designed for and used in this work (nicknamed the "CoCo" electrodes, after co-constructors Conti and Corwin) are of the "filled" variety (Figure 4-8). The body of the electrode is constructed of high-quality, annealed Plexiglas.

Figure 4-6

Salt Bridge System Background Noise



11-1-51
M.A.P.

Figure 4-7

Salt Bridge System Handling Noise

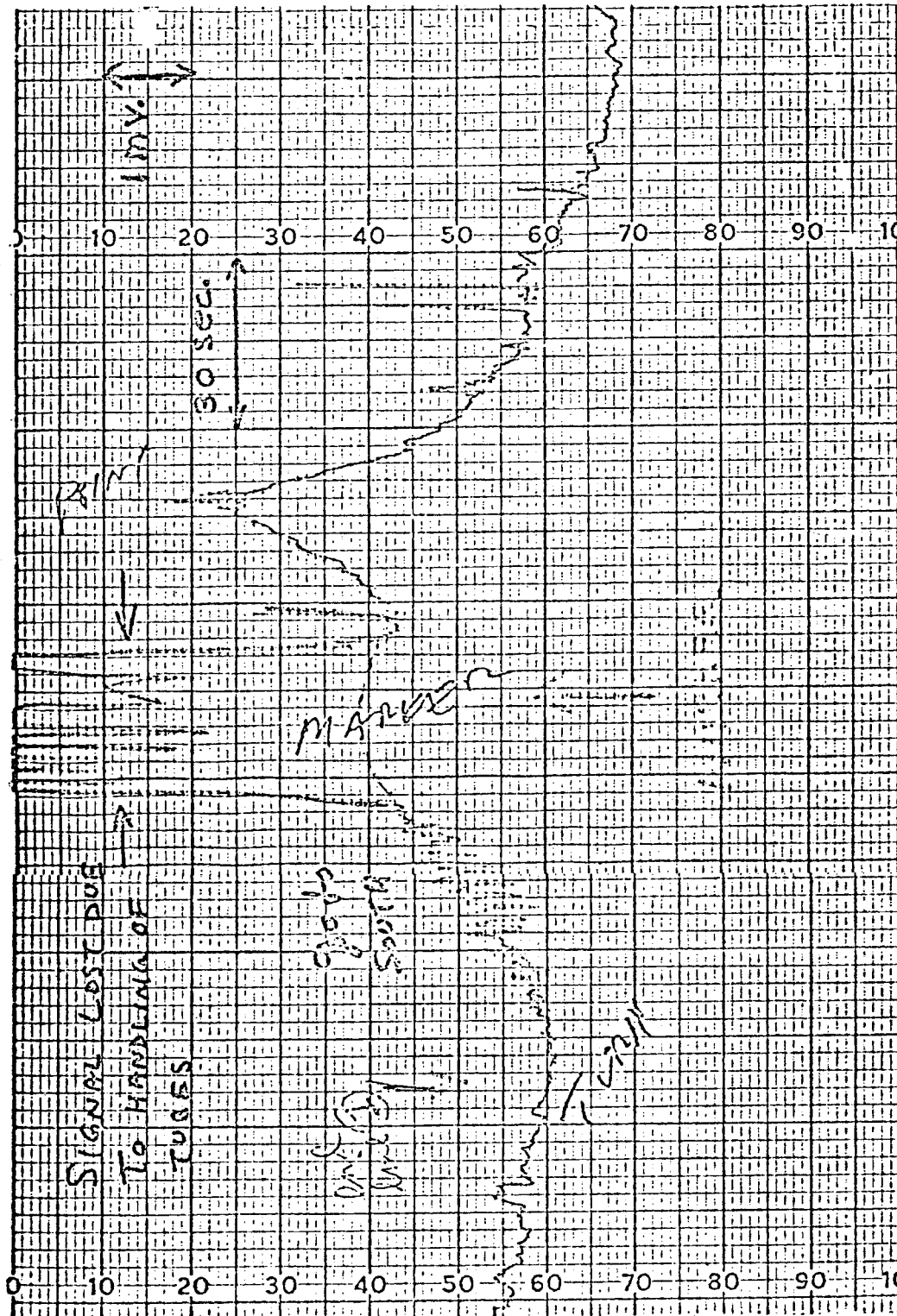
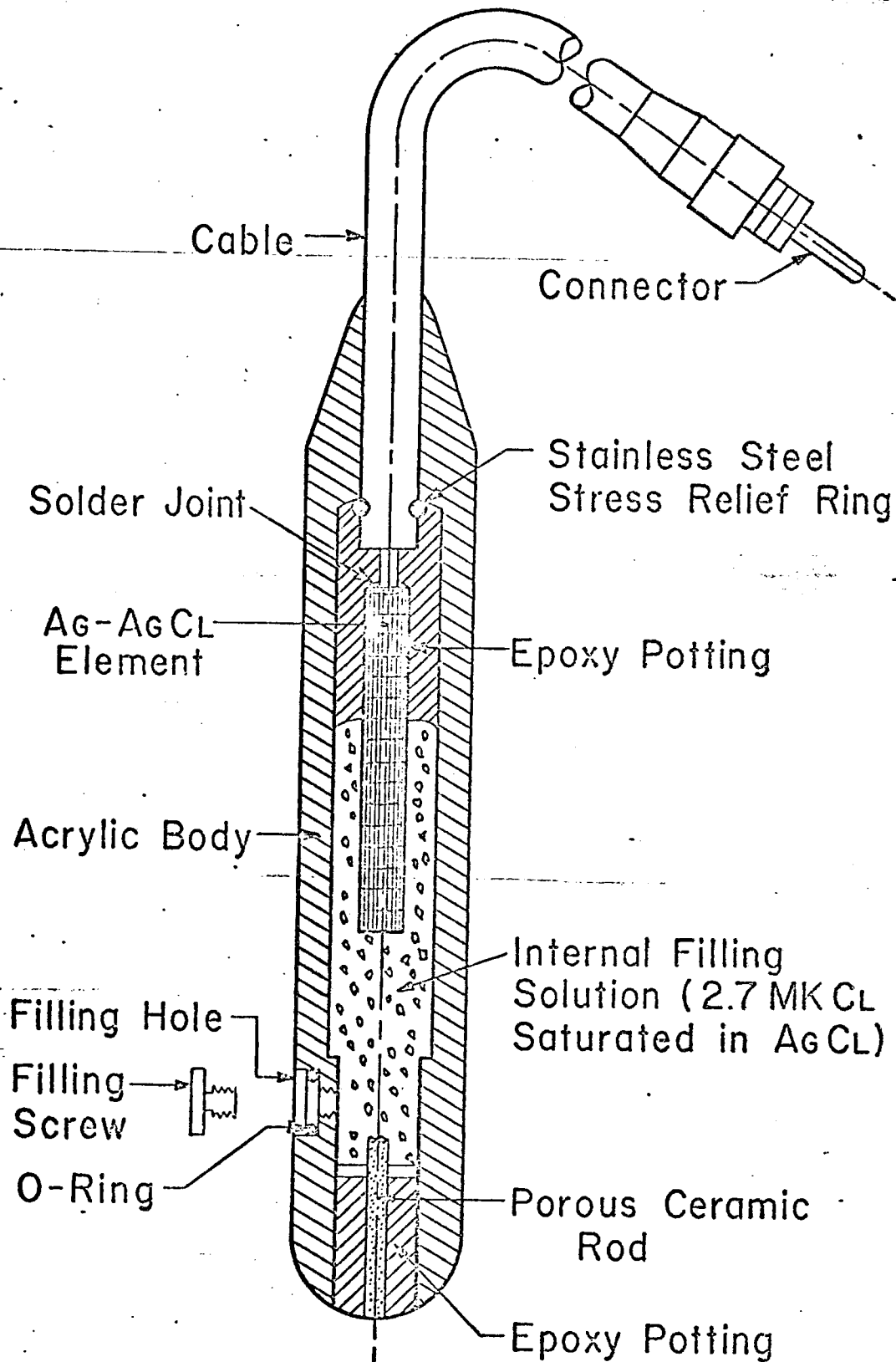


Figure 4-8

"CoCo" Electrode



The filling solution is potassium chloride (KCl) saturated with silver chloride. The KCl solution may be saturated if only relatively warm water temperatures are expected, but if water temperatures near 0°C may be encountered, the KCl solution is made 2.7 M (see the section in this chapter on electrode temperature response). The solution is replenished or changed through the filling hole.

Contact with the sea water is made through a rod of porous ceramic (Coors #70001), which combines low impedance with a low fluid leakage rate. The electrode is capped when not in use by slipping an ordinary crutch tip (1" diameter) over the end of the body. The electrode has been stored for six months in this way, with storage drift of less than one millivolt.

The thermally coated silver-silver chloride element is made according to the "recipe" given by von Arx (1962, p. 276), using a firing time of 20 minutes at 460°C as suggested by Sanford (1967, p. 71). The solder joint connecting the element to the lead-out cable is fully potted in epoxy resin, precluding the possibility of spurious potentials arising from corrosion at the joint. Field experience proved that the towing cable will break before it is pulled out of the electrode.

The "CoCo" electrodes have an impedance of 1000 ohms and have been used extensively for offshore and onshore self-potential and resistivity studies. They have proven to have very low levels of noise and drift, excellent reproducibility, and acceptably low response to changes in environmental parameters. They also have proven to be extremely rugged and have survived a wide variety

of abuse, including being repeatedly stepped on, smashed against rocks, and inserted in boiling hot springs. The response of the "CoCo" electrodes to changes in salinity, temperature, and Eh is examined later in this section. Response to other parameters, including agitation, mechanical shock, and applied electric fields is discussed briefly at the end of the section.

Standard potential

The potential of a silver-silver chloride electrode in a chloride solution, measured against a standard hydrogen electrode, is given by:

$$E = E^{\circ} - \frac{2RT}{f} \ln \gamma_{\pm} \quad (4-9)$$

(Ives and Janz, 1961, p. 188), where γ_{\pm} is the activity coefficient of the chloride solution and E° is the value of the standard oxidation potential at infinite dilution (i.e. $\gamma_{\pm} = 1$ and $\ln \gamma_{\pm} = 0$). E° is a function of temperature, varying from +236 mv at 0°C to +165 mv at 95°C. For a "filled" electrode with the filling solution at a fixed concentration, it is convenient to define an electrode potential, E_e , for the electrode at the given filling solution concentration and temperature.

If E_e also is expressed as an oxidation potential, algebraic signs will agree with the polarities read on a voltmeter. For example, with a platinum electrode connected to the positive terminal and the "CoCo" electrode to the negative terminal of a voltmeter, the value of the redox potential (Eh) will be ($\Delta V_{\text{read}} - E_e$). Using Equation 4-9 and the values of γ_{\pm} for KCl as given by Latimer (1952, p. 355), E_e for a silver-silver chloride electrode filled with 2.7 M KCl at 20°C is found to be +198 mv, and for 4.2 M (saturated) KCl, the value

for E_e also is + 198 mv (Durst, 1969, p. 117).

To check these values, a solution with an Eh value of +430 mv was prepared (ZoBell, 1946, p. 495). A platinum electrode was connected to the positive terminal of a Keithley Model 600B electrometer, the electrode to be tested to the negative terminal, and both electrodes inserted in the standard solution. The results are tabulated below:

Positive Electrode	Negative Electrode	ΔV (mv)	E_e (mv)
1. Platinum	Beckman #39070 (Ag-AgCl, Sat. KCl)	+235	+195
2. Platinum	"CoCo", Sat. KCl	+236	+194
3. Platinum	"CoCo", 2.7 M KCl	+215	+215

In 1 M NaCl, the following result was obtained:

4. Beckman #39070	"CoCo", 2.7 M KCl	-13	+208
-------------------	-------------------	-----	------

(Ideal E_e is calculated as +198 mv in all cases).

The value for the saturated KCl "CoCo" electrodes is found to agree well with the theoretical value, but the values for the 2.7 M electrode differ considerably from those predicted. The discrepancy may be due to diffusion-adsorption potentials generated in the porous ceramic rod of the "CoCo" electrode; to an anomalous liquid junction potential in the ceramic rod; or to very slow reaction kinetics, i.e., many days may be required for the potentials to come to their final values (the tests were run in the space of several hours).

For practical purposes, in most natural media, the E_e value for the "CoCo" electrode filled with 2.7 M KCl may be taken as +210mv.

Response to salinity changes

The salinity of sea water is a defined parameter related to the concentration of dissolved salts in the water. The salinity of a seawater sample may be determined by a chemical titration process (Knudson, 1901), or by measurement of electrical conductivity (Cox, 1966). A Hytech (Bisset-Berman Corp., San Diego, Calif.) Model 6220 conductivity-type laboratory salinometer was used to measure salinity for this work. It is assumed for the following discussion that the relative abundance of the major constituents of sea water remains constant, regardless of salinity (Sverdrup and others, 1942, p. 166).

The average salinity of the oceans is about 35 ‰, and it ranges between about 33 ‰ and 37 ‰ in the open ocean (Sverdrup and others, 1942, p. 55). Most offshore prospecting, however, would be done in near-shore and estuarine environments, where the salinity range may be much greater. Mineral deposits in Alaska and Maine, for example, are found in coastal areas where fresh-water rivers empty into the sea, so salinity in the area of interest may range from oceanic values to near zero. On the other hand, bodies of warm, shallow, stagnant water may have salinities appreciably higher than oceanic values. The salinity of the Red Sea is about 43-45 ‰, and some lagoons off the Gulf of Mexico have even higher salinities (Neumann and Pierson, 1966, p. 39).

It is evident, then, that electrode pairs used in the near-shore and shallow water environments may be subjected to much larger changes in salinity, over shorter periods, than those used in the open ocean, where salinity gradients are unlikely to exceed 0.0001‰ over a distance of 100 meters, and the change of salinity with

respect to time may be a maximum of 0.5‰ per minute (von Arx, 1950, p. 46).

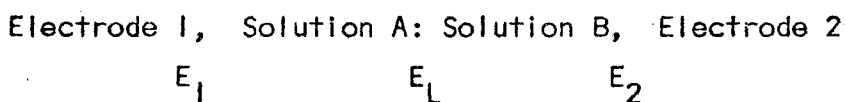
Response to simultaneous salinity change at both electrodes

Ideally, the potential difference between a pair of identical electrodes will not change as the salinity of the water in which they are both immersed is varied, if the salinity variation is identical and simultaneous at both electrodes. In practice, small manufacturing differences will produce potential changes. Figure 4-9 shows the variation as a function of time, and Figure 4-10 shows the variation as a function of salinity change, for a pair of "CoCo" electrodes.

It may be seen from Figure 4-9 that the response is quite rapid. From Figure 4-10, it is evident that, for any salinity change likely to be encountered while towing an electrode pair offshore, the response will be less than one millivolt. Over most of the range of S_2 the response varies linearly with the log of S_2/S_1 , where S_1 is the initial salinity and S_2 is the final value. ΔV approaches a limiting value of about one millivolt at very low values of S_2 .

Differential salinity changes

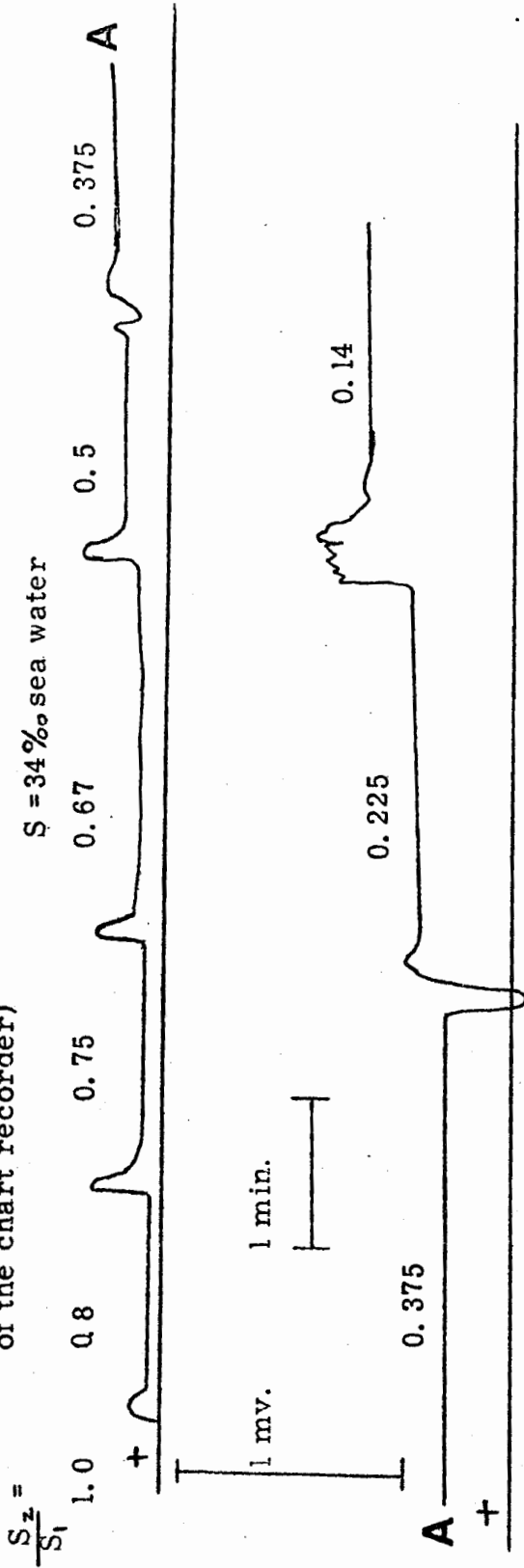
Two electrodes, immersed in different solutions A and B and connected by a liquid junction, may be represented by the formulation:



(4-10) (the colon indicates a liquid junction)

The potential between the two electrodes will be $(E_1 + E_L + E_2)$, where E_1 is the potential between electrode 1 and solution A, E_L

(the electrode in the more dilute solution was connected to the positive input terminal of the chart recorder)



Time Response to Simultaneous Salinity Change at Both Electrodes

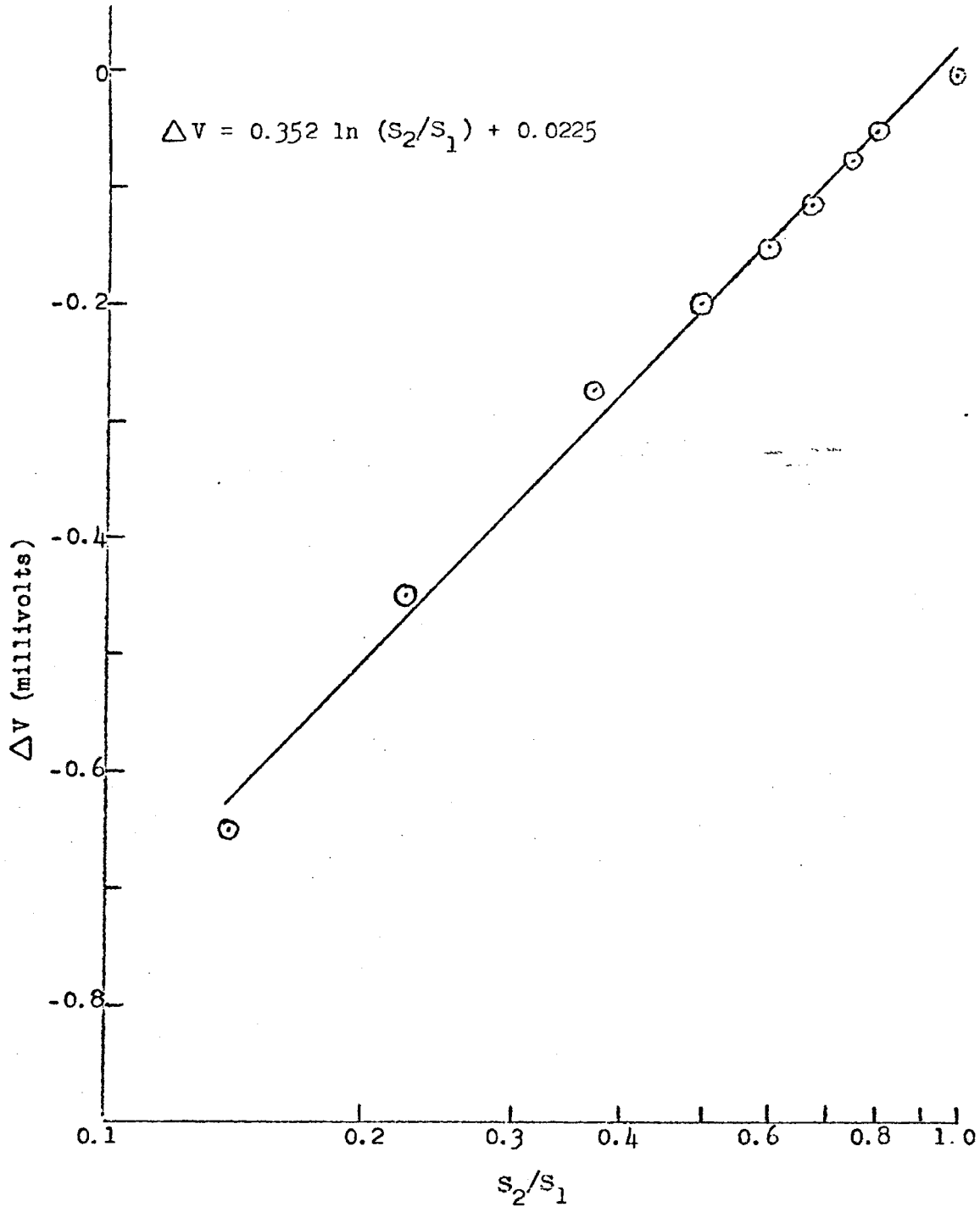
FIGURE 4-9

Figure 4-10

Potential Difference Due to Simultaneous Salinity Change
at Both Electrodes

"CoCo" Electrodes

S_1 = Sea water, 34 ‰



is the liquid junction potential, and E_2 is the potential between solution B and electrode 2. The electrode potentials E_1 and E_2 may be calculated as described previously in this section, while the liquid junction potential E_L may be found by use of the Henderson

equation:
$$E_L = \frac{RT}{\mathcal{F}} \frac{\sum_n \frac{u_i}{z_i} (C_{iB} - C_{iA})}{\sum_n u_i (C_{iB} - C_{iA})} \ln \frac{\sum_n C_{iA} u_i}{\sum_n C_{iB} u_i}$$

(4-11)
where:

u_i = the mobility of ion i

z_i = the valence of ion i

C_i = the molarity of ion i in solution A or B,

as defined by MacInnes (1961, p. 231).

For the simplest situation, where A and B are two solutions of the same univalent salt at concentrations C_1 and C_2 , the total potential ($E_1 + E_L + E_2$) between the two electrodes reduces to

$$(E_1 + E_L + E_2) = E = \frac{-2RT}{\mathcal{F}} \int_{C_1}^{C_2} t_+ d \ln a_{\text{solution}}$$

(4-12)

where t_+ is the transport number of the positive ion, and a_{solution} is the activity of the solution as a function of concentration.

Specifically, when the solutions are sodium chloride,

$$E = \frac{-2RT}{\mathcal{F}} \int_{C_1}^{C_2} t_{\text{Na}^+} d \ln a_{\text{NaCl}}$$

(4-13)

Because sea water is an extremely complex solution, for which all the ion mobilities are not well established, it would be impossible to calculate the liquid junction potential E_L for a sea water concentration cell. In order to compare the theoretical and the actual response of an electrode to a concentration change at one of the electrodes, it is necessary to use a concentration cell with simple solutions, such as sodium chloride, and extrapolate the

results to sea water.

Sanford (1967, p. 140) performed an experiment in which "packed" Ag-AgCl electrodes were inserted in containers holding 1.0 M NaCl solution, joined by a salt bridge. Distilled water was then added to one container to lower the concentration to 0.8 M, and the potential between the electrodes was recorded as a function of time (Figure 4-11). A similar experiment was performed using sea water, with distilled water added to one container to bring the salinity to 0.8 times the initial value. The final potential for the NaCl experiment, as determined from Equation 4-13 for a temperature of 20°C, t_{Na^+} assumed constant at 0.382, and using activity values from Latimer (1952, p. 356), is + 4.2 mv, in good agreement with the experimental results. (The computation of this value is given in Appendix 4-1). The final potential for the sea water experiment was + 3.94 mv, slightly lower than that from NaCl. By assuming that sea water behaves as an NaCl solution of equal ionic strength, Sanford arrived at an "apparent transport number" for sea water, t_{sw^+} , of 0.355, for salinities between 33 ‰ and 38 ‰. This value may be used in Equation 4-12 to predict the potential of a sea water concentration cell for "packed" electrodes.

The concentration cell potential between a pair of "filled" electrodes, such as the "CoCo" design, will be different from the potential measured by a pair of "bare" or "packed" electrodes. The situation may be represented by

Electrode 1, Solution 1:Solution 2:Solution 3:Solution 1, Electrode 2

E_1 E_2 E_3 E_4 E_5

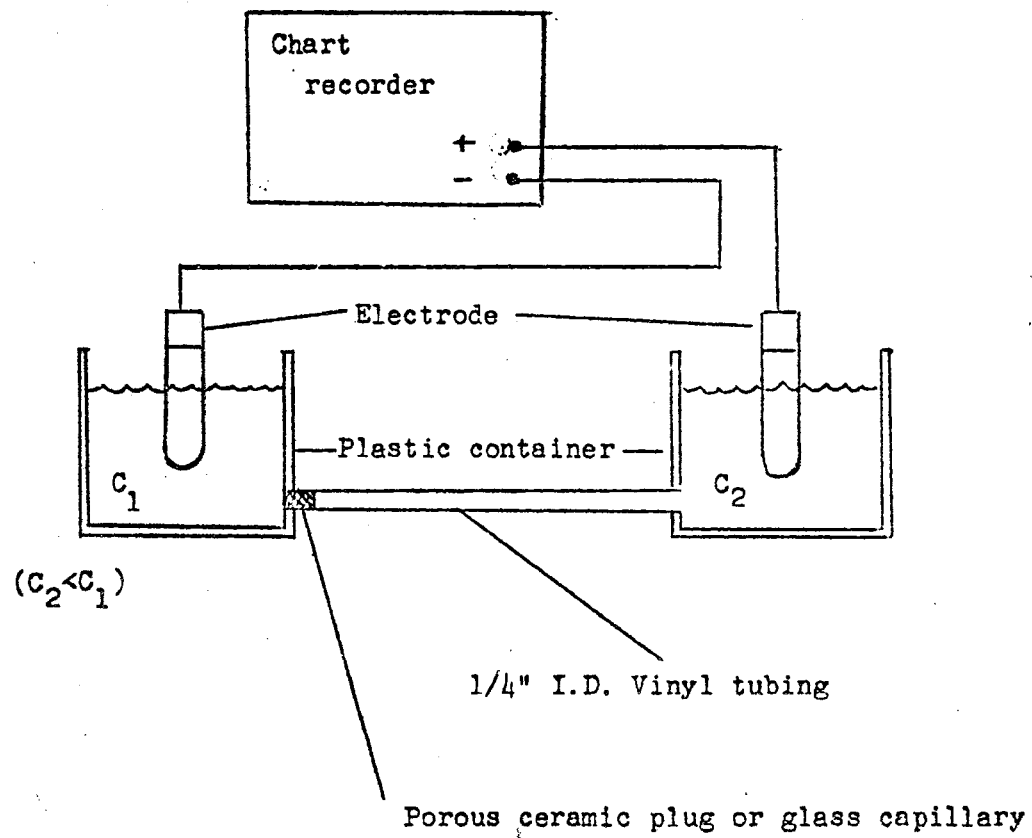
(4-14)

and the potential between electrodes 1 and 2 by $(E_1 + E_2 + E_3 + E_4 + E_5)$. Because electrodes 1 and 2 are in identical solutions, $E_5 = -E_1$, so the potential is the sum of the liquid junction potentials, $(E_2 + E_3 + E_4)$. These potentials for simple solutions such as NaCl and KCl may be calculated by Equation 4-11, but if ions appear on one side of the junction that are not present on the other (e.g. a KCl: NaCl junction), the potentials have been found to depend upon the manner in which the junction was formed (MacInnes, 1961, p. 226).

The liquid junction potential E_3 , between the two sea water solutions 2 and 3, may be calculated by the use of Equation 4-12, using 0.355 for the value of t_{sw+} . The potentials E_2 and E_4 , which are for the junctions KCl: sea water ₂ and sea water ₃: KCl will depend upon the nature of the distribution of sea water and KCl in the porous ceramic rod, and will be difficult to predict analytically. Again, NaCl test solutions may be used to infer the behavior of the more complex sea water case.

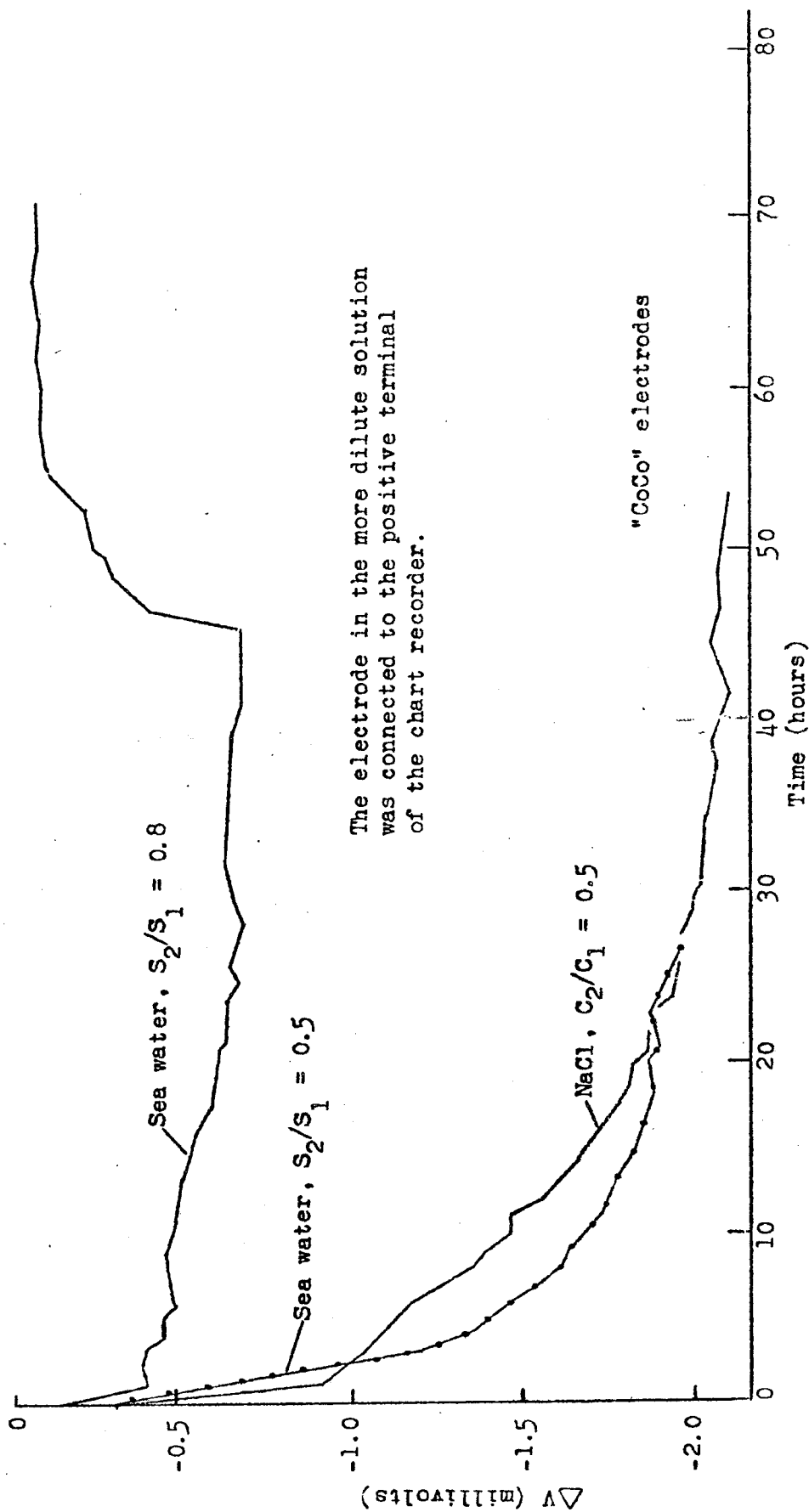
The potential across the cell

Ag, AgCl, KCl (2.7 M): NaCl (1 M): NaCl (0.5 M): KCl (2.7 M), AgCl, Ag calculated by Equation 4-11, is -2.6 mv (see Appendix 4-2). This cell was constructed in the laboratory (Figure 4-12), and the response of the system to a step change from 1.0 to 0.5 M NaCl recorded as a function of time (Figure 4-13). The potential after 53 hours, when the test was terminated, was -2.1 mv. The response curve consists of a small, rapid initial response, followed by a very slow drift to the final value. It is possible that the value might have been somewhat more negative had more time been allowed to elapse. The experiment was repeated for sea water concentration cells with $S_2/S_1 = 0.5$ and 0.8, with the results shown



Concentration Cell Test Arrangement

Figure 4-12



Long-Term Response to Differential Concentration Change

Figure 4-13

6 11 19

in Figure 4-13. From Figure 4-14, the relationship between ΔV at 29 hours and S_2/S_1 is

$$(4-15) \quad \Delta V = 2.9 \ln \frac{S_2}{S_1} ; S_2 < S_1 ; 9 \leq S \leq 35 ; T = 20^\circ \text{C}.$$

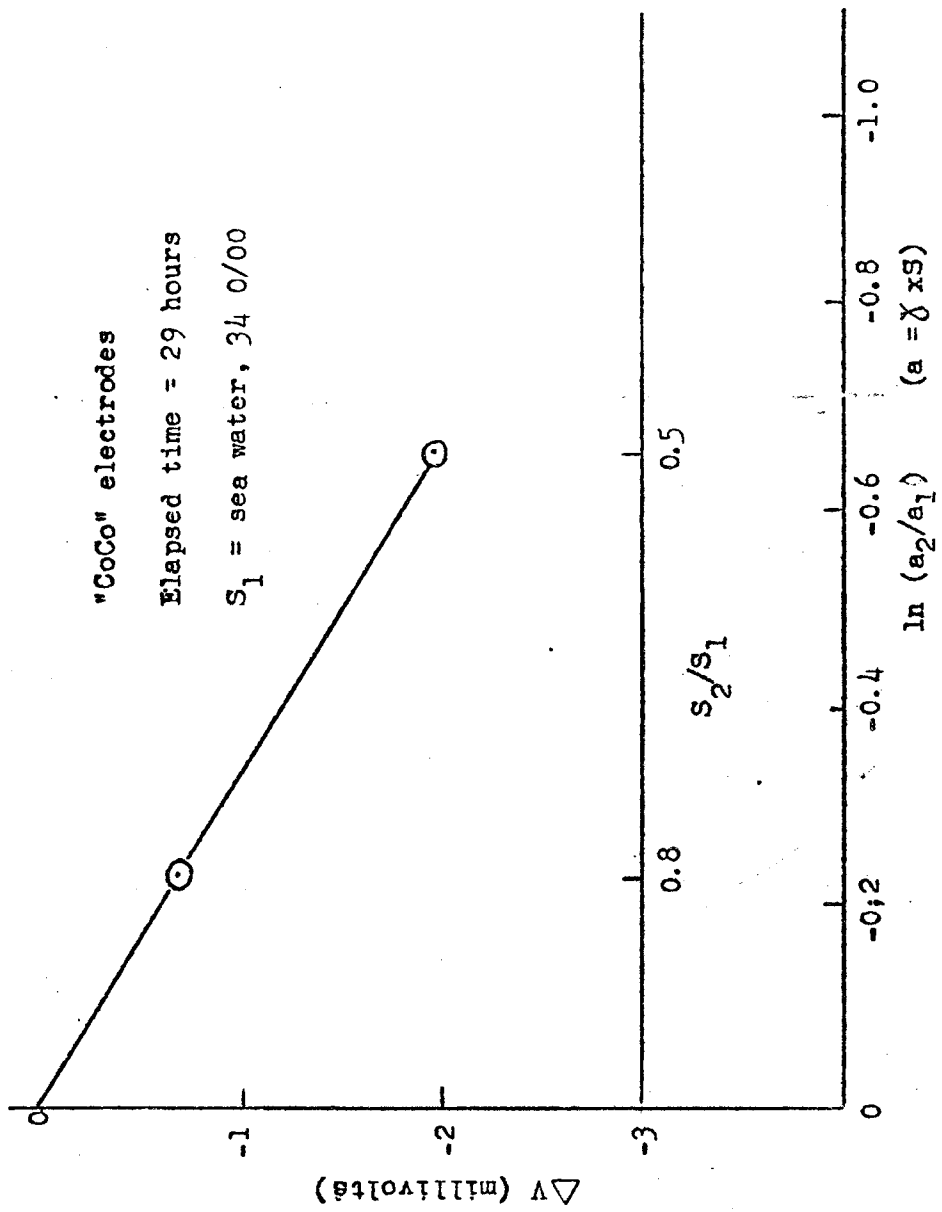
The small, rapid response also was measured over a range of S_2/S_1 values, with the results shown in Figures 4-15 and 4-16. Although the response varied somewhat as the experimental arrangement was changed, the formula

$$(4-16) \quad \Delta V = 0.52 \ln \frac{S_2}{S_1} ; S_2 < S_1 ; 9 \leq S \leq 35 ; T = 20^\circ \text{C}.$$

may be used to calculate, with an accuracy of about $\pm 20\%$, the potential difference between two "CoCo" electrodes, one minute after a differential step change in salinity.

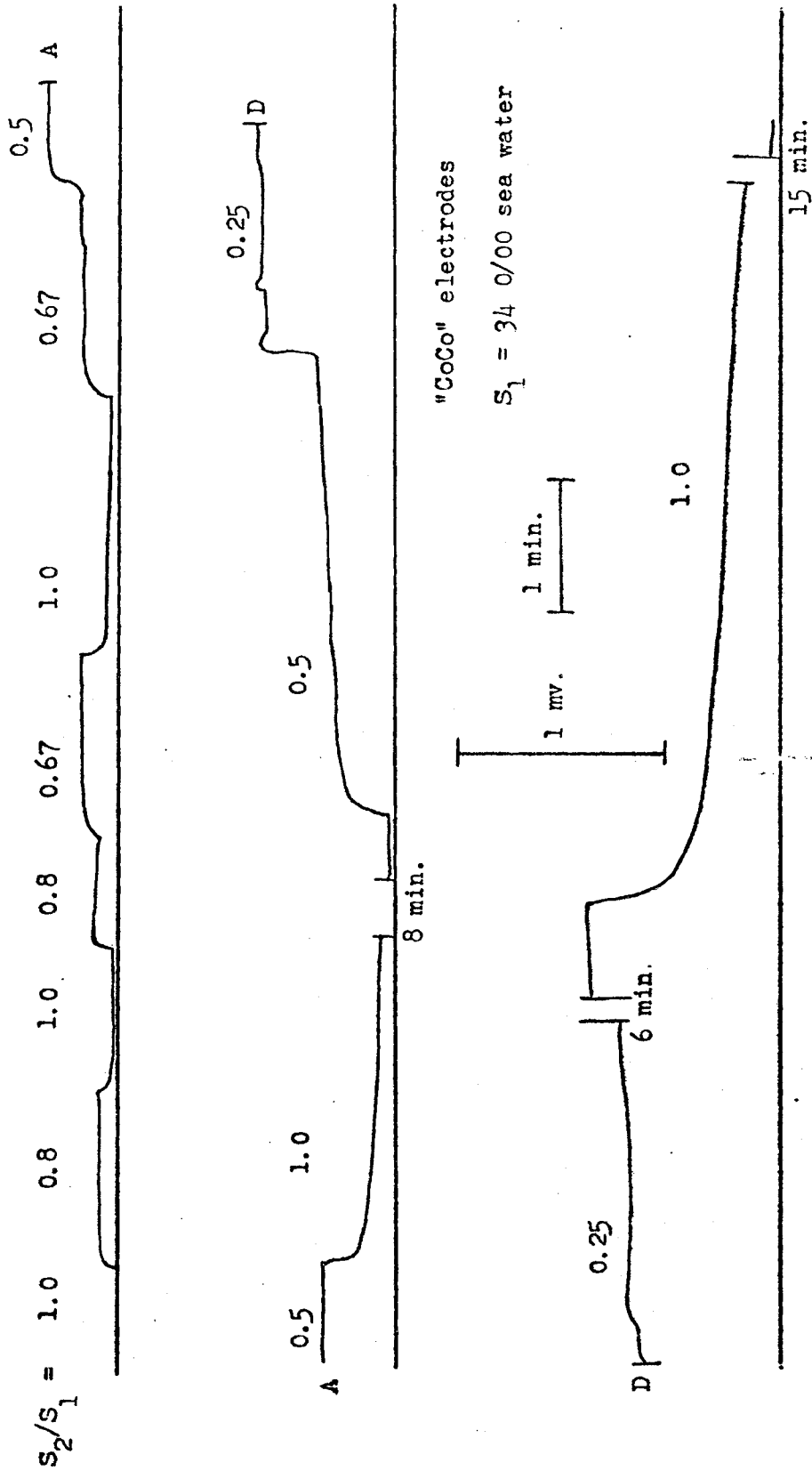
Response to temperature changes

Open ocean water temperatures range from about -2°C to $+30^\circ\text{C}$, with higher maxima possible in landlocked areas (Sverdrup and others, 1942, p. 55). Temperatures in shallow estuaries and in areas of geothermal activity may be considerably higher than 30°C . An electrode pair used in an offshore self-potential survey, then, may be subjected to simultaneous or differential temperature changes when being towed through currents, areas of upwelling, internal waves, or geothermal areas; past the mouths of rivers entering the sea; or when used to make vertical measurements in the water column. The magnitude of these changes generally will not exceed a few degrees, although changes of a few tens of degrees may be possible in some cases.



Long-Term Potential Difference vs. Differential Salinity Change
Figure 4-14

NOV 1964



Short-Term Response to Differential Salinity Change

Figure 4-15

Handwritten notes and markings on the right margin of the page.

Figure 4-16

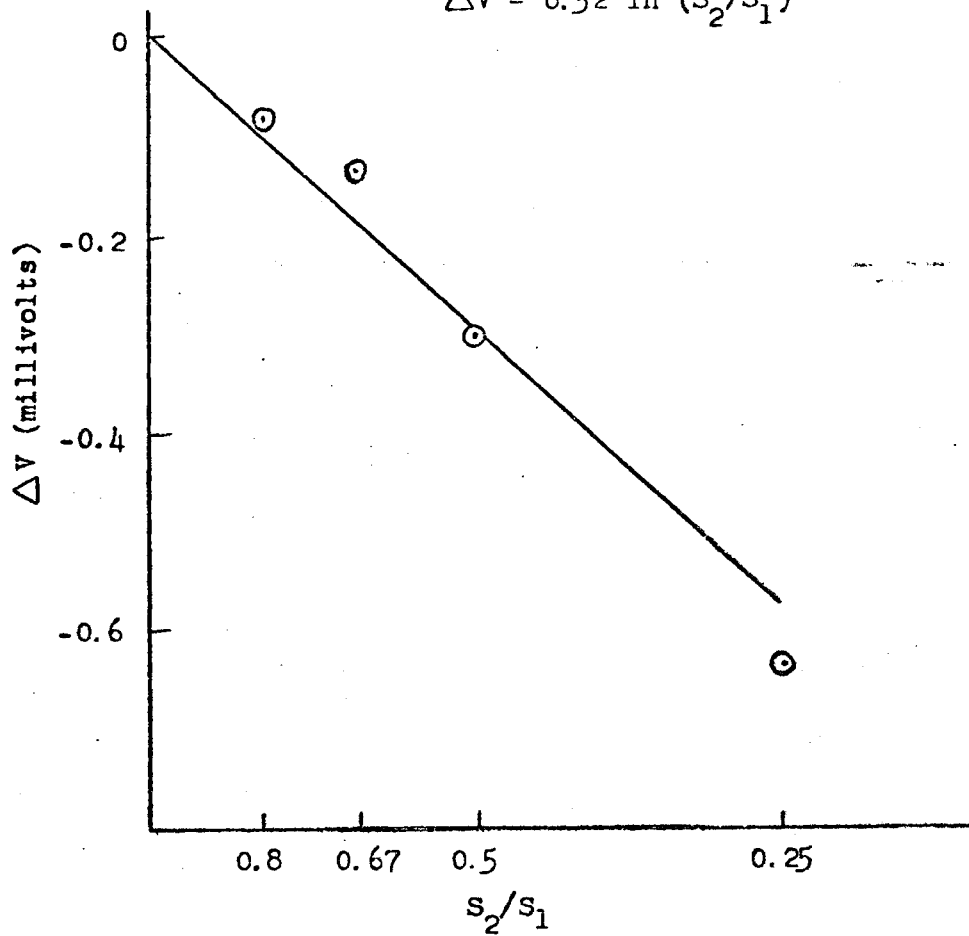
Short-Term Potential Difference vs.
Differential Salinity Change

"CoCo" electrodes

$S_1 = 34.0/00$ sea water

Elapsed time = 1 min.

$$\Delta V = 0.52 \ln (S_2/S_1)$$



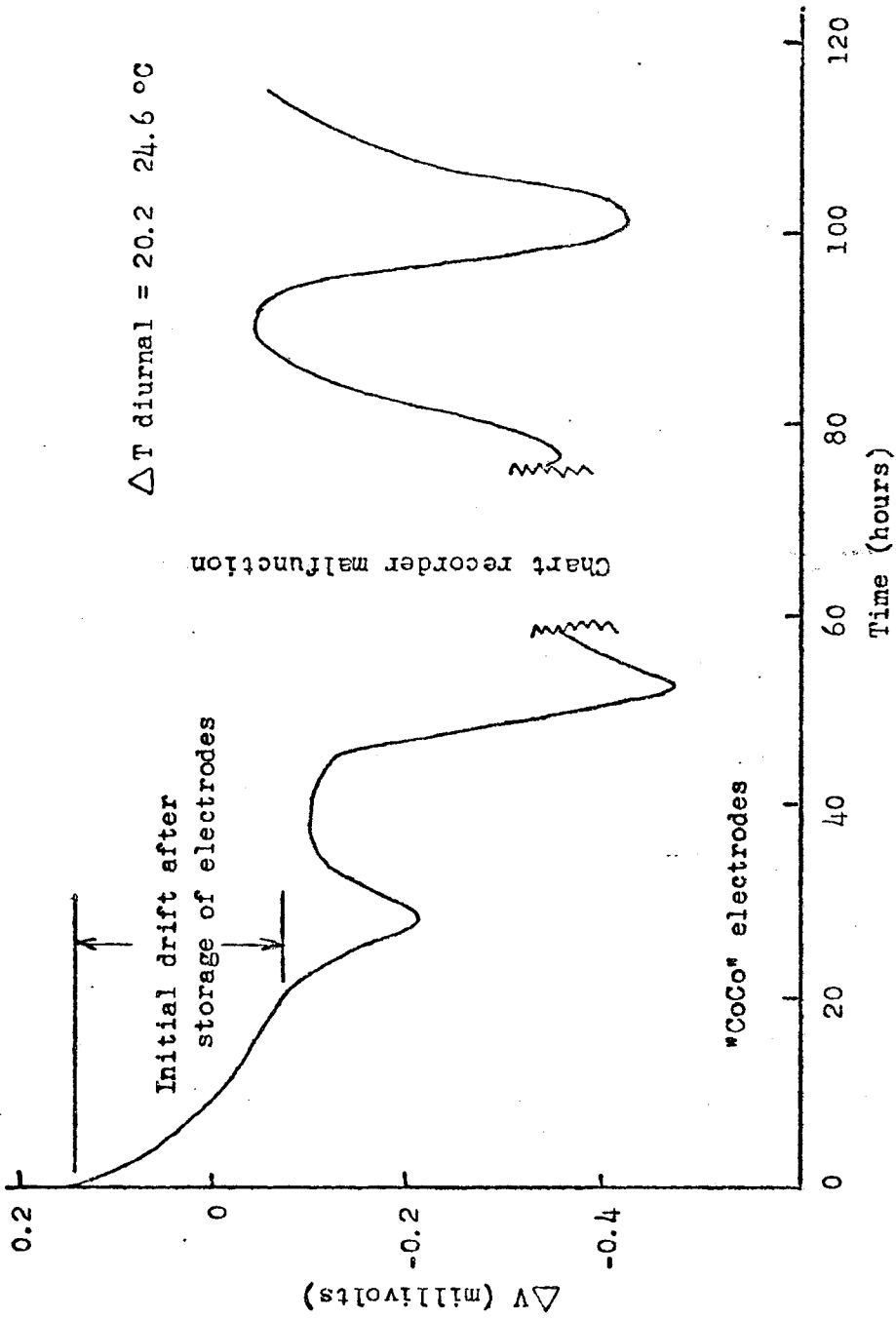
Simultaneous temperature change at both electrodes

An identical and simultaneous temperature change at both electrodes should produce no change in the potential difference between the two electrodes. Manufacturing differences, however, could lead to such changes.

To test the effect of such a temperature change, a pair of "CoCo" electrodes was placed in a container of sea water ($S = 34.7‰$) at 24.3°C. Chilled sea water was added to reduce the temperature to 17.7°, followed by addition of heated sea water to raise the temperature to 42.5°C. No significant change in the potential between the electrodes was observed over a period of 11 minutes from the change from 17.7° to 42.5°, nor was any voltage change observed during a 7 minute period following the change from 23.4° to 17.7°. In a longer term (five days) drift test, a diurnal potential change with an amplitude of about 0.3 mv was observed (Figure 4-17). The period of this change appeared to correlate with the diurnal change in the temperature of the sea water in which the electrodes were immersed (about 4.4°C). The value of $\Delta V / \Delta T$ from this data is about 0.1 mv/ °C.

Differential temperature changes

The potential V of the cell
 Electrode, Solution (C_1, T_1): Solution (C_2, T_2), Electrode
 where C is the concentration and T is temperature, cannot be calculated from the conventional temperature coefficient of the electrode (Tyrell and Hollis, 1949; Tyrell and Colledge, 1954). The potential is a function of the concentration and temperature of the solution and of the nature of the dissolved ions which form the solution. This potential has been measured for Ag-AgCl



Long-Term Drift Test

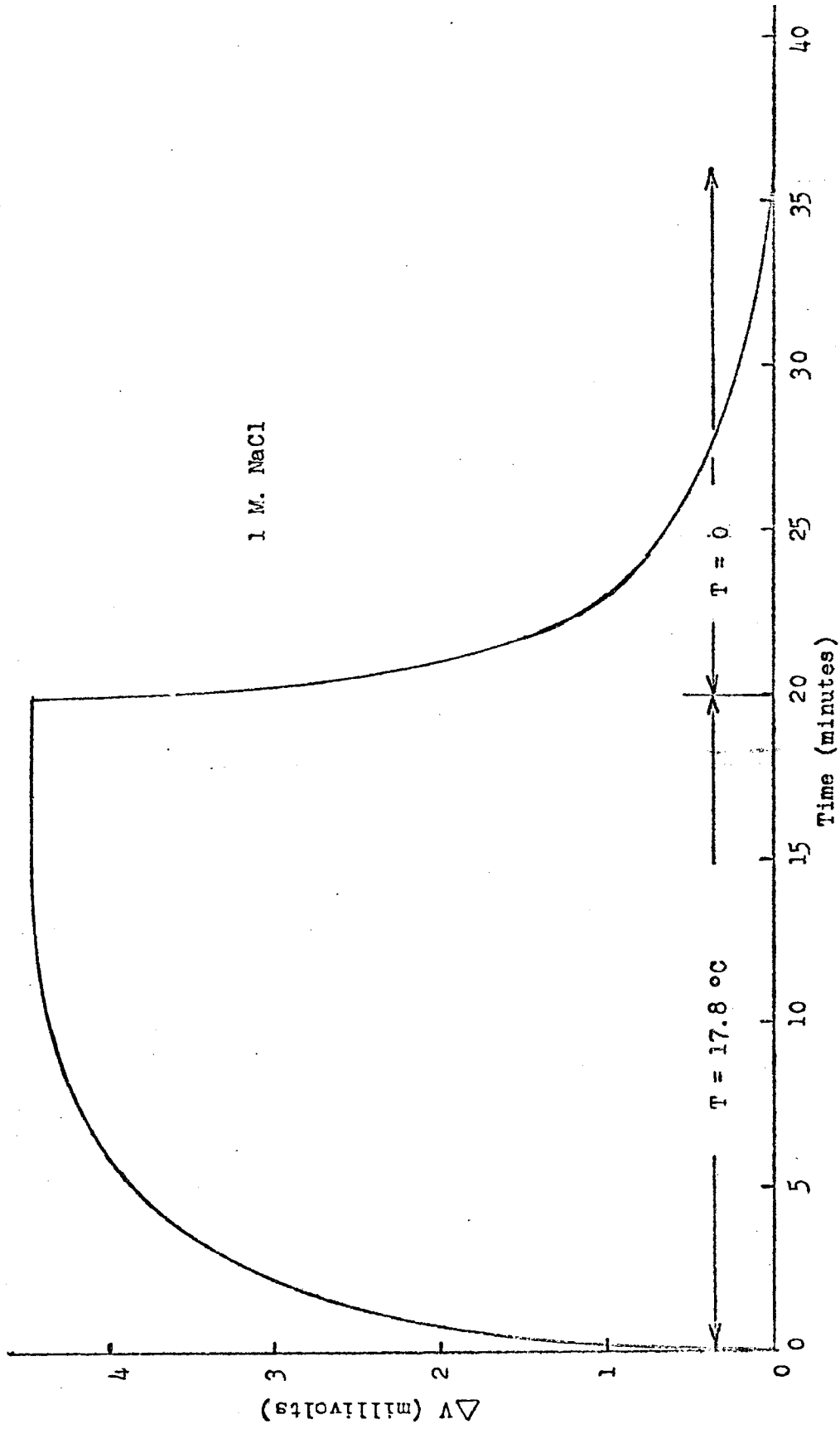
Figure 4-17

electrodes in thermal cells of various solutions by Haase and Schönert (1960) who present value of E_o , where E_o is defined as dV/dT in $\mu v/^\circ C$, as a function of solution type, concentration and temperature.

Sanford (1967, p. 147) measured the value of E_o for a "packed" electrode in 0.75 M NaCl at $3^\circ C$ to $20^\circ C$ and found E_o to be $277 \pm 11 \mu v/^\circ C$, close to the value predicted by Haase and Schönert. Sanford then repeated the experiment for sea water, $S = 36.98 \text{ ‰}$ and $T_1 = 22^\circ$, and found a value for E_o of $364 \mu v/^\circ C$. (The warmer electrode was positive).

I conducted similar experiments with "packed" electrodes and with the "CoCo" electrodes to determine both the magnitude and the time nature of the response to a step change in temperature. As suggested by Sanford, I used a 1000 ml graduate, filled with 1 M NaCl, as the electrode container. The upper end was at room temperature ($20^\circ C$) and the lower end was chilled in a bucket of ice, so a temperature step function could be applied to one electrode by moving it rapidly from the top to the bottom of the graduate or vice versa, while the other electrode was held stationary.

Results of these tests on the "packed" electrodes are shown in Figure 4-18. The electrodes reached equilibrium in about 20 minutes, and the final value of E_o was $250 \mu v/^\circ C$, close to the value of $237 \mu v/^\circ C$ given by Haase and Schönert for 1 M NaCl at a mean temperature of $25^\circ C$ (the value of E_o for other chloride solutions increases as the temperature decreases, and it should be different for the mean temperature of about 10° used in these tests.)

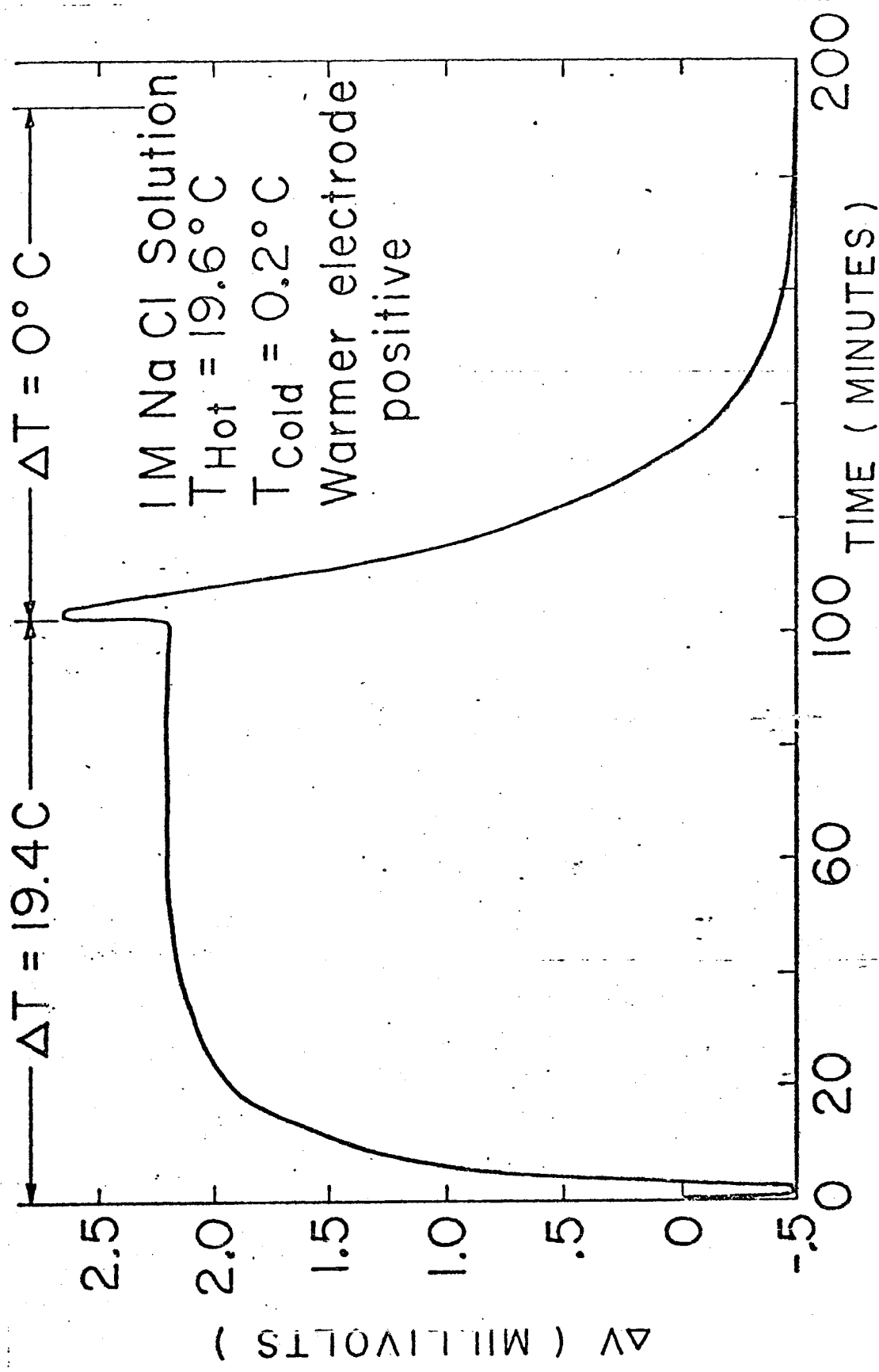


Temperature Step Response for "Packed" Electrodes
Figure 4-18

The result of a temperature step of 19.4°C applied to a pair of "CoCo" electrodes filled with 2.7 M KCl is shown in Figure 4-19. The electrodes required about an hour to come to equilibrium (probably due to the greater thermal insulation provided by the "CoCo" electrode housing) and the average final value of E_o for several such tests with a mean temperature of 10°C was 140 $\mu\text{v}/^\circ\text{C}$. The data of Haase and Schönert for KCl goes only to 2.0 M, but by assuming their results can be extrapolated to 2.7 M, a value of 210 $\mu\text{v}/^\circ\text{C}$ for E_o at 10°C may be obtained. This value differs considerably from that obtained experimentally, and may be due to liquid junction potentials across the KCl-NaCl interface. Another possible explanation for the discrepancy is that it may not be possible to simply extrapolate the data of Haase and Schönert from 2.0 M to 2.7 M. The value of 140 $\mu\text{v}/^\circ\text{C}$ for dV/dt (warmer electrode positive) was repeatable to $\pm 15\%$ over a range of 8°C to 12°C mean temperature, and seems to represent a good working number.

Several important points about thermal potentials must be noted. First, in order for a thermal potential to appear across the electrodes, the temperatures of the electrolyte solutions in contact with the electrode elements must be different. This is why the salt bridge system shows no response to a temperature cell - the electrode elements are aboard ship, and temperature changes in the sea are not transmitted to the electrode elements.

Second, a filling solution which is saturated with KCl at room temperature is not satisfactory for use in an electrode which may be subjected to cold (near 0°C) water temperatures.



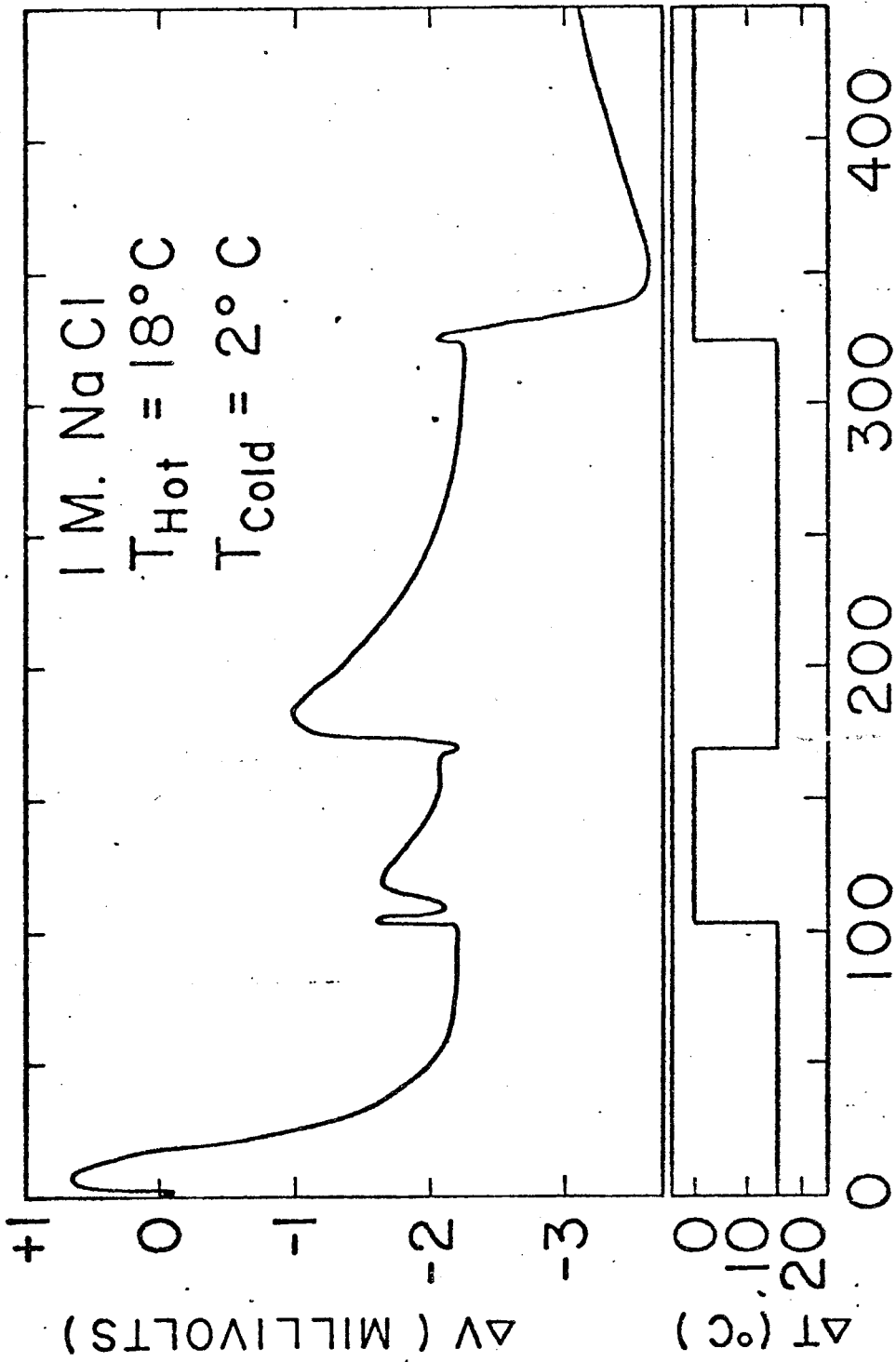
Temperature Step Response for 2.7 M. "CoCo" Electrodes

Figure 4-19

Apparently, when the ambient temperature is reduced KCl will precipitate in the pores of the ceramic junction. When the temperature is increased, the KCl comes out of solution very slowly. These precipitation and dissolution processes apparently generate potential differences across the junction which are, over short periods, irreversible. The result of applying several successive temperature steps of 16°C to a pair of "CoCo" electrodes filled with saturated KCl is shown in Figure 4-20. Two days were required for the electrodes to return to their original zero potential at the same temperature. To avoid this problem, the concentration of KCl in the filling solution is made low enough so that KCl will not precipitate out of solution at 0°C . Ben-Yaakov and Kaplan (1968) used a 2.7 M KCl solution, which is 75% of the 3.6 M KCl concentration which will just precipitate at 0°C (Goldhaber, 1972, personal communication). The 2.7 M KCl concentration also was used in the "CoCo" filling solution, and no further problems were encountered with reversibility of response to temperature steps.

Third, for "filled" electrodes, the nature of the thermal cell response is determined only by the filling solution, and not by the external medium (discounting possible liquid junction effects). Thus, the thermal cell response for the "CoCo" electrodes should be the same in NaCl as in sea water.

Fourth, from Figure 4-19, it may be seen that the response curve shows an initial "kick" of about 3 to 5 minutes in the opposite direction from the equilibrium value (i.e., the warmer electrode goes negative before going positive). In a towing situation, it is likely that many temperature profiles will be



Temperature Step Response for Saturated "CoCo" Electrodes

Figure 4-20

traversed in less than 3 to 5 minutes, so interpretation of temperature anomalies from the self-potential record must take this "kick" into account.

Finally, it has been noticed that the "CoCo" electrodes must be soaked for at least 12 hours after storage before a repeatable thermal cell response may be obtained. Apparently, during long-term storage the porous ceramic junctions tend to dry out, allowing the KCl solution in the junctions to become saturated, and leading to non-repeatable responses as shown in Figure 4-20. Soaking the electrodes in NaCl solution or sea water overnight gives results as shown in Figure 4-19.

Response to Eh changes

The definition and measurement of Eh (also called oxidation potential or redox potential) are discussed in Chapter 2. An electrode of the second kind which gains and loses electrons at a constant potential (Equation 4-6) theoretically will not respond to changes in Eh. However, a change in Eh necessarily implies a change in the concentration of the chemical components controlling the Eh, and thus the existence of a concentration cell. But, because the concentration of the ions controlling the Eh of normal, oxidizing sea water is so low, it is unlikely that the "CoCo" electrodes would respond to any measurable degree to the concentration cell potential corresponding to a difference in Eh.

In strongly reducing water or bottom muds, however, the concentration of the sulfide ions controlling the Eh is high enough to produce measurable concentration cell potentials across the "CoCo" electrodes. The experimental arrangement shown in

Figure 4-21 was used to study the response of the "CoCo" electrodes to an extreme change in Eh. The oxidizing solution had an Eh value of + 430 mv (ZoBell, 1946, p. 495), and the reducing mud (from San Francisco Bay), an Eh of about 0 (the Eh of the mud varied by several tens of millivolts from point to point and from time to time). The total difference in Eh between the mud and the oxidizing solution was, then, about 430 mv.

The potential between a pair of "CoCo" electrodes both inserted in the mud was -0.2 mv. When the positive electrode was moved into the oxidizing solution, the potential jumped to -5 mv, drifting slowly to a value of - 8 mv in a period of 19 hours, when the test was terminated. Several days of soaking in normal sea water were required for the electrode pair to return to their initial potential difference.

Response to agitation and mechanical shock

A pair of "CoCo" electrodes was immersed in a plastic container holding sea water at 32.7 ⁹⁰⁰ and 17°C. The pair was agitated violently and knocked against each other and the container for a period of about one minute, with the result shown in Figure 4-22. The positive peaks were due to one electrode being removed completely from the water; the negative peaks due to removal of the other electrode. There appears to be essentially no response to the agitation or shock.

Response to applied electric fields

A lag in the time response of the electrodes to a rapidly varying external electric field would be extremely undesirable, as the true signal in the water would have to be obtained by deconvolution of the apparent signal and the electrode response.

Figure 4-21

Test Arrangement for Eh Response

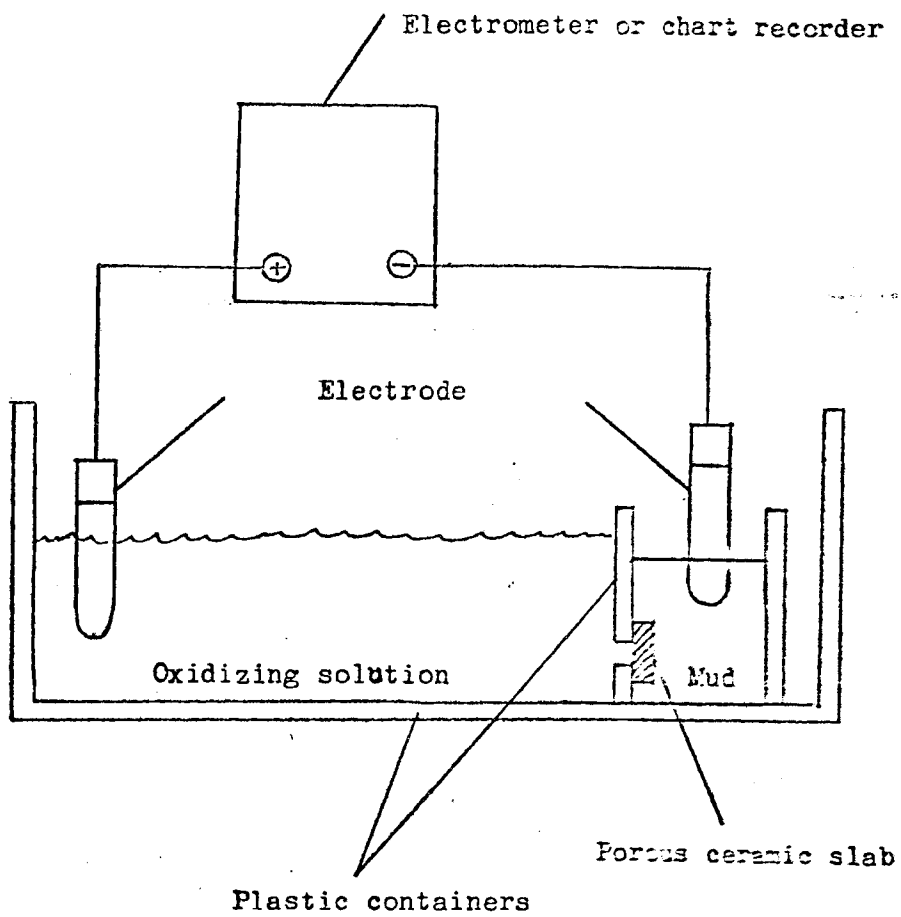


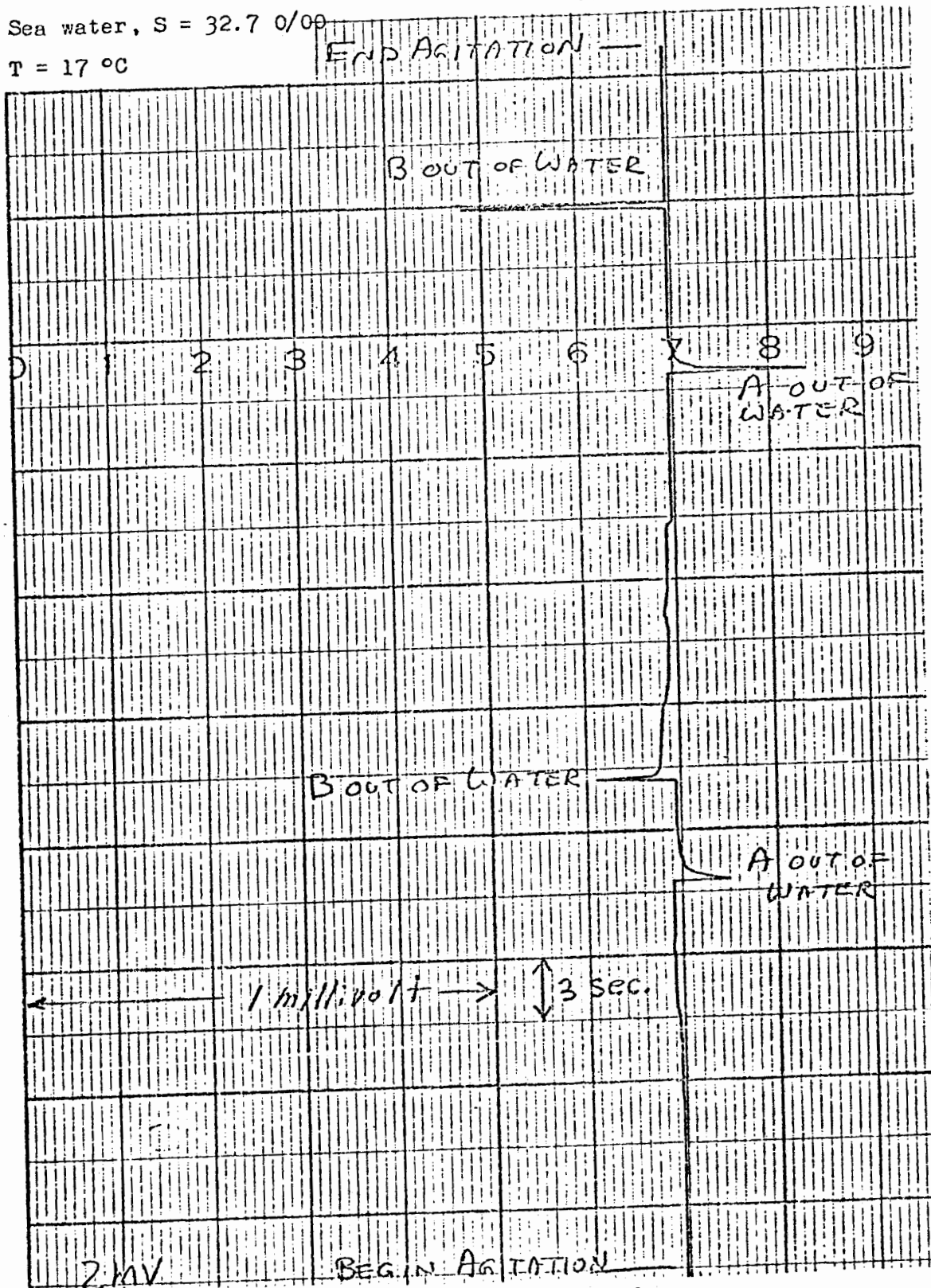
Figure 4-22

Response to Shock and Agitation

"CoCo" electrodes

Sea water, S = 32.7 ‰

T = 17 °C



To check the electrode time response, a pair of "CoCo" electrodes was inserted into a plastic container filled with sea water at 20°C and 32.7‰ salinity, together with a pair of graphite current electrodes connected to a power supply. The power supply was turned on and off, and the potential between the "CoCo" electrodes recorded on a Keithley model T 171B chart recorder. The output is shown in Figure 4-23. Response is essentially instantaneous, with the negative drift while the power supply is on being due to polarization of the current electrodes.

To test the electric field response under actual operating conditions, an electric field was generated in San Francisco Bay, using the arrangement shown in Figure 4-24. The ship was run on lines parallel to the dock at distances DB of 20, 40, 80, 160 and 320 feet. The signal measured at DB = approximately 40 ft (12 m) is shown in Figure 4-25, along with the theoretical signal from a point source and sink of current on the surface of the water at DB = 10 and 12 m, assuming the water to be a perfect half-space. The measured signal is seen to be quite close to the theoretical curve, with the differences probably mainly due to the fact that the ship's course was neither perfectly straight, nor perfectly parallel to the dock.

The theoretical and measured peak values of the signal are plotted against distance DB in Figure 4-26. The fact that the measured values are higher than the theoretical values probably is due to the fact that the water was not a perfect half-space, but had a depth of about 40 ft. at the dock.

Chart recorder

The chart recorder used throughout these studies is the

Figure 4-23

Response to Electric Field Step Input

"CoCo" electrodes

Sea water; S = 32.7 0/00, T = 17 °C

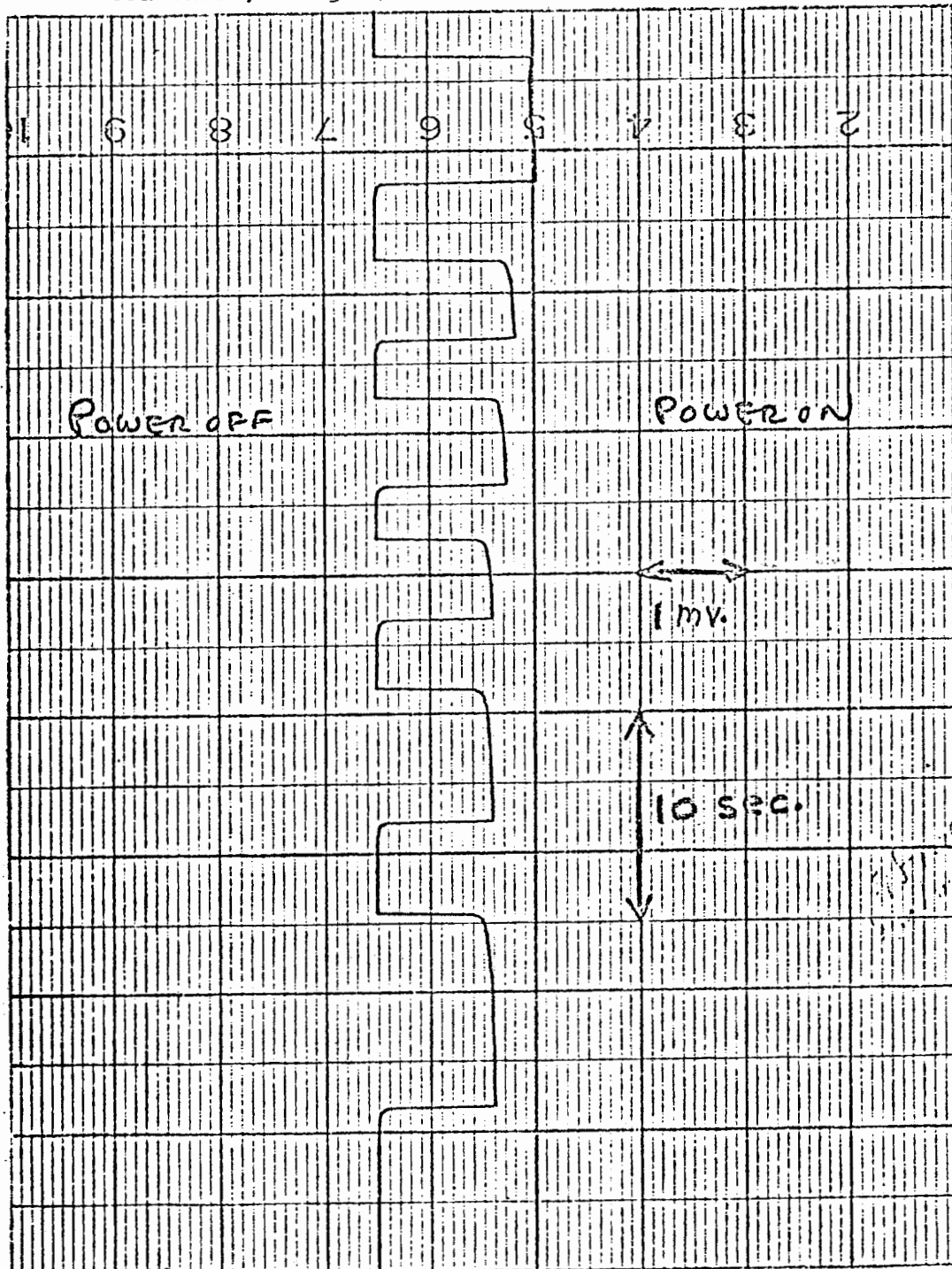
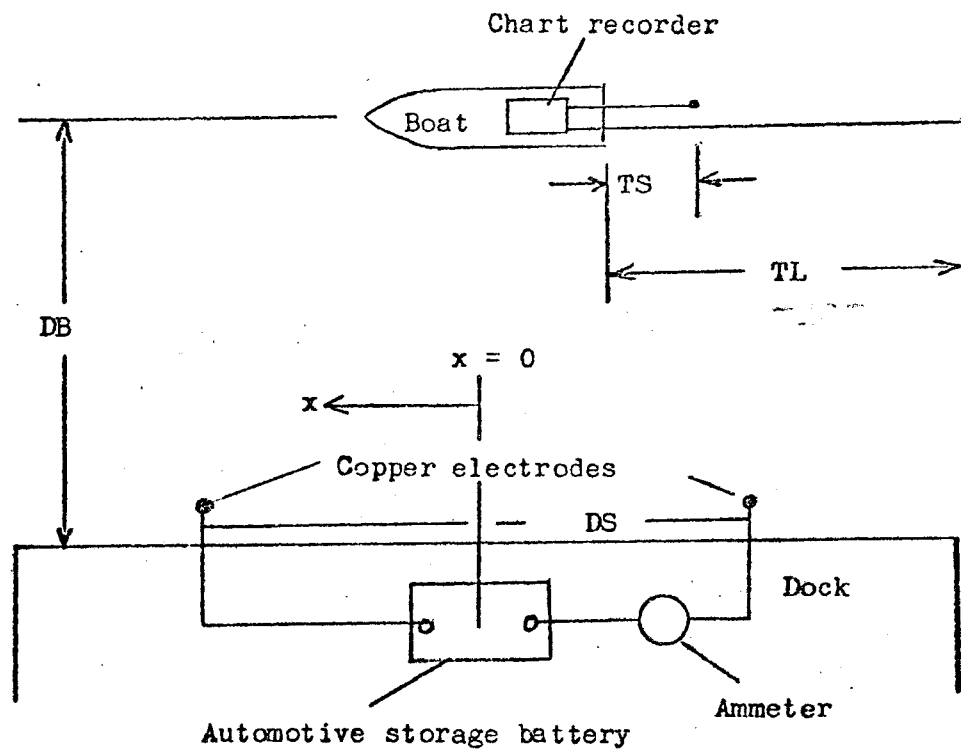
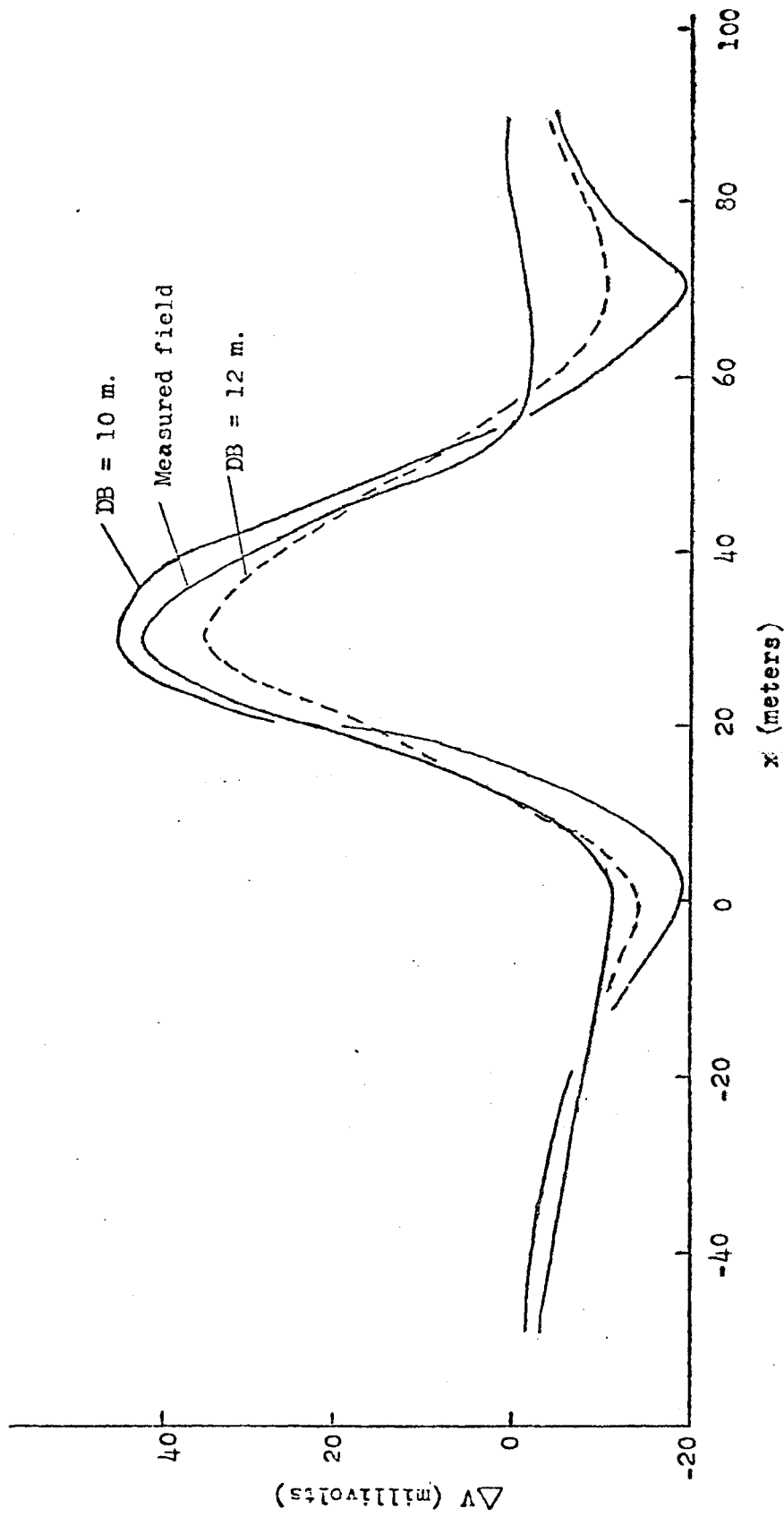


Figure 4-24
Dock Test Arrangement

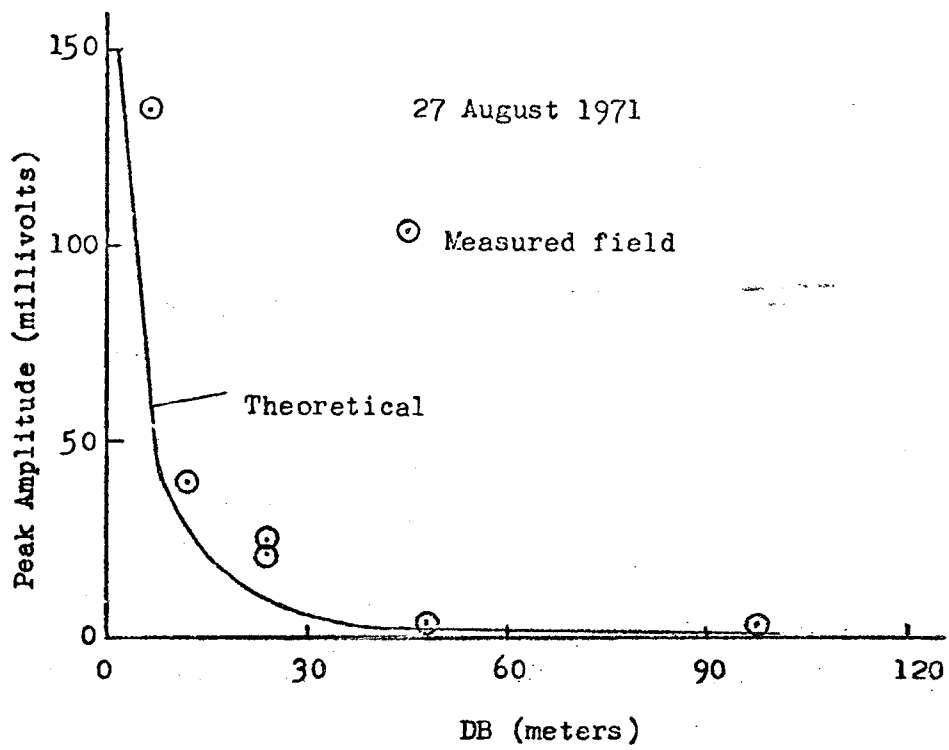




Dock Test Results
Figure 4-25

Figure 4-26

Peak Amplitude vs. Distance DB



Esterline-Angus model T 171 B (Esterline Corp., Box 24000, Indianapolis, Indiana). The recorder is fully portable, with its own nickel-cadmium battery power supply, and offers full-scale ranges from 2 mv to 50 volts. Input impedance on all ranges is 1.8 megohms, and response time is 1/2 second for full scale pen travel.

To test the effect of recorder input impedance on electrode performance, several of the short and long term tests described previously in this chapter, including the sea trials described in the preceding paragraphs, were run with a Keithley model 600 B (Keithley Instruments, Inc., 28775 Aurora Rd., Cleveland, Ohio) electrometer used as a impedance isolation amplifier between the electrodes and the recorder (the Keithley has an input of 10^8 megohms when used in this way). No difference was observed in the electrode response with the Keithley in or out of the circuit.

Cable and connectors

RG 58A/U transmission line cable is used for towing the electrodes. This cable, which is 0.195 inches (0.5 cm) in outside diameter, consists of a central stranded conductor enclosed by polyethylene insulation, a woven metal shield, and an outer vinyl jacket. The multiple layers surrounding the central conductor strengthen the cable and protect the conductor from contact with the sea water (the shield is not electrically connected to the electrode or chart recorder).

EnviroCon RMG-2-FS and RMG-2-MP underwater cable connectors (Brantner and Associates, San Diego, Calif.) are used to connect the electrode to the towing cable, and the towing cable to the

chart recorder . When used with the locking sleeves supplied by the manufacturer, these connectors have proven adequate in strength and water resistance. The connector splice to the cable is made using the materials supplied in the Dow Corning (Midland, Mich.) 5-15 cable splicing kit.

Complete system

The complete system, then, consists of a pair of "CoCo" electrodes, two lengths of towing cable (50 m for the forward electrode and 200 m for the after electrode usually are more than adequate), a reel on which to store the cable, appropriate connectors, and the Esterline-Angus T 171B chart recorder (Figure 4-27). The chart recorder is secured to the boat and covered with a clear plastic shroud before getting under way, and, after deployment, the cables are tied off to the stern of the boat (tying them to the lifting handle of the outboard motor helps keep them clear of the propeller).

Summary of "CoCo" electrode characteristics (2.7 M KCl filling solution)

Standard potential(E_e)

$$E_e = + 210 \text{ mv}$$

Simultaneous salinity change at both electrodes

$$\Delta V (\text{mv}) = 0.325 \ln (S_2 / S_1) + .0225$$

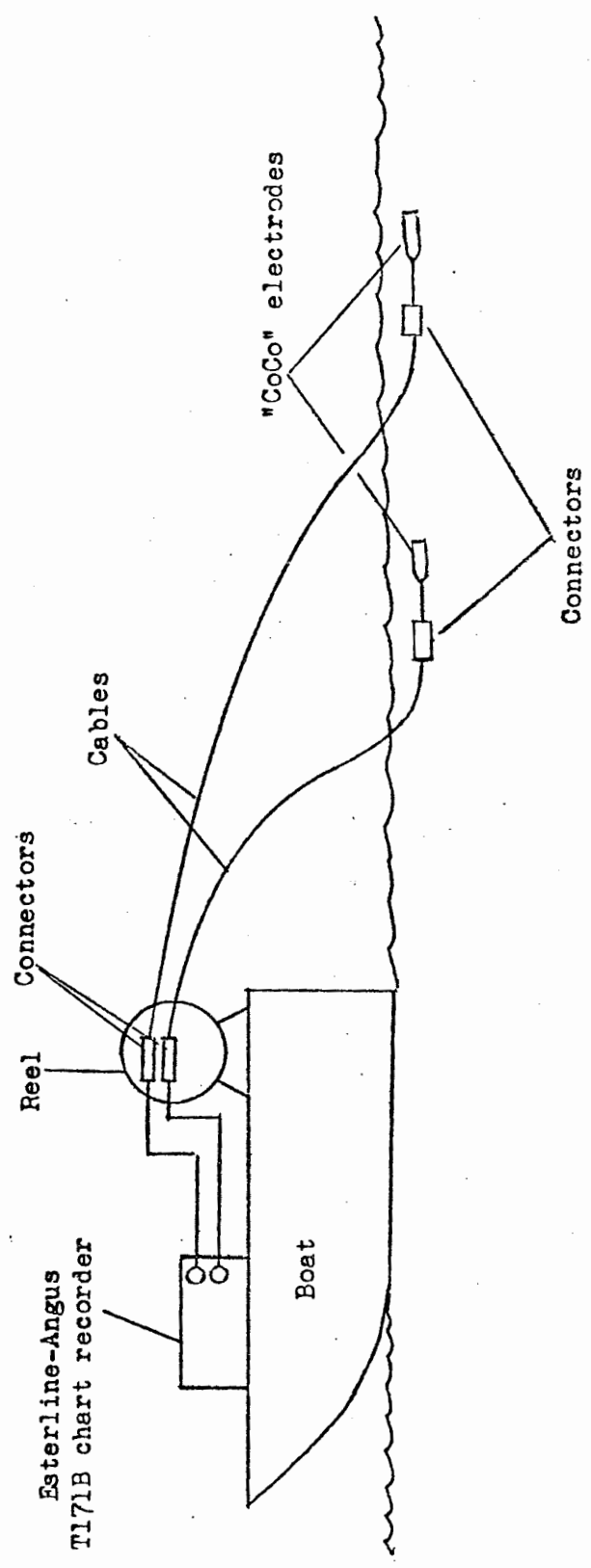
$$0.15 \leq S_2 / S_1 \leq 1.0$$

Differential salinity change

a) equilibrium value:

$$\Delta V (\text{mv}) = 2.9 \ln (S_2 / S_1)$$

$$0.25 \leq (S_2 / S_1) \leq 1.0$$



Complete System

Figure 4-27

b) short-term value:

$$\Delta V \text{ (mv)} = 0.52 \ln (S_2 / S_1)$$

$$0.25 \leq (S_2 / S_1) \leq 1.0$$

Simultaneous temperature change at both electrodes

a) equilibrium value:

$$\Delta V \text{ (mv)} \approx 0.1 \times \Delta T \text{ (}^\circ\text{C)}$$

b) short-term response:

none

Differential temperature change

$$\Delta V \text{ (mv)} = 0.14 \times \Delta T \text{ (}^\circ\text{C)}$$

(warmer electrode positive)

Eh change

$$\Delta V \text{ (mv)} \approx 0.018 \times Eh \text{ (mv)}$$

Agitation and mechanical shock

no measurable response

Applied electric field

response limited only by chart recorder characteristics

CHAPTER 5

NOISE

"... the voices of many waters"

Psalms 93.4

For the purpose of offshore self-potential prospecting, "noise" is considered to be any recorded signal which is not generated by a mineral deposit. Much of this "noise" may be considered valuable signal in other studies; for example, the potential fields due to water currents, corrosion, impressed current anodes, and geothermal activity. Other noise, such as that generated within the instrumentation, benefits no one.

Noise may be divided into two general categories: instrumental (inherent in the measuring system or generated by interaction between the instrumentation and the environment), and environmental (actual potential fields generated in the water by processes other than self-potential). The smallest scale division on the chart recorder used in the final system (see below) is 0.02 mv, so any noise signal of less than 0.02 mv will be considered undetectable by this system.

Instrumental noise

The sources and magnitude of instrumental noise depend on the particular system used. The noise characteristics of the salt bridge system shown in Figure 4-5 will be different from those of the towed electrode system shown in Figure 4-27; in a towed electrode system lead electrodes will differ in noise characteristics from "CoCo" silver-silver chloride electrodes. The system discussed in this section will be that shown in Figure 4-27, consisting of "CoCo" electrodes, RG/U shielded cable, and an Esterline-Angus T 171B battery-operated chart recorder. This system, used for the field work in Maine and Mexico (Chapter 6), has proven to be the most practical and noise-free of those tested.

Other systems and components will be mentioned only in comparison with the system described above.

Electrodes

The response of the "CoCo" electrodes to mechanical shock and agitation is undetectable (Figure 4-22), and their response to changing electric fields is immediate and reversible (Figure 4-23) so no electrode noise will be generated by either of these sources. Changes in water temperature or salinity, on the other hand, do generate measurable signals (Figures 4-13 through 4-20).

In an extreme case, such as passage by a hot-water outfall or by a fresh-water river entering sea water, it is conceivable that a signal of several mv amplitude could be generated by rapid temperature and/or salinity changes. In most cases, however, the source of such a signal would be obvious. If desired, the noise signal could be removed from the total signal by measurement of temperature and salinity and use of the appropriate response curves. In field experience, such noise has not proven troublesome. In several instances, survey lines have passed the mouths of rivers entering salt water; in no case was any spurious "anomaly" observed.

Cables

The motion of the cables through the Earth's magnetic field generates potentials which are an annoying source of noise. With the boat moving straight ahead in calm water, the velocity vector of a cable is directed along the length of the cable, and no potential is generated in the cable. If, however, the boat is turning, or is subjected to wave motion, a component of the cable's velocity will be perpendicular to the lines of force of the Earth's magnetic field, and a potential will be generated in the cable.

As one cable is always longer than the other, the potentials generated are not equal, and the difference between the potentials generated in the two cables will appear as a signal at the chart recorder.

A first estimate of this turning noise is shown in Figure 5-1. The boat has just made an abrupt 90° turn to the right, and is travelling at a velocity (v) of 5 knots (2.6 m/sec). The separation S between electrodes is 20 m, and the cable is considered to be moving as a rigid bar, with the after electrode stationary (the actual cable motion is, of course, much more complex). The average velocity of the cable in a direction perpendicular to its length is 1.3 m/sec. Faraday's law:

$$\vec{v} \times \vec{E} = - \frac{\partial \vec{B}}{\partial t} \quad (5-1)$$

reduces to

$$\Delta V = - H_z S v \quad (5-2)$$

for this simple case, where:

H_z = vertical component of Earth's magnetic field (Webers/m²)

S = electrode separation (m)

v = boat speed (m/sec)

V = potential (volts).

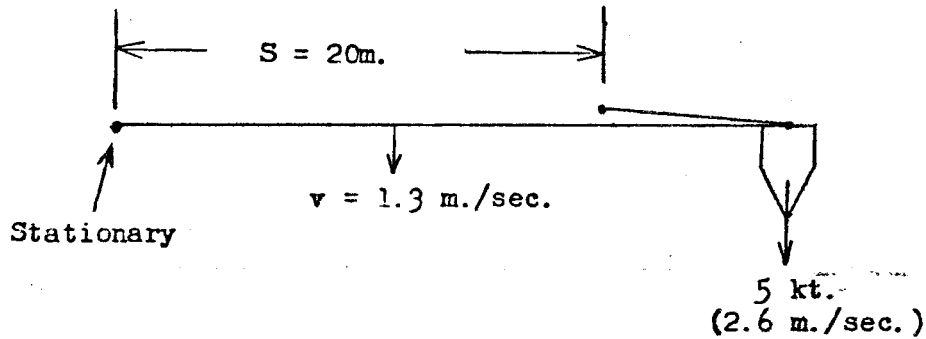
For a total field intensity of 0.5 gauss and a dip angle of 67° (typical of the northern mid-latitudes), the generated potential is about 1 millivolt.

Figure 5-1

Potential Generated by Turn

Northern mid-latitudes:

Earth's magnetic field intensity = 0.5 gauss

Dip angle = 67° northHorizontal intensity $H_h = 0.5 \cos 67^\circ = 0.2$ gaussVertical intensity $H_z = 0.5 \sin 67^\circ = 0.46$ gauss

$$\begin{aligned}
 V &= H_z S v \\
 &= 0.46 \times 10^{-4} \times 20 \times 1.3 \\
 &= 11.8 \times 10^{-4} \text{ volts} \\
 &= 1.2 \text{ millivolts}
 \end{aligned}$$

Actual signals ranging from a few tenths of a millivolt to greater than one millivolt are observed during turning maneuvers (Figure 5-2). Such signals are particularly annoying during runs along irregular shorelines, when frequent sharp turns must be made. Although it may be obvious that at least part of the signal is due to the turn, another part might be due to an ore body. In practice, if very small (less than one millivolt) signals due to ore bodies are anticipated, turning noise may be reduced by using slow boat speeds and keeping maneuvers to a minimum.

Similar signals are generated by wave action on the cables. Often, a noise component with the same period as the waves is observed on the recorder output (Figure 5-3), with the amplitude increasing as the wave height increases. Part of this noise is due to the electric field generated by wave particle motion (see the section of this chapter on waves); the remainder, to vertical motion of the cables through the Earth's magnetic field. Although wave noise may reach several millivolts with large arrays, its periodicity makes it relatively easy to remove from the record, if desired (the period of a self-potential signal, generally greater than one minute, is considerably longer than that of most shallow-water waves).

Connections

Connections are a constant source of trouble in the marine environment. A loose or poorly soldered connection will cause intermittent jumps in the record (Figure 5-4), and a leaky underwater connection will result in rapid drift as the exposed wire corrodes or galvanic couples add to the signal. Also, if a true signal is present in the water, a leaky connection will act as a

Figure 5-2
Signals Due to Turns
Penobscot Bay, Maine 8 Sept 1971

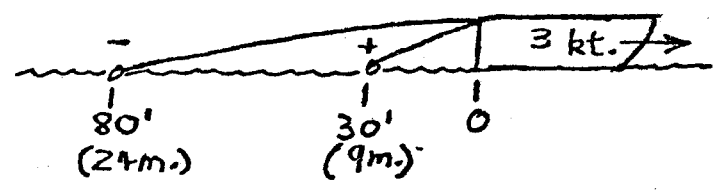
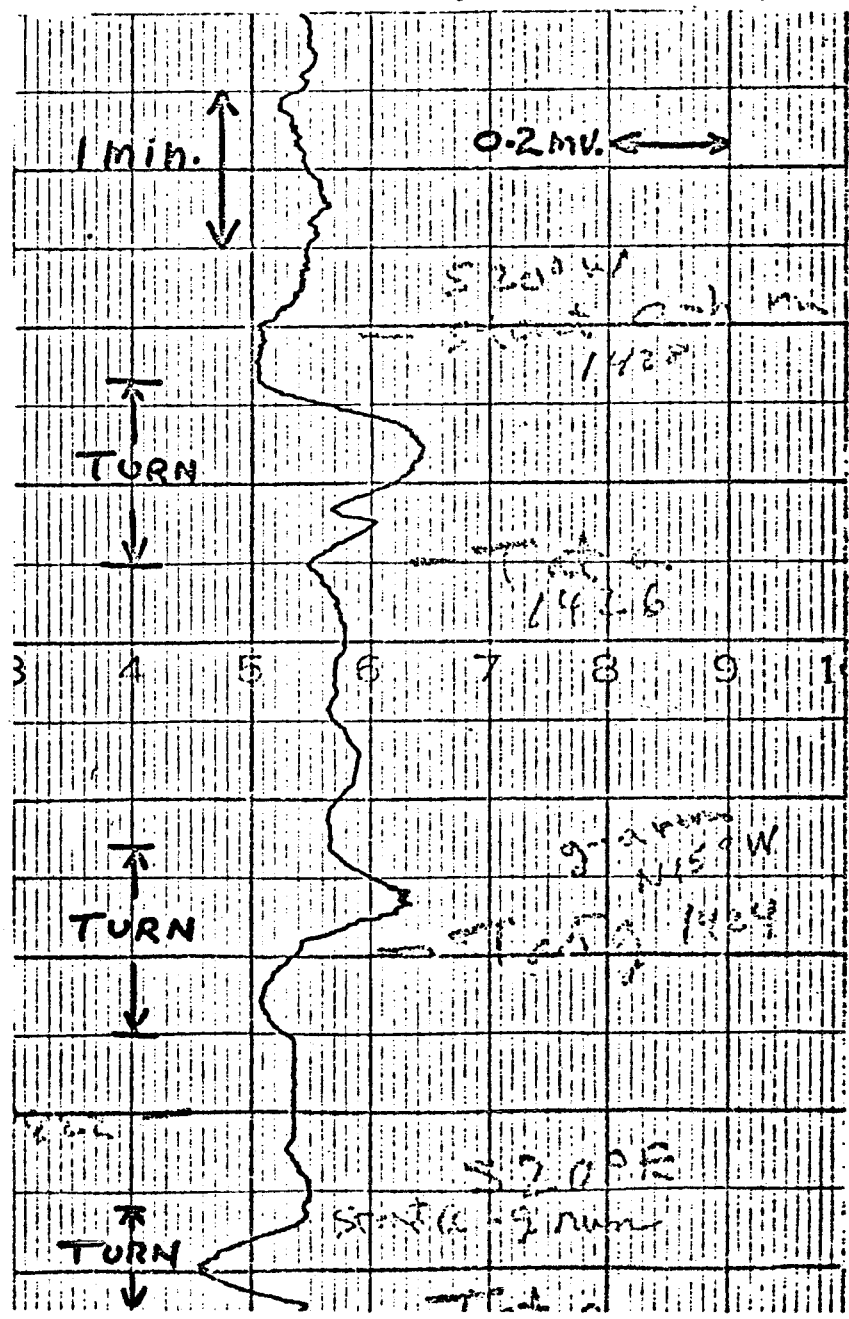


Figure 5-3

Noise Due to Waves

Punta Banda, Baja California, Mexico

28 Dec. 1971

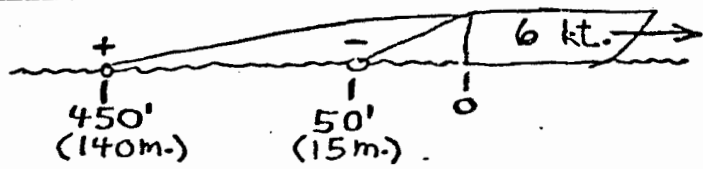
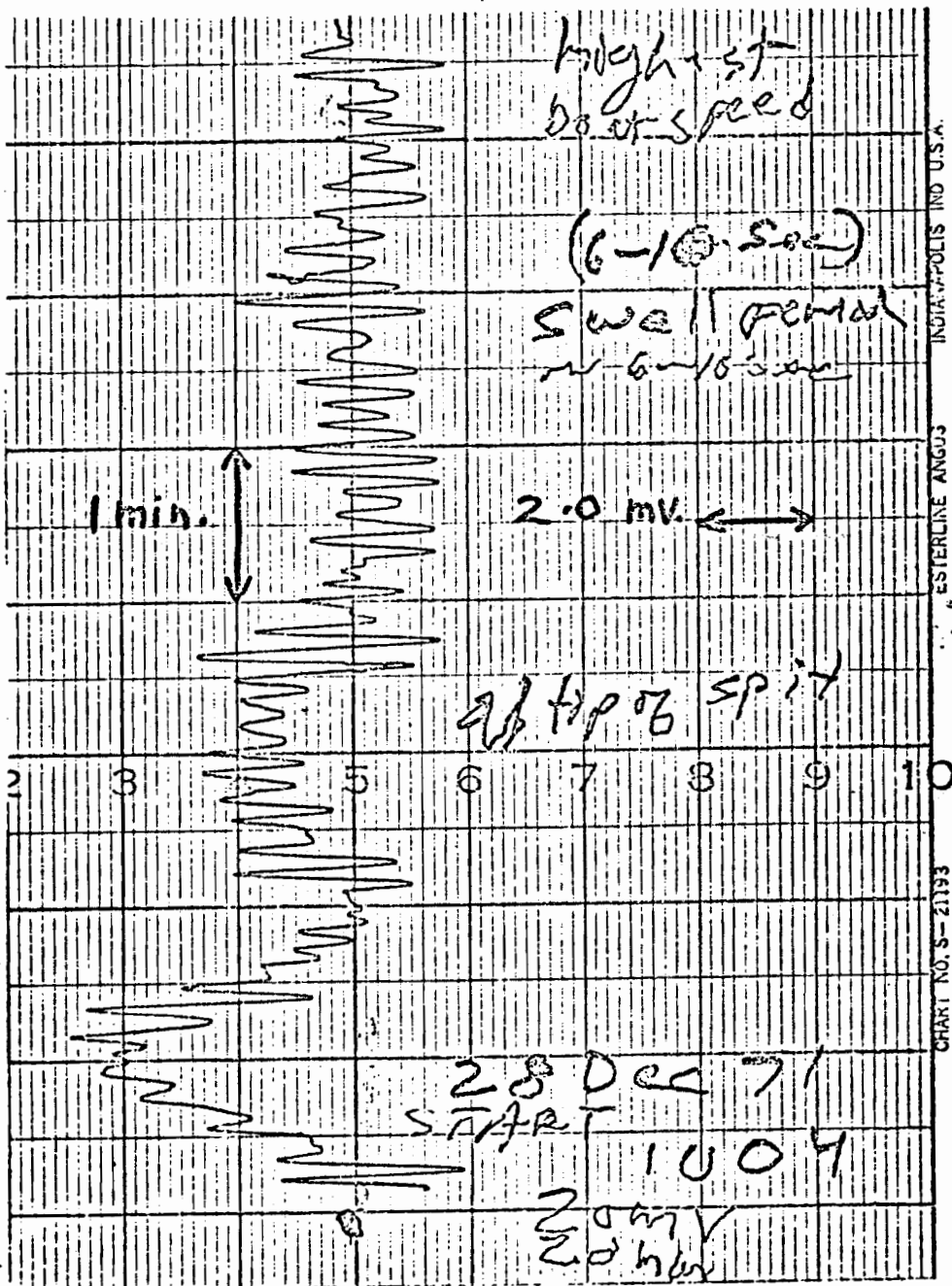
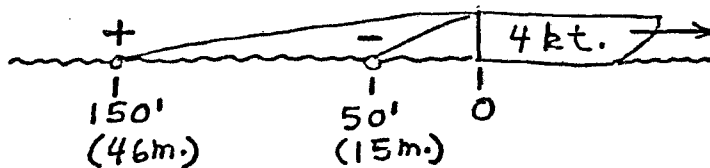
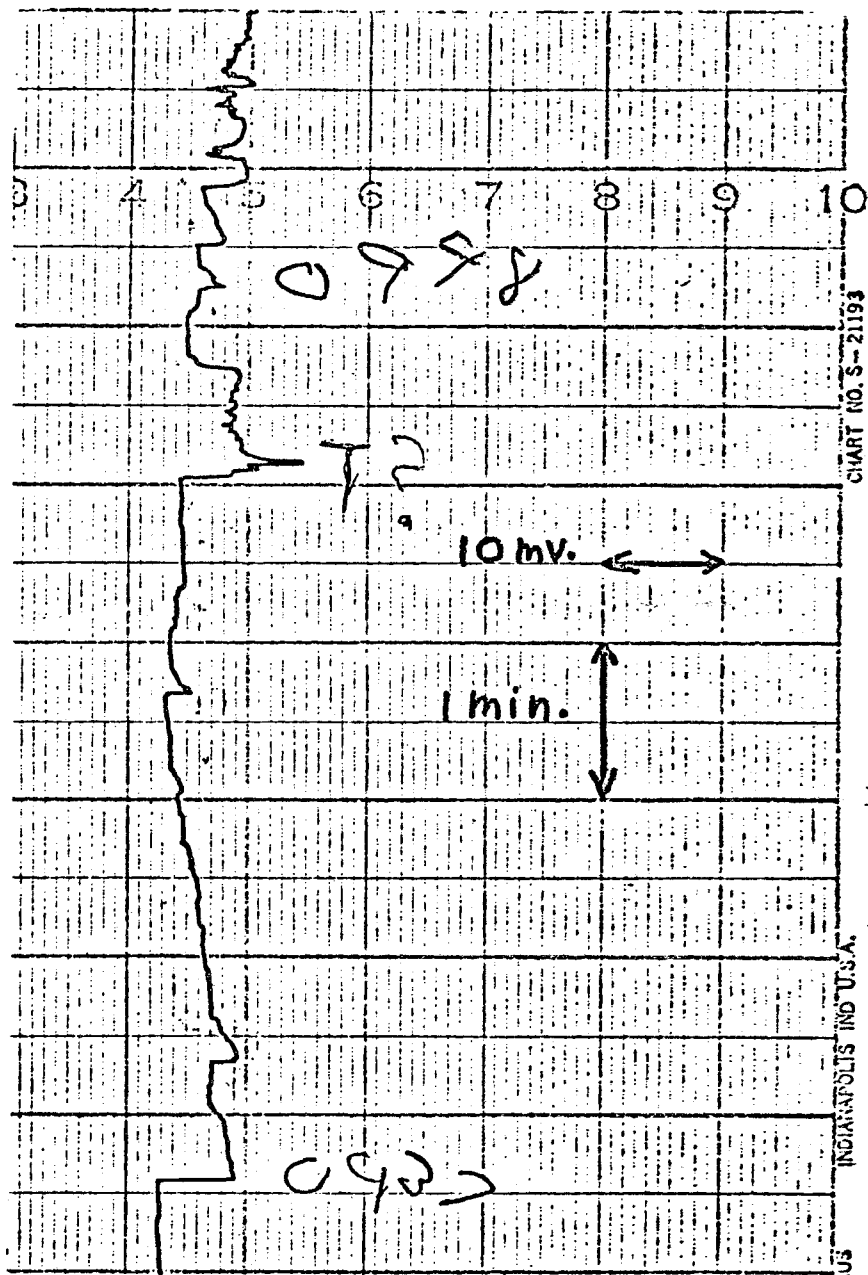


Figure 5-4

Noise Due to Poor Connection

Punta Banda, Baja California, Mexico

30 Dec., 1971



third electrode, making analysis of the data virtually impossible. For these reasons, all underwater splices must be made carefully, and tested thoroughly for electrical continuity and for leaks, before field use.

Although the connections to the reel and chart recorder are not submerged, they are subject to the action of damp salt air and occasional spray, both of which can lead to corrosion, variable resistance, or short-circuiting. Therefore, above-water splices must be made carefully, and connectors preferably should be of the underwater type, such as the EnviroCon RM series (Brantner and Associates, San Diego, Ca.) used on the "CoCo" electrodes.

Chart recorder

The noise level of the Esterline-Angus T 171B chart recorder is specified by the manufacturer as less than 10 microvolts peak-to-peak, and drift as less than 10 microvolts per hour. Both of these values are well below the observable level. In very rough seas, the recorder pen may be deflected by violent pounding of the boat (Figure 5-5). When such conditions are encountered in a small boat, it is generally the better part of valor to head for port. A more serious problem is created by moist, salty air, often encountered in late afternoon and evening. Under such conditions, touching the case or controls of the chart recorder often results in a jump of the pen. Grounding the recorder to the sea may help alleviate this condition.

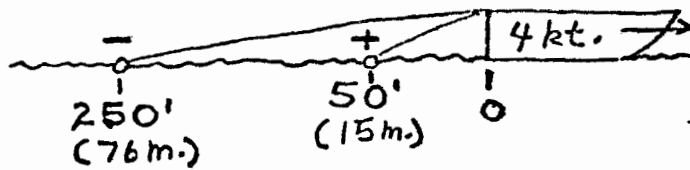
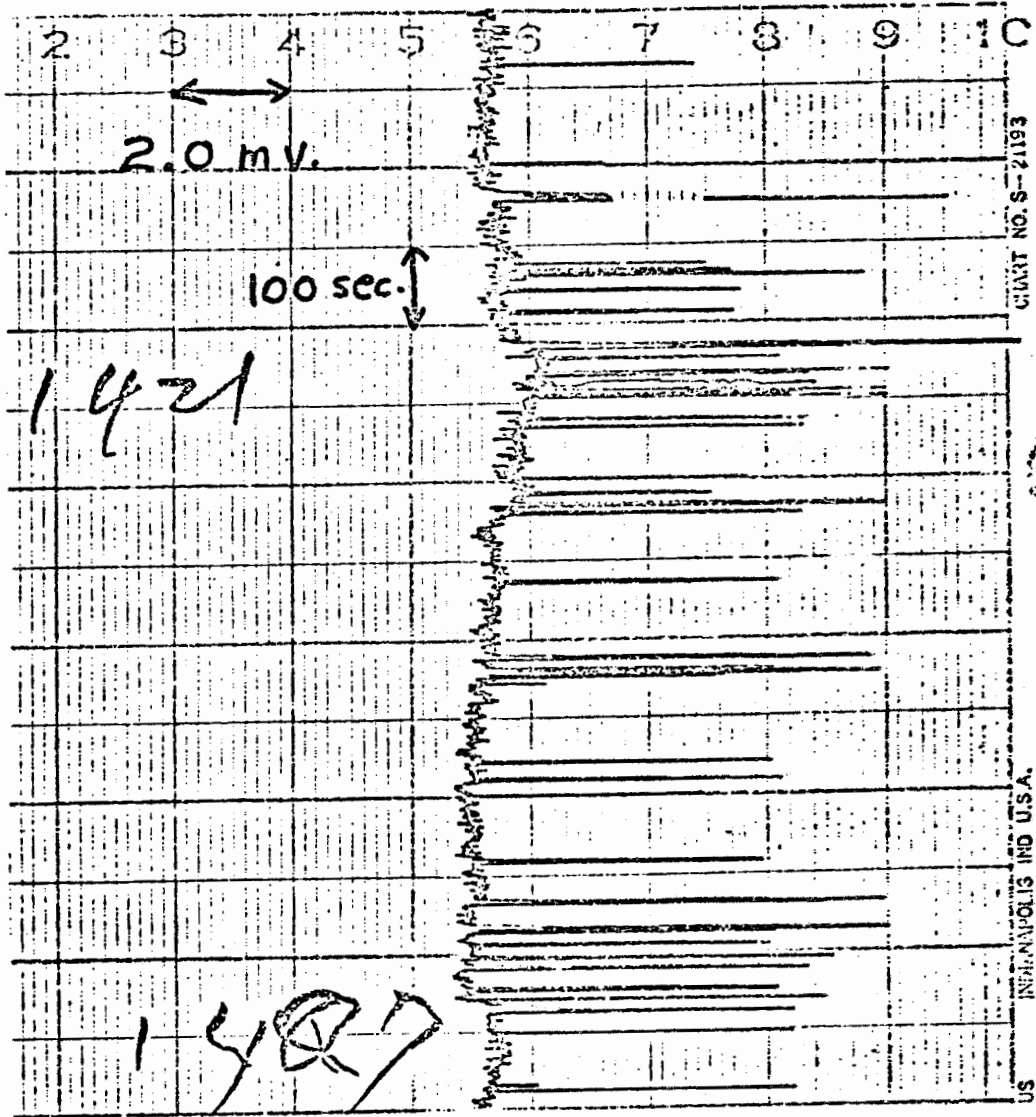
Electrical noise generated aboard the boat does not seem to affect the recorder, which has been used within a meter of an operating outboard motor with no ill effects noticed.

Figure 5-5

Noise Due to Pounding of Boat

Punta Banda, Baja California, Mexico

29 Dec. 1971



Radio transmission was sometimes seen to generate a large noise signal with the salt bridge system (Chapter 4) , but no such effect has been observed with the present system.

Environmental noise

In contrast to instrumental noise, which is generated within the measuring system, environmental noise is caused by an electrical field which is present in the water and which is not generated by mineral deposits. Some of these fields, such as those due to water currents or corrosion processes, are useful in studying the phenomena involved; for the purpose of self-potential prospecting, they are noise. Other fields, such as that due to the turbulent wake of the boat, are a general nuisance.

Currents

"Theoretically, it seems a necessary consequence that where water is flowing, there electric currents should be formed: thus, if a line be imagined passing from Dover to Calais through the sea, and returning through the land beneath the water to Dover, it traces out a circuit of conducting matter, one part of which, when the water moves up or down the channel, is cutting the magnetic curves of the earth, whilst the other is relatively at rest." Thus the omniscient Michael Faraday (1832) laid the groundwork for the "deep sea electromagnetic method" (von Arx , 1950) of measuring the velocities of ocean currents from a ship under way.

The history, theory, and practice of such measurements are covered thoroughly by von Arx (1950; 1962, p. 260), Stommel (1948), and Sanford (1967, 1971); only the portion of the theory relevant to this thesis will be discussed briefly below. The equipment used to measure electromagnetically induced electric fields in the

sea, named the "Geomagnetic Electrokinetograph" (mercifully abbreviated as "GEK") by von Arx, although primarily designed for deep sea use aboard large ships, is identical in purpose to that used for offshore self-potential prospecting. The experience gained by the designers of this equipment helped me greatly in developing the present system.

The magnitude in volts of the horizontal electric field induced in the water, ΔV_{xy} , is ideally

$$(5-3) \quad \Delta V_{xy} = S (\vec{i} C_y H_z - \vec{j} C_x H_z)$$

(Figure 5-6), where:

S = electrode separation (meters)

C_y = y - component of water current velocity (meters/sec)

C_x = x - " " " " "

H_z = intensity of vertical component of Earth's magnetic field (webers/meter²)

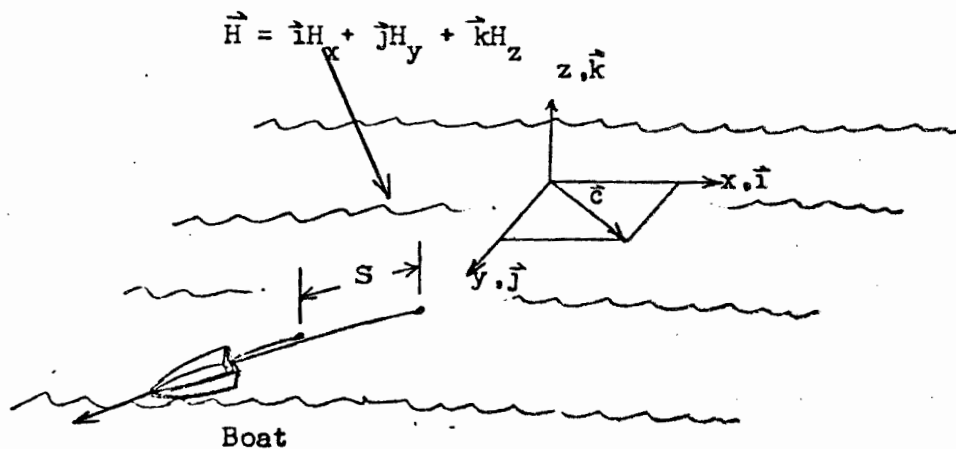
Although it must be modified for finite sea-floor conductivity, or for current velocity which is not constant with depth, Equation 5-3 is sufficiently accurate for a first estimate. For a boat travelling in the x direction, a water current velocity of 1 knot (0.5 m/sec) in the y direction, and H_z of 0.46 gauss (Figure 5-1),

$\Delta V_{xy}/S$ is about 0.024 millivolts/meter, and ΔV is about 0.5 millivolts for $S = 20$ m.

This signal is constant as long as boat and current velocity remain unchanged, and is noticeable only as an offset in the electrode zero level as the boat gets under way, and as a change in the zero

Figure 5-6

Potential Due to Water Current



$$\text{Water current velocity } \vec{c} = \vec{i}c_x + \vec{j}c_y$$

$$\frac{\Delta V}{s} = \vec{c} \times \vec{H}$$

$$= \begin{vmatrix} \vec{i} & \vec{j} & \vec{k} \\ c_x & c_y & 0 \\ H_x & H_y & H_z \end{vmatrix}$$

$$= \vec{i}c_y H_z - \vec{j}c_x H_z + \vec{k}(c_x H_y - c_y H_x)$$

$$\text{In the x-y plane, } \frac{\Delta V}{s_{xy}} = \vec{i}c_y H_z - \vec{j}c_x H_z$$

level when a turn is completed. In practice (Figure 5-7) such offsets are easy to recognize. As their magnitude usually does not exceed a millivolt or two, they may be removed, if desired, simply by resetting the chart recorder zero.

Waves

Waves generate noise on the record by two processes: (1) motion of the towing cables through the Earth's magnetic field (see above); and (2) electromagnetically induced potentials, similar to those generated by water currents, caused by the wave water particle motion through the Earth's magnetic field. The particle velocity within a travelling wave is extremely complex (Wiegel, 1964, p. 11), and it would be difficult to estimate the electric field which would be measured by a pair of electrodes towed through surface waves, especially as the position of the electrode relative to the water surface is not known precisely. Sanford (1967, p. 158) calculated a signal of 0.13 mv at a stationary surface electrode due to waves of amplitude 80 cm and period 5 seconds, and measured 0.8 mv under these conditions. The wave noise observed on offshore self-potential surveys, however, appears primarily to be due to the cable motion described above, as it decreases with decreasing cable length.

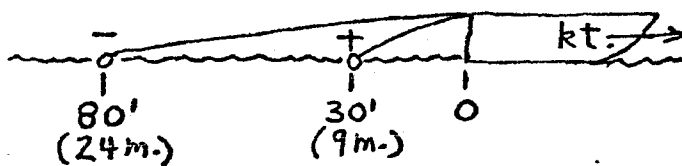
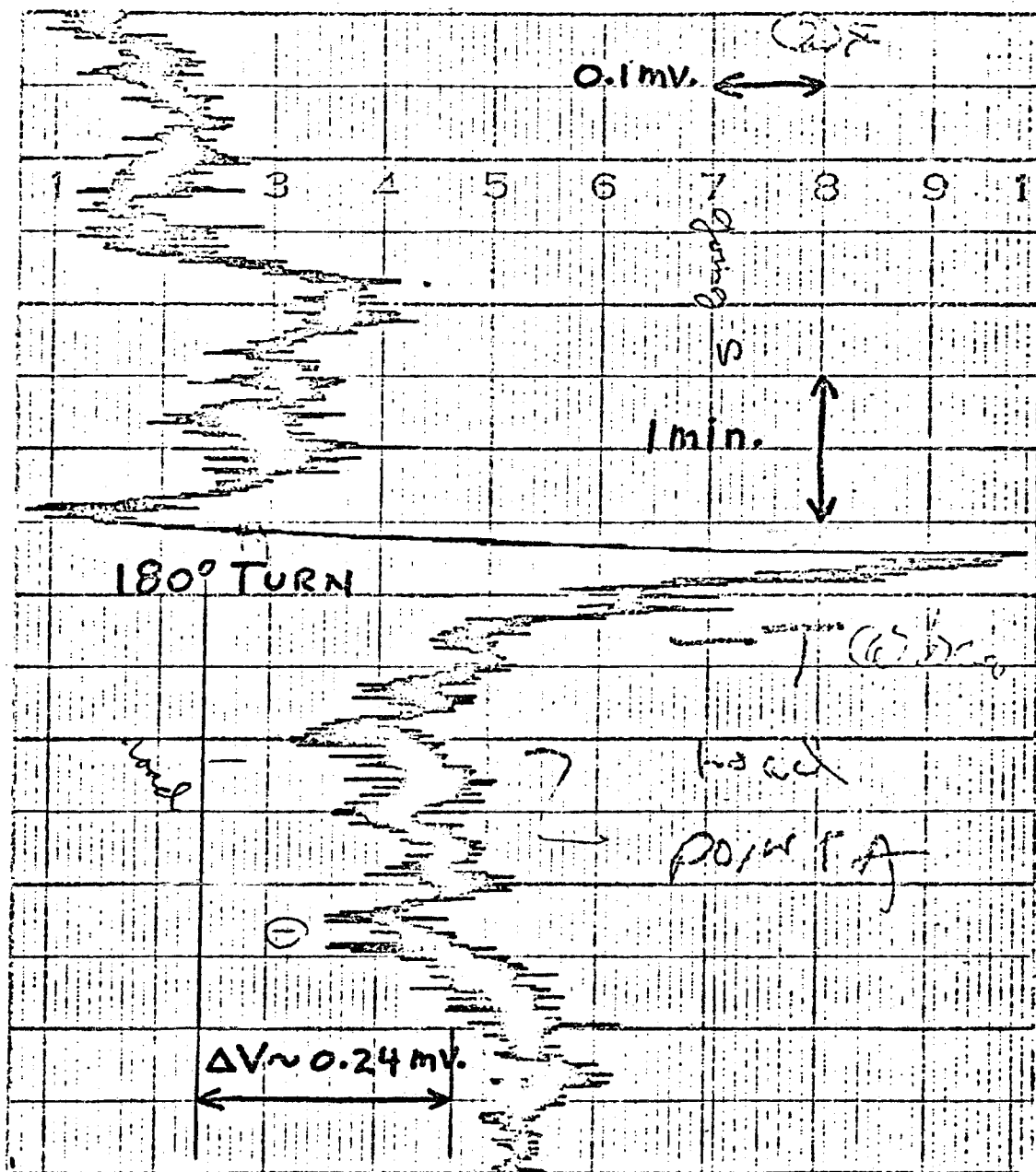
Wake turbulence

Turbulence in the wake of the towing vessel may generate noise by the process described above for waves, in addition to creating air bubbles which could cause an electrode to break contact with the water. von Arx (1962, p. 277) recommends towing the GEK electrodes one ship's length astern to remove them from the galvanic and magnetic effects of the ship's hull. This distance also appears sufficient

Figure 5-7
Signal Due to Water Current

Penobscot Bay, Maine

8 Sept. 1971



to remove any effects of the wake on the forward electrode at normal towing speeds (up to 5 knots), although a minimum distance of 5 or 10 meters usually is used with small boats. Figure 5-8 shows the increased noise level caused by high towing speeds. The forward electrode was 20 m astern, and the towing boat was an LCM (Landing Craft Mechanized), about 17 m long, making 9.5 kt.

Magnetic field variations (telluric noise)

A pair of electrodes in the earth will record potential changes over a wide spectrum of frequencies and amplitudes (Keller and Frischknecht, 1966, p. 197). These signals, which at frequencies greater than one Hz are generated by temporal variations in the Earth's magnetic field, may reach amplitudes of 100 mv per km, with periods of about 30 sec, during magnetic storms. Amplitudes of a few mv per km, however, are more typical in the 10 to 40 second period range.

Shuleikin (1962) presents the results of telluric noise measurements taken at sea. He states (in translation) : During days, and from one day to another day, the intensity of electrical field fluctuated with an amplitude equalling several millivolts per kilometer, whereby sometimes the amplitude reached even tens of millivolts per kilometer". Apparently, then, the normal telluric background noise level in the sea is below 10 mv per km (0.2mv for an electrode separation S of 20 m). During large magnetic storms (Figure 5-9), the noise level may rise to 40 mv per km.

Geologic background noise

The background noise level for onshore self-potential surveys varies widely in amplitude and spatial frequency, ranging from

Figure 5-8

Noise Due to Increased Boat Speed

San Francisco Bay, California

11 Sept. 1972

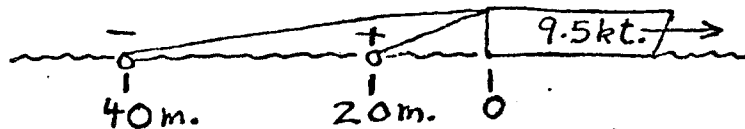
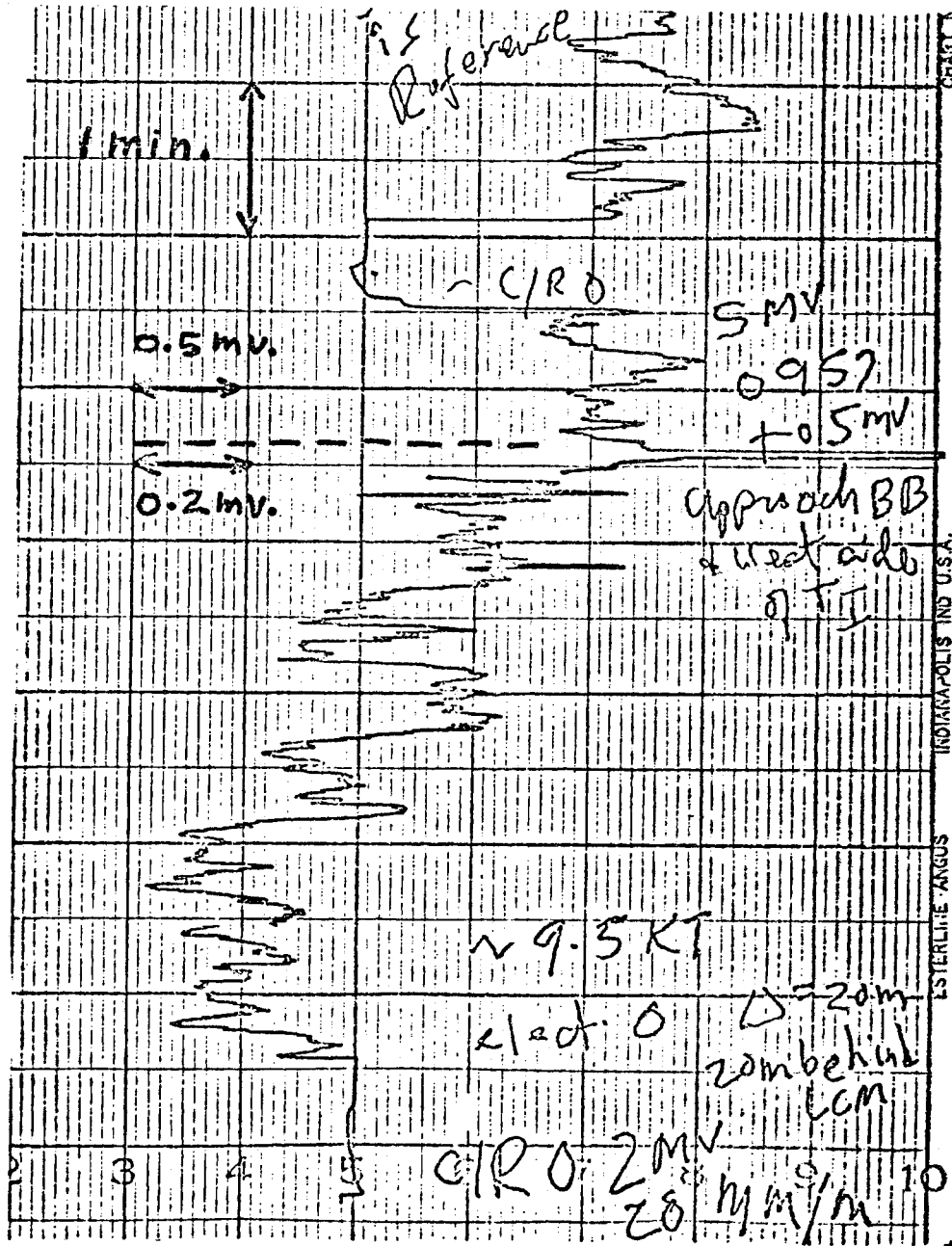


Figure 5-9

Potentials Due to Magnetic Storm

From Shuleikin (1962)

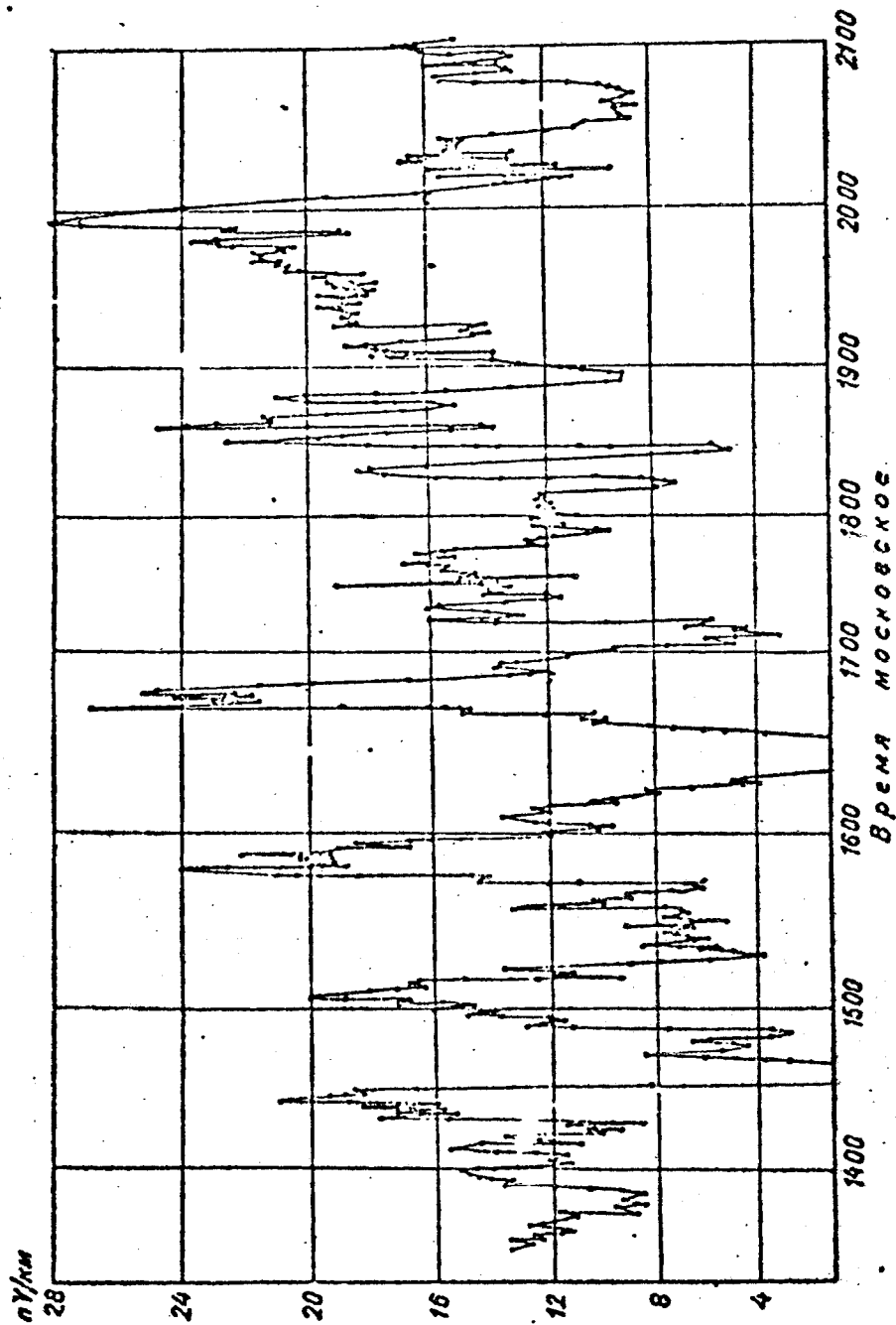


Fig. 304. Fluctuations of currents in the sea (according to Mironov).

[during magnetic storm]

Key: Abscissa: Moscow time.

nearly zero to about 10 or 20 mv in amplitude, and from a few meters up to about 50 meters in spatial wavelength. Noise levels generally are greatest in heavily wooded areas; in areas where the soil is rich in soluble salts; in rugged topography; and in areas of geothermal activity (geothermal areas are discussed in a later section of this chapter). In my experience, surveys conducted along sea water-saturated sandy shorelines have exhibited very low noise levels -- generally less than 5 millivolts (see Figures 6-39 and 6-47).

Onshore geologic noise is caused by surface and subsurface water flow (streaming potentials); chemical, biological, moisture, and temperature differences in the soil; local telluric currents generated in conductive non-metallic bodies such as clay lenses; and geologic contacts. The effect of chemical and temperature changes on the electrodes is discussed in Chapter 4. Of the other factors, only streaming potentials and geologic contacts might be expected to be of importance in offshore work. These are discussed separately below.

Streaming potentials

A fluid forced through a capillary tube generates an electromotive force called the streaming potential (Mac Innes, 1961, p. 437). This potential is due to the Helmholtz double layer which forms at the wall of the capillary, with the wall acquiring charge of one sign, and the fluid the opposite sign. According to Dakhnov (1962, p. 313) most rocks preferentially adsorb anions (negative ions), so the pore liquid becomes enriched in cations (positive ions), and carries a positive charge. Clays and some carbonate rocks, on the other hand, tend to adsorb cations, causing

the pore liquid to become negative in charge.

The net effect of this charge separation is that motion of the pore water results in a transport of charge, constituting an electric current flow, and a potential difference is developed along the length of rock or soil through which pore water is moving. MacInnes (1961, p. 439) shows that the streaming potential E may be calculated from the equation

$$(5-4) \quad E = \frac{P D J}{4 \pi L \eta}$$

where:

P = the pressure difference

D = the dielectric constant of the fluid

J = the "zeta potential" (a property of the fluid)

L = the specific conductance of the fluid

η = the viscosity of the fluid.

It is important to note that E does not depend on the length or cross-sectional area of the capillary, and is inversely proportional to the conductivity of the fluid.

The falloff in streaming potential with increasing fluid conductivity is confirmed by the work of Meyer (1972) and Oglivy and others (1969). They showed that distilled water moving through sand generated potentials of about -3 to -12 mv per cm pressure head (of water), whereas for a 10^{-3} M solution of NaCl the potential dropped to about -0.5 mv per cm; and Meyer states "Voltages for all head differences in sand with sea water were found to be zero". Sea water flowing through a clay bearing mud was found

by Meyer to generate potentials of about + 0.3 mv per cm.

Although streaming potentials may reach large values on land (Poldini, 1939, reports an extreme value of - 300 mv on the crest of a hill in Serbia, and 10 to 20 mv as a common value), it appears from the preceding paragraph that streaming potentials generated in a sandy sea floor by the movement of sea water are negligible. (This possibly accounts for the very low noise level observed in self-potential surveys along sandy beaches, where wave and tide action might be expected to produce vigorous subsurface water flows). Fresh water flows or seepages, or the movement of sea water through a clay sea floor may, however, generate measureable potentials. Oglivy and others (1969) report potentials of up to 25 mv over seepage zones in a fresh-water reservoir. This would probably represent an upper limit for any streaming potential generated on the sea floor.

Geologic contacts

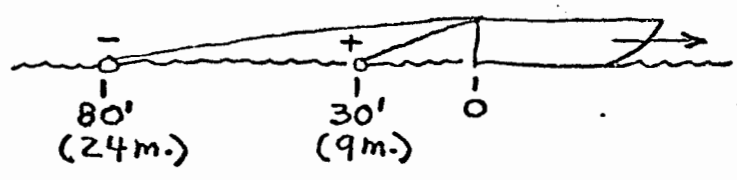
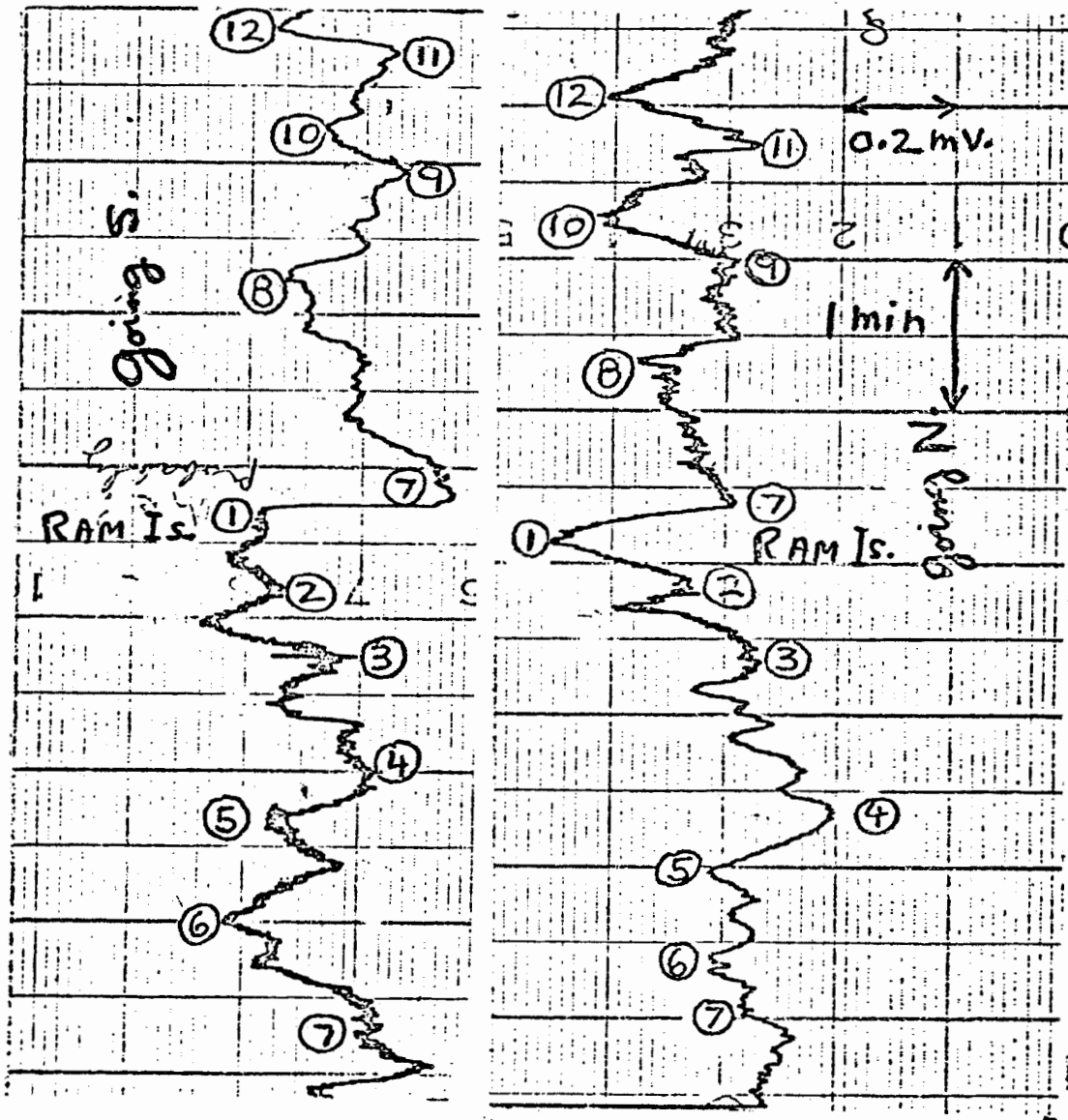
The spontaneous potentials developed across geologic contacts are used to map the contacts in borehole logging (Wyllie, 1963; Schlumberger Well Surveying Corporation, 1958; Dakhnov, 1962, p. 287). These potentials develop when the pore waters of adjacent formations, having different concentrations of dissolved ions, are allowed to interact through the drilling mud filling the borehole. Although these formation waters had come to equilibrium with each other over geologic time, the introduction of a new flow path, via the mud, allows ionic currents to flow between formations as the formation waters attempt to approach a new equilibrium. These potentials have been studied extensively and are discussed in detail by the authors cited above.

Similar potentials may be developed across faults and other geologic contacts on the surface of the Earth. Jakosky (1950, p. 451) states, "Contacts of different materials containing ground waters of different chemical properties often give rise to earth potentials which may not be related to ore occurrence. In addition different geological formations usually possess different electrical conductivities; hence they cause a distortion of the normal regional ground currents with a resultant redistribution of the surface potentials. Fault zones filled with wet clay gouges, or other conducting materials, cause severe distortion of the surface potentials".

On the sea floor, the cover of salt water or saturated sediments probably damps out most of this geochemical activity, with the conductive layer allowing electrochemical imbalances between formations to be equalized. Two surveys conducted in Maine, in which one electrode was held stationary at the shoreline while the other was towed in along the bottom, showed potential variations of less than 2 mv in 500 feet (153 m). A towed offshore survey in the same area showed repeatable short-period signals of about 0.2 mv amplitude in very shallow (less than 1 m) water (Figure 5-10).

Whether such signals were due to the sources of geologic noise mentioned above, or to tiny amounts of sulfide minerals in the bottom, or to water current velocity variations caused by the underwater topography, is impossible to say. It appears, however, that geologic noise for towed offshore self-potential surveys does not seem to exceed 0.2 mv, even in very shallow water.

Figure 5-10
 Geologic Noise
 Penobscot Bay, Maine
 8 Sept. 1971



Corrosion

The process of metallic corrosion requires a flow of electrical current, so a corroding object in the sea will produce a potential field in the surrounding water. That such fields may reach detectable values was demonstrated by Grice (1968; Ocean Industry, 1967), who detected a 2.5 mv anomaly in 38 ft (12 m) of water, caused by the 2,100 ton Civil War ironclad "Tecumseh", sunk 102 years before. The 2.5 mv value is the gradient anomaly -- Grice does not give the electrode separation used, so the total anomaly is not known.

Greater fields may be produced by larger (or fresher) objects, such as pipelines or large ships, or by impressed current protection systems used to reduce corrosion (these systems are discussed in the following section). Also, submerged objects composed of two or more metals may produce large potential fields by galvanic current flow between the dissimilar metals. A zinc-copper couple installed on French Navy training torpedoes generated a 5 mv field at a distance of 11 m, which was used to aid in the recovery of lost torpedoes (Grice, 1968). Pipelines corroding in the soil generate potentials greater than 100 mv at the surface (Heiland, 1940, p. 680); such potentials would produce easily detectable fields in sea water.

Corrosion fields, then, may be a source of considerable noise in waters near populated areas. Sunken (or floating) ship hulls, pipelines, cables, or metallic junk on the bottom all may produce measurable potential fields at the water surface. In some cases, such as a pipeline or cable crossing marked on a chart, or

a steel-hulled ship passing nearby, the source of the signal may be obvious. In other instances, the longer spatial wavelength of a self-potential signal may help to distinguish it from one caused by corrosion, as geologic phenomena are generally on a larger scale than those which are man-made.

Corrosion control systems

Corrosion control systems, used to protect ships, piers, and other submerged structures, are of two types: galvanic and impressed current (Uhlig, 1963, p. 182). In a galvanic system, an electrolytically active metal, such as zinc or magnesium, is electrically connected to the metal to be protected. The active metal functions as a sacrificial anode, with ions of the sacrificial metal going into solution and electrons spontaneously flowing to the protected metal.

The current flow generated by such systems may be substantial. Zinc galvanic anodes used on boats are consumed at a rate of about 26 lb per square foot per year (128 kg/m²-year), implying a current flow of about 12 amps per m² (Lenk, 1966, p. 31). A single anode of an impressed current system on a large ship may have a current capacity of 150 amps (Lenk, 1966, p. 86), and the system protecting the San Francisco-Oakland (California) Bay Area Rapid Transit District (BART) transbay tube employs impressed current anodes of 250 ampere capacity (Bomar and Marchand, 1970).

Such current flows, of course, produce enormous potential fields. A survey run over one 250 amp anode of the BART tube mentioned above gave the gradient anomaly shown in Figure 5-11a. When integrated, this field is one volt in amplitude, as shown in

Figure 5-11a

Potential Field Due to BART Transbay Tube Protective Anode

San Francisco Bay, California

11 Sept. 1972

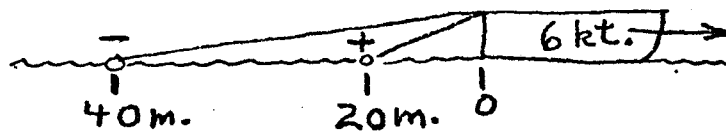
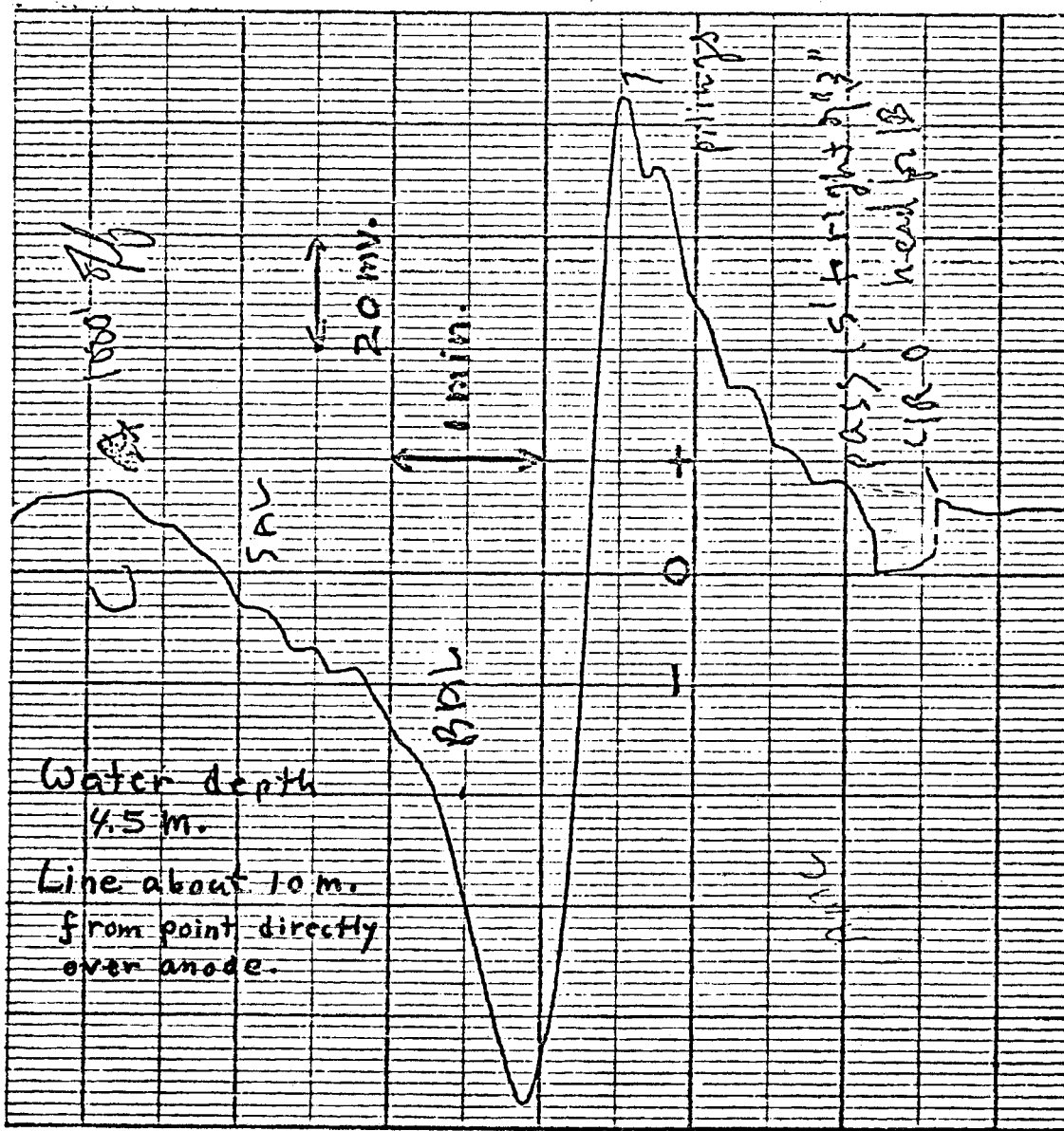


Figure 5-11 b (Cornet, 1972). Bomar and Marchand (1970), using a different system, measured fields of similar magnitude over other BART anodes. A survey run parallel to a large steel-hulled freighter gave the signal shown in Figure 5-12, undoubtedly caused by the ship's impressed current system.

The source of such fields, unless emanating from an uncharted shipwreck or underwater structure, usually is easy to identify. However, if such large signals are present in areas of geophysical interest, they could mask sulfide self-potential fields. A special danger is presented by any corrosion control system employed by the towing vessel. If the system cannot be turned off during self-potential profiling, the electrodes must be streamed far enough astern to remove them from the field of the corrosion control system.

Stray currents

Stray currents include any electrical currents generated by human activity. The corrosion control currents described above are in this category. Other sources of stray currents include direct-current electrical equipment and leaking electrical and communication cables. Direct current electrical equipment such as welders and motors installed on the towing vessel or on other ships, or near the shore in industrial or mining areas, may be grounded to the sea and thus generate a potential field in the water. If the self-potential survey is being conducted in conjunction with other onshore or offshore geophysical work, such as direct-current resistivity or induced polarization surveys, the fields generated by these activities may interfere with the self-potential readings.

Figure 5-11b

Total Field and Ship's Course

BART Transbay Tube Protective Anode

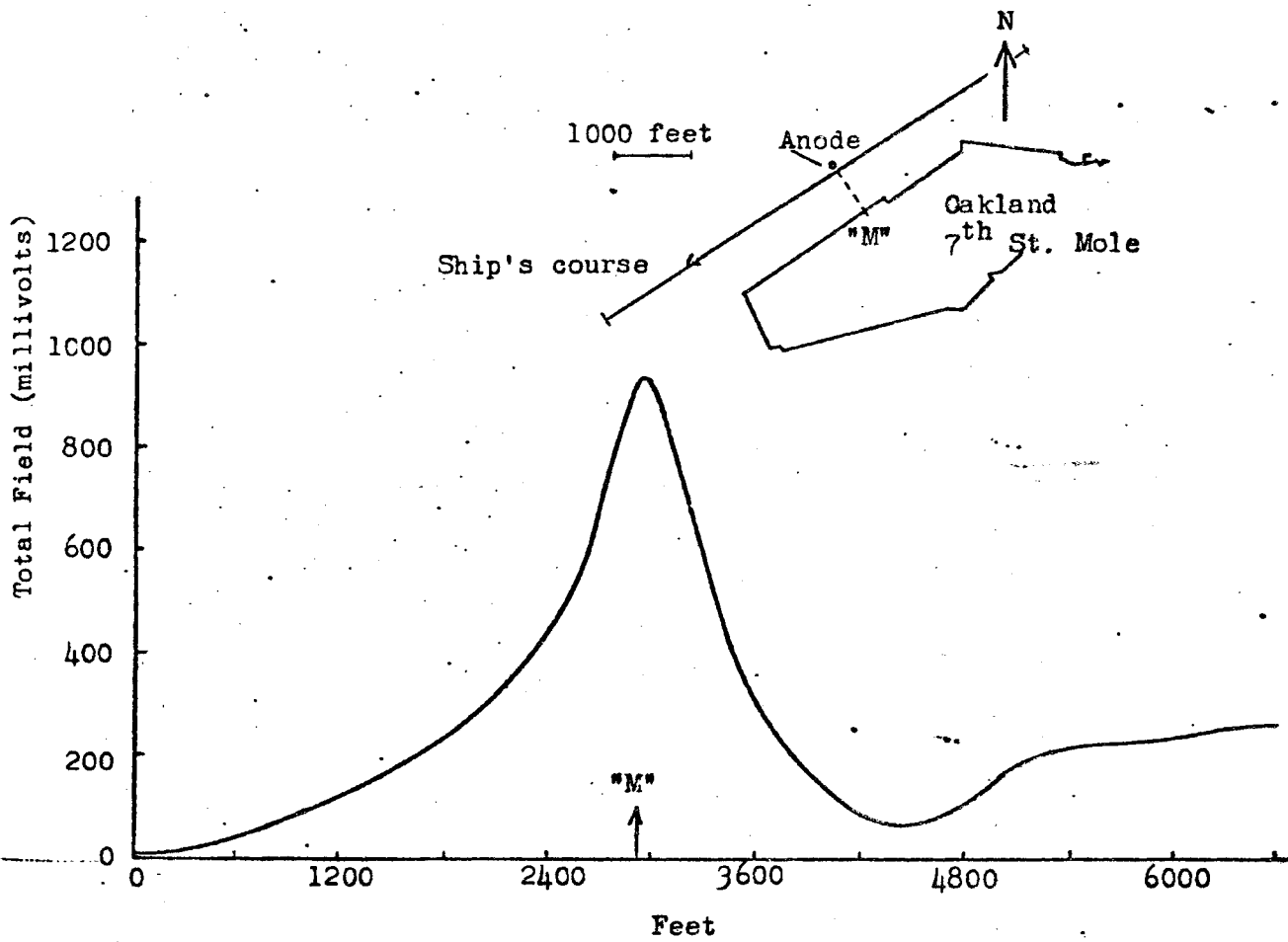
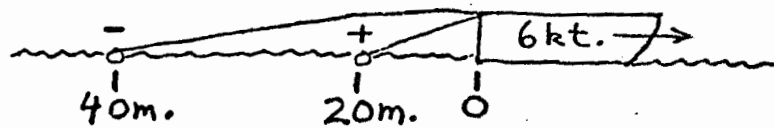
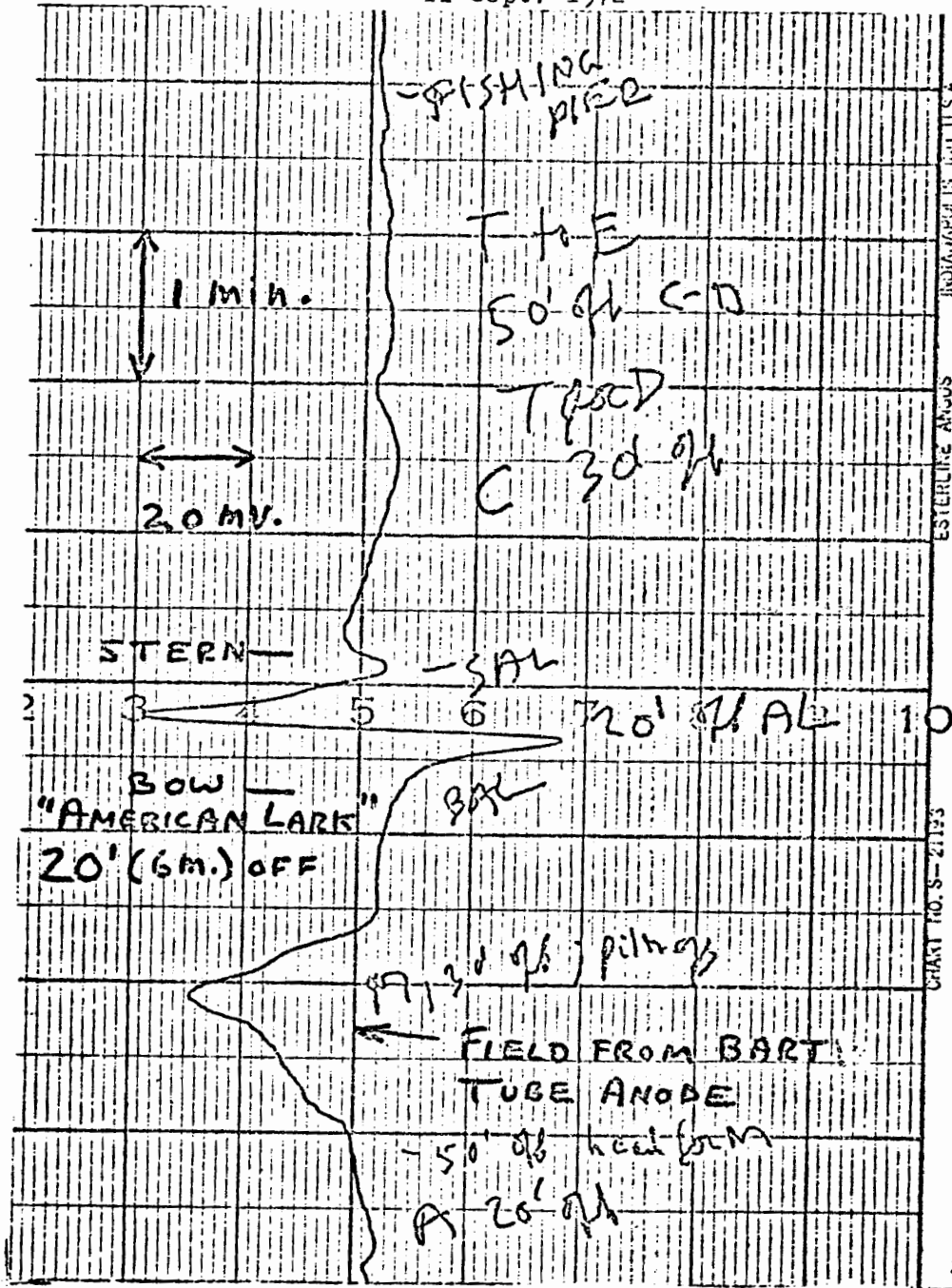


Figure 5-12

Potential Field Due to Ship's Impressed Current System

San Francisco Bay, California

11 Sept. 1972



Geothermal activity

Geothermal activity is thought to be caused by the heating of groundwater by an underlying chamber of hot magma (White, 1969; Grose, 1971). The heated groundwater tends to rise and, if permeable channels to the surface exist, to escape as hot springs or geysers (Figure 5-13b). If no path to the surface exists, the groundwater would tend to circulate in a convection cell (Figure 5-13a).

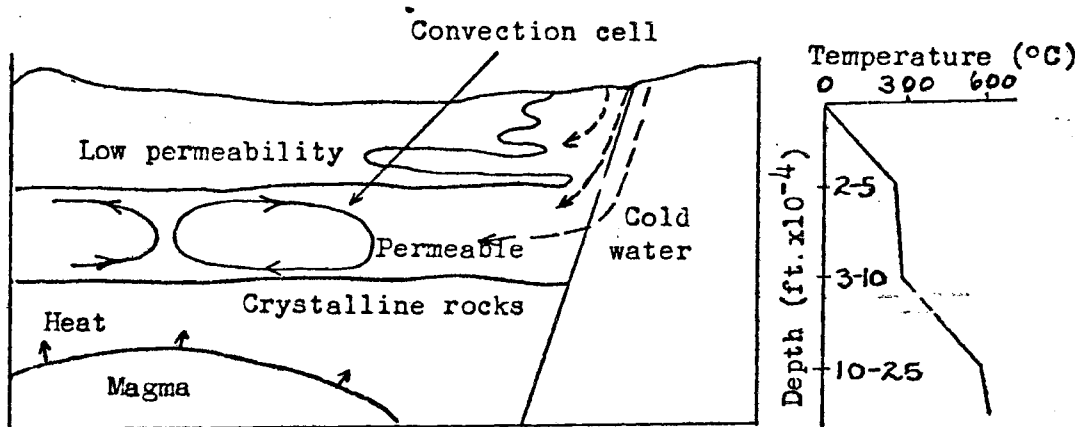
Workers conducting direct current resistivity surveys in geothermal areas have noticed a high level of background self-potential (personal communication, Dr. R.B. McEuen, San Diego State College, California, 1971), and indeed have suggested that self-potential may be useful as a survey technique for locating or delineating geothermal areas. Banwell (1970) states:

"Time-variable electrical and acoustic noise is known to be present in the neighborhood of active geothermal areas... High natural electrical potentials are commonly observed in the course of resistivity surveys of thermal areas, and their effect on measurements is removed by injecting suitable backoff potentials into the receiving circuit.

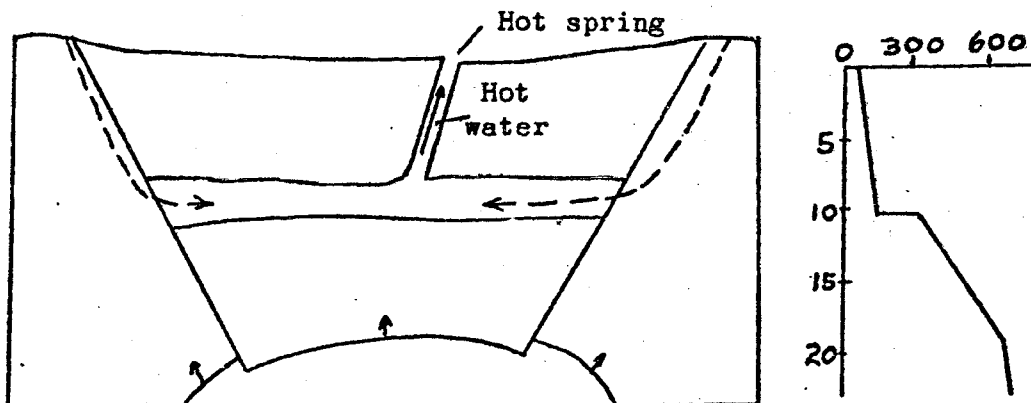
However, these natural potentials have never been measured systematically over a thermal area and its surroundings, and it is possible that the potential vectors, which are easily observed, may form a recognizably different pattern over the thermal area. Methods of this kind are sometimes used for the detection of certain types of buried ore bodies characterized by electro-chemical activity, and there are

Figure 5-13
Geothermal Systems
After White (1969)

13a
Insulated Reservoir



13b
High Rate of Upflow



theoretical reasons for expecting that thermal gradients in pore water electrolytes and contact potentials between bodies of ground water of differing temperature and chemical composition may also give rise to measurable electrical anomalies. Potential surveys of this type would be attractive in that they will have some depth-penetration and point by point observations can be made with relatively small electrode spacing."

Several mechanisms may contribute to surface self-potential fields in geothermal areas: streaming potentials, caused by the flow of heated water through the subsurface; thermoelectric coupling; chemical diffusion; and electrode reactions.

Streaming potentials would be generated as described earlier in this chapter, with negative potentials created at the surface by downward water flow through most geologic materials except clay, in which the polarity could be reversed. Thus, in Figure 5-13b, the central portion of the geothermal area might be expected to be positive with respect to the outer areas, as water is ascending at the center and descending at the edges. The potentials would be weakened by the high temperature and high dissolved solid content, and hence high electrical conductivity, of geothermal waters (Equation 5-4). Even so, the large volume of moving water typical of such areas still might generate appreciable streaming potentials.

Thermoelectric potentials are generated by a temperature difference applied across geologic inhomogeneities (Nourbehecht, 1963). Nourbehecht has calculated the thermoelectric potentials generated at the surface by a buried sphere of elevated temperature

(Figure 5-14). For $(a/d) = 1.0$, $R_{21} = 0.5$, and $(C_1 - C_2) = 0.2$, the maximum potential generated at the surface is about 8 mv per 100 °C of temperature difference. Thus, the magma chamber or the hot water reservoir could generate significant thermoelectric potentials at the surface.

The soil in areas of surface geothermal activity generally contains a large amount of various soluble salts, and the amount and type of salt vary widely from place to place. If the soil contains enough moisture to dissolve these salts, the salt ions will tend to diffuse away from areas of high concentration, creating a flow of charge, and thus a potential gradient, along the surface. These diffusion potentials may contribute to the large self-potentials observed in geothermal areas.

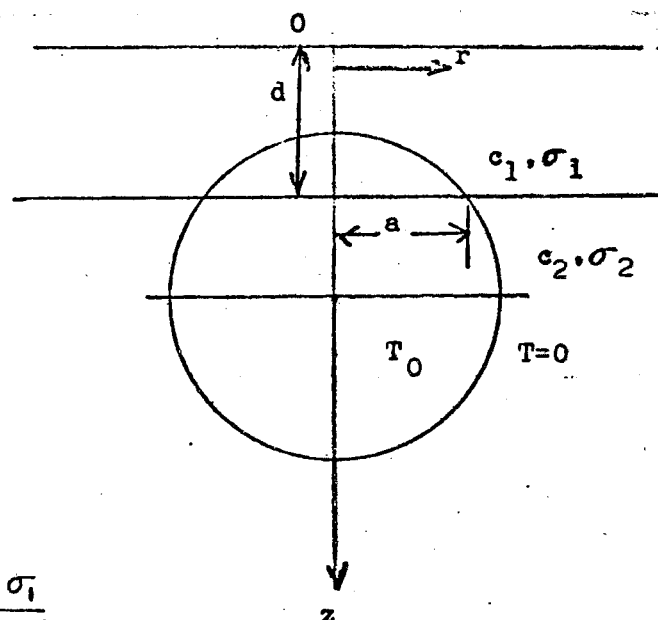
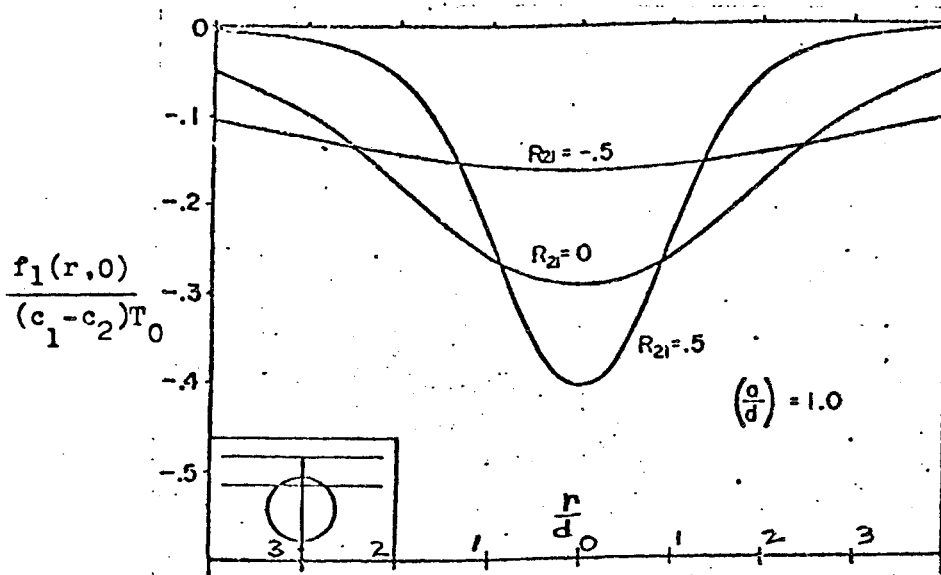
As discussed in Chapter 4, electrodes respond to temperature and concentration gradients (the copper-copper sulfate electrodes usually used for self-potential surveys are particularly sensitive to temperature changes, according to Ewing, 1939). If the two electrodes are placed in soil of different temperature, a potential difference will be generated: about 1 mv/°C for a Cu-CuSO₄ electrode pair, and about 0.14 mv/°C for a "CoCo" Ag-AgCl pair. Similarly, if the electrodes are placed in soils of different salt content, liquid junction potentials will appear across the electrode pair.

As temperature and concentration differences may act simultaneously on an electrode pair, considerable potentials may be developed. It is good practice, when conducting a self-potential survey in a geothermal area, to measure and record the ground temperature at each electrode location, and possibly to take soil

Figure 5-14

Thermoelectric Potential Generation

(From Nourbehecht, 1963)



$$R_{21} = \frac{\sigma_2 - \sigma_1}{\sigma_2 + \sigma_1}$$

$f_1(r,0)$ is potential in millivolts

T_0 is temperature in $^{\circ}\text{C}$

c_1, c_2 are thermoelectric coupling coefficients,
ranging from -0.086 to +1.36

σ_1, σ_2 are electrical conductivities

samples for later analysis. As salty mud clinging to an electrode may create diffusion potentials, the electrodes should be cleaned thoroughly each time they are removed from the soil.

Offshore and onshore self-potential surveys were run in several geothermal areas, as described in Chapter 6. Although the results of these surveys were inconclusive, it appears that a high level of self-potential variation does characterize areas of geothermal activity. This variation may prove useful as a tool for the study of geothermal systems, but would constitute noise in an offshore self-potential survey for sulfide minerals in a geothermal area.

An example of possible geothermal background noise is shown in Figure 6-48; with an electrode separation S (Figure 5-3) of 400 ft (124 m), it has an amplitude of about 1 mv and a spatial wavelength of about 600 m in about 6 m of water. The larger (about 10 mv) anomaly shown in Figure 6-49 also may have been due to geothermal activity, or it may have been caused by corroding material on the sea floor.

Offshore gas and oil fields

According to Pirson (1971), "Gas and oil fields and certain metallic deposits act as underground 'fuel cells' which generate electric current. Distribution and vectorial properties of these currents may be traced at the surface of the earth by processing surface electrical potential measurements." The "fuel cell" activity apparently is due to the existence of a reducing environment above the oil or gas reservoir, which interacts with the surrounding oxidizing environment to produce a flow of

electrical current toward the reducing zone, generating a negative anomaly above the reservoir.

From Pirson's discussion, it appears that such anomalies may be of the order of -60 mv. at the Earth's surface. A sea-floor anomaly of this magnitude could be detectable at the surface. A survey for such anomalies over a known offshore oil reservoir, therefore, would be of great interest.

Summary

All of the noise conditions discussed in this chapter would not (hopefully!) exist at the same time. In calm water more than 1 meter deep, in an unpopulated area, the noise levels shown in Figures 5-7 and 5-15 are typical: less than 0.1 mv with an electrode separation of 20 to 40 m and a towing speed of less than 5 knots. Under these conditions, anomalies of one mv amplitude, such as that shown in Figure 6-24, are easily discernible by eye. In rougher water, or at higher towing speeds, the noise level may increase to 0.3 to 0.8 mv, as shown in Figure 5-8.

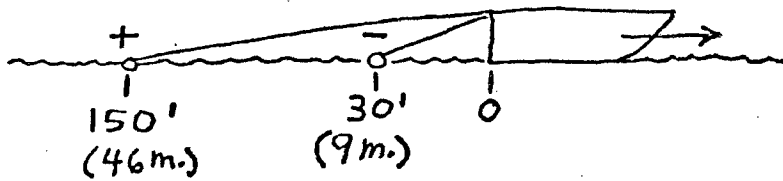
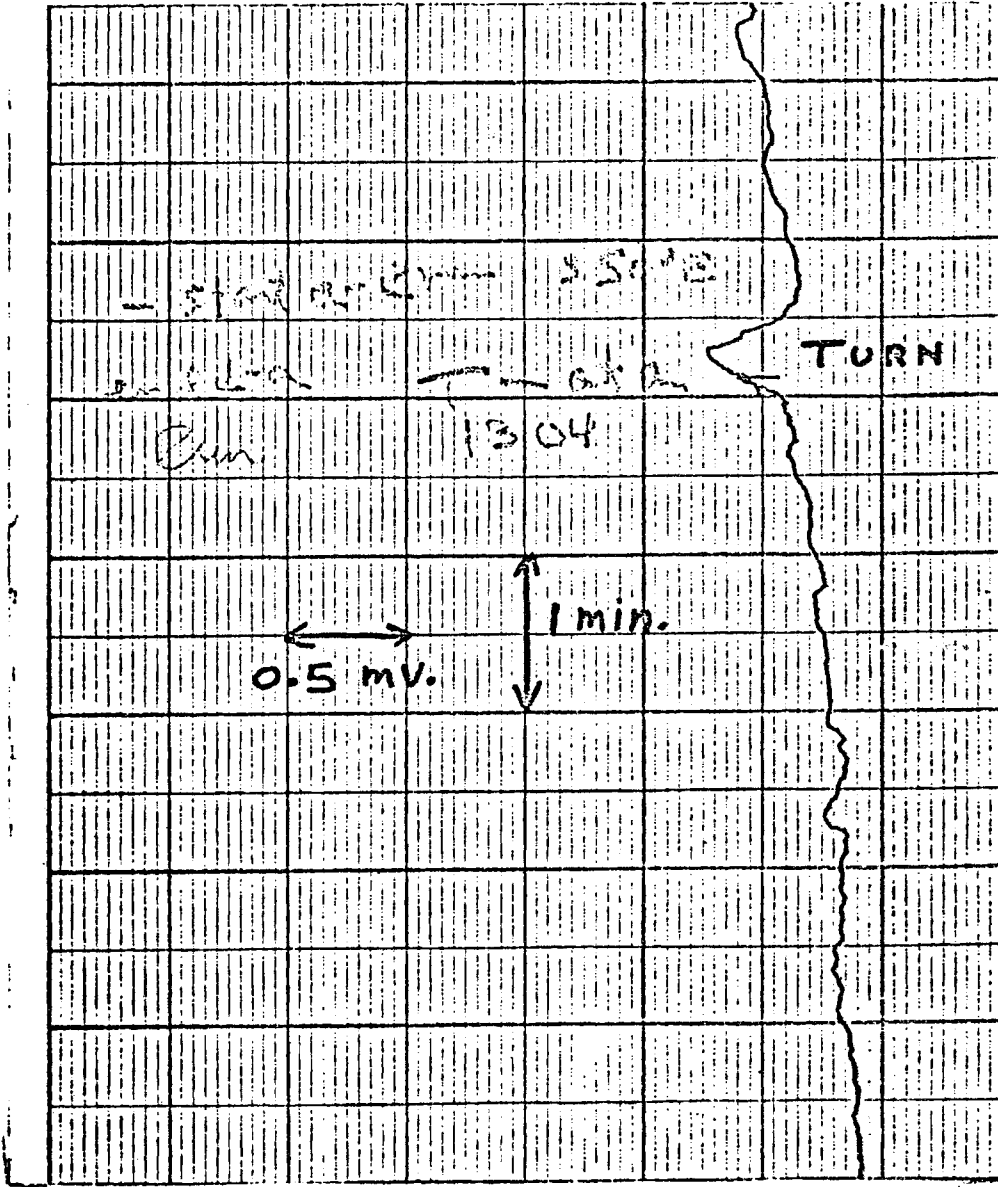
Noise levels higher than those mentioned above are not usual. In most cases their source is easily determined, and may be removed from the record, if desired, by judicious treatment of the data. (For example, von Arx (1962) uses a low-pass filter on the Geomagnetic Electrokinetograph to remove wave-generated noise). A noise level of a few tenths of a millivolt, then, appears to be the expected background for most offshore self-potential surveys, and at this noise level anomalies of greater than one millivolt should be easily distinguishable.

Figure 5-15

Typical Noise Level

Penobscot Bay, Maine

9 Sept. 1971



Summary of Noise Sources

Electrodes: No noise observed.

Cables: About 1 mv signal caused by turns; up to several mv caused by waves. Amplitude of cable noise increases with electrode separation.

Connections: Good connections cause no noise.

Chart Recorder: Case should be grounded to sea in wet weather. Noise spikes generated by pounding of boat in heavy seas.

Currents: Up to 1 or 2 mv zero shift when turning 180° in strong current field.

Waves: See cables.

Wake turbulence: Several tenths of a mv noise increase when boat speed is increased from 5 to 10 kt.

Magnetic field variations: Normally below 0.1 mv; may increase to 1 mv for long cables during magnetic storms.

Geologic background noise: 0.1 to 0.2 mv in water depth less than 1 m, otherwise negligible except in geothermal areas (see below).

Corrosion:

Corrosion control systems:

Stray currents:

} May range up to one volt, when present.

Geothermal activity: Geologic background level increased. Large anomalies may be noted.

CHAPTER 6

FIELD WORK

"Anomalies are like assholes -
every geophysicist has at least one!"

Fred Wolper
Ketchikan, Alaska

Introduction

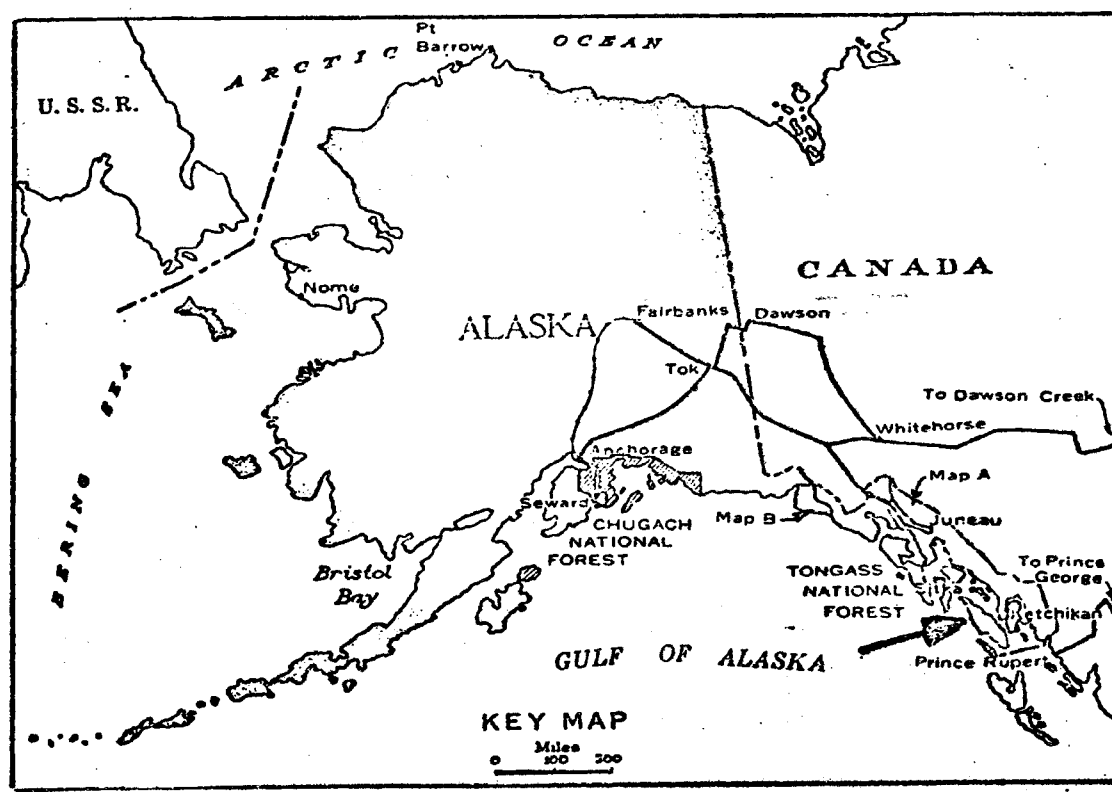
Field trials of offshore self-potential systems were conducted in three areas: Southeastern Alaska, in the vicinity of the city of Ketchikan; Penobscot Bay, Maine, near Blue Hill; and Punta Banda, Baja California, Mexico, near the city of Ensenada. The first two were areas where sulfide deposits were known to occur at or close to shorelines; the last is an area of known offshore geothermal activity. The results obtained in Alaska and Mexico, although interesting, were inconclusive. In Maine, on the other hand, two very large offshore self-potential anomalies proved to be related to onshore sulfide and graphite deposits, and several small anomalies appeared to be related to submerged sulfide deposits. The results from each of these three areas are discussed below.

Alaska

The area around Ketchikan, Alaska (Figure 6-1) contains a large number of rich sulfide deposits, many of which occur at or near shorelines (Wright and Wright, 1908; Buddington and Chapin, 1929). The sulfide-bearing formations are known to strike offshore in many locations, presenting ideal targets for offshore self-potential surveying. For this reason, and because excellent liaison with U.S. Bureau of Mines personnel in the area was available, the Ketchikan area was chosen as the first test site.

With the invaluable aid of Mr. Tom Pittman, a U.S. Bureau of Mines field geophysicist with encyclopedic knowledge of the area, a 38 foot salmon gill-netter, the M.V. "Maggie Deare", was chartered, and four working locations were selected. The general locations

Figure 6-1
Location of Ketchikan, Alaska



are shown in Figure 6-2, and more detailed maps of each area are given later. In most of the areas, Mr. Pittman conducted onshore self-potential surveys while the offshore surveys were being done. A variety of offshore self-potential systems and configurations was used, as described in the following sections.

Hump Island

"The Hump Island-Back Island area is the most favorably located area for initial trials. This is a copper-molybdenum prospect that has not been examined by the USGS or the USBM. A zone of sulfides, mostly pyrite in schist, is reported to extend two miles from the south end of Hump Island to the north end of Back Island. At the south end of Hump Island the schist is reported to contain about 10% total sulfides. The reports are considered to be reliable." (Letter from Mr. John J. Mulligan, U.S. Bureau of Mines, Juneau, Alaska).

The south end of Hump Island (Figure 6-3), where the sulfide zone outcropped at the shoreline and appeared to strike offshore, was selected as the first test site. Two onshore self-potential surveys were run across the strike of the zone, one about 15 m north of the shoreline and one directly at the shoreline (Figure 6-4). (All onshore surveys were made with a Sharpe model SP5-R S-P-Resistivity Unit and Cu-CuSO_4 electrodes). A third survey was made just offshore, using a Keithley model 600A portable electrometer and lead electrodes (Figure 4-3). The results of these three surveys, shown in Figure 6-4, indicate that the sulfide deposit generated an S-P anomaly which decreased in amplitude toward the shoreline.

The offshore survey was run around the entire island, as

Figure 6-2
 Test Sites in Ketchikan Area



Figure 6-3
Hump Island



INTERIOR-GEOLOGICAL SURVEY, WASHINGTON D.C. 20540
M R-3750

1:63,360

4 MILES

18000 21000 FEET

5 KILOMETERS

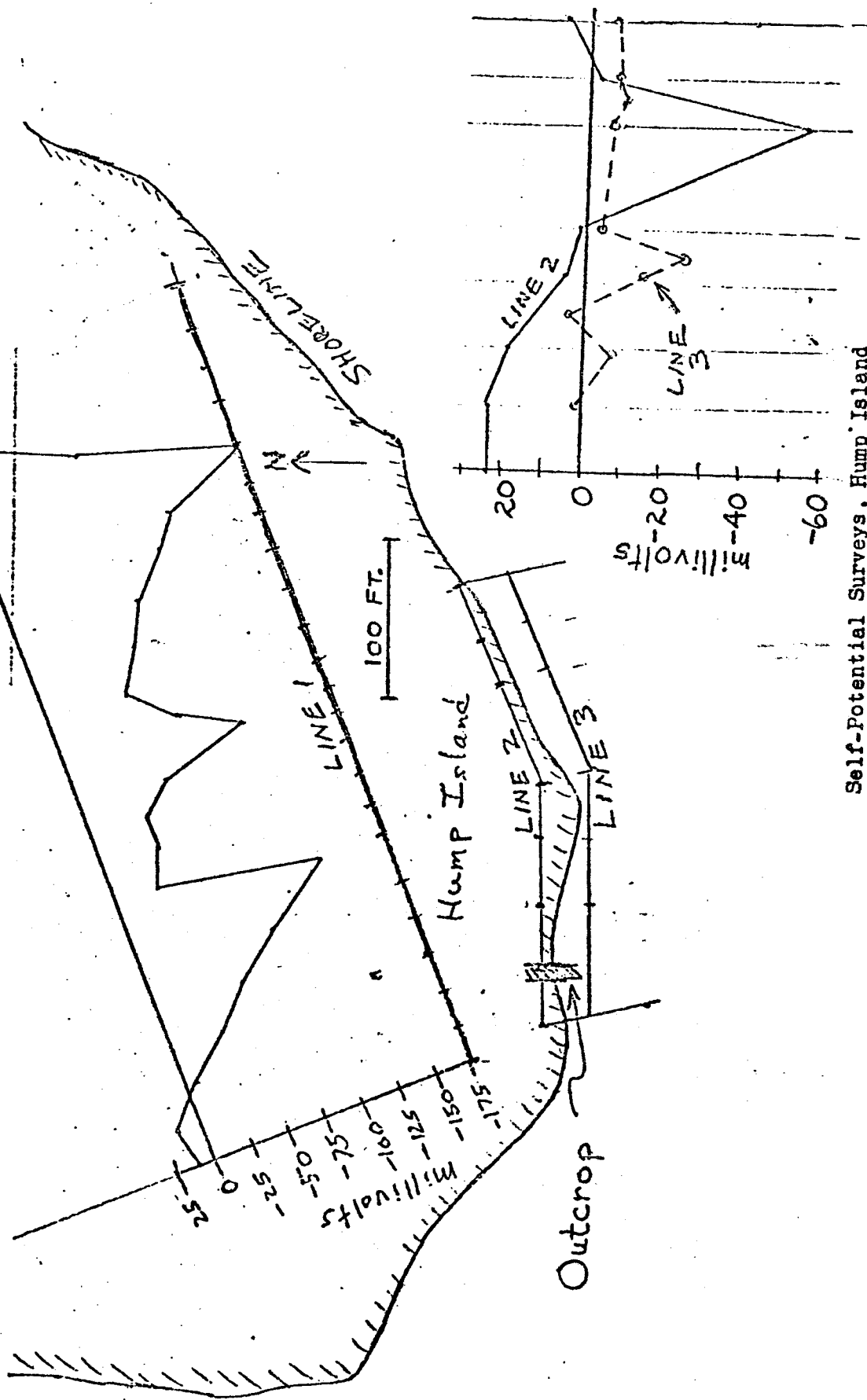
Depth curves
in feet



ROAD CLASSIFICATION

ALL WEATHER ROADS		DRY WEATHER ROADS	
Hard-surface	None	Improved dirt	None
Other	None	Unimproved dirt	None
Trails			

KETCHIKAN (C-6), ALASKA
N5530-W1314G/1520



Self-Potential Surveys, Hump Island

Figure 6-4

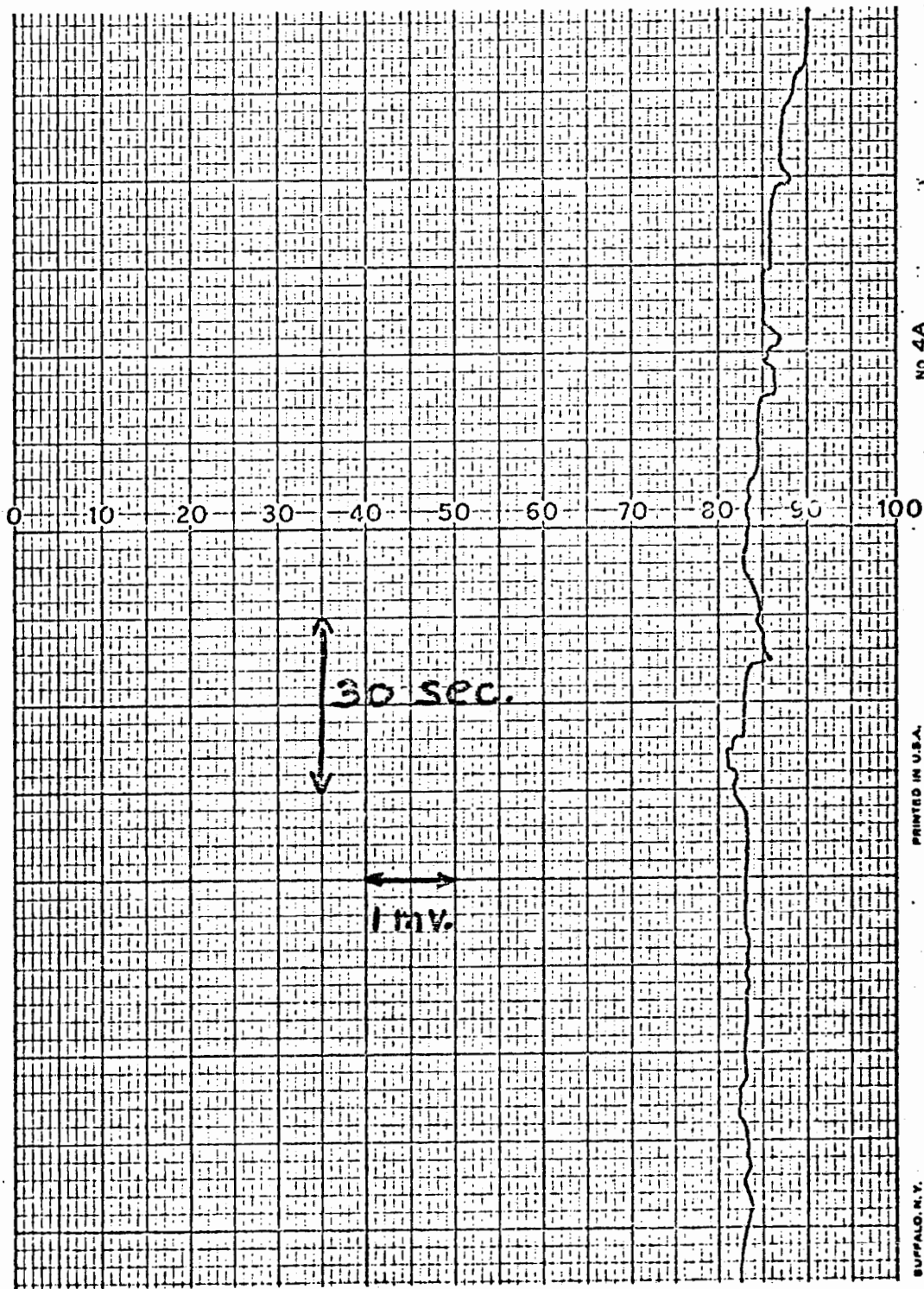
close to shore as the draft of the vessel (4 feet) permitted. As the bottom topography was rugged, with numerous shoal areas, it was usually not possible to approach closer than about 20 m from shore. Water depth at this distance averaged about 15 m. The system consisted of a pair of lead electrodes directly connected to a Varian model G-14A-5 chart recorder. The recorder was powered by an inverter run from the boat's 12 volt system, and was grounded to the sea with a separate lead electrode.

The lead electrode exhibited little noise while being towed through calm water at about 1 or 2 knots (Figure 6-5), but drift and non-repeatability were problems. The electrodes would drift 5-10 mv per hour during towing, and a test signal (wires from a 9 volt transistor battery dipped in the water near the electrode) often would polarize the electrode several millivolts.

Several different towing configurations were tried, including a horizontal array (Figure 3-8) with separation S of 50 m and a vertical array with one electrode at the surface and the other held close to the bottom with a V-fin. No definite S-P anomalies were seen in any of the towed tests, indicating that (1) the sulfide zone pinched out or plunged very steeply offshore, or (2) the sulfides continued offshore but generated no S-P signal, or (3) the equipment used was unable to detect an existing S-P signal.

Judging by the rapid decrease in the onshore signal, (1) appears to be the most reasonable assumption. As we were unable to get closer than 40 or 50 m to shore at the points of maximum anomaly shown on Figure 6-4, it is not surprising that no extension

Figure 6-5
Signal from Lead Electrodes



BUFFALO, N.Y.

of the onshore signal was detected. A brief survey by SCUBA divers found no evidence of sulfide outcrops a few meters past the low tide line. Although the lead electrodes used certainly inspired little confidence, any signal greater than a few millivolts should have been detectable.

Roe Point

A sulfide deposit containing pyrite, pyrrhotite, chalcopyrite, gold, and silver in mica schist is located on the shoreline of Behm Canal, two miles south of Roe Point (Wright and Wright, 1908, p. 347). As shown in Figure 6-6, the deposit strikes offshore, and a small (about 2 m wide) mineralized vein can be seen entering the water on the face of a shoreline cliff (Figure 6-7). Unfortunately, it was not determined whether the vein at the shoreline was continuous with the main deposit. An onshore S-P survey conducted across the strike of the deposit (Figure 6-8) showed an anomaly of -225 mv just to the north of the deposit, and -475 mv just to the south (the survey was run about 75 m inshore, parallel to the shoreline).

The bottom dropped off steeply from the shoreline, and water depth was 20 m at a point 15 m from the shore, opposite the location where the mineralized vein entered the water. This was as close to shore as the offshore survey could be run from the "Maggie Deare", due to numerous shoals and snags closer in. All offshore S-P surveys were made with the salt bridge system shown in Figure 4-5, at a speed of 2-3 knots.

The first offshore run was made using a surface array (Figure 3-8) with a separation S of 50 m, with the forward electrode 6 m astern. Unfortunately, the chart recorder was set at 100 mv full scale for this run, and no anomaly was observed opposite the

Figure 6-7
Mineralized Vein at Shoreline
Roe Point

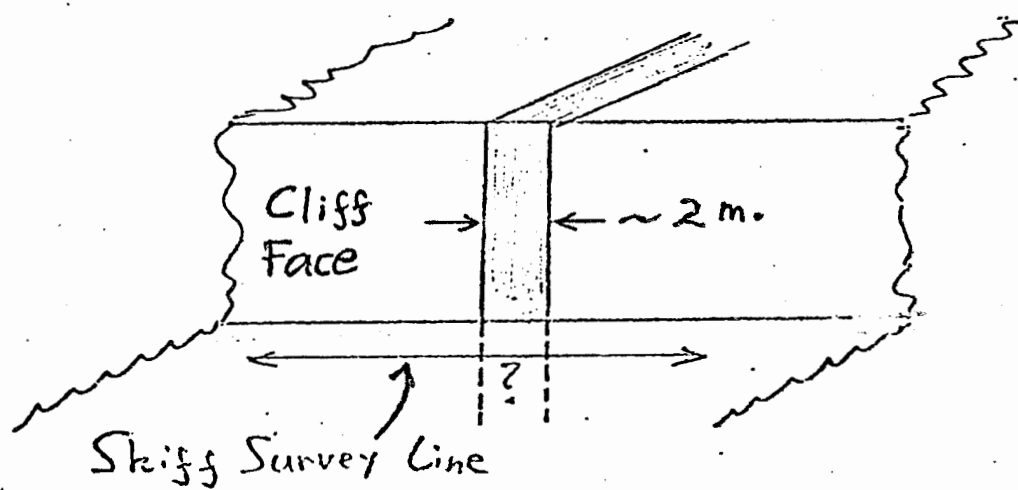
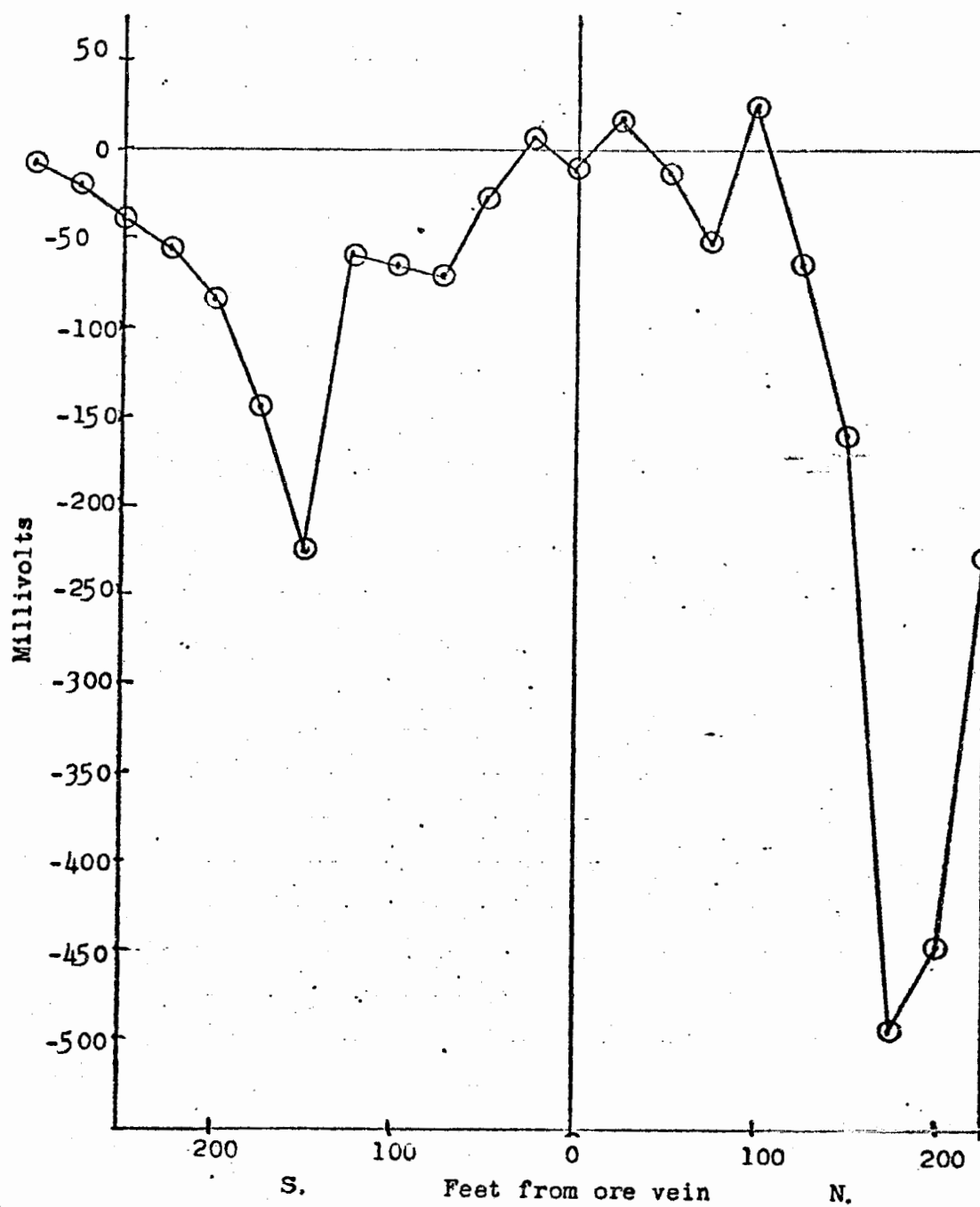


Figure 6-8
Onshore Self-Potential Survey
Roe Point



vein (Figure 6-9). From the discussion in the next paragraph, it appears that an anomaly would have been seen had a more sensitive scale been used (10 or 1 mv full scale). The noise level seen in Figure 6-8, which appears to be about 1 mv, actually was inherent in the chart recorder and isolation amplifier, as it did not increase as the sensitivity was increased in later runs (Figure 6-10).

The second run was made using a vertical array with the reference tube at the surface and a V-fin used to hold the lower tube to a depth of 20 m (water depth was just over 20 m). A small, but definite and repeatable, anomaly of about 0.5 mv amplitude was seen opposite the vein, about 15 m offshore (Figure 6-10). The anomaly was easily detectable above the background noise level of about 0.1 mv. Stepping on or handling of the salt bridge tubes produced noise spikes of several mv.

As the "Maggie Deare" was unable to approach closer than about 15 m to shore, a skiff was used to tow one tube past the vein, about 1 m offshore, while the reference tube and chart recorder remained aboard the "Maggie Deare". A surprisingly small, but repeatable anomaly of about 4 mv amplitude was observed when crossing the vein (Figure 6-11). If the shoreline vein was continuous with the main ore body, the anomaly along the shoreline should have been at least of the same order of magnitude as that shown in Figure 6-8. Apparently, it was not continuous, and the observed field either was the extension of the field from the main body, or was generated by the vein. Due to the rough topography no onshore survey was run at the shoreline. As the geometry of the vertical array shown in Figure 6-10 was not known accurately

Figure 6-9

Horizontal Array Survey

Roe Point

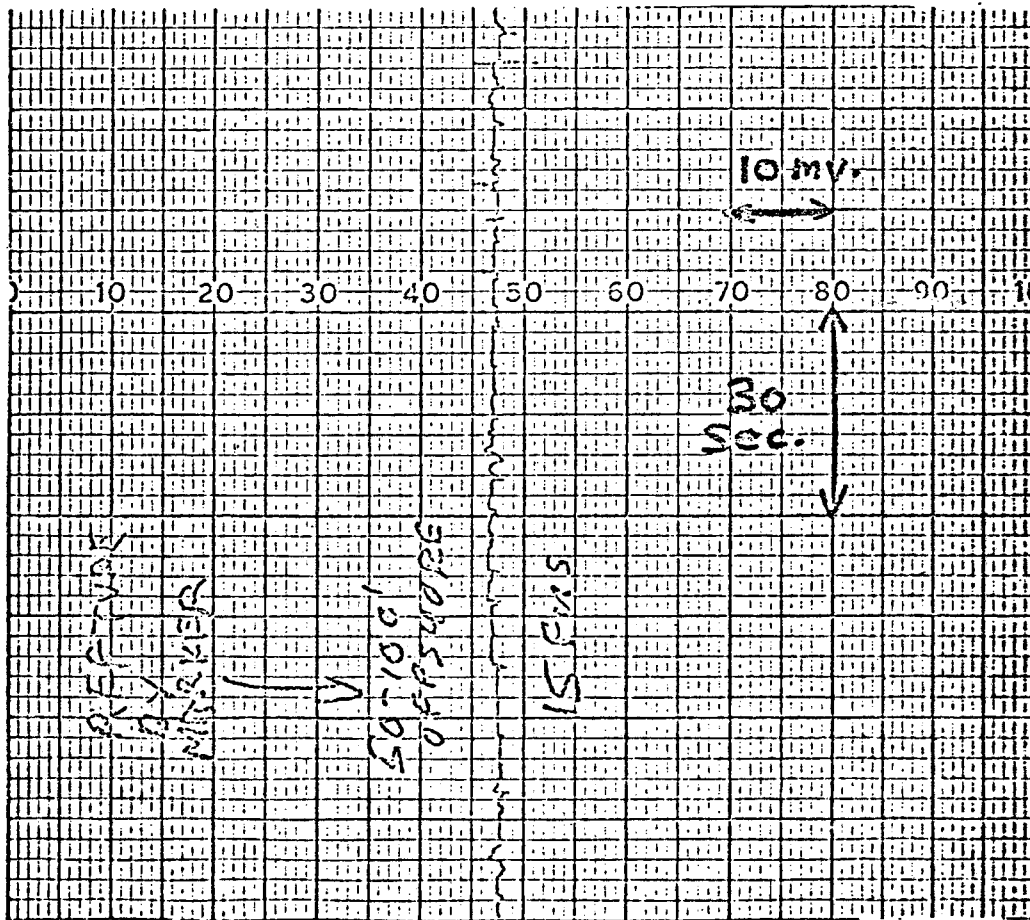
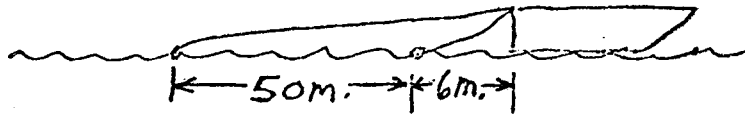


Figure 6-10

Vertical Array Survey

Roe Point

("Marker" refers to vein location)

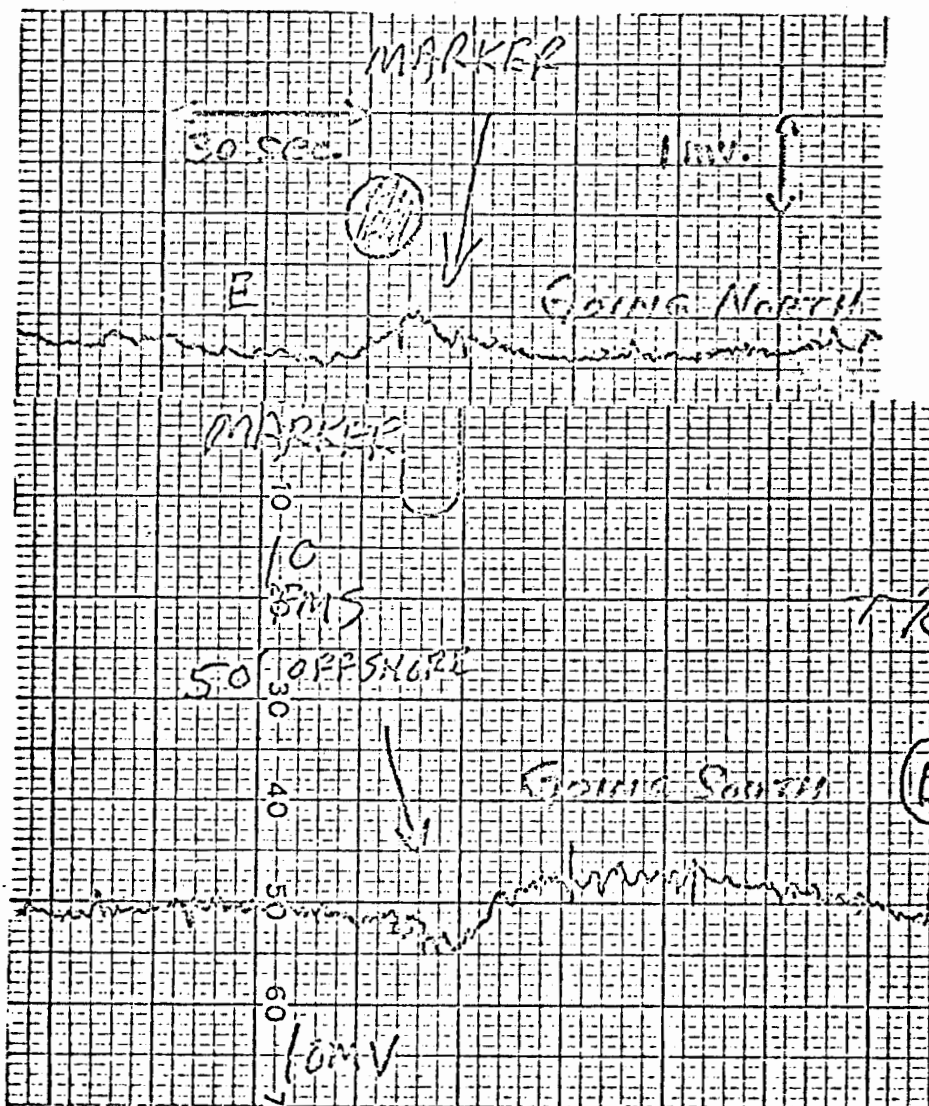
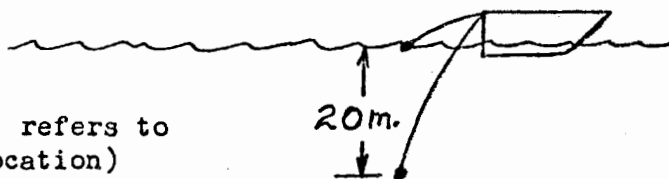
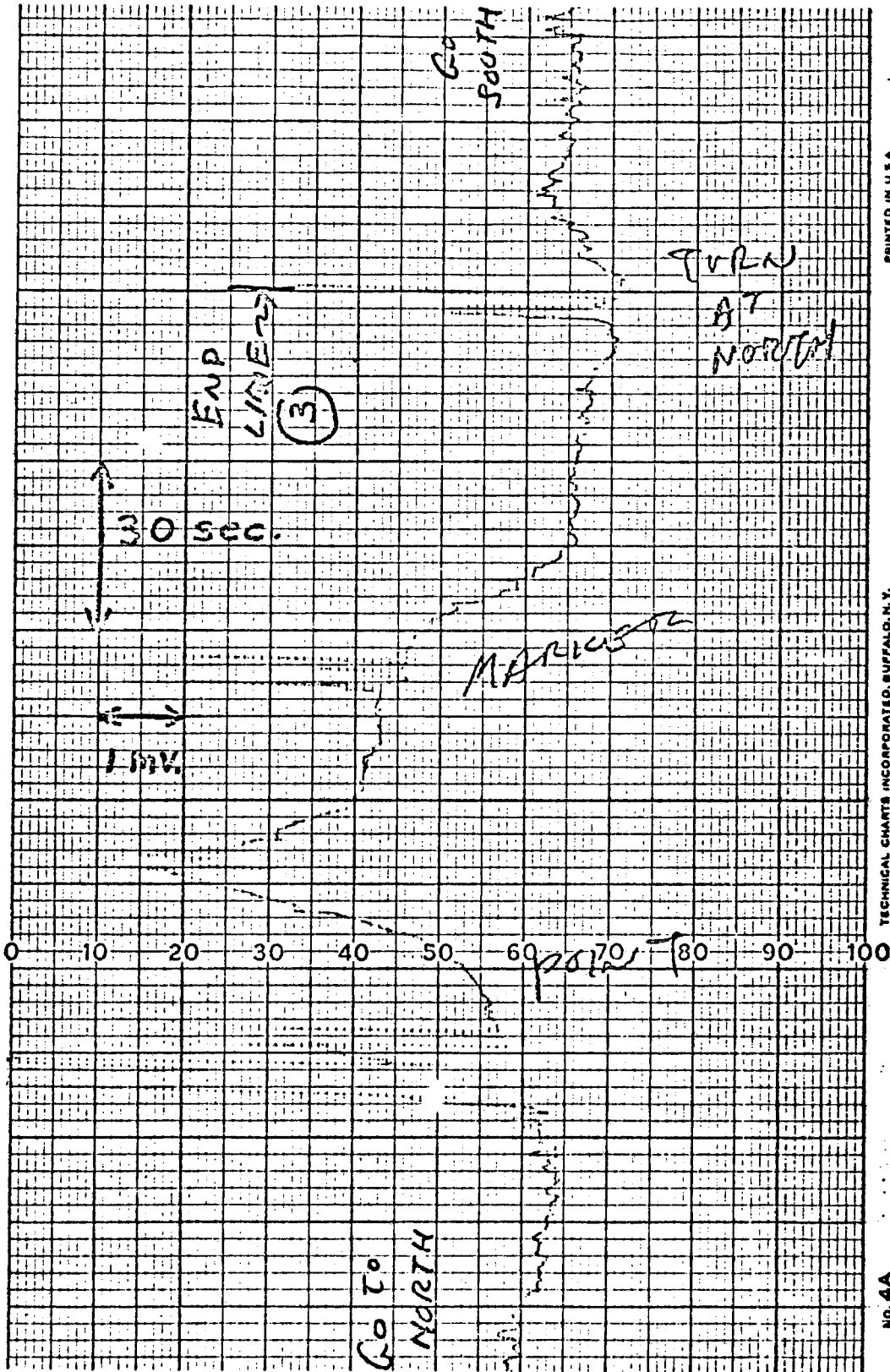


Figure 6-11

Skiff Survey Results

Roe Point



PRINTED IN U.S.A.

TECHNICAL CHARTS INCORPORATED, BUFFALO, N. Y.

NO. 4A

it is impossible to state whether the anomaly shown in Figure 6-10 is solely the offshore extension of the field shown in Figure 6-11, or is partly due to an underwater extension of the vein.

Obviously, the profiling technique used for the near-shore survey was slow and clumsy, and the necessary handling of the salt bridge tube aboard the skiff produced the noise spikes shown in Figure 6-11. A self-contained system, carried aboard the skiff, such as that used in Maine (see below) surely would have produced better results. However, it was encouraging that a signal generated by an onshore ore body (and possibly its offshore extension) was detected offshore.

Niblack Anchorage

"The Niblack mine, at the head of the Niblack Anchorage (Figure 6-12) operated from 1902 to 1909 and consisted of a 300-foot shaft and about a mile of underground workings. Production, estimated on the basis of incomplete records was at least 1,400,000 pounds of copper, 1,100 ounces of gold, and 15,000 ounces of silver. The ore bodies were replacement deposits in schistose greenstone and consisted of masses of chalcopyrite and pyrite containing small amounts of sphalerite, galena, and hematite." (Buddington and Chapin, 1929, p. 174). Wright and Wright (1908, p. 128-131) give additional information on the Niblack mine.

An onshore self-potential survey run across the strike of the deposit gave a self-potential anomaly of -421 mv (Figure 6-13), indicating that sulfides still remained in the deposit. A parallel traverse run at the shoreline, however, showed no anomaly. Offshore self-potential surveys were made using the salt bridge system in a variety of configurations, towed parallel and as

Figure 6-12

Niblack Anchorage

C&GS # 8086
 1:40,000
 Depths in fathoms

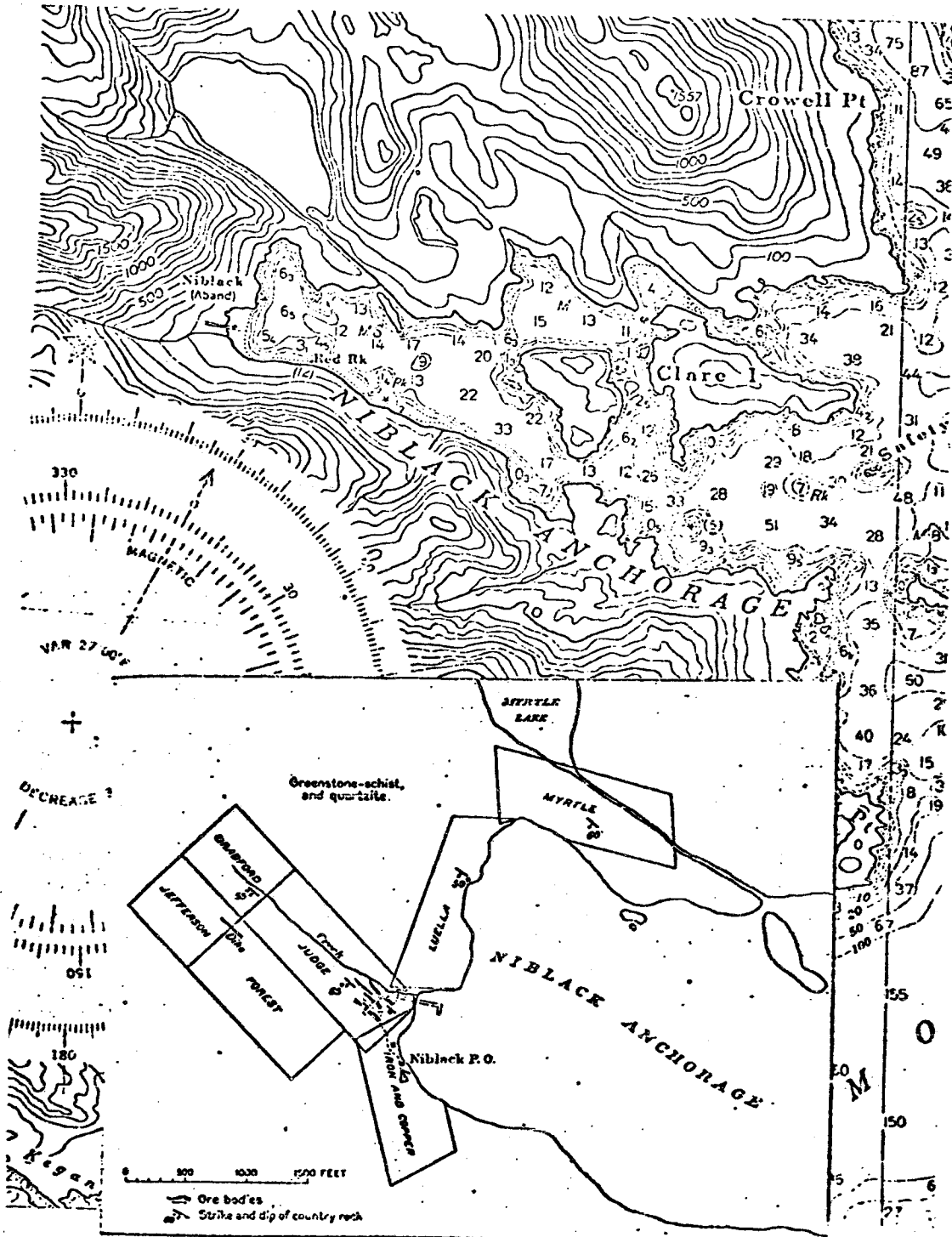
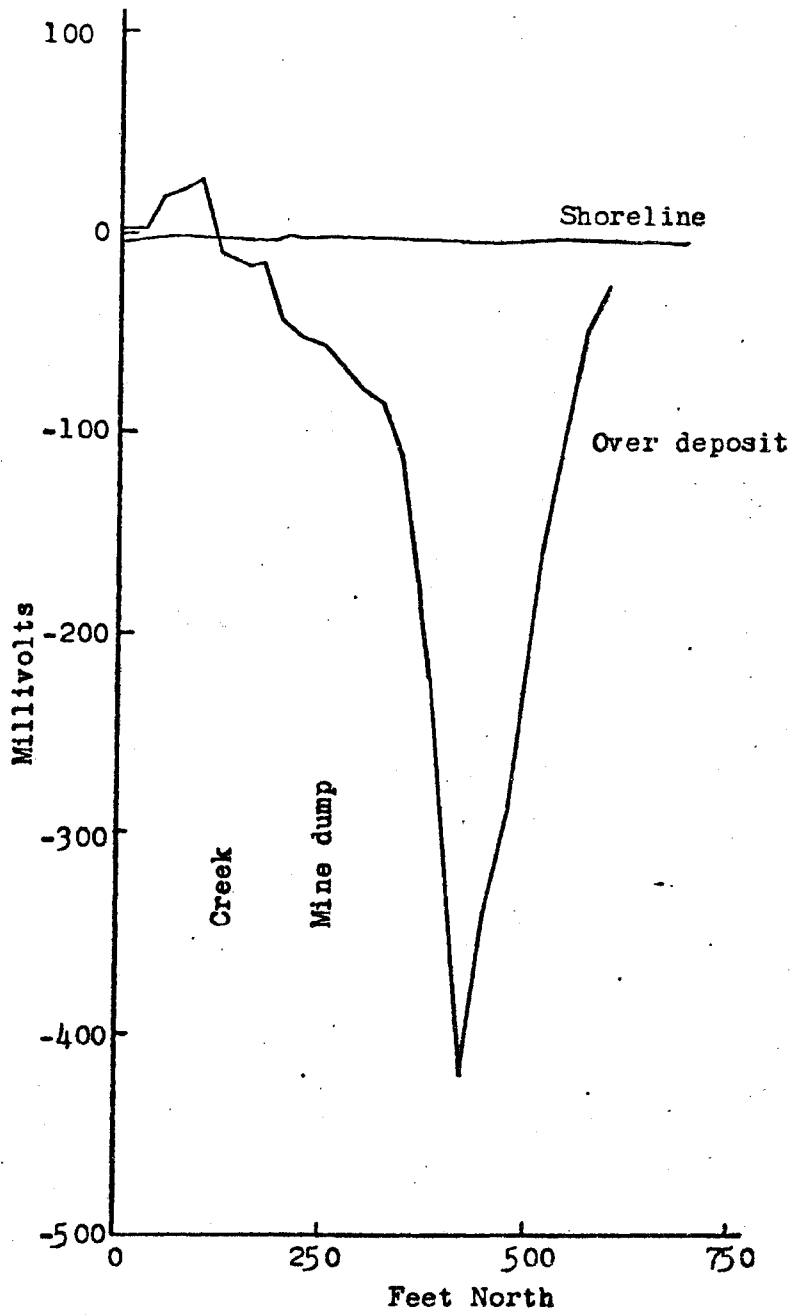


Figure 6-13
Onshore Self-Potential Surveys
Niblack Anchorage

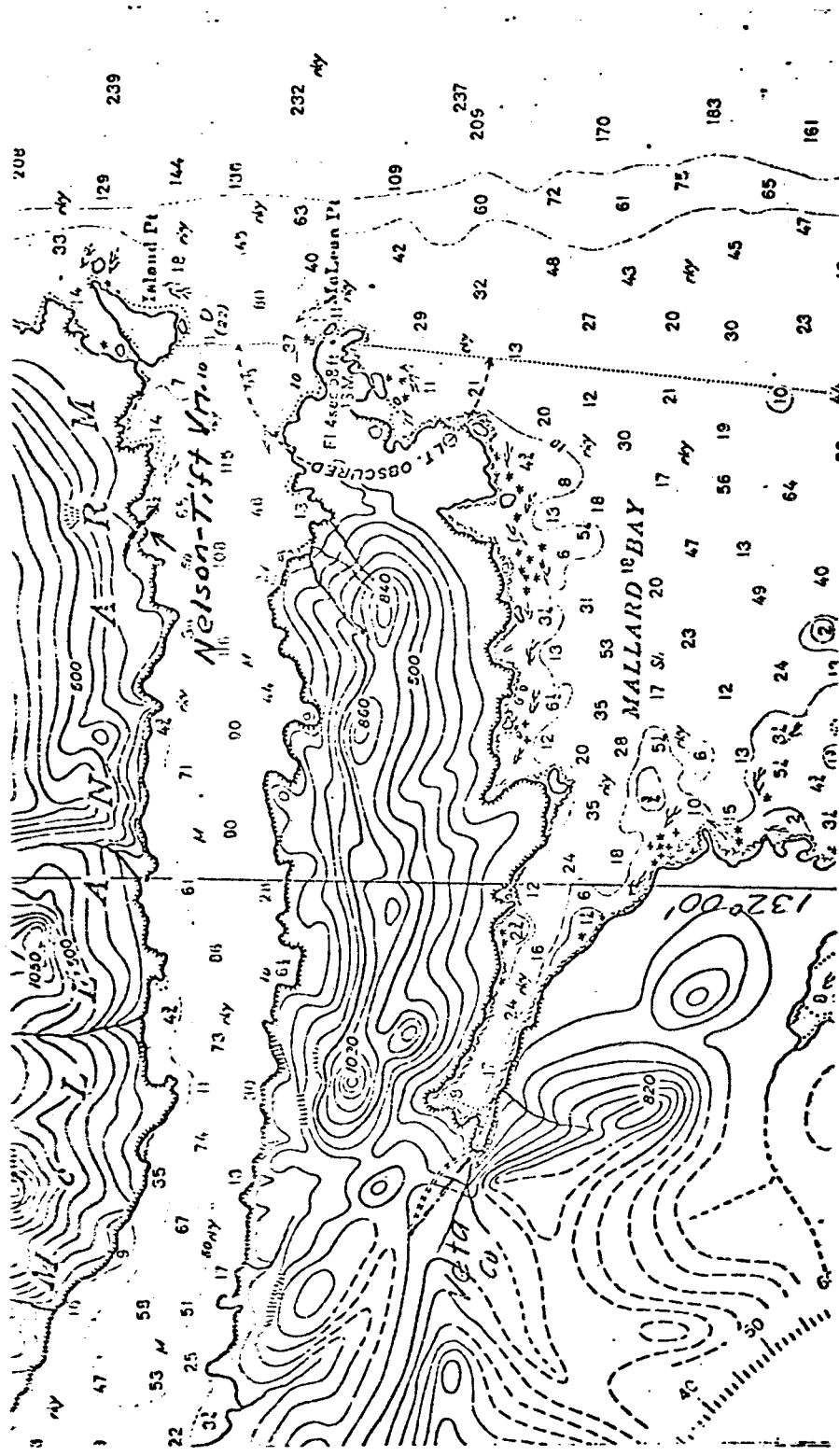


close to shore as possible (about 10 to 20 meters water depth). No anomalies were observed. SCUBA divers recovered samples of an offshore rock outcrop on strike with the former ore body; on analysis the samples proved barren of sulfides. From this evidence, it seems reasonable to conclude that there is no offshore extension of the Niblack ore body.

McLean Arm

The Nelson and Tift mine, discovered in 1935, is located on the southern shore of McLean Arm (Figure 6-14). "The deposit, which was mined out, was a lens composed mostly of auriferous pyrite and probably other sulfides in a roof pendant of cherty marble in quartz diorite. About 1,300 tons of ore were shipped, from which gold, silver, some copper, and a little lead were recovered. The precious-metal content ranged from 0.12 to 2.08 ounces of gold and from 0.05 to 0.40 ounce of silver per ton; data on the copper and lead content are not available." (Berg and Cobb, 1967, p. 175). A large notch had been cut into the rock at the shoreline to allow removal of ore (Figure 6-15). An onshore self-potential survey across the strike of the former ore body showed an anomaly of only -15 mv (Figure 6-16); apparently, the ore had been thoroughly mined out.

Maneuverability was so restricted in the area of the mine that no offshore self-potential surveys were attempted with the "Maggie Deare"; instead, all surveys were made with one tube of the salt bridge held at the anchored "Maggie Deare" while the other was carried on the skiff (Figure 6-15). Great excitement was occasioned when a large, but rather suspicious-looking,



C&GS # 6145
 1:40,000
 Depths in fathoms

McLean Arm
 Figure 6-14

Figure 6-15
Skiff Survey
Nelson & Tift Mine

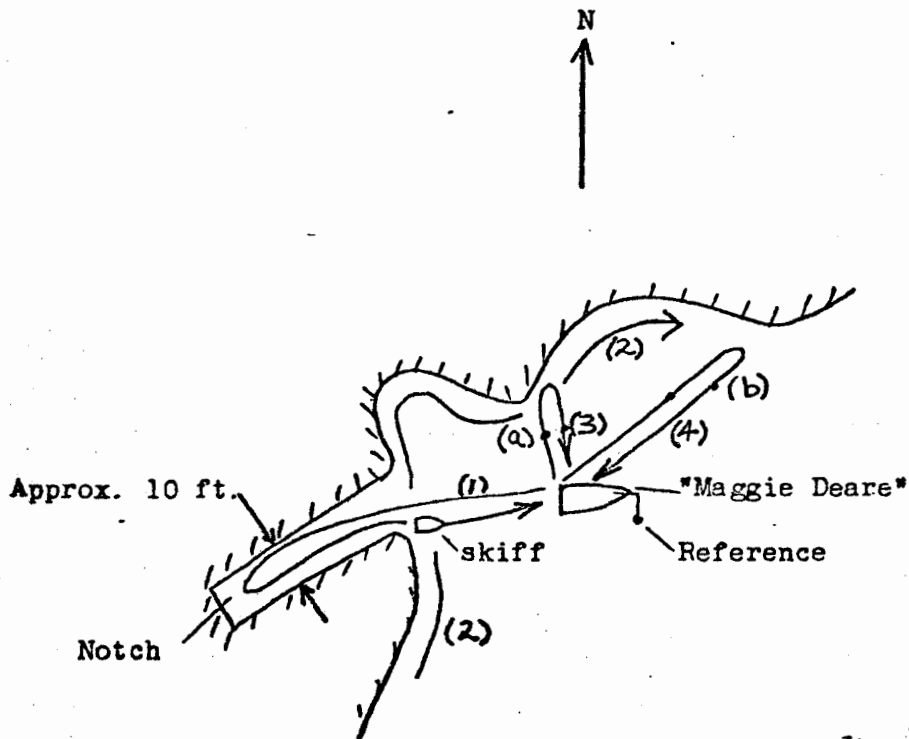
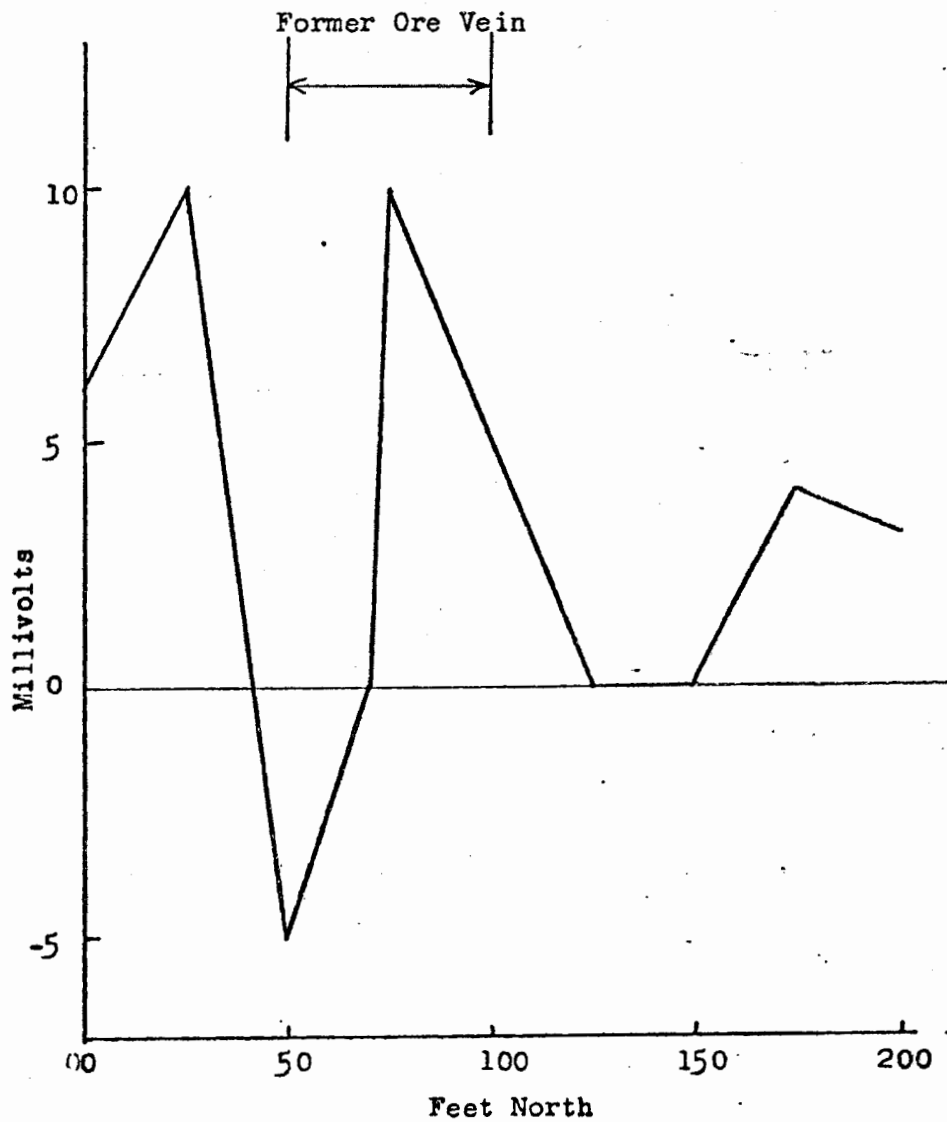


Figure 6-16
Onshore Self-Potential Survey
Nelson & Tift Mine



signal was repeatedly recorded at point (a) on survey line (3) and point (b) on survey line (4) (Figure 6-17), apparently on line with the strike of the former ore body. After the anomaly had been thoroughly surveyed, the excitement died when it became apparent that the "anomaly" was due to a leaky connection in the salt bridge tube which entered and left the water as the tube was pulled out and fed in from the "Maggie Deare". As our time in Alaska had run out, the expedition thus came to an inglorious end.

Maine

In September, 1971, at the invitation of Mr. Frederick M. Beck of the Callahan Mining Corporation, an offshore self-potential survey was run in the waters north of Cape Rosier, Maine (Figures 6-18 and 6-19). Many onshore sulfide deposits are known to exist in the area (prospects are indicated by the circled numbers in Figure 6-20; from Young, 1962). The Penobscot Mine, currently (in 1971) producing copper and zinc ore, is indicated on Figure 6-19, and is shown as location 7 on Figure 6-20 (Beck, 1970). The submerged area around Ram Island was of particular interest, due to its proximity to the Penobscot Mine, and some shows of sulfides on the island.

The onshore sulfide deposits in the area are known to produce self-potential fields (Young, 1962), and an onshore survey run over a recently discovered massive sulfide deposit, located south of the Penobscot Mine and covered by about 60 m of overburden, showed an anomaly of about -200 mv (Figure 6-21). Thus, the

Figure 6-17

Spurious Offshore Self-Potential Signal

Nelson & Tift Mine

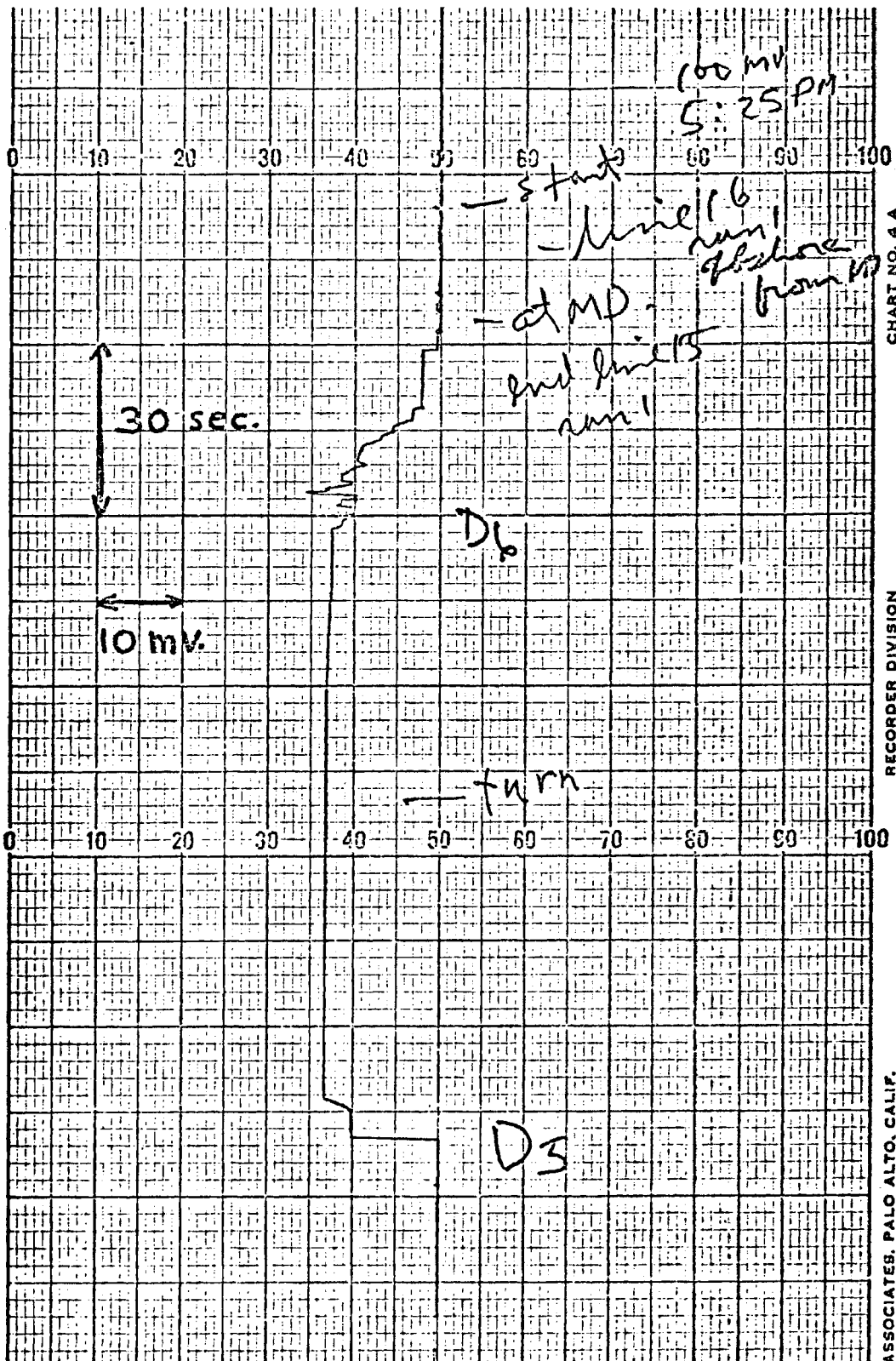


CHART NO. 4 A

REORDER DIVISION

ASSOCIATES, PALO ALTO, CALIF.

Figure 6-18
Location Map, Maine
From Beck (1970)

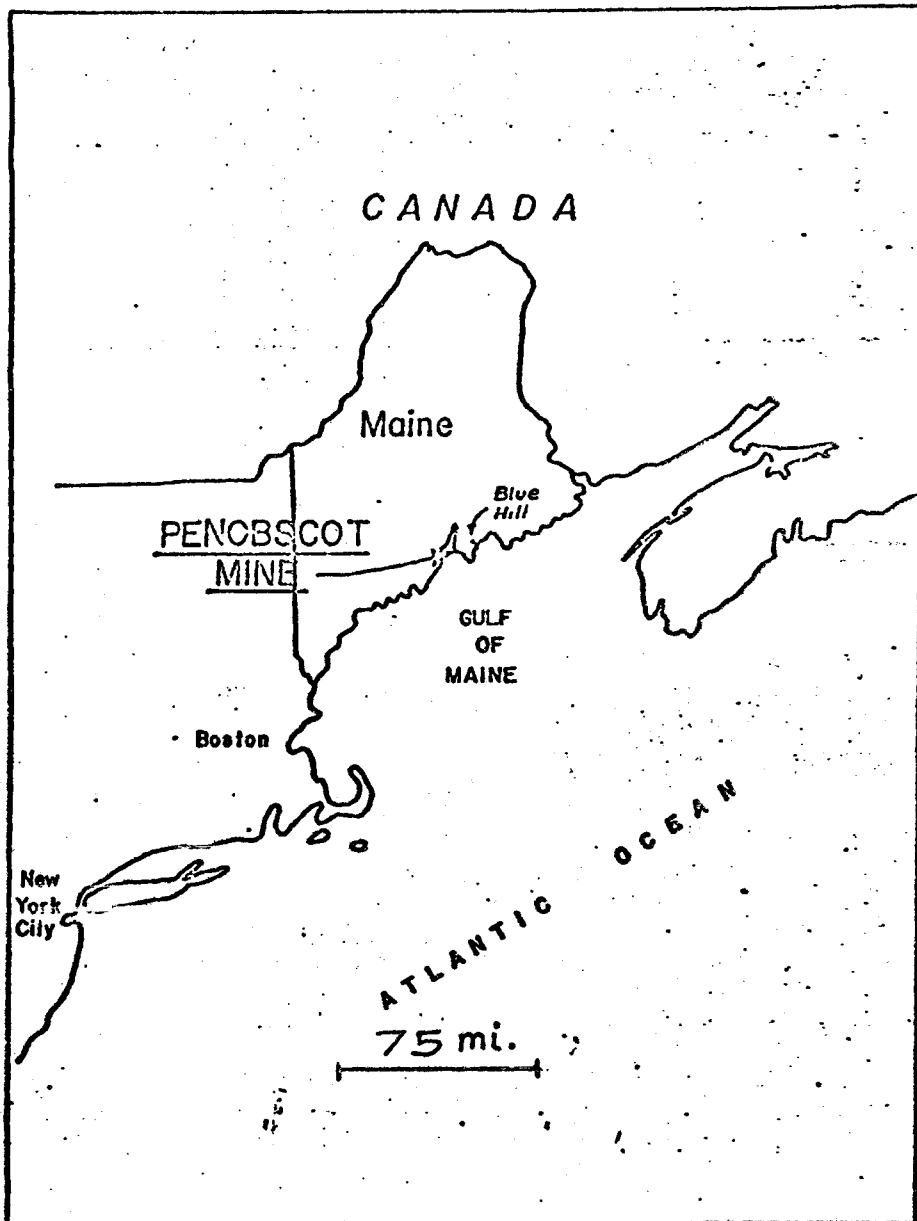
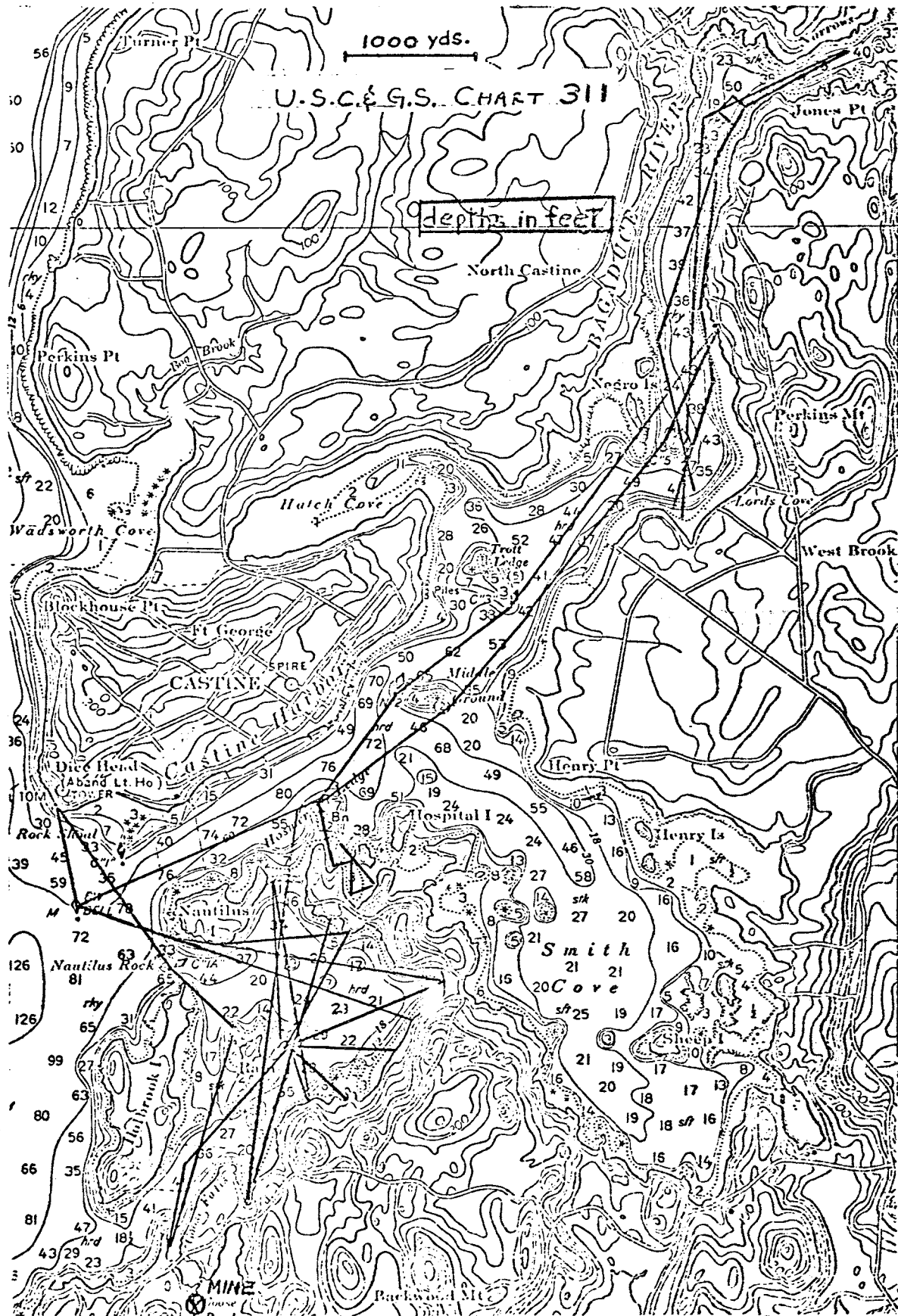


Figure 6-19
Survey Lines, Maine



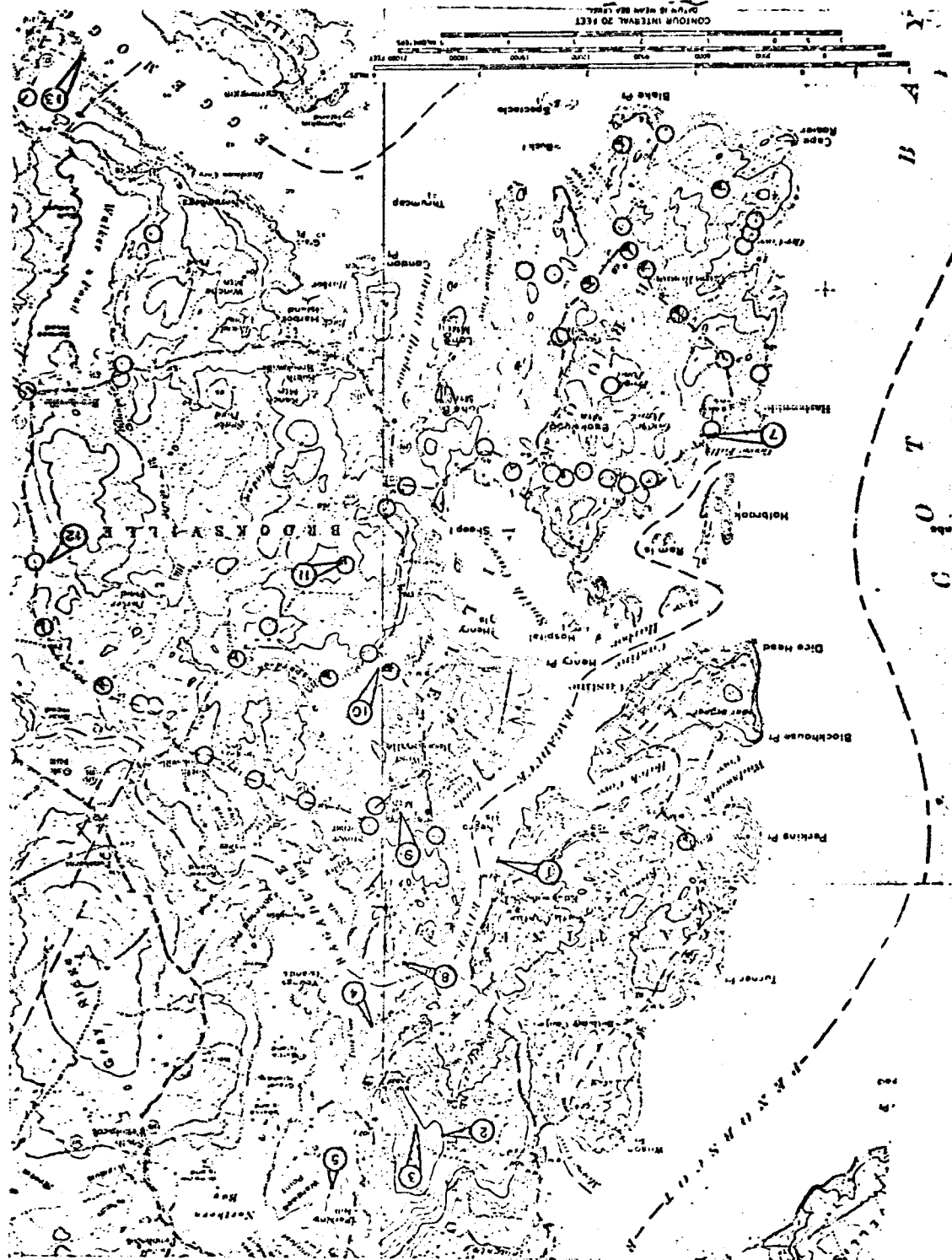
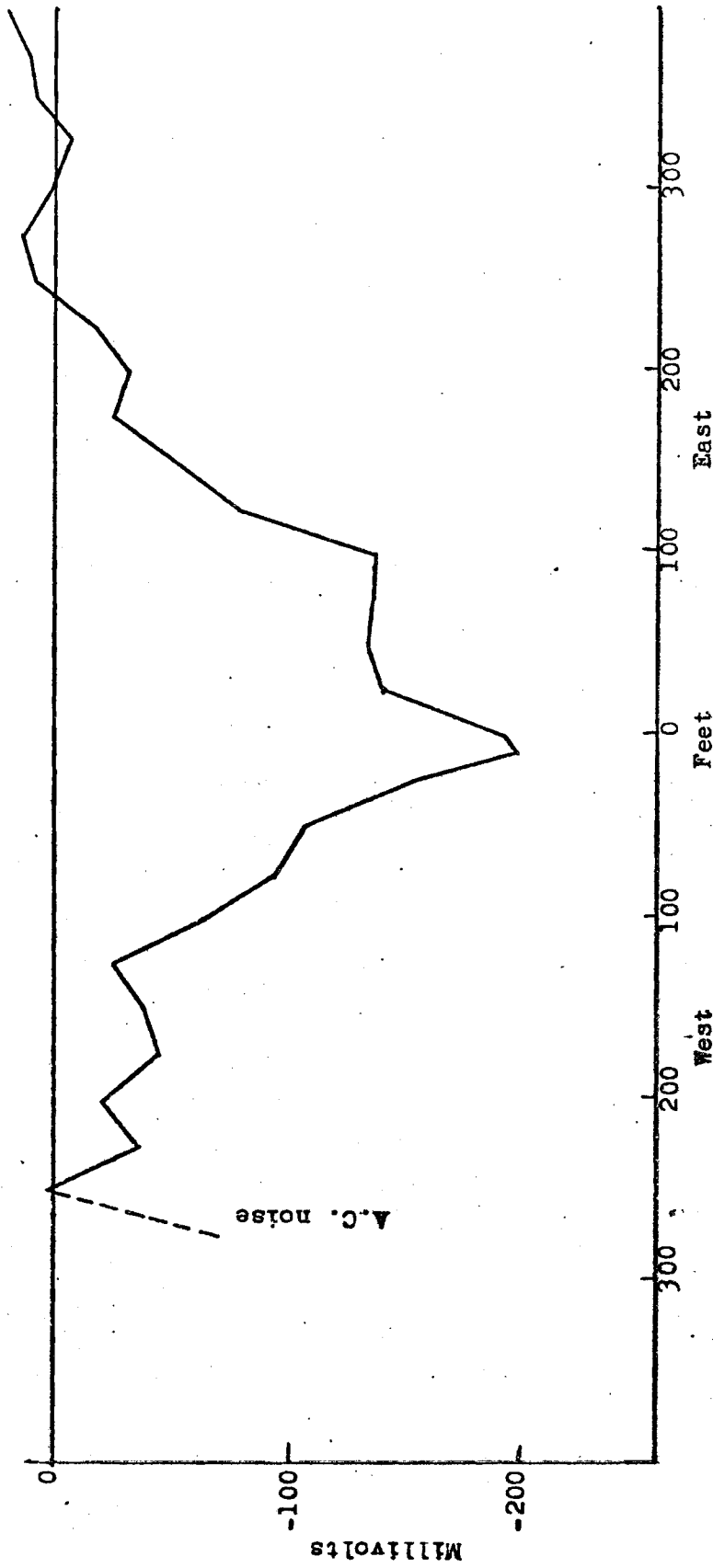


Figure 6-20
 Prospect Locations, Maine
 From Young (1962)



11 Sept. 1971

Onshore Self-Potential Survey Cape Rosier, Maine

Figure 6-21

prospects for the existence of offshore self-potential fields, caused by submerged or onshore sulfide deposits, appeared good.

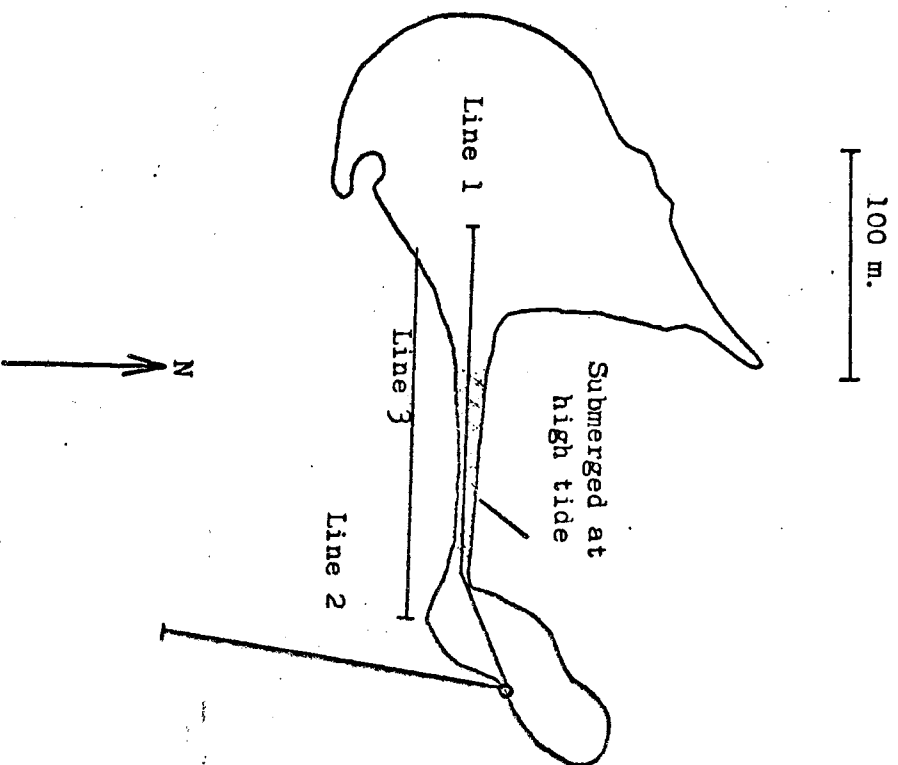
The offshore self-potential surveys were run in two general areas: the body of water surrounding Ram Island and bounded by Holbrook and Nautilus Islands on the east; and up the Bagaduce River, from Castine to the area labelled "Narrows" (the survey lines are shown in Figure 6-19). All offshore surveying was done using the system shown in Figure 4-27, which was carried aboard an open 14 foot (4.3 m) aluminum skiff powered by a 10 horsepower outboard motor. As the water generally was calm, and population sparse, noise levels usually were very low -- typically less than a few tenths of a millivolt (Figure 5-15).

Because of its proximity to the operating Penobscot Mine, the water area surrounding Ram Island was of the greatest interest, and was surveyed first. Despite the dense survey pattern (Figure 6-19), only one self-potential anomaly was recorded in the area. It was located off the northern end of Holbrook Island, and is discussed (as Anomaly #1) below. Otherwise, the record in the area was as shown in Figures 5-10 and 5-15.

Two land-based self-potential surveys were conducted from Ram Island, (lines 2 and 3 in Figure 6-22) with the reference electrode and the operator located at the shoreline. The scanning electrode was carried out 500 feet (153 m) by the boat, and then was towed in over the bottom toward shore. The signal level along these lines was very low; less than two millivolts. Line 1 (Figure 6-22), an onshore survey on Ram Island, showed similar low levels, even near shows of disseminated sulfides.

Figure 6-22

Ram Island Self-Potential Surveys



This lack of bottom self-potential activity apparently is reflected in the quiet nature of the offshore record in this area.

Beside the anomaly mentioned above, three other large offshore self-potential anomalies were recorded (Figure 6-23); one between Middle Ground and Trott Ledge, one east of Negro Island, and one west of Jones Point. Each of these is discussed in turn below.

Area #1 (North end of Holbrook Island)

An anomaly of about one millivolt amplitude was observed repeatedly just off the northern end of Holbrook Island (Figure 6-24). The anomaly was detected over an interval of about 150 meters along the line from Nautilus Rock to Ram Island which ran closest to Holbrook Island. Integration of the observed gradient anomaly gives a total field anomaly amplitude of about 0.5 mv (Figure 6-25). The source for this total field anomaly may be simulated by a buried, inclined current dipole, with the sink closer to the surface and toward the northwest.

A brief investigation of the rocks near the north end of Holbrook Island showed no sulfides, but some disseminated sulfides were found (in very small quantities) in rocks along the southern shore of Nautilus Island. Analysis of these rocks showed 0.11% copper, 0.09% lead, and 9.38% zinc.

Whether these sulfide-bearing rocks were responsible for the offshore self-potential anomaly is difficult to say. As the anomaly amplitude was greatest close to Holbrook Island, and decreased to zero on the line close to Nautilus Island, it is curious that the sulfide-bearing rocks were found only on the island. There was no evidence of cables, pipelines, or

Figure 6-23
Anomaly Locations



Figure 6-24

Anomaly # 1.

(North End of Holbrook Island)

11 Sept. 1971

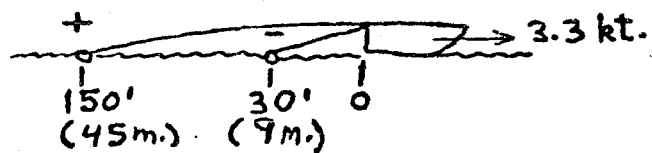
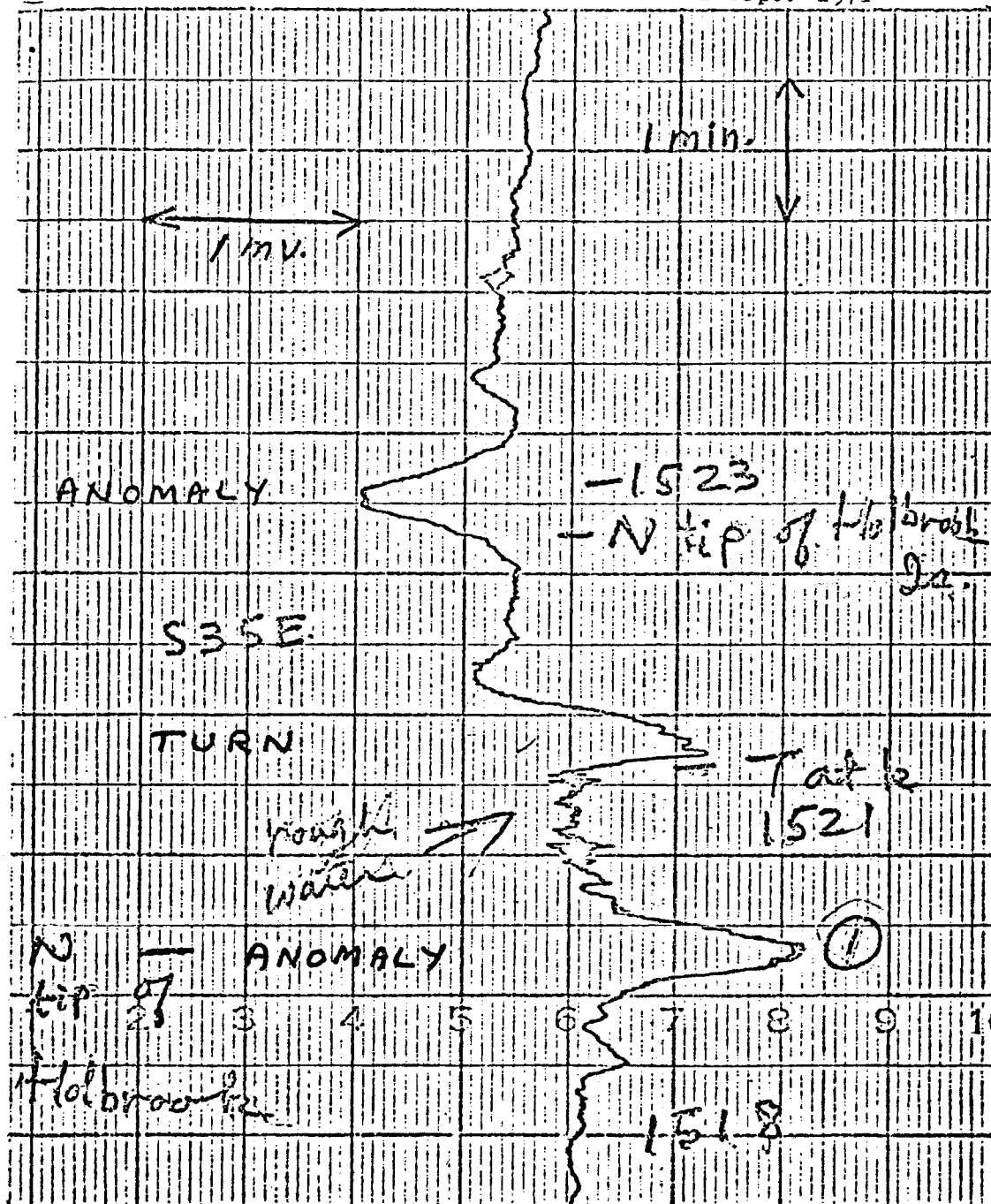
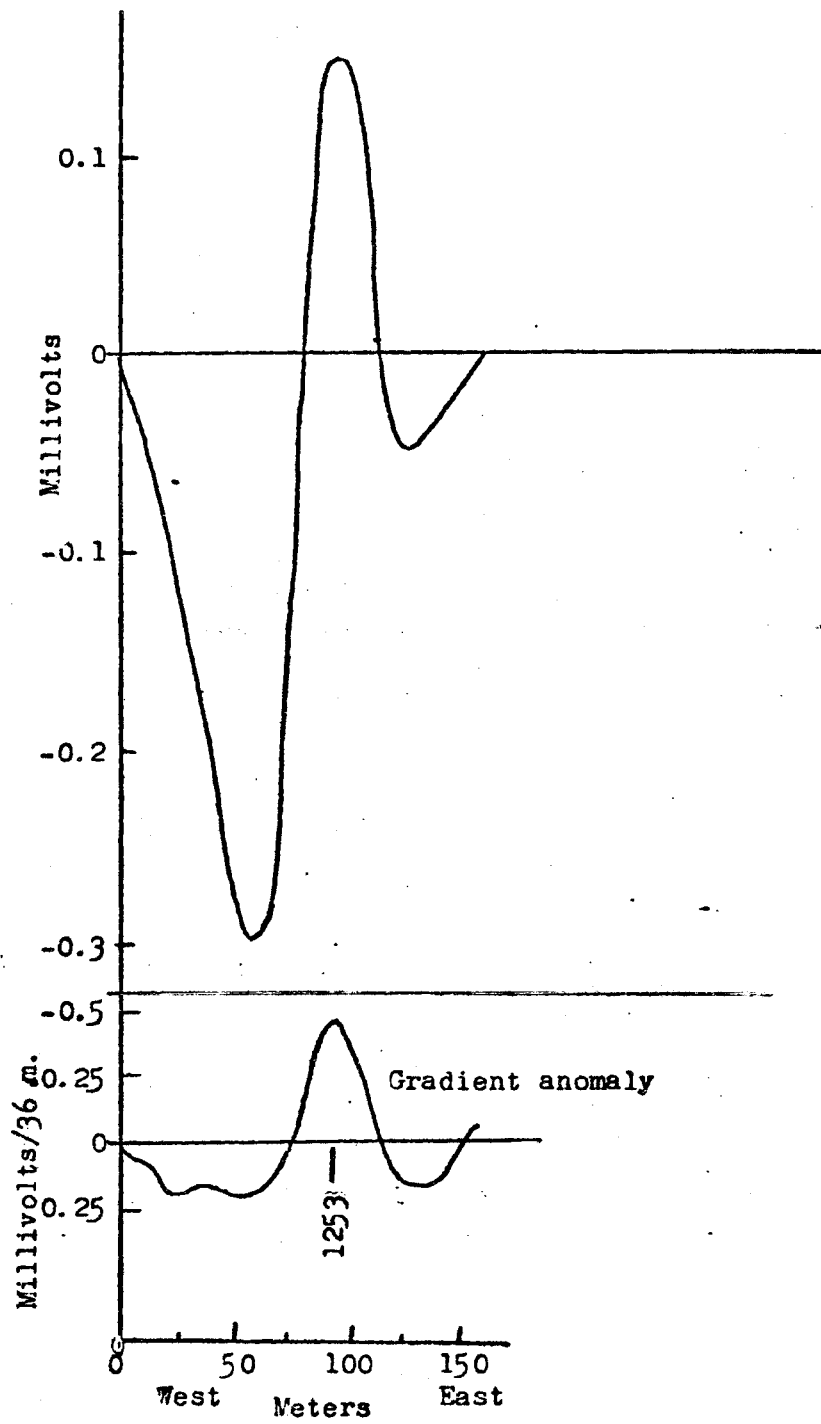


Figure 6-25
Integration of Anomaly # 1



human activity in the area, so it seems reasonable to assume that the observed anomaly was a self-potential signal, generated by a submerged mineral deposit. This assumption is strengthened by the negative polarity of the total field anomaly, which would be expected of a sulfide self-potential field.

The onshore geology was complex, and it was impossible to determine, in the time available, whether the strike of the sulfide bearing formation on Nautilus Island was in the direction of the observed offshore anomaly. However, it was encouraging that an offshore self-potential field did lead to the discovery of sulfide-bearing rocks nearby.

Area #2 (Middle Ground to Trott Ledge)

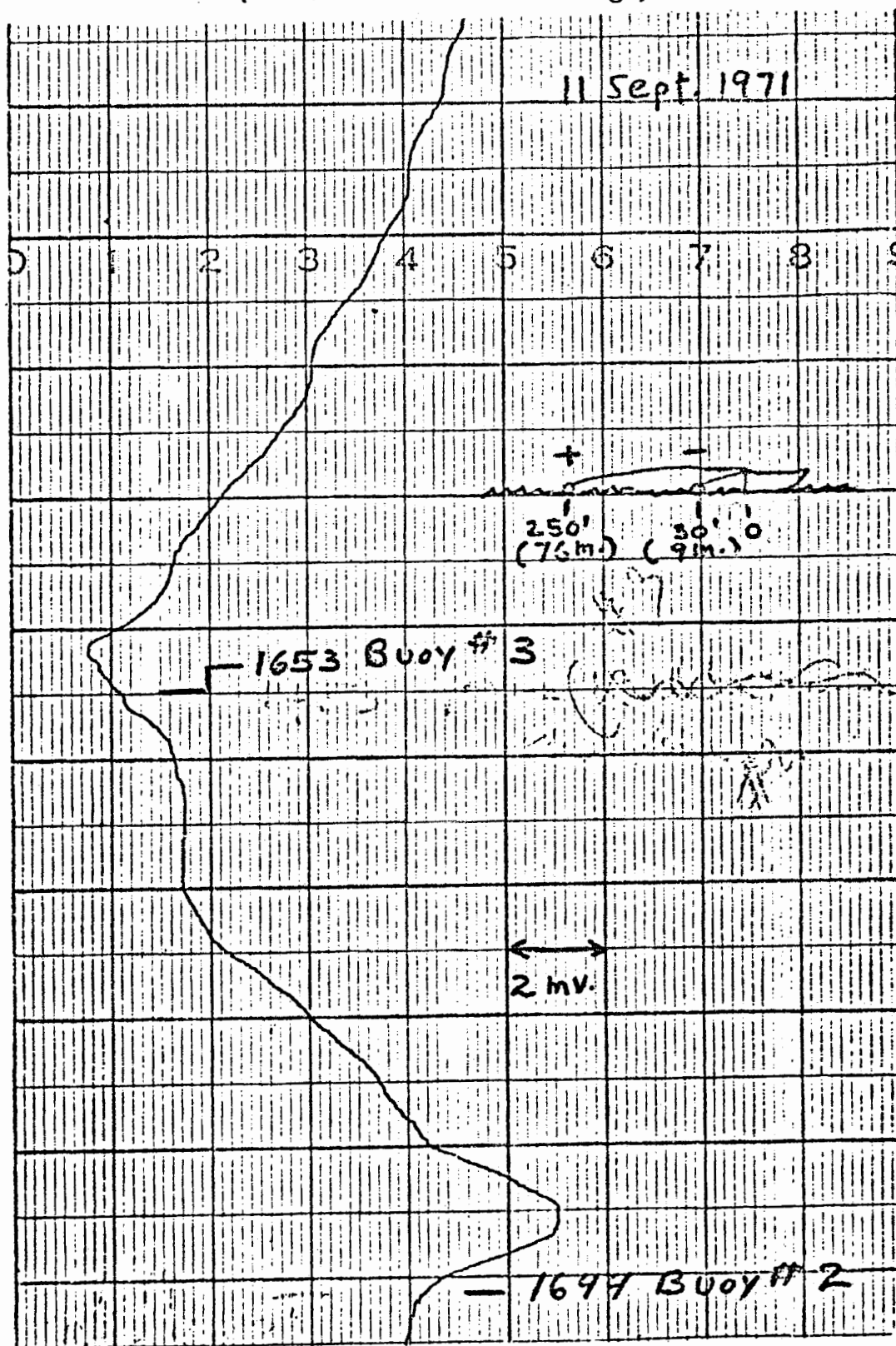
An anomaly with an observed amplitude of about 9 mv. was measured over an area extending from south of Middle Ground to north of Trott Ledge (Figure 6-23). The measured anomaly, which was of equal amplitude on both survey lines, is shown in Figure 6-26, and the integration of the anomaly in Figure 6-27. The integrated anomaly has a total amplitude of about 35 mv, but, as the zero level of the observed anomaly was uncertain, the zero level of the integration is somewhat arbitrary. This total field anomaly could be generated by an inclined current dipole with the sink closer to the surface and toward the southwest.

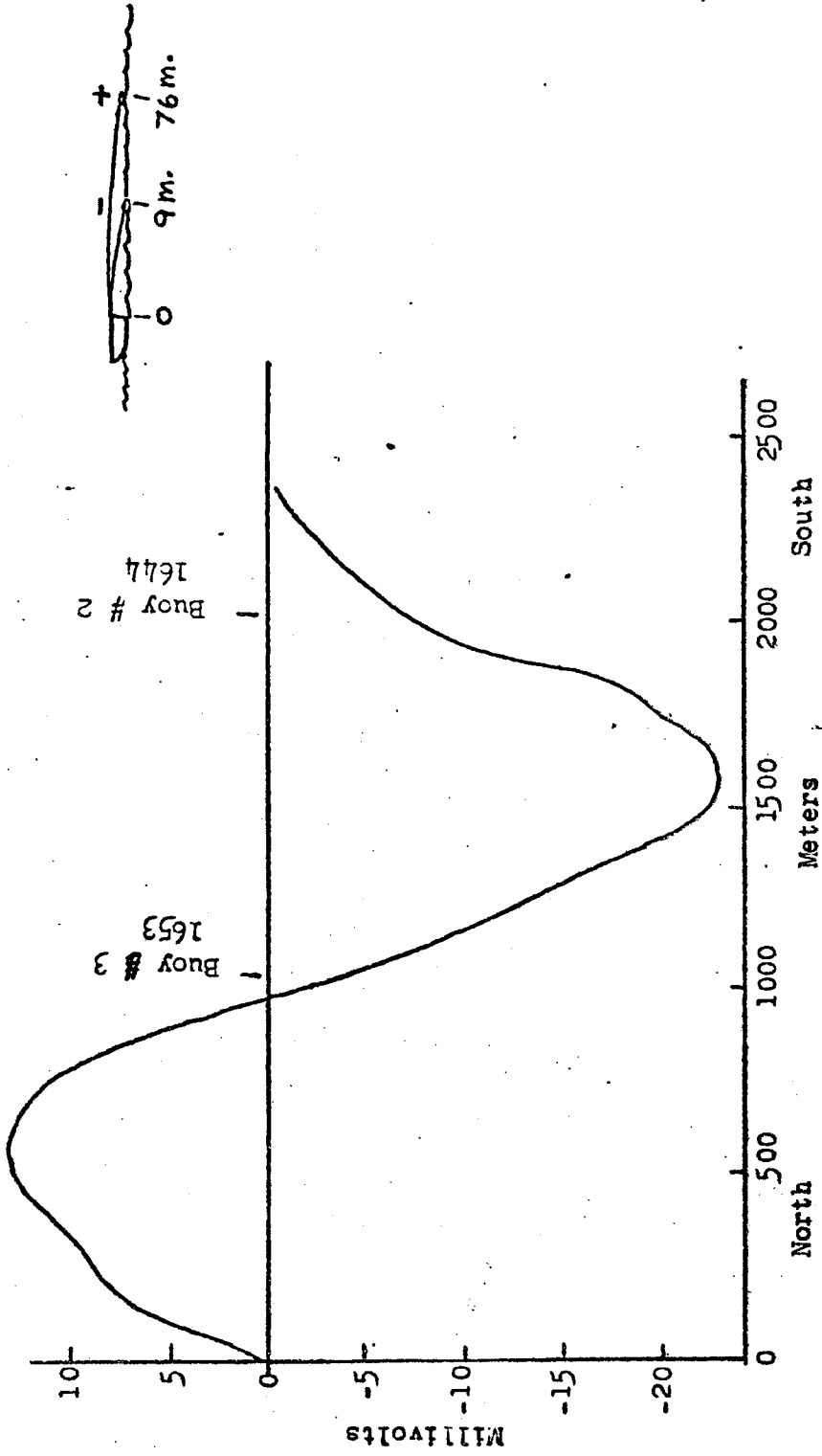
The anomaly extends over a considerable distance; nearly 1 km between peaks, and about 2.5 km overall. As the survey lines were several hundred meters from both shores, and as no pipelines or wrecks were indicated on the chart, it does not appear that any human activity could be responsible for the anomaly. The lack of known onshore sulfide deposits in the area, and the approximate

Figure 6-26

Anomaly # 2

(Middle Ground to Trott Ledge)





Integration of Anomaly # 2 13 Sept. 1971

Figure 6-27

correspondence of the peaks of the anomaly with the shoal areas at Middle Ground and Trott Ledge, suggest that the signal emanated from the bottom, quite possibly from a submerged mineral deposit. As with anomaly #1, the fact that the current sink was closer to the surface argues in favor of a mineral self-potential field. Unfortunately, lack of time precluded further exploration of the area.

Area #3 (Opposite Negro Island)

A very large self-potential anomaly was observed in the Bagaduce River, just north of Negro Island (Figure 6-23). Three runs were made across the anomalous area, at estimated distances of 100 ft. (30 m), 400 ft (122 m) and 700 ft (213 m) from the eastern shore. The length of the anomaly ranged from about 1 km at 100 ft to 1.4 km at 700 ft offshore. At 100 ft the amplitude of the gradient anomaly was about 110 mv, and the total field anomaly was about - 210 mv (Figures 6-28 and 6-29). At 400 and 700 ft the gradient amplitude was about 25 mv and the total field amplitude about -65 mv (Figures 6-30 through 6-33).

The formation responsible for the anomaly outcropped on the eastern shore of the Bagaduce River (point m, Figure 6-23), directly opposite the point of maximum amplitude of the total field anomaly. It consisted of graphite shales and quartzites, heavily interlaced with pyrite; the amount of pyrite reaching up to 25% in places (estimated by eye). Analysis of the rocks showed 0.02% copper, 0.05% lead, and 1.45% zinc. The graphite was highly conductive: the resistance of a hand specimen measuring about 16 cm by 6 cm by 2.5 cm was about 250 ohms, giving a resistivity of about 2.5 ohm-meters.

This formation is undoubtedly that described by Wingard

Figure 6-28

Anomaly # 3a (100 ft. offshore)

14 Sept. 1971

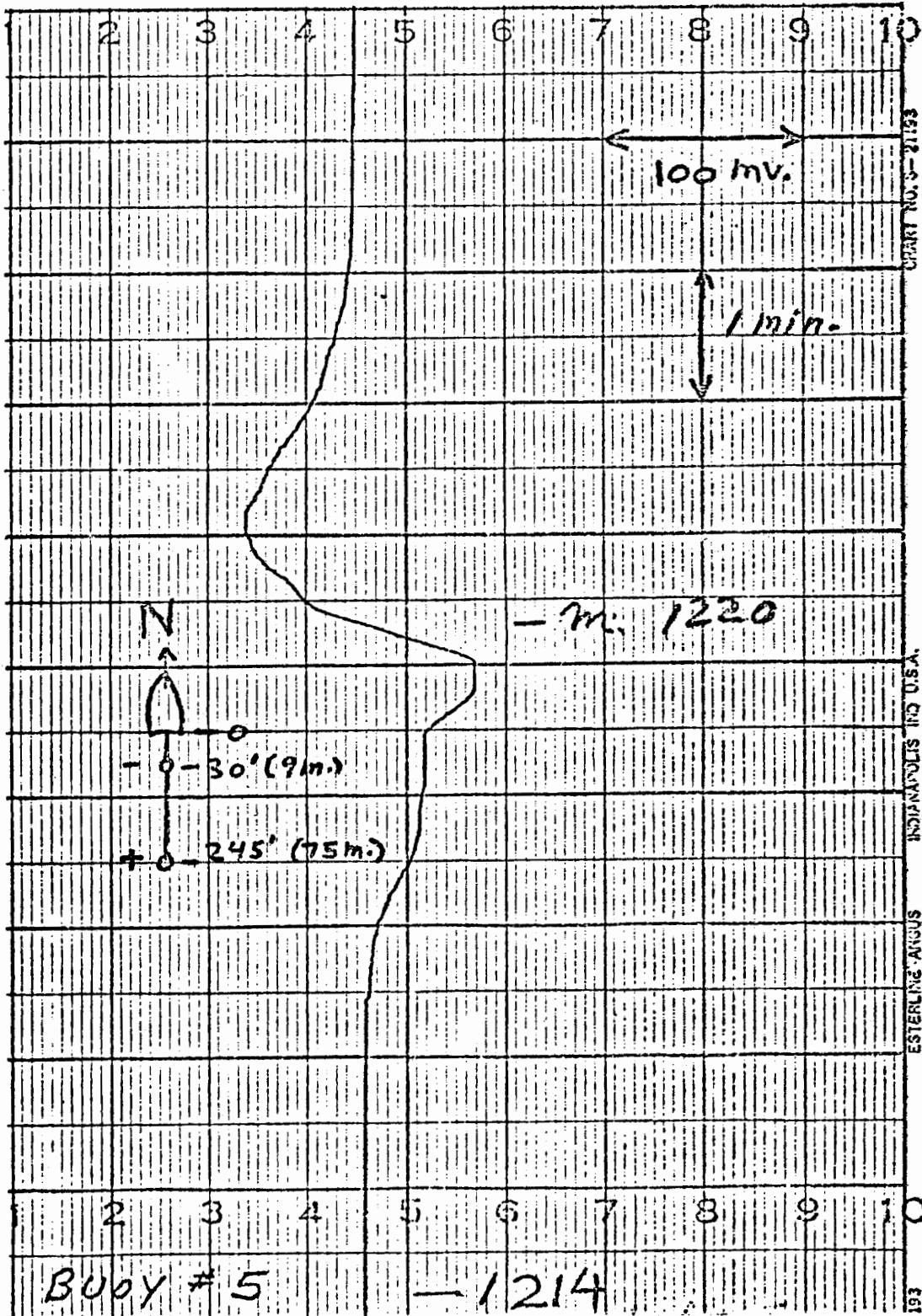


Figure 6-29

Integration of Anomaly # 3a

14 Sept. 1971

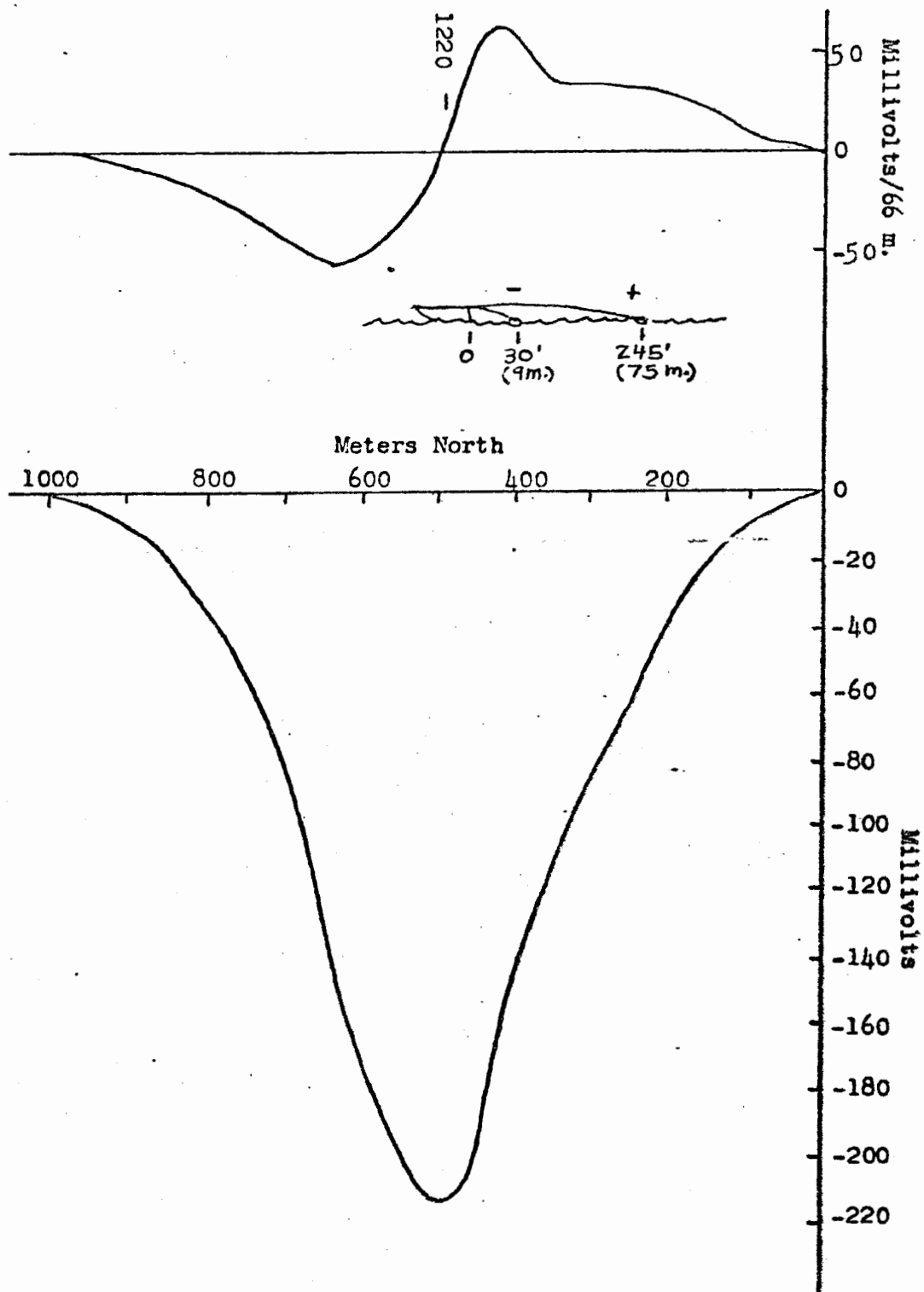
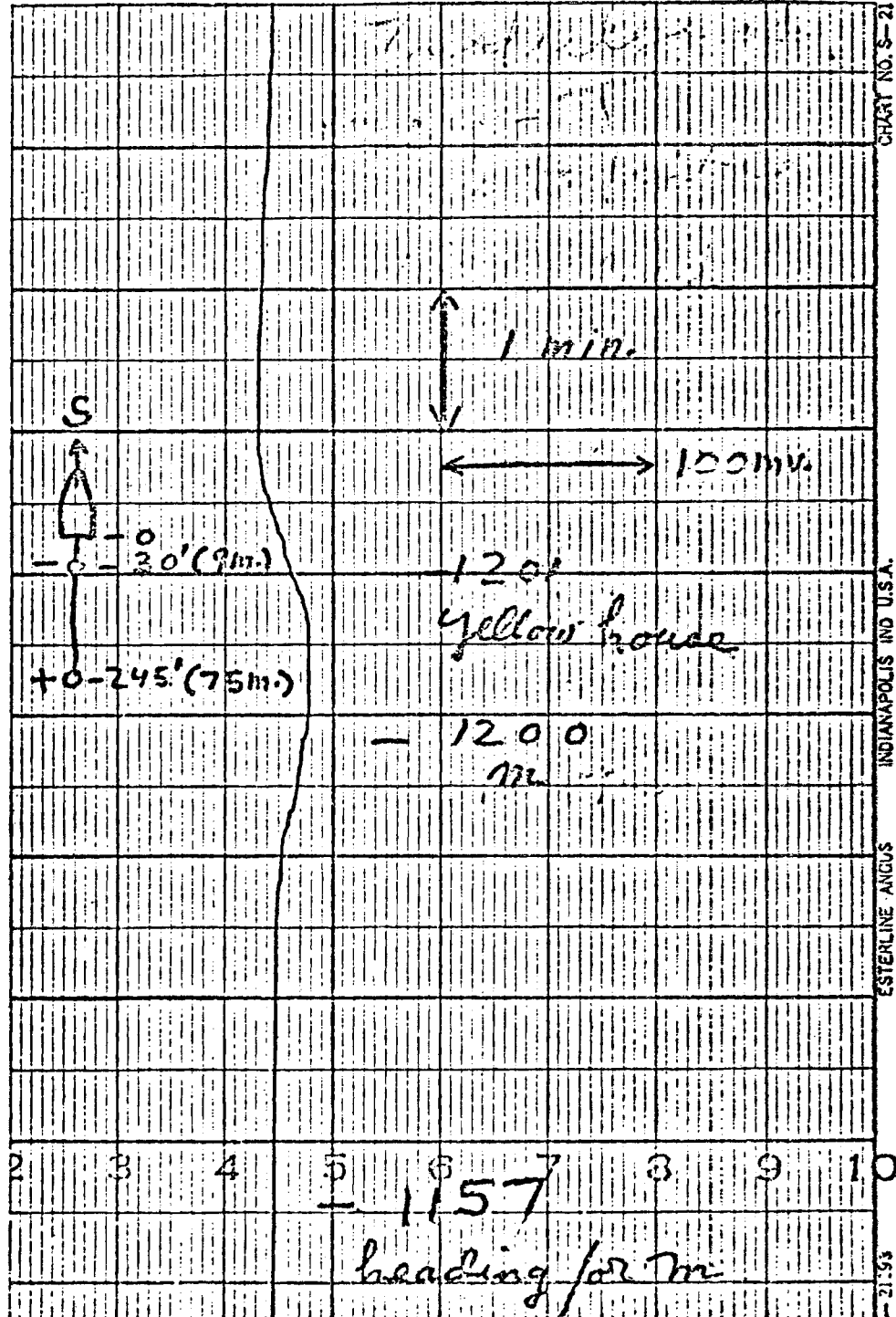
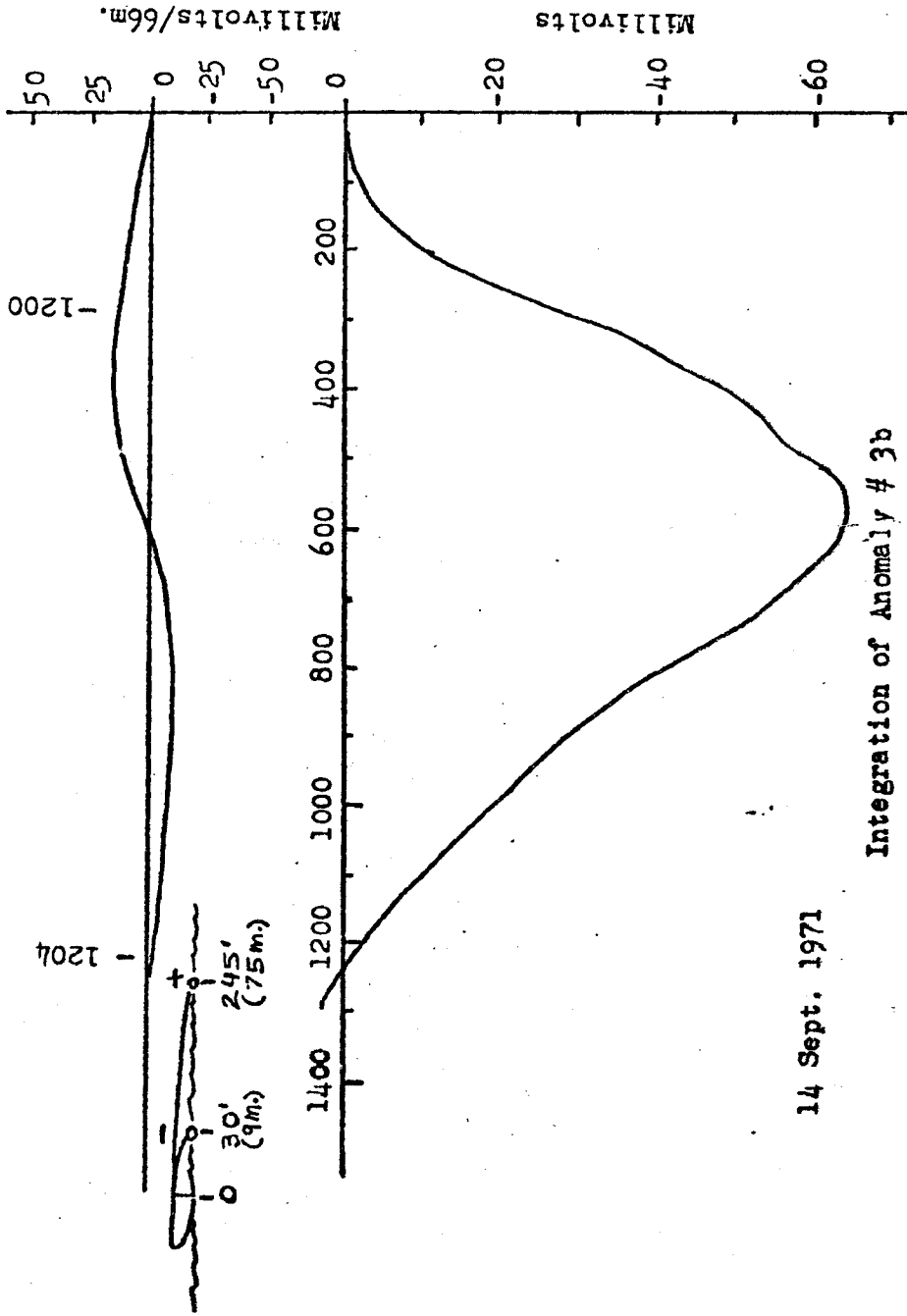


Figure 6-30

Anomaly # 3b (400 ft. offshore)

14 Sept. 1971





14 Sept. 1971

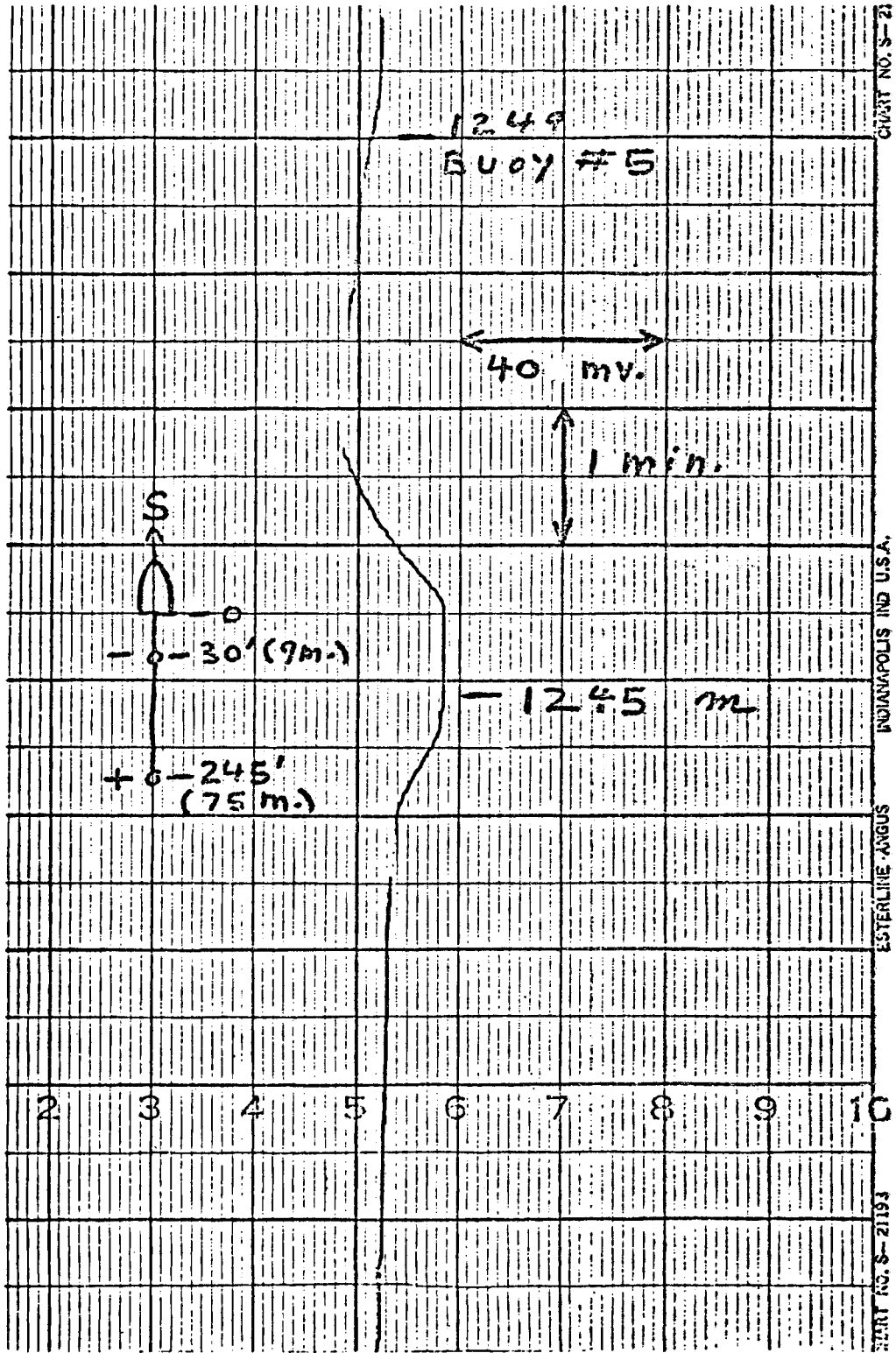
Integration of Anomaly # 3b

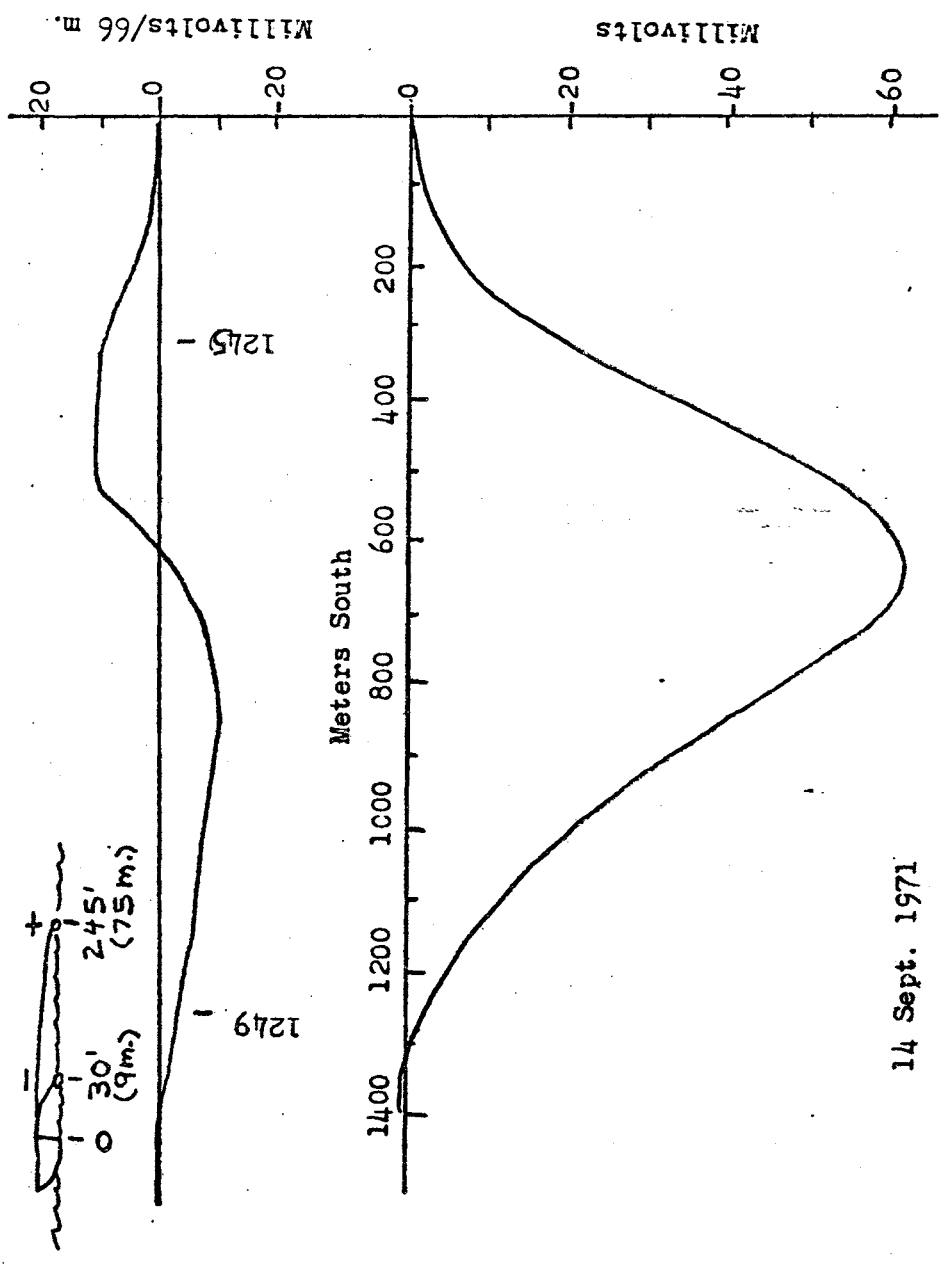
Figure 6-31

Figure 6-32

Anomaly # 3c (700 ft. offshore)

14 Sept. 1971





14 Sept. 1971

Integration of Anomaly # 3c

Figure 6-33

(1961, p. 41): "East of Negro Island, a series of black, graphite slates and quartzites occurs but soon disappears beneath cover. The same rock types on the south shore of Hatch Cove also disappear beneath cover." Thus, the formation would seem to extend to the southwest beneath the Bagaduce River. This possibility is reinforced by the fact that the amplitude of the offshore anomaly was virtually the same at 400 ft and 700 ft from the eastern shore, implying that at least part of the signal emanated from the river bed.

This interpretation is complicated by the fact that the Emerson-North Castine prospect (number 1, Figure 6-20) is located on the opposite (west) shore of the river, just north of the anomalous area. Young (1962, p. 19), describes a self-potential anomaly of -125 mv over this prospect, which showed pyrite, sphalerite, galena, and chalcopyrite mineralization. However, this anomaly was oriented roughly parallel with the river, and decreased in amplitude toward the shoreline, so it is doubtful whether the offshore extension of the Emerson-North Castine anomaly significantly contributed to the observed offshore anomaly. It is more probable that the offshore anomaly was generated by the highly conductive graphitic formation described by Wingard.

Using Figure 3-18, the point current sink magnitude necessary to generate an offshore signal of -200 mv at 30 m may be estimated as about -60 amps (water salinity was 29.4 ‰). As the formation outcrops, this current sink exists directly at the surface, and must generate a very large self-potential field on shore. Unfortunately, access to the shore (which was privately owned) was difficult, and lack of time precluded any attempt at an onshore self-potential survey.

Area #4 (Jones Point)

Another very large anomaly (Figure 6-34) was seen off the northwestern tip of Jones Point (point n, Figure 6-23). Unfortunately our visibility was restricted by driving rain (the remnants of hurricane Heidi) which, together with a powerful tidal current and headwind, prevented us from completing the run through the anomalous area. However, the data taken was sufficient to establish the total field anomaly amplitude as about -300 mv, along a line about 100 ft (30 m) offshore (Figure 6-35). Two samples of sandy shale taken from outcrops at the shoreline showed about 8% disseminated pyrite by visual inspection, and on analysis were found to contain 10.86 and 11.33% zinc, 0.03 and 0.02% copper, and 0.0002% and 0% lead.

Young (1962, p. 47) describes the Jones prospect, located at the northern end of Jones Point (number 8, Figure 6-20), as being locally rich in sphalerite, galena, chalcopryrite, chalcocite, and pyrite. His self-potential survey of the area showed peak values of -225 mv at the locations indicated by the "X" marks in Figure 6-23. As the offshore self-potential anomaly is of greater amplitude than that measured on shore, the probability is strong that the deposit extends beneath the river bed, possibly with an even greater degree of mineralization. This area definitely seems to be worthy of further investigation.

Summary

The results of the field work in Maine were, obviously, very encouraging. Two of the four offshore self-potential anomalies (#3 and #4) were found to be related directly to nearby conductive deposits; one of graphite and pyrite and the other of ore-grade

Figure 6-34

Anomaly # 4 (100 ft. offshore)

14 Sept. 1971

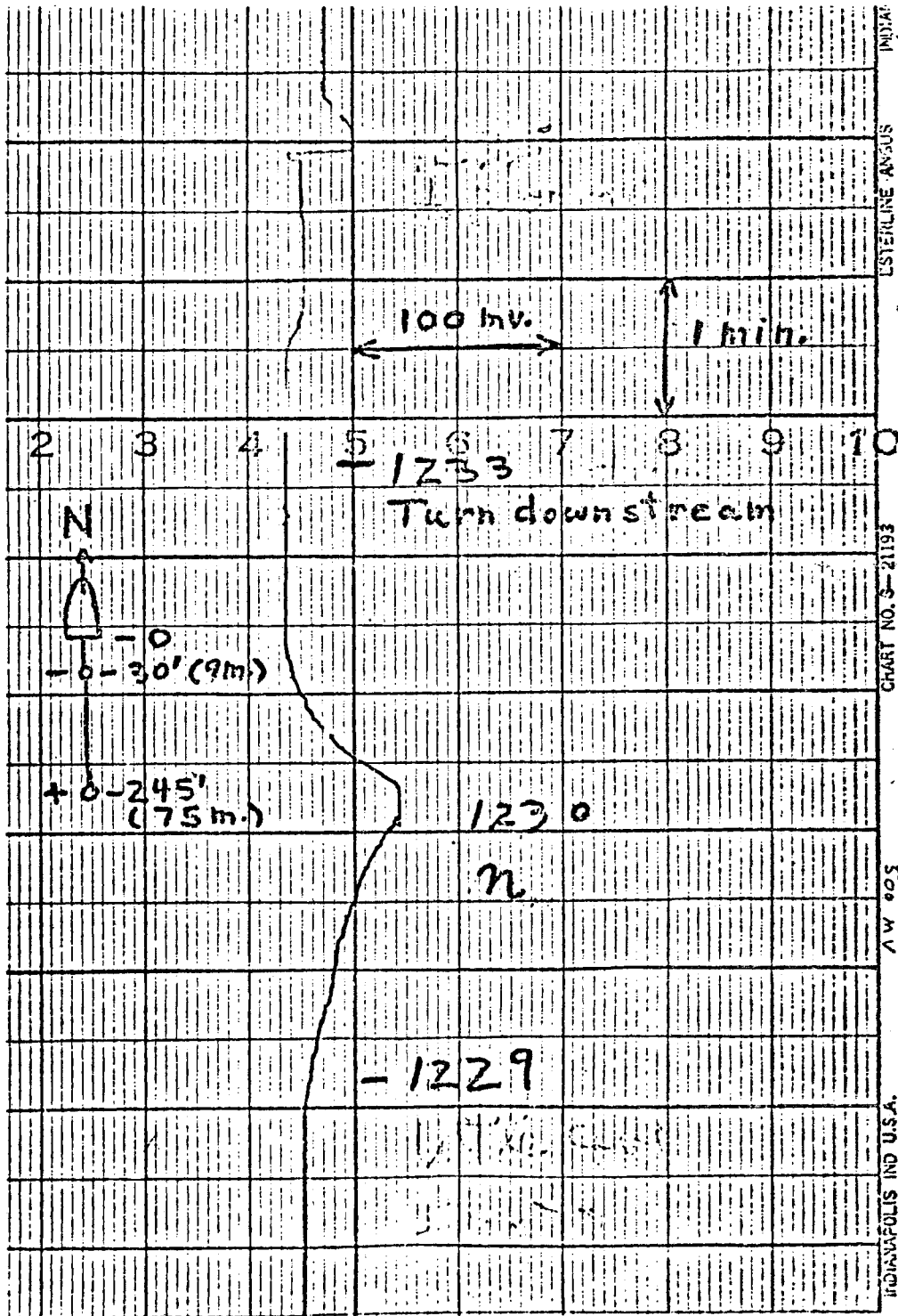
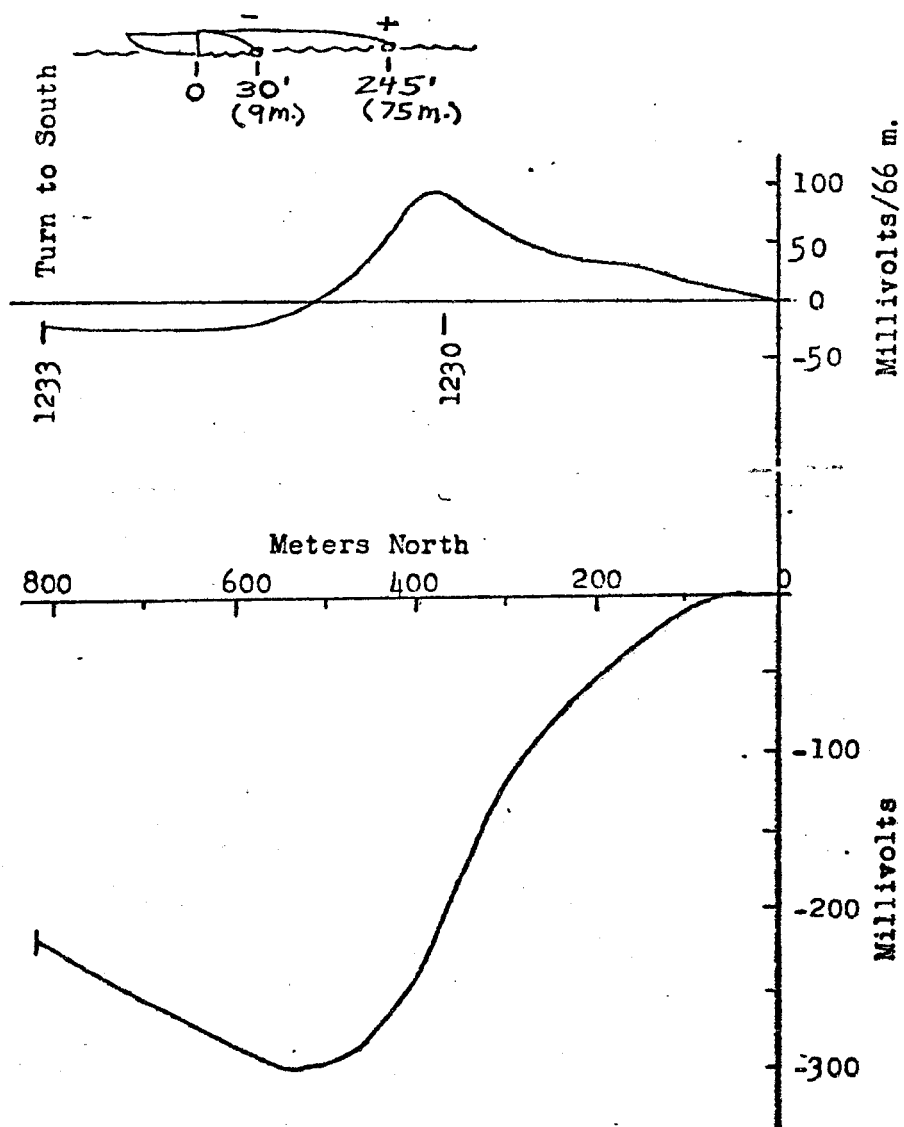


Figure 6-35

Integration of Anomaly # 4

14 Sept. 1971



sulfides. Anomaly #1 led to the discovery of zinc-rich rocks on shore (although the anomaly may have been generated by a submerged deposit). Only the origin of anomaly #3 remains a complete mystery, although it is difficult to imagine any source other than mineral self-potential for a potential field with a length of 4 km.

It was unfortunate that anomalies #3 and #4 were discovered at the very end of our allotted time in Maine, and that delineation of these anomalies had to be carried out in a single day, in a blinding rainstorm. Careful delineation and analysis of these offshore self-potential fields and their relation to the local geology would be of great value in the study of offshore and onshore self-potential generation.

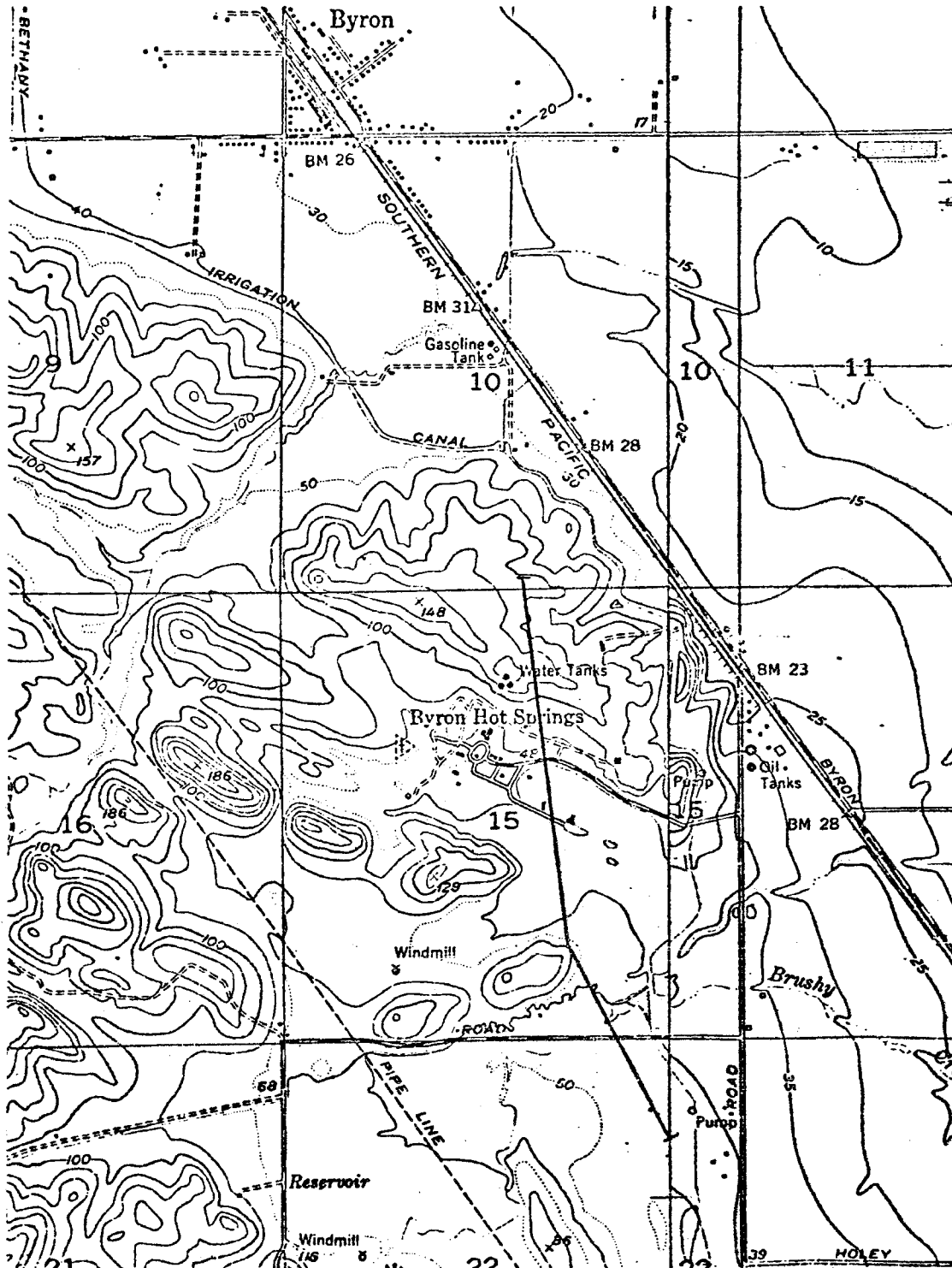
Geothermal field work

As discussed in Chapter 5, areas of geothermal activity may have high levels of surface self-potential. The results of onshore self-potential surveys conducted in geothermal areas in California and Nevada, and onshore and offshore surveys conducted near Ensenada, Baja California, Mexico are presented below, and discussed in a summary section.

Byron Hot Springs, California

Byron Hot Springs, about a mile south of the town of Byron in Contra Costa County, California (Figure 6-36), was the location of a thriving resort in the late 1800's and early 1900's (Bohm, 1971, p. 94; Irelan, 1888, p. 163; Waring, 1915, p. 109; Root, 1927, p. 17). According to Irelan, "The springs are situated in a small valley leading from the San Joaquin plains westward toward Mount Diablo. The center of this valley is filled with a light-colored adobe clay, caused by the decomposition of the calcareous shales, of which a great

Figure 6-36
Byron Hot Springs



BYRON HOT SPRINGS QUADRANGLE
CALIFORNIA
7.5 MINUTE SERIES (TOPOGRAPHIC)

portion of the neighboring hills are formed. The clay is covered in many places by sand, resulting from disintegration of adjacent sandstones. It is in this clay that Byron Springs rise."

Apparently, sometime between 1927 and the present the springs went dry. The resort is now in ruins, and no geothermal activity is observable. Nevertheless, as the area was conveniently located, and as the present owners, Mr. and Mrs. R.H. Burr, were interested in the possible rejuvenation of the springs, a self-potential survey was run across the valley floor on January 12, 1971. The survey line, centered between the Liver and Kidney Spring and the Swimming Pool, is shown in Figure 6-36, and the survey results in Figure 6-37.

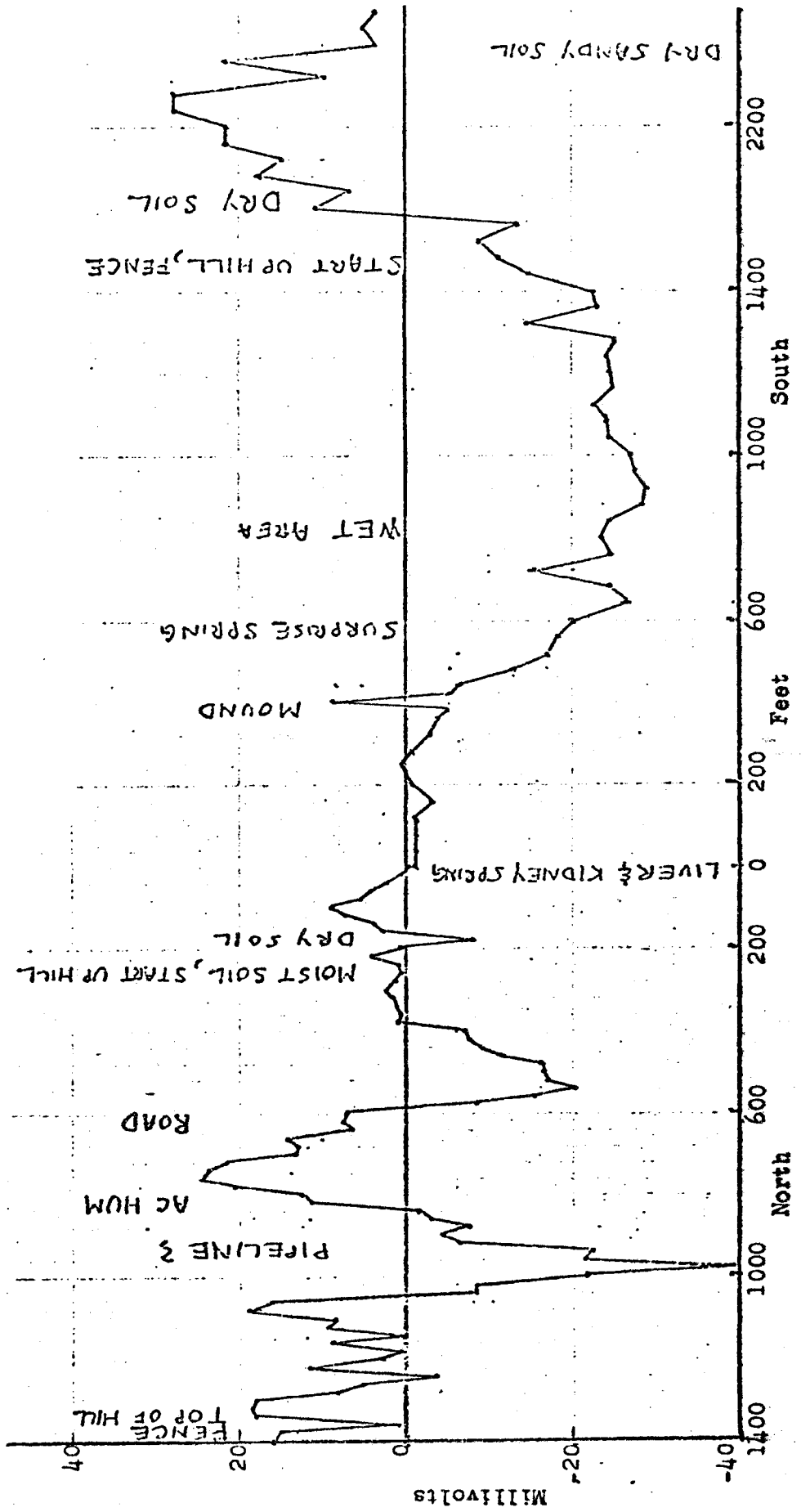
Rocky Point, California

"A warm spring that is mildly sulphurated rises on the beach about 6 miles northwest of Point Bonita. It is locally known as Rocky Point Spring, but it is exposed only at low tide and is of little importance" (Waring, 1915, p. 80). Even though "of little importance", the occurrence of shoreline geothermal activity was of interest for this work. Accordingly, a self-potential survey was run along the tideline, across the warm spring area (Figure 6-38).

Temperature and self-potential are shown in Figure 6-39.

Spencer Hot Springs, Nevada

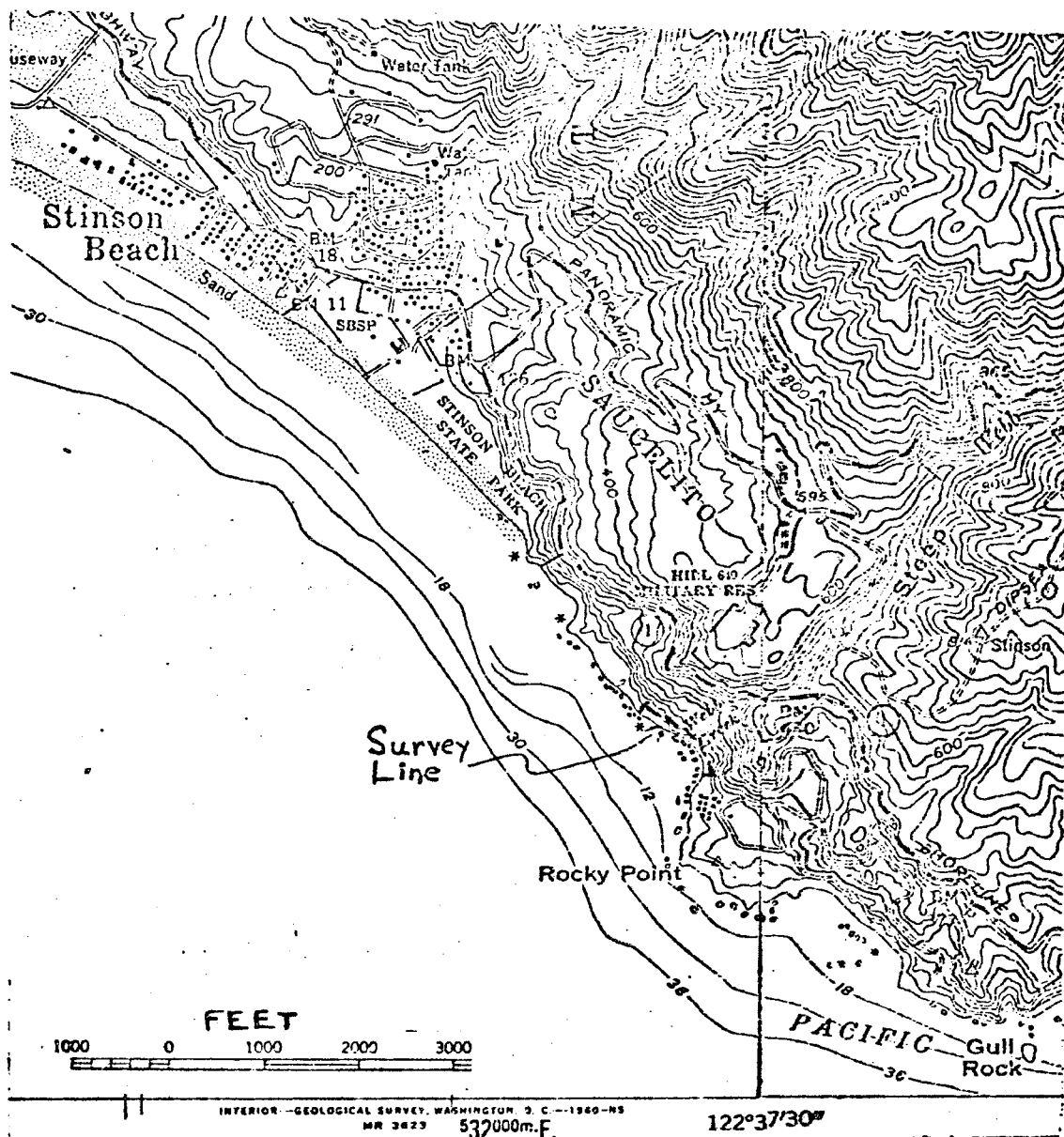
Spencer Hot Springs is an active geothermal area in central Nevada (Figure 6-40). A geophysical survey of the area, including ground magnetics, shallow electromagnetics, self-potential, and dipole-dipole resistivity, was performed by a group from the University of California, Berkeley, on November 10-12, 1972. The self-potential lines are shown in Figure 6-41, and the data in Figures 6-42 through 6-44.



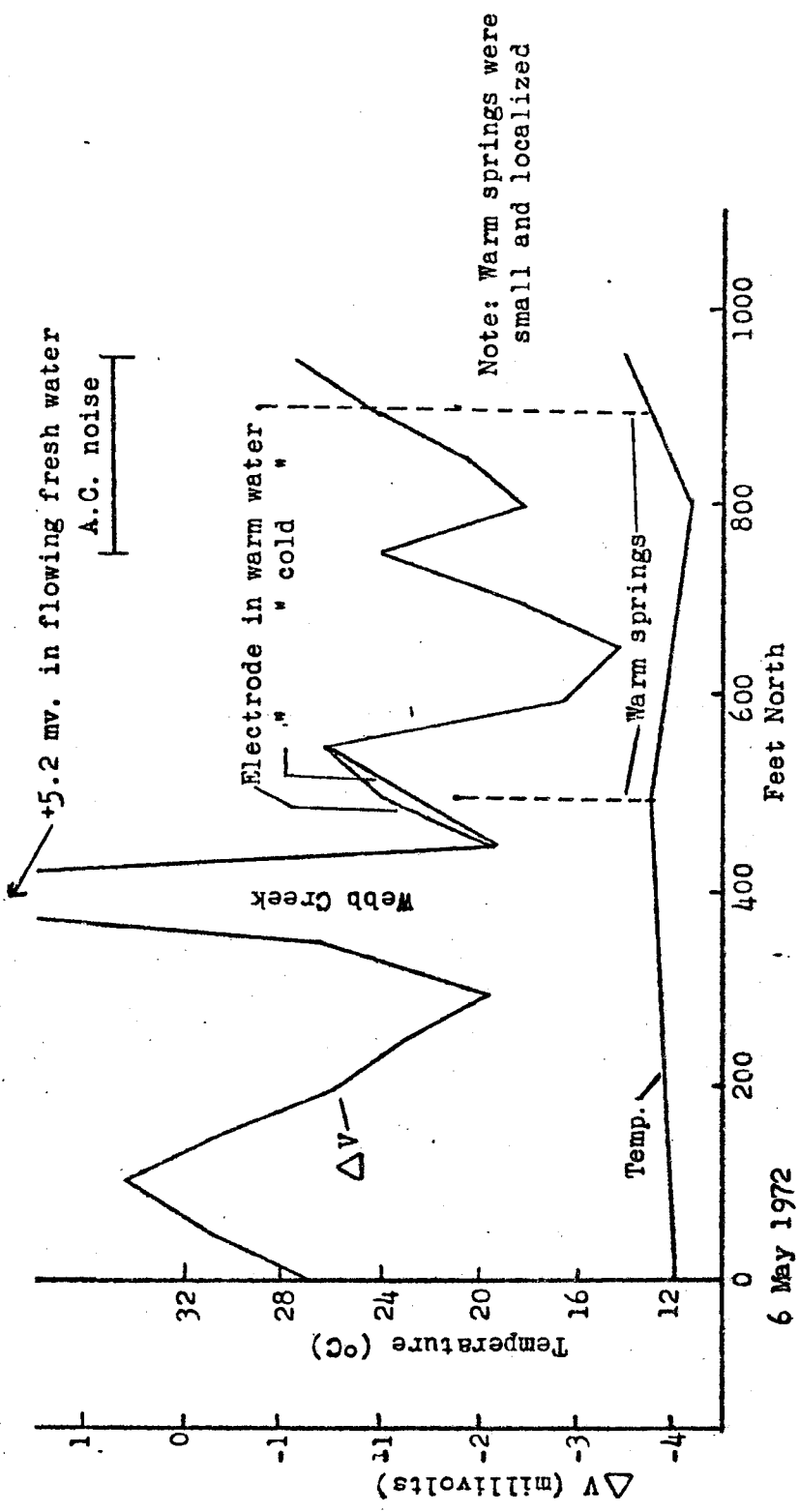
Self-Potential Survey, Byron Hot Springs 12 Jan. 1971

Figure 6-37

Figure 6-38
Rocky Point, California



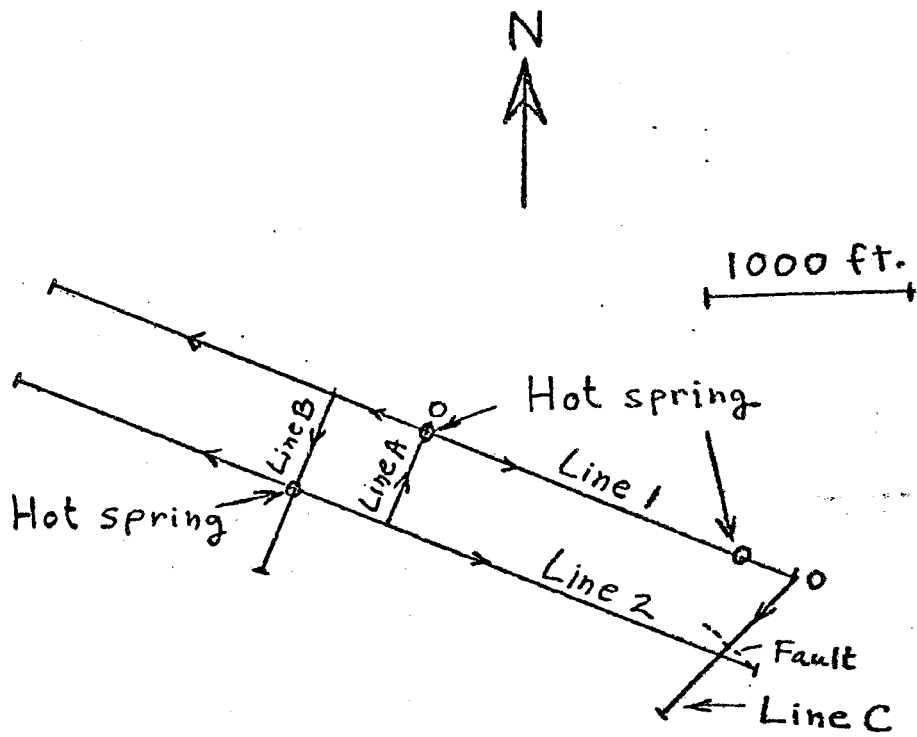
Bolinas and San Rafael, California 7.5' Quadrangles

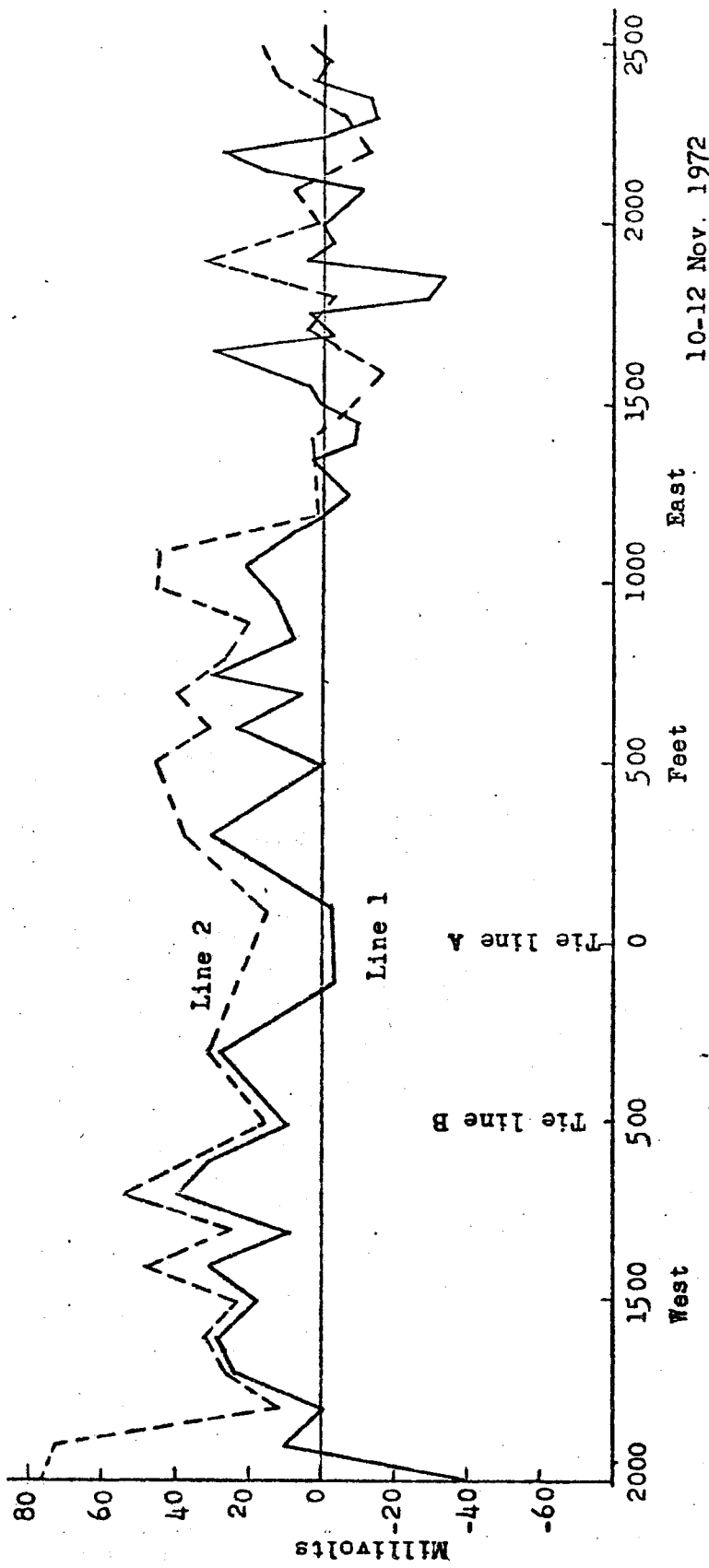


Self-Potential Survey, Rocky Point, California

Figure 6-39

Figure 6-41
Self-Potential Survey Lines
Spencer Hot Springs, Nevada





Self-Potential Data - Spencer Hot Springs, Nevada

10-12 Nov. 1972

Figure 6-42

Figure 6-43

Self-Potential on Tie Lines A & B

Spencer Hot Springs, Nevada

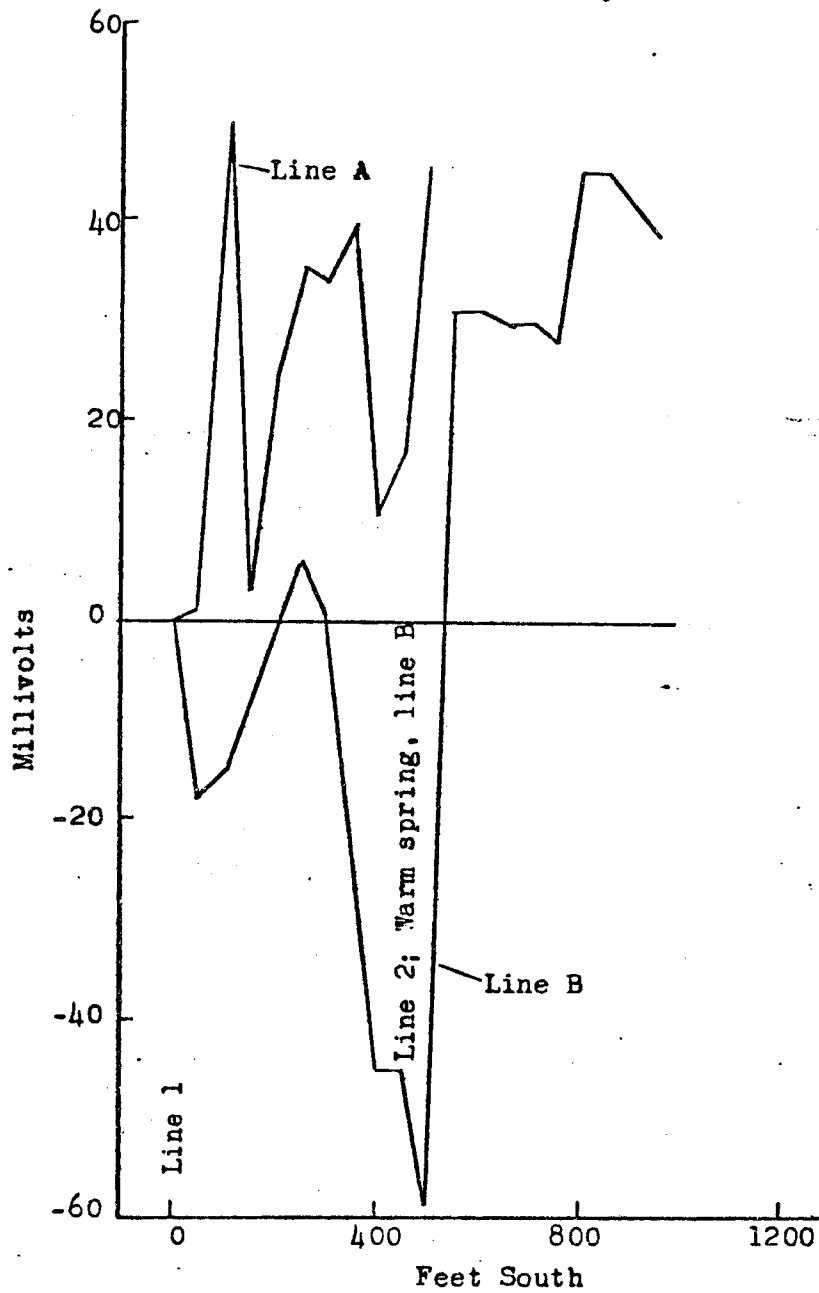
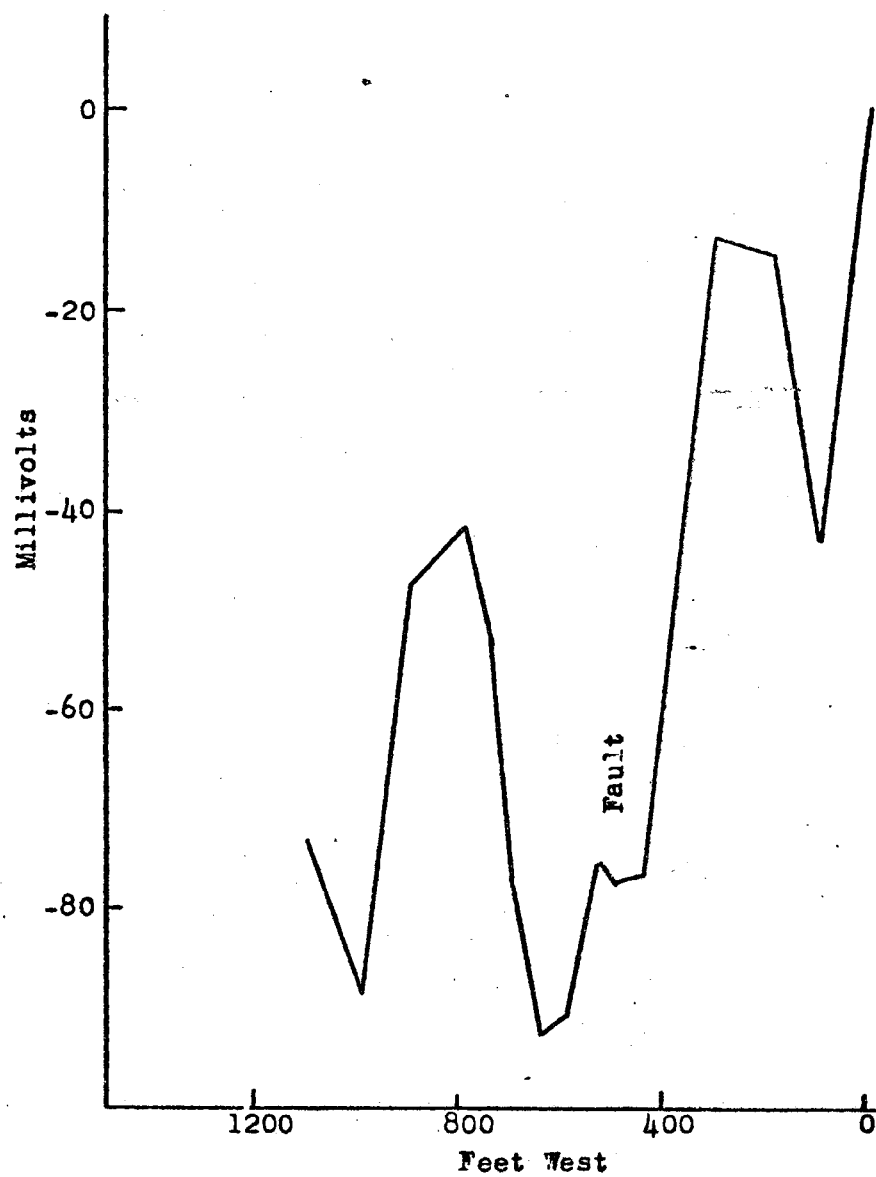
Note: Zero level for both lines
is arbitrary

Figure 6-44

Self-Potential on Line C
Spencer Hot Springs, Nevada

Note: Zero level is arbitrary



Considerable difficulty was experienced with electrode polarization, resulting from the accumulation of salty mud on the electrodes, during these surveys. Cleaning the electrodes thoroughly between readings helped alleviate this problem, and the data is probably accurate to within ± 5 millivolts.

Punta Banda, Baja California, Mexico

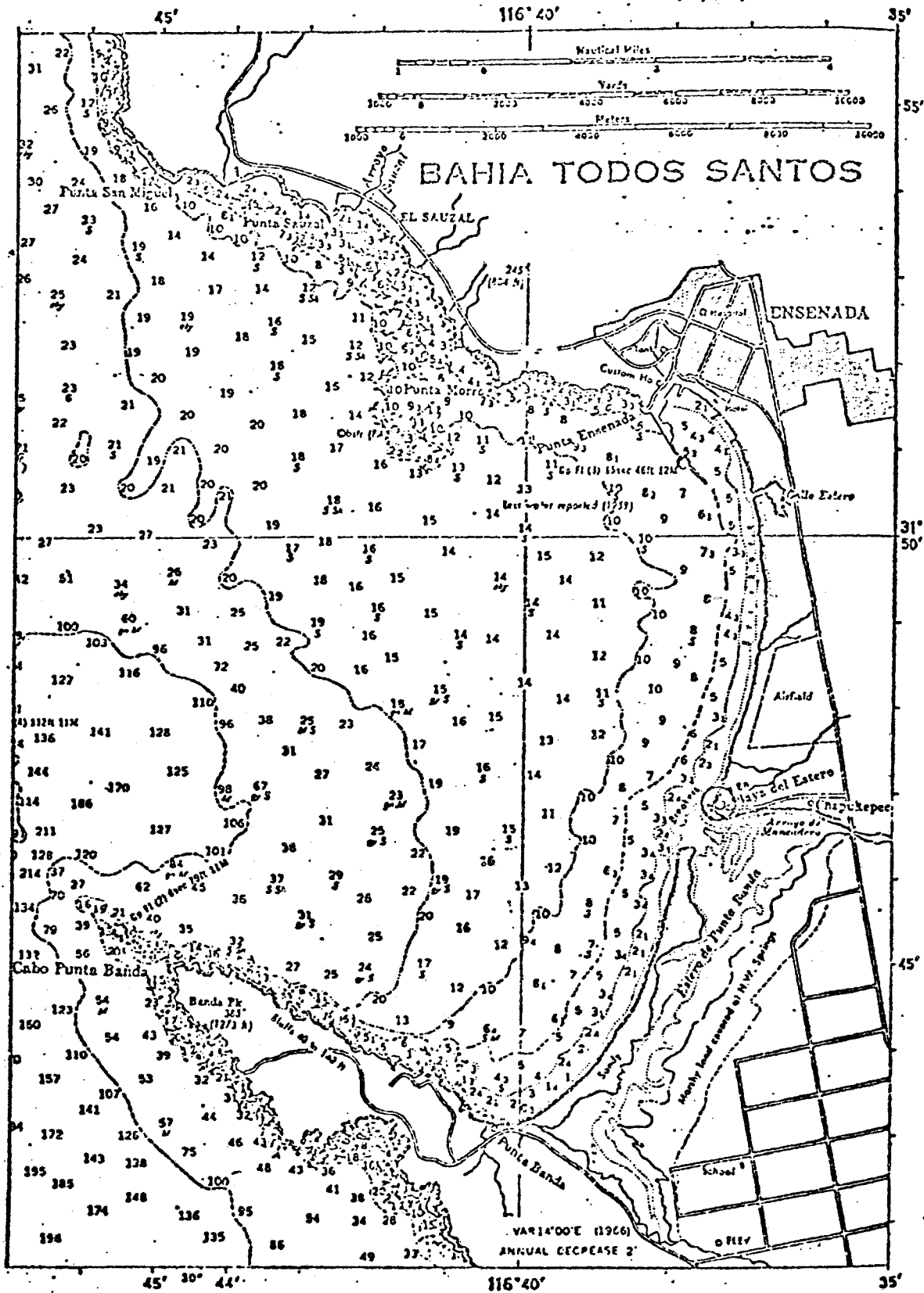
The Punta Banda peninsula forms the southern boundary of Bahia Todos Santos, Baja California, Mexico (Figure 6-45). Onshore and offshore geothermal activity is associated with the Agua Blanca fault system. Hot springs emerge from the beach just east of the town of Punta Banda, (location A, Figure 6-46), and from the sea floor, in 30 m deep water, off the southwestern shore of the peninsula (location B, Figure 6-46).

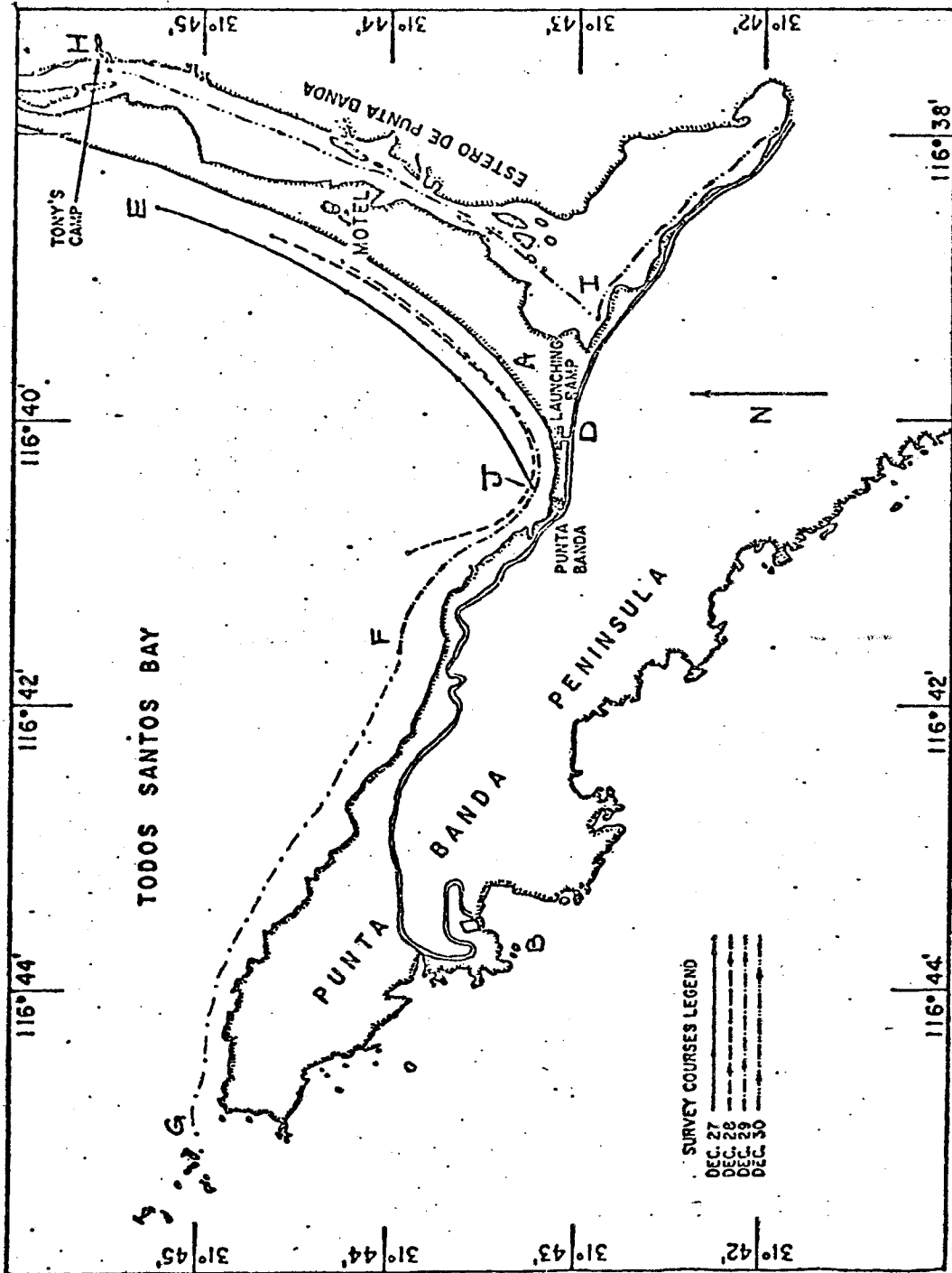
At the invitation of Dr. R.B. McEuen of San Diego State University, California, who was conducting geophysical studies of the area with a group from the Universidad Autonoma de Baja California, offshore self-potential surveys were run along the lines shown in Figure 6-46. The work was done in conjunction with Dr. Ugo Conti, of the University of California, Berkeley, who used an underwater environmental monitor (Conti, 1972), to record temperature, salinity, dissolved oxygen, pH, Eh, and ambient light level along the survey course.

An onshore self-potential survey was run along the beach, east of the town of Punta Banda, where the hot springs emerge (point D to point A, Figure 6-46), with the results shown in Figure 6-47. Good offshore data was obtained between points E and F, Figure 6-46. Runs between points F and G were hampered by heavy seas, (Figure 5-5) and a survey run inside Estero de Punta Banda (points H to I,

Figure 6-45

From Conti (1972)





(FROM AERIAL PHOTOS SUPPLIED BY THE INSTITUTO DE INVESTIGACIONES OCEANOLÓGICAS)

From Conti (1972)

Punta Banda
Figure 6-46

Figure 6-47

Shoreline Self-Potential Survey

Punta Banda, Baja California, Mexico

30 Dec. 1971

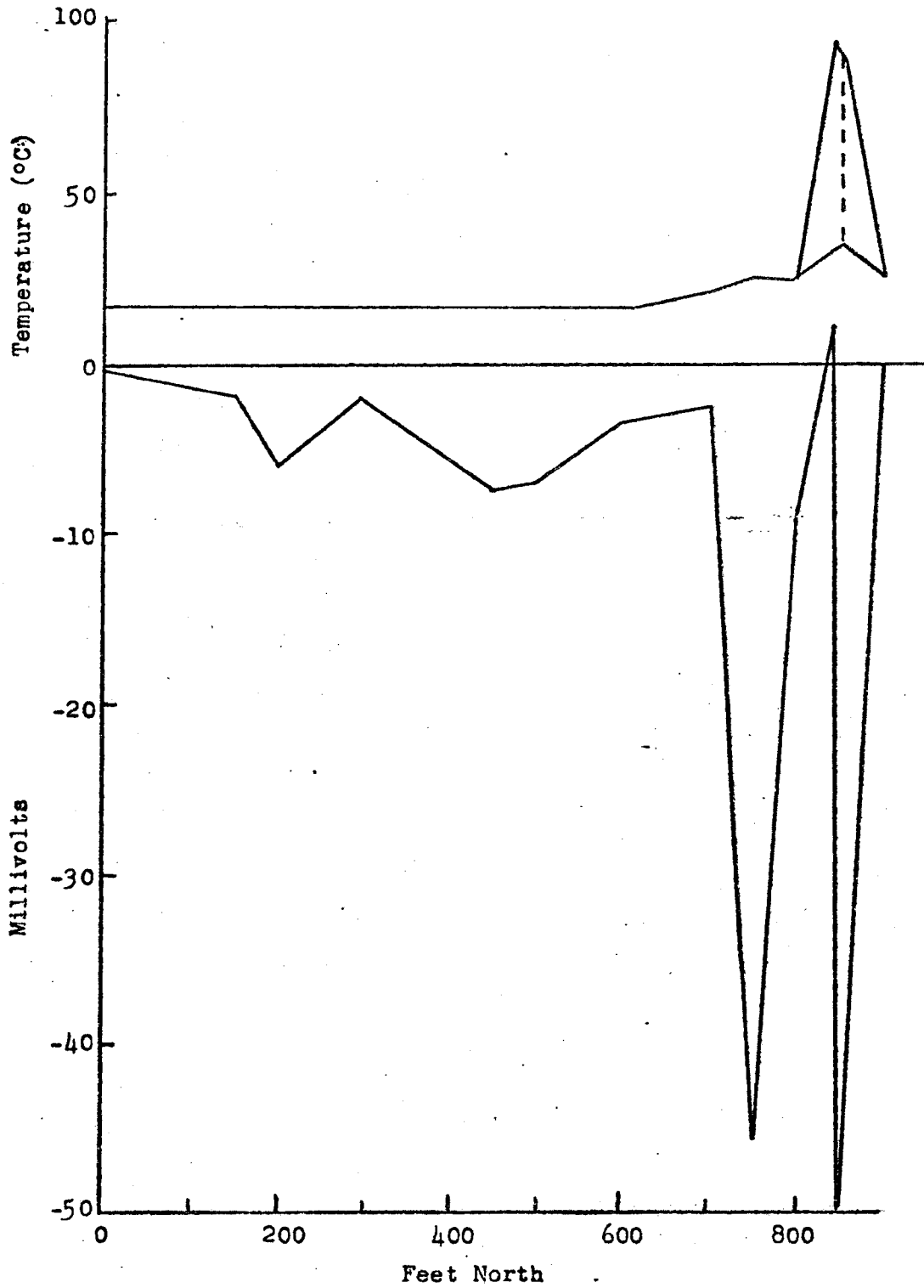


Figure 6-46) gave invalid data (Figure 5-4) due to a leaky cable splice made after the cables were cut by the propeller of the towing vessel (a 24 foot, open, diesel powered boat).

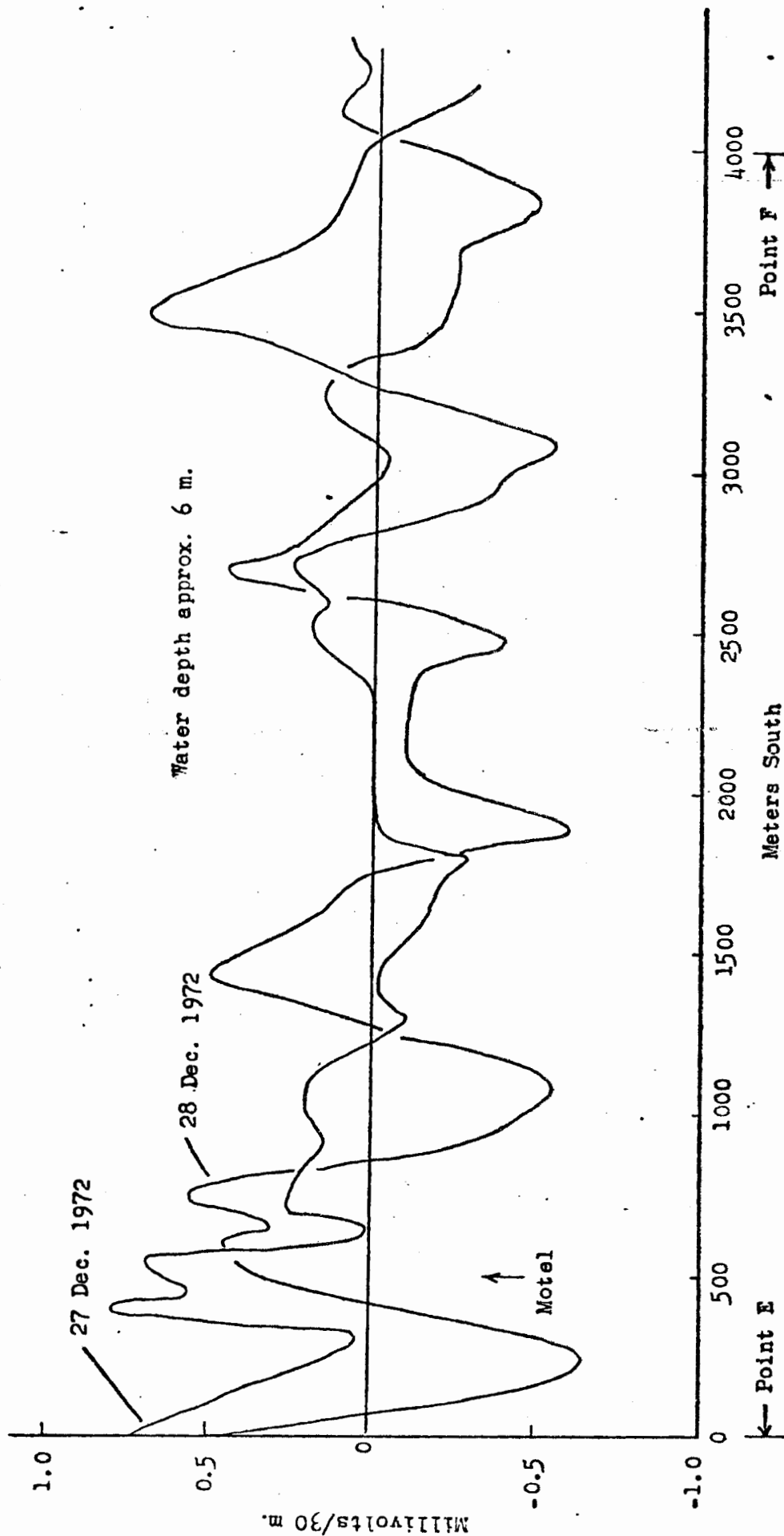
The offshore data, with wave noise (Figure 5-3) removed, is shown in 6-48. A large anomaly observed at point J, Figure 6-46, is shown in Figure 6-49, and the integration of the anomaly in Figure 6-50.

Discussion of geothermal data

Except for higher-than-normal background noise levels, it is difficult to see any truly distinct patterns in the self-potential data taken in onshore geothermal areas. The onshore surveys conducted at Byron Hot Springs (Figure 6-37) and Spencer Hot Springs (Figure 6-42) appear to show that the central area of warm spring activity (former activity in Byron) is positive with respect to the outer edges of the area, by about 25 mv at Byron, and about 35 mv at Spencer Hot Springs. This trend is not pronounced and may be associated with topography as well as geothermal activity.

The tie lines run at Spencer Hot Springs (Figures 6-43 and 44) show strong self-potential activity. The large (-100 mv) anomaly at 450 ft on line B is associated with a large warm spring (which once fed a swimming pool) and appears also to show on line A, 500 feet further east. A similar large anomaly is seen on line C, in this case associated with a fault. Whether any of these onshore anomalies are due to water moving along a fault zone, to chemical diffusion, or to some other cause is impossible to say without further geologic study of the areas.

In contrast to the inland locations, the self-potential surveys run along sandy shorelines show very little self-potential acti

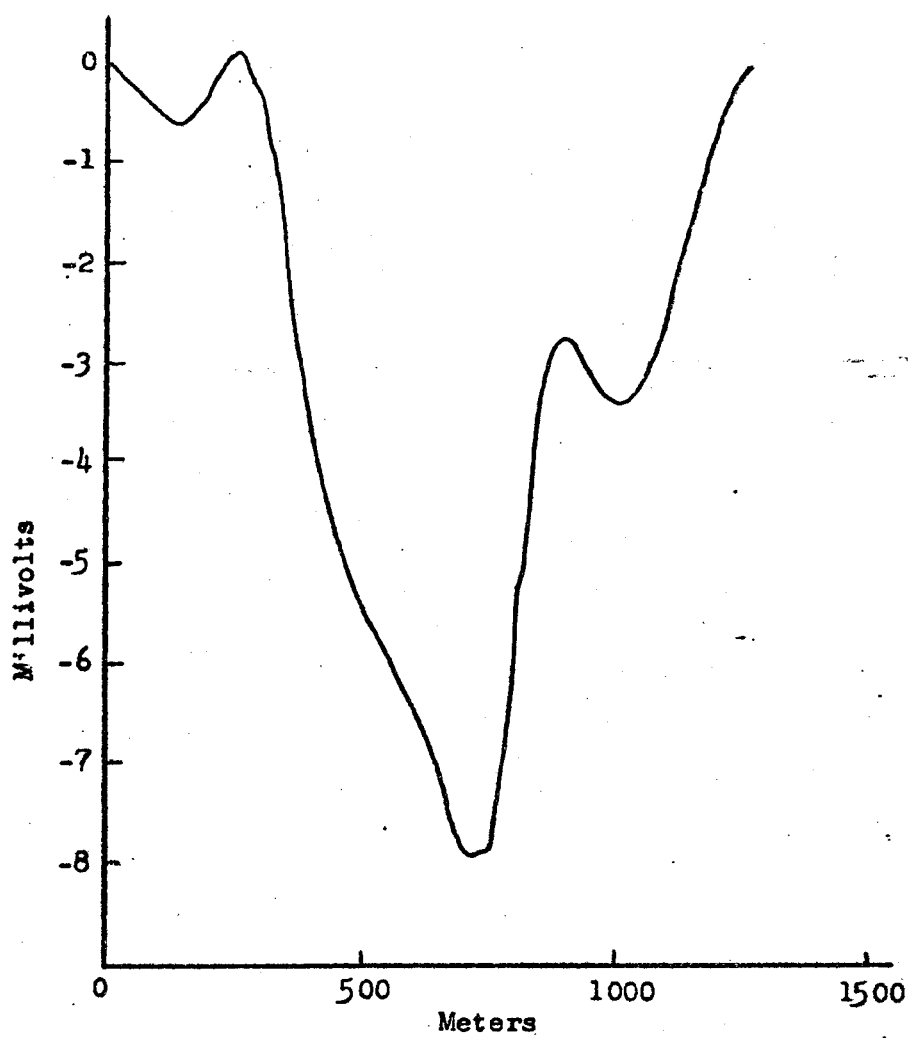


Punta Banda, Baja California, Mexico
Offshore Self-Potential

Figure 6-48

Figure 6-50

Integration of Gradient Anomaly at Point J



with one exception. The survey at Rocky Point (Figure 6-39) showed signal levels of less than 5 mv over 1000 feet, except when the scanning electrode was immersed in a fresh-water creek. Potential differences of only a few tenths of a millivolt were observed when the "CoCo" electrode was immersed in a warm spring and then in cool sand a short distance away, as at 500 feet. The area of warm spring activity, from about 500 to 900 feet, was not significantly different in potential from the inactive area south of Webb Creek.

The survey run along the shoreline near Punta Banda (Figure 6-47) showed a similar quiet background level until the hot spring area was reached at about 700 feet. Two large self-potential "spikes" were seen in this area: one of -46 mv at 750 ft, where the temperature was 25°C (the background temperature of the sand was 17°C); and one of -44 mv at 850 ft where the temperature was 35° to 90°C (these two temperature readings were taken only a few cm apart).

Obviously, the self-potential readings (which were repeatable to 1 or 2 mv) did not correlate directly with temperature, nor were they due to changes in water chemistry, as the readings are too great by an order of magnitude (see Chapter 4). As no evidence of pipelines or other metallic objects was seen nearby, the origin of these large self-potential signals is not clear. It can only be said that they appear to correlate with the hot spring activity--in direct contrast with the results obtained at Rocky Point.

The offshore record at Punta Banda (Figure 6-48) shows a higher geologic background signal level (by about an order of magnitude, in water six times as deep) than that seen in either Alaska or Maine. That the signal is associated with the sea floor is evident

from the correlation of the records taken on different days. Although the courses were not exactly the same on both days, and the boat's speed was not constant, the two records in Figure 6-48 do appear to correlate in many areas, particularly between 0 and about 750 meters, and between 1800 and 2300 meters.

Whether this signal is due to geothermal activity is not clear. Simultaneous records taken by Conti (1972, p. 153-154) show no outstanding anomalies in the monitored parameters, indicating that no large scale geothermal activity occurs at the sea floor. Deeper geothermal activity, however, could have been responsible for the high self-potential signal level.

A relatively large self-potential anomaly (Figure 6-49), about four times greater in amplitude than the background described above, was observed at point J on Figure 6-46. The integral of the measured gradient anomaly, shown in Figure 6-50, has an amplitude of about -8 mv. Data taken by Conti (1972, p. 153-154) at the same location shows a slight anomaly in the salinity, temperature, and dissolved oxygen levels, indicating that geothermal activity may have been responsible for the self-potential anomaly (the area was not far from the hot springs on the beach). Unfortunately, the presence of fishing nets in the area hampered further detailing of the anomaly, and logistic problems precluded a planned investigation by SCUBA divers.

In summary, the relationship between geothermal activity and self-potential remains unclear. If offshore sulfide deposits are being sought in a geothermal area, the increased noise level and possible large anomalies might prove a nuisance. If the geothermal activity itself is of interest, self-potential may prove useful in

locating or delineating geothermal areas. The subject is of great practical interest, and is worthy of further theoretical and field investigation.

Costs

An estimate of the cost of offshore self-potential prospecting may be made, based on the field work done in Maine and Mexico. Assuming a towing speed of 4 miles per hour, and 5 hours of actual profiling per day, 20 line miles (32 km) would be a conservative estimate for daily coverage.

The type of boat required depends upon the expected sea state. In calm, sheltered waters, a 10 ft (3 m) inflatable rubber boat, or a 14 foot (4 m) aluminum skiff, available with motor and fuel for less than \$20 per day, has been found satisfactory. In rougher water a high-freeboard boat of 15-25 feet (5-8 m) length, generally available for less than \$100/day, usually will suffice.

Although an individual could run a survey alone, the use of two people, one to run the boat and one to navigate and watch the chart recorder, is recommended. Estimated daily expenses, based on the use of two operators, are tabulated below:

Boat and fuel	\$100
Equipment rental and depreciation	\$ 50
Operator salary and overhead	\$300
Data reduction and analysis	<u>\$150</u>
	\$600/day

For 20 line miles per day, this would be about \$30 per line mile (or \$19 per line km.), less travel expenses. It might be possible to run a magnetometer or other geophysical instrument

simultaneously with the self-potential, thus reducing the line-mile cost for both.

Appendix 2-1

Current FlowInside Pipe

The resistance R of a conductor of cross-sectional area A , length L , and resistivity is

$$R = \frac{\rho L}{A} .$$

The current I for a given potential drop ΔV is thus

$$I = \frac{A \Delta V}{\rho L} .$$

For the first Duriron pipe used, the inside diameter was 6.7 cm, and the resistivity of the water was 30.7 ohm-cm. Therefore,

$$I = \frac{1.15 \Delta V}{L} .$$

For the segment from $z = 0$ to $z = 15$ cm, ΔV was (690-160) or 530 mv, so the current I was 40.6, or about 41 ma. For the segment from $z = 15$ to $z = 50$ cm, ΔV was (160-100) or 60 ma, so I was about 2 ma.

Outside pipe

The portion of the current flowing outside the pipe may be estimated roughly by considering the pipe to be a point current source at large r . The current would then be

$$I = \frac{2\pi r V}{\rho} = 0.2 r V ,$$

with V measured at the water surface. From Figure 2-28, $V = 0.6$ mv at $r = 30$ cm and 0.2 mv at $r = 60$ cm. so I is roughly 3 ma. This estimate is crude, but sufficient for a first approximation.

Total current and surface area

The total current flowing in the upper part of the pipe, then, was about $(41 + 3)$ or 44 ma. The total surface area of the pipe exposed to the water and mud was about 0.4 square meters, so the current generated was about 100 ma per square meter. As the Duriron appeared to generate a current an order of magnitude greater than the ore sample tested, a first estimate for an actual ore body might be 10 ma/m^2 .

Applying this current density to a cylindrical ore body of, say, 20 m diameter by 100 m long, with a surface area of 6900 m^2 , the total current generated would be 69 amps. As discussed in Chapter 3, this appears to be a reasonable magnitude (rather surprising in view of the crudeness of the analysis!).

Appendix 3-1

The Potential Field Generated by a Point Source of Current Buried
in the Sea Floor

The problem, conveniently, has been solved by Van Nostrand and Cook (1966, p. 84). The situation is shown in Figure A3-1. The potential V (in volts) in the water layer is given by

$$V = \frac{I \rho_s}{4\pi} \left\{ \frac{1}{R} + \int_0^{\infty} (A_w e^{\lambda z} + B_w e^{-\lambda z}) J_0(\lambda r) d\lambda \right\}$$

CA3-11

where: I = current

ρ_s = resistivity of the sediment

$$R = (r^2 + z^2)^{1/2}$$

λ = dummy parameter of integration

J_0 = the Bessel Function of the order zero

$$A_w = \frac{k_{aw} (1 + k_{ws}) e^{-2\lambda z_2}}{1 + k_{ws} k_{aw} e^{-2\lambda b}}$$

$$B_w = \frac{k_{ws} - k_{ws} k_{aw} e^{-2\lambda b}}{1 + k_{ws} k_{aw} e^{-2\lambda b}}$$

$$k_{aw} = (\rho_a - \rho_w) / (\rho_a + \rho_w)$$

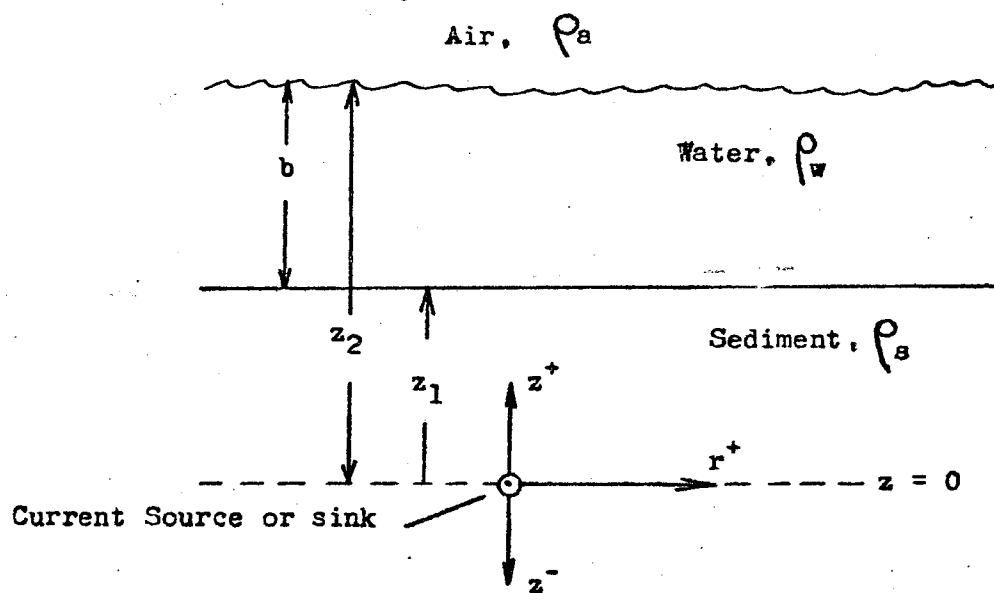
$$k_{ws} = (\rho_w - \rho_s) / (\rho_w + \rho_s)$$

ρ_a = the resistivity of the air

ρ_w = the resistivity of the sea water.

Figure A3-1

Point Source or Sink of Current Buried in the Sea Floor



If the resistivity of the air approaches infinity, k_{aw} becomes 1 and using the relation

$$(A3-2) \quad \int_0^{\infty} e^{-\lambda z} J_0(\lambda r) d\lambda = \frac{1}{\sqrt{r^2 + z^2}}, \quad z \geq 0.$$

expression A3-1 becomes

$$(A3-3) \quad V = \frac{I P_s}{4\pi} (1 + k_{ws}) \int_0^{\infty} \left[\frac{e^{\lambda(z-2z_2)}}{1 + k_{ws} e^{-2\lambda b}} + \frac{e^{-\lambda z}}{1 + k_{ws} e^{-2\lambda b}} \right] J_0(\lambda r) d\lambda$$

Equation (A3-3) cannot be solved in closed form, but may be evaluated conveniently by using a series approximation. Using the relation

$$(A3-4) \quad \frac{1}{1-a} = \sum_{n=0}^{\infty} a^n, \quad a < 1,$$

and the fact that $k_{ws} = -k_{sw}$ and that $(2z_2 - z) = (2b + 2z_1 - z)$,

$$\begin{aligned} \frac{1}{1 + k_{ws} e^{-2\lambda b}} &= \frac{1}{1 - k_{sw} e^{-2\lambda b}} \\ &= \sum_{n=0}^{\infty} (k_{sw} e^{-2\lambda b})^n \\ &= \sum_{n=0}^{\infty} k_{sw}^n e^{-2n\lambda b}, \end{aligned}$$

and

$$V = \frac{I P_s}{4\pi} (1 + k_{ws}) \sum_{n=0}^{\infty} \int_0^{\infty} \left[e^{-\lambda(2b+2z_1-z)} e^{-2n\lambda b} + e^{-\lambda z} e^{-2n\lambda b} \right] J_0(\lambda r) d\lambda$$

or

$$V = \frac{I P_s}{4\pi} (1 + k_{ws}) \sum_{n=0}^{\infty} \int_0^{\infty} \left[e^{-\lambda(2b+2z_1-z+2nb)} + e^{-\lambda(z+2nb)} \right] J_0(\lambda r) d\lambda.$$

but

$$\int_0^{\infty} e^{-\lambda x} J_0(\lambda r) d\lambda = \frac{1}{(x^2+r^2)^{1/2}}, \quad x \geq 0$$

and, as

$(2b+2z, -z+2hb)$ and $(z+2hb)$ are ≥ 0 ,

$$(A3-5) \quad V = \frac{I\rho_s}{4\pi} (1+k_{sw}) \sum_{n=0}^{\infty} k_{sw}^n \left[\frac{1}{\sqrt{(2z_1+2b-z+2hb)^2+r^2}} + \frac{1}{\sqrt{(z+2hb)^2+r^2}} \right].$$

The speed of convergence of the series portion of (A3-5) depends strongly on the value of k_{sw} . If the sediment resistivity ρ_s is much greater than the water resistivity ρ_w , k_{sw} approaches one, and k_{sw}^n goes to zero slowly as n increases. For ρ_s close to ρ_w , k_{sw} approaches zero, and k_{sw}^n goes to zero rapidly with increasing n . The table below shows the value of n for which $k_{sw}^n < 10^{-6}$, for different values of ρ_s/ρ_w .

ρ_s/ρ_w	2	3	4	5	8	10	100
n	13	20	28	35	55	69	691

A computer program (VSP) has been written for the CDC 6400 computer to calculate V , the potential in the water layer, from Equation (A3-5). The program is included as Appendix 3-2.

Appendix 3-2

Computer Program

09/22/72 CALIDOSCOPE (SCM) VER.01.1-A 09/06/72 MACHINE A
14.47.27.HI CR 05 J7387, 200, 45000, 100. MORRISON-CORWIN.
14.47.30.HI CR 05 80 CARDS
14.47.31.\$!JOB INITIATED. J7387NL CPL4.
14.47.31.\$!RUN.S.
14.47.31.\$!CM=18944(45000B), EC=0, CS=0, PP=0.017, SP=0
14.47.33.\$!LGO.
14.47.35.\$!CM=4416(10500B), CP=0.553, PP=3.465, SP=0.095
14.47.35. BEGIN EXECUTION VSP
14.49.52. STOP VSP
14.49.52.\$!EXIT.
14.49.52.\$!JOB COMPLETED. CP=88.700, PP=6.031, SP=0.205
14.49.52.\$!PRINTED LINES = 743, PUNCHED CARDS = 0
14.49.52.\$!EFFECTIVE TIME = 90.014 SEC, JOB COST = \$7.771

 RUN-FORTRAN COMPILER VERSION 2.3-B.3

```

PROGRAM VSP (INPUT,OUTPUT)
000003 DIMENSION R(20), Z1(50), B(50), RS(50)
000003 PI = 3.14159
000004 RW = .25
000006 CUR = -60.
000010 READ 102, (R(I), I=1, 12)
000021 102 FORMAT(6F12.6)
000021 PRINT 200
000025 200 FORMAT(1H1)
000025 DO 6 K=1, 27
000027 IB = K
000030 IZ1 = K
000031 READ 103, RS(K), R(IB), Z1(IZ1)
000042 103 FORMAT(3F12.6)
000042 AKWS = (RW-RS(K))/(RW+RS(K))
000047 AKSW = -1.*AKWS
000051 FO = ((RS(K)*(1.+AKWS))/(4.*PI)) *CUR
000050 Z = Z1(IZ1)+B(IB)
000064 DO 4 IR= 1, 12
000065 S = 0.
000056 SD = 0.
000066 R2 = R(IR)**2
000070 DO 5 J=1, 100
000072 EN = J-1
000074 FA = (2.*B(IB)+2.*Z1(IZ1)-Z+2.*EN*B(IB))**2.
000106 FB = (Z+2.*EN*B(IB))**2.
000115 FC = 1./(SQRT(FA+R(IR)**2.))
000125 FD = 1./(SQRT(FB+R(IR)**2.))
000136 FF = AKSW**EN
000142 FH = -R(IR)*((FA+R2)**(-1.5)+(FB+R2)**(-1.5))
000156 SD = SD+(FF*FH)
000161 FG = FF*(FC+FD)
000164 S = S+FG
000156 5 CONTINUE
000171 V = FO*S*1000.
000173 DVDR = FO*SD*1000.
000174 TDVDR = 20.*DVDR
000177 PRINT 202, RS(K), B(IB), Z1(IZ1), Z, R(IR), V, DVDR, TDVDR
000222 202 FORMAT(5X, 8F12.6, /)
000222 4 CONTINUE
000224 6 CONTINUE
000226 STOP
000230 END

```

Sample Output

ρ_s	b	z_1	z	r	v	$\partial v / \partial r$	$20x\partial v / \partial r$
1.250000	20.000000	20.000000	40.000000	.001000	-163.921616	.000069	.001377
1.250000	20.000000	20.000000	40.000000	.010000	-163.921613	.000688	.013766
1.250000	20.000000	20.000000	40.000000	.100000	-163.921272	.006883	.137654
1.250000	20.000000	20.000000	40.000000	1.000000	-163.887217	.068768	1.375364
1.250000	20.000000	20.000000	40.000000	3.000000	-163.613093	.204884	4.097690
1.250000	20.000000	20.000000	40.000000	10.000000	-160.622058	.632918	12.658366
1.250000	20.000000	20.000000	40.000000	30.000000	-141.276287	1.123587	22.471748
1.250000	20.000000	20.000000	40.000000	60.000000	-110.687566	.862865	17.257304
1.250000	20.000000	20.000000	40.000000	100.000000	-83.692597	.521285	10.425706
1.250000	20.000000	20.000000	40.000000	200.000000	-51.082983	.202684	4.053685
1.250000	20.000000	20.000000	40.000000	300.000000	-36.444261	.105529	2.110570
1.250000	20.000000	20.000000	40.000000	1000.000000	-11.803763	.011556	.231111
.300000	20.000000	20.000000	40.000000	.001000	-68.260946	.000041	.000823
.300000	20.000000	20.000000	40.000000	.010000	-68.260944	.000412	.008234
.300000	20.000000	20.000000	40.000000	.100000	-68.260740	.004117	.082336
.300000	20.000000	20.000000	40.000000	1.000000	-68.240371	.041130	.822604

Appendix 4-1

Computation of potential between "bare" or "packed" electrodes in
a NaCl concentration cell; $C_1 = 1 \text{ M}$ & $C_2 = 0.8 \text{ M}$.

$$E = -\frac{2RT}{zF} \int_{C_1}^{C_2} t_{\text{Na}^+} d \ln a_{\text{NaCl}}$$

$R = 8.314 \text{ joules/degree-mole}$

$T = 20^\circ\text{C} = 293.2^\circ\text{K}$

$F = 96,500 \text{ coulombs/mole}$

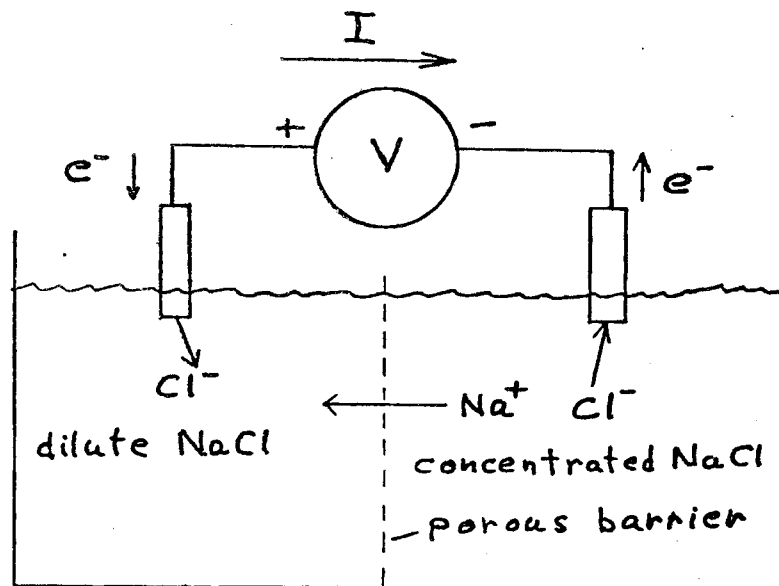
$t_{\text{Na}^+} = 0.382 \text{ for } C_{\text{NaCl}} \geq 0.2 \text{ M}$

$a_{\text{NaCl}} = 0.665 \text{ for } 1.0 \text{ M}, 0.67 \text{ for } 0.8 \text{ M}$

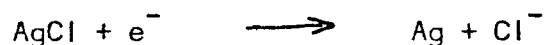
$$E = \frac{(-2)(8.314)(293.2)}{96,500} (0.382) [\ln(0.8)(0.67) - \ln(1)(0.665)]$$

$E = 0.00417 \text{ volts} = 4.17 \text{ millivolts}$

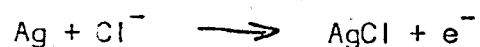
The sign of the potential as measured on a voltmeter may be determined by consideration of the sketch below. The electrodes are reversible



to chloride ions, so when current is drawn from the cell they provide chloride to the dilute solution by the reaction



At the same time, chloride ions are removed from the concentrated solution by the reaction



while sodium ions are transported across the porous barrier to maintain electrical neutrality. Because the electron flow through the voltmeter is from concentrated to dilute, the conventional current flow is from dilute to concentrated, and the voltmeter indicates that the electrode in the dilute solution is positive relative to the electrode in the concentrated solution. Getman and Daniels (1931, p. 453) discuss the determination of polarity for concentration cells.

Appendix 4-2

Calculation of the potential across KCl:NaCl liquid junctions

If all of the ions involved in a liquid junction between solutions A and B are univalent, the Henderson equation (4-11) takes the form

$$E_L = \frac{RT}{F} \frac{(U_1 - V_1) - (U_2 - V_2)}{(U_1 + V_1) - (U_2 + V_2)} \ln \frac{(U_1 + V_1)}{(U_2 + V_2)}$$

(4-2-1)

(MacInnes, 1961, p. 232), where:

$$U_1 = C_{1A}^+ U_{1A}^+ + C_{2A}^+ U_{2A}^+$$

$$V_1 = C_{1A}^- U_{1A}^- + C_{2A}^- U_{2A}^-$$

$$U_2 = C_{1B}^+ U_{1B}^+ + C_{2B}^+ U_{2B}^+$$

$$V_2 = C_{1B}^- U_{1B}^- + C_{2B}^- U_{2B}^-$$

and C_{1A}^+ and U_{1A}^+ represent, respectively, the concentration in moles and the mobility in cm/sec of the positive ion of constituent 1 of solution A, with the same convention followed for the other definitions.

For a KCl:NaCl junction, with KCl as solution A and NaCl as solution B,

$$U = C_{K^+A} U_{K^+} \quad ; \quad U_{K^+} = 6.85 \times 10^{-4} \text{ cm/sec}$$

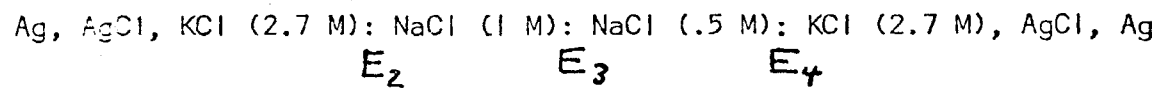
$$V = C_{Cl^-A} U_{Cl^-} \quad ; \quad U_{Cl^-} = 7.12 \times 10^{-4} \text{ cm/sec}$$

$$U_2 = C_{Na^+B} U_{Na^+} \quad ; \quad U_{Na^+} = 4.67 \times 10^{-4} \text{ cm/sec}$$

$$V_2 = C_{Cl^-B} U_{Cl^-}$$

(mobilities are for 20°C, from Glasstone and Lewis, 1960, p. 455).

For the cell



the values of E_2 , E_3 , and E_4 are found from Equation 4-2-1 to be + 6.75, - 4.13, and - 5.18 mv, respectively. The potential across the cell ($E_2 + E_3 + E_4$), then, is - 2.56 mv.

REFERENCES

- Alfano, L. , 1962, Geoelectrical Prospecting with Underground Electrodes: Geophysical Prospecting, v. 10, no. 3, p.290 - 303.
- Allen, S. J., 1971, Geophysical Activity in 1969: Geophysics, v. 36, no. 1, p. 189 - 196.
- Archie, G. E., 1942, The Electrical Resistivity Log as an Aid in Determining Some Reservoir Characteristics: Transactions, A.I.M.E., v. 146, p. 54 - 62.
- Baas Becking, L. G. M., Kaplan, I. R., and Moore, D., 1960, Limits of the Natural Environment in Terms of pH and Oxidation - Reduction Potentials: The Journal of Geology, v.68, no.3, p.243-284.
- Banister, D.A., 1962, Point Astley Zinc - Copper Deposits: U. S. Bureau of Mines, Alaska Office of Mineral Resources, Juneau, Alaska, report No. 54 (unpublished), 7 p.
- Banwell, C. J., 1970, Geophysical Techniques in Geothermal Exploration, in United Nations Symposium on the Development and Utilization of Geothermal Resources, Pisa, Italy.
- Barnes, B.B., Corwin, R.F., Beyer, J. H., Jr., and Hildenbrand, T. G., 1972, Geologic Prediction: Developing Tools and Techniques for the Geophysical Identification and Classification of Sea - Floor Sediments: NOAA Technical Report ERL 224-MMTC 2, U. S. Government Printing Office, Washington, D.C., 163 p.
- Bates, R.G., 1954, Electrometric pH Determinations: Wiley, New York, 331 p.
- Beck, F. M., 1970, Marine Challenges Encountered by a Small Mine on the Maine Coast: Preprints, Second Annual Offshore Technology Conference, Houston, Texas, Volume 2, p. 279 - 286.
- Becker, A., and Telford, W.M., 1965, Spontaneous Polarization Studies: Geophysical Prospecting, v. 13, no. 2, p. 173 - 188.
- Ben-Yaakov, S., 1970, An Oceanographic Instrumentation System for in-situ Measurements: Ph.D. thesis, University of California, Los Angeles, 342 p.
- Berg, H. C., and Cobb, E. H., 1967, Metalliferous Lode Deposits of Alaska: U.S. Geological Survey Bulletin 1246, U. S. Government Printing Office, Washington, D.C., 254 p.
- Bohn, D., 1971, East of these Golden Shores: Scrimshaw Press, San Francisco.

- Bomar, H. E., and Marchand, R.H., 1970, Guarding a Cathodic Protection System from Outside Interference: *Materials Protection*, v. 9, no. 4, p. 19 - 22.
- Bouma, A. H., Sweet, W.E., Chmelik, F.B., and Huebner, G.L., 1971, Shipboard and In-Situ Electrical Resistivity Logging of Unconsolidated Marine Sediments: Preprints, Third Annual Offshore Technology Conference, Houston, Texas, Volume 1, p. 253 - 268.
- Boyce, R.E., 1967, Electrical Resistivity of Modern Marine Sediments from the Bering Sea: M.S. Thesis, San Diego State College, California, 172 p.
- Breck, W.G., 1972, Redox Potentials by Equilibration: *Journal of Marine Research*, v. 30, no. 1, p. 121-139.
- Brooks, R.R., Kaplan, I.R., and Peterson, M.N.A., 1969, Trace Element Composition of Red Sea Geothermal Brine and Interstitial Water, in Degens, E.T., and Ross, D.A., eds., *Hot Brines and Recent Heavy Metal Deposits in the Red Sea*: Springer - Verlag, New York, 600 p.
- Buddington, A.F., and Chapin, T., 1929, *Geology and Mineral Deposits of Southeastern Alaska*: U.S. Geological Survey Bulletin 800, U.S. Government Printing Office, Washington, D.C., 378 p.
- Canadian Institute of Mining and Metallurgy, 1957, *Methods and Case Histories in Mining Geophysics*: Sixth Mining and Metallurgical Congress, Montreal, 359 p.
- Conti, U., 1972, Study of an Underwater Towable Environmental Monitor: Ph.D. Thesis, University of California, Berkeley, 184 p.
- Cooper, L.H.N., 1937, Oxidation - Reduction Potential in Sea Water: *Journal of the Marine Biological Association of the United Kingdom*, v. XXII, p. 167 - 175.
- Cornet, I., 1972, Steel, Concrete, and Sea Water: Third International Congress on Marine Corrosion and Fouling (in press).
- Corwin, R.F., Ebersole, W.C., and Wilde, P., 1970, A Self-Potential Detection System for the Marine Environment: Preprints, Second Annual Offshore Technology Conference, Houston, Texas, Volume 2, p. 305 - 314.
- Corwin, R., 1970, Berkeley Aquatic Park Water -- an Analysis: Term Report, Civil Engineering 201 B, University of California, Berkeley, 20 p.
- Covington, A.K., 1969, Reference Electrodes, in Durst, R.A., ed., *Ion-Selective Electrodes*: National Bureau of Standards Special Publication 314, U.S. Government Printing Office, Washington, D.C., 452 p.

- Cowan, E.W., 1963, Basic Electromagnetism: Academic Press, New York, 476 p.
- Cox, R.A., 1966, International Oceanographic Tables: Unesco, Place de Fontenoy, Paris 7e, France, 117 p.
- Curtin, T.B., 1970, Towed Electrodes in the Sea: Theory and Use: M.S. Thesis, Oregon State University, Corvallis, Oregon, 96 p.
- Dakhnov, V.N., 1959, Geophysical Well Logging: Quarterly of the Colorado School of Mines, v. 57, no. 2, p. 1-445.
- Demenitskaya, R.M., Gorodnitskiy, A.M., Litvinov, E.M., and Trubyatchinskiy, N.N., 1970, Vertical Distribution of the Natural Electric Field in the Sea, in Shuleykin, V.V., ed., Electromagnetic Phenomena in the Sea: Joint Publications Research Service JPRS 50173, U.S. Department of Commerce, p. 95-102.
- deWitte, L., 1948, A New Method of Interpretation of Self-Potential. Field Data: Geophysics, v. XIII, no. 4, p. 600 - 608.
- Drever, R.G., and Sanford, T.B., 1970, A Free - Fall Electromagnetic Current Meter - Instrumentation: Proceedings of the I.E.R.E. Conference on 'Electronic Engineering in Ocean Technology', p. 353 - 370.
- Durst, R.A. (ed.), 1969, Ion - Selective Electrodes: National Bureau of Standards Special Publication 314, U.S. Government Printing Office, Washington, D.C., 474 p.
- Edge, A.B., and Laby, T.H., 1931, The Principles & Practice of Geophysical Prospecting: Cambridge University Press, London, 372 p.
- Emery, K.O., and Rittenberg, S.C., 1952, Early Diagenesis of California Basin Sediments in Relation to Origin of Oil: Bulletin of the American Association of Petroleum Geologists, v. 36, no. 5, p. 735 - 806.
- Erchul, R.A., and Nacci, V.A., 1971, The Use of Electrical Resistivity Measurements to Predict Porosity of Marine Sediments, in Proceedings, The International Symposium on the Engineering Properties of Sea - Floor Sc. Is and Their Geophysical Identification: Sponsored by UNESCO, Seattle, Washington, p. 296 - 308.
- Ewing, S., 1939, The Copper - Copper Sulfate Half - Cell for Measuring Potentials in the Earth: Technical Section, American Gas Association Distribution Conferences, 1939.

- Fox, R.W., 1830, On The Electro-Magnetic Properties of Metaliferous Veins in the Mines of Cornwall: Royal Society of London, Philosophical Transactions, Part 2, p. 399 - 414.
- Faraday, M., 1832, The Bakerian Lecture. - Experimental Researches in Electricity - Second Series: Philosophical Transactions of the Royal Society of London, v. 122, p. 163 - 176.
- Garrels, R.M., and Christ, C.L., 1965, Solutions, Minerals, and Equilibria: Harper and Row, New York, 450 p.
- Gay, S.P., Jr., 1967, A 1,800 Millivolt Self - Potential Anomaly near Huagayoc, Peru: Geophysical Prospecting, v. 15, no. 2, p. 236 - 245.
- Getman, E.H., and Daniels, F., 1931, Outlines of Theoretical Chemistry: Wiley, New York, 643 p.
- Glasstone, S., and Lewis, D., 1960, Elements of Physical Chemistry (Second Edition): D. Van Nostrand, Princeton, New Jersey, 758 p.
- Grice, C.E., 1968, Finding Underwater Objects: Ocean Industry, v. 3, no. 1, p. 25 - 42.
- Grose, L.T., 1971, Geothermal Energy: Geology, Exploration, and Developments, Part 1: Mineral Industries Bulletin, Colorado School of Mines, v. 14, no. 6, 14 p.
- Haase, R., and Schönert, H., 1960, Untersuchungen an Thermoketten iv. Messungen: Zeitschrift für Physikalische Chemie Neue Folge, v. 15, 1. 193 - 204.
- Hayes, F.R., 1964, The Mud-Water Interface: Oceanography and Marine Biology Annual Review (Barnes, H., ed.), v. 2, p. 121-145.
- Heiland, I.A., 1940, Geophysical Exploration: Prentice - Hall, New York, 1313 p.
- Hood, P., and Kellogg, W.C., 1969, Mining Geophysical Activity in 1968: Geophysics, v. 34, no.6, p. 848 - 858.
- Irrel, W., Jr., 1883, Eighth Annual Report of the State Mineralogist: California State Mining Bureau, Sacramento.
- Ives, D.G., and Janz, G.J., 1961, Reference Electrodes - Theory and Practice: Academic Press, London, 651 p.
- Jakovlev, J.J., 1950, Exploration Geophysics (Second Edition): Terra Publishing Co., Newport Beach, California, 1195 p.
- Kellogg, W.C., and Frischknecht, F.C., 1966, Electrical Methods in Geophysical Prospecting: Pergamon Press, Oxford, 519 p.

- Kelly, S.F., 1945, Discussion on paper by Rao, M.B.R., Spontaneous Polarization Surveys near Guddarangavvanahalli, Chitaldrug, Mysore State, India: Transactions, American Institute of Mining and Metallurgical Engineers, v. 164, p. 107 - 116.
- Kermabon, r., Gehin, C., and Blavier, P., 1969, A Deep - Sea Electrical Resistivity Probe for Measuring Porosity and Density of Unconsolidated Sediments: Geophysics, v.34, no. 4, p. 554 - 571.
- Knudsen, M., 1901, Hydrographic Tables: G.E.C. GAD, Copenhagen, 63 p.
- Krauskopf, K.E., 1967, Introduction to Geochemistry: Mc Graw - Hill, New York, 721 P.
- Kruger, F.J., and Lacy, W.C., 1949, Geological Explanation of Geophysical Anomalies near Cerro de Pasco, Peru: Economic Geology, v. 44, no. 6.
- Latimer, W.M., 1952, The Oxidation States of the Elements and their Potentials in Aqueous Solutions: Prentice - Hall, Englewood Cliffs, New Jersey, 392 p.
- Lenk, J. D., 1966, Electronic Corrosion Control for Boats: Howard W. Sams & Co., Indianapolis, Indiana, 128 p.
- Mac Innes, D.A., 1961, The Principles of Electrochemistry: Dover Publications, Inc., New York, 478 p.
- Manglesdorf, P.C., Jr., 1962, The World's Longest Salt Bridge, in Marine Sciences Instrumentation, Volume 1, Gaul, R.D., Ketchum, D.D., Shaw, J. T., and Snodgrass, J.M., eds: Plenum Press, New York, p. 173 - 195.
- Manheit, F., 1961, In Situ Measurements of pH and Eh in Natural Waters and Sediments: Stockholm Contributions in Geology, v. 8, no. 3, p. 27 - 36.
- Marke, F.A.B., 1965, The Development and Use of Off-Shore Mineral Exploration Techniques: Ph.D. Thesis, Imperial College of London, 186 p.
- Meiser, F., 1952, A Method for Quantitative Interpretation of Self-potential Measurements: Geophysical Prospecting, v. X, no. 2, p. 203 - 218.
- Merkle, F.E., 1955, Oxidation - Reduction Processes in Soils, in Ess. F.E., Chemistry of the Soil: Reinhold, New York, p. 200 - 218.
- Meyer, v. r., 1972, Laboratory Streaming Potential Measurements: Term Report, Civil Engineering 201 C, University of California, Berkeley.

- Morris, J.C., and Stumm, W., 1967, Redox Equilibria and Measurements of Potentials in the Aquatic Environment, in Stumm, W. (Chairman), Equilibrium Concepts in Natural Water Systems: American Chemical Society, Washington, D.C., Advances in Chemistry Series, no. 67, 344 p.
- Neumann, G., and Pierson, W.J., Jr., 1966, Principles of Physical Oceanography: Prentice - Hall, Inc., Englewood Cliffs, New Jersey, 545 p.
- Nourbehecht, B., 1963, Irreversible Thermodynamic Effects in Homogeneous Media and Their Applications in Certain Geoelectric Problems: Ph.D. Thesis, Massachusetts Institute of Technology, Cambridge, 121 p.
- Ocean Industry, 1967, Spontaneous Potential Will Play Big Part in Future Sea Exploration: Ocean Industry, v.2, no. 8, p. 58-62.
- Oglivy, A.A., Ayed, A.A., and Bogoslovsky, V.A., 1969, Geophysical Studies of Water Leakages from Reservoirs: Geophysical Prospecting, v. XVII, no. 1, p. 36 - 62.
- Parasnis, D.S., 1966, Mining Geophysics: Elsevier, New York, 356 p.
- Parasnis, D.S., 1970, Some Recent Geoelectric Measurements in the Swedish Sulfide Ore Fields Illustrating Scope and Limitations of the Methods Concerned, in Mining and Groundwater Geophysics/1967, Morley, L.W., ed., Geological Survey of Canada, Ottawa, Canada, Economic Geology Report no. 26, p. 290 - 301.
- Paul, M.K., 1955, Direct Interpretation of Self - Potential Anomalies Caused by Inclined Sheets of Infinite Horizontal Extensions: Geophysics, v. 30, no. 3, p. 418 - 423.
- Petrowsky, A., 1928, The Problem of a Hidden Polarized Sphere: Philosophical Magazine, v. 5, no. 28, p. 334 - 353; no. 31, p. 914 - 933.
- Pirson, S.J., 1971, New Electric Technique can Locate Gas and Oil: World Oil, v. 172, no. 5, p. 69 - 72; no. 6, P. 72 - 74.
- Poldini, E., 1938, 1939, Geophysical Exploration by Spontaneous Polarization Methods: The Mining Magazine, v. 59, p. 278 - 282; 347 - 352; v. 60, p. 22-27; 90 - 94.
- Pourbaix, M.J.N., 1949, Thermodynamics of Dilute Aqueous Solutions: Edward Arnold & Co., London, 136 p.
- Riley, J.P., and Skinner, G., eds., 1965, Chemical Oceanography, Volumes 1 and 2: Academic Press, London and New York, 712 p. (Vol. 1); 508 p. (Vol. 2).

- Root, L.A., 1927, Report XXIII of the State Mineralogist: California State Mining Bureau, California State Printing Office, Sacramento.
- Roy, A., 1963, New Interpretation Techniques for Telluric and some Direct Current Fields: Geophysics, v. 28, no. 2, p. 250 - 261.
- Roy, A., and Chowdhury, D.K., 1959, Interpretation of Self Potential Data for Tabular Bodies: Journal of Science and Engineering Research, v. III, part I, p. 35 - 54.
- Sanford, T.B., 1967, Measurement and Interpretation of Motional Electric Fields in the Sea: Ph.D. Thesis, Massachusetts Institute of Technology, Cambridge, 161 p.
- Sanford, T.B., 1971, Motionally Induced Electric and Magnetic Fields in the Sea: Journal of Geophysical Research, v. 76, no. 15, p. 3476 - 3492.
- Sato, M., 1960 a, Oxidation of Sulfide Ore Bodies, I. Geochemical Environments in terms of Eh and pH: Economic Geology, v. 55, p. 928 - 961.
- Sato, M., 1960 b, Oxidation of Sulfide Ore Bodies, II. Oxidation Mechanisms of Sulfide Minerals at 25 °C: Economic Geology, v. 55, p. 1202 - 1231.
- Sato, M., and Mooney, H.M., 1960, The Electrochemical Mechanism of Sulfide Self - Potentials: Geophysics, v. 25, no. 1, p. 226 - 249.
- Schlumberger Well Surveying Corporation, 1958, Introduction to Schlumberger Well Logging: Schlumberger Document Number 8, 176 p.
- Sengupta, S.N., Bose, R.N., and Mitra, S.K., 1969, Geophysical Investigation for Copper Ores in the Singhana -Gotro area, Khetri Copper Belt, Rajasthan (India): Geoexploration, v. 7, no. 2, p. 73 - 82.
- Shuleikin, Y.V., 1962, Magnetic and Electric Phenomena in the Sea: U.S. Navy, Hydrographic Office, Washington, D.C., 43 p. (Reproduced by National Technical Information Service, Springfield, Virginia, 22151).
- Snyder, R.M., 1966, Spontaneous Potential: Geo-Marine Technology, v. 2, no. 3, p. 12 - 13.
- Starkey, R.L., and Wight, K.M., 1945, Anaerobic Corrosion of Iron in Soil: American Gas Association, New York, 108 p.

- Stern, W., 1945, Relation Between Spontaneous Polarization Curves and Depth, Size, and Dip of Ore Bodies: Transactions of the American Institute of Mining and Metallurgical Engineers, v. 164, p. 189 - 196.
- Stommel, H., 1948, The Theory of the Electric Field Induced in Deep Ocean Currents: Journal of Marine Research, v: 7, no. 3, p. 386 - 392.
- Sverdrup, H. U., Johnson, M.W., and Fleming, R. H., 1942, The Oceans: Prentice - Hall, Englewood Cliffs, New Jersey, 1087 p.
- Tooms, J.S., Taylor Smith, D., Nichol, I., Ong, P., and Wheildon, J., 1965, Geochemical and Geophysical Mineral Exploration Experiments in Mounts Bay, Cornwall, in Whittard, W.F., and Bradshaw, R., eds., Submarine Geology and Geophysics: Butterworths, London, p. 363 - 391.
- Tyrrell, H. J. V., and Colledge, R., 1954, Thermal Diffusion Potentials in Non-Isothermal Electrolytic Systems - Part 3: Transactions of the Faraday Society, v. 50, part 10, no. 382, p. 1056 - 1066.
- Tyrrell, H. J. V., and Hollis, G.L., 1949, Thermal Diffusion Potentials in Non - Isothermal Electrolytic Systems: Transactions of the Faraday Society, v. 45, part 4, no. 316, p. 411 - 423.
- Uhlig, H.H., ed., 1948, The Corrosion Handbook: John Wiley and Sons, New York, 1188 p.
- Uhlig, H.H., 1963, Corrosion and Corrosion Control: Wiley, New York, 371 p.
- Van Nostrand, R.G., and Cook, K.L., 1966, Interpretation of Resistivity Data: Geological Survey Professional Paper 499, U. S. Government Printing Office, Washington, D.C., 310 p.
- von Arx, W.S., 1950, An Electromagnetic Method for Measuring the Velocities of Ocean Currents from a Ship Under Way: Papers in Physical Oceanography and Meteorology (M.I.T. - Woods Hole), v. 11, no. 3, p. 1 - 62.
- von Arx, W.S., 1962, An Introduction to Physical Oceanography: Addison - Wesley, Reading, Mass., 422 p.
- Waring, G.A., 1915, Springs of California: U.S. Geological Survey, Water Supply Paper 338, U.S. Government Printing Office, Washington, D.C.
- White, D.E., 1969, Natural Steam for Power: U.S. Geological Survey (Pamphlet), U.S. Government Printing Office, Washington, D.C.

- Wiegel, R.L., 1964, Oceanographical Engineering: Prentice - Hall, Englewood Cliffs, New Jersey, 532 p.
- Wilde, P., 1956, pH of Deep - Sea Sediments: Program, The Geological Society of America, 1966 Annual Meeting, San Francisco, California, p. 240 - 241.
- Wilson, I.F., and Rocha, V.S., 1955, Geology and Mineral Deposits of the Boleo Copper District, Baja California, Mexico: U. S. Geological Survey Professional Paper 273, U. S. Government Printing Office, Washington, D.C., 134 p.
- Wingard, P. S., 1961, Geology of the Castine - Blue Hill Area, Maine: Ph.D. Thesis, University of Illinois, Urbana, 137 p.
- Wright, F.E., and Wirght, C.W., 1908, The Ketchikan And Wrangell Mining Districts, Alaska: U. S. Geological Survey Bulletin 347, U. S. Government Printing Office, Washington, D.C., 210 p.
- Wyllie, M. R. J., 1963, The Fundamentals of Well Log Interpretation (Third Edition): Academic Press, New York, 238 p.
- Young, R.S., 1962, Prospect Evaluations, Hancock County, Maine: Special Economic Studies Series No. 2, Maine Geological Survey, Department of Economic Development, Augusta, Maine, 113 p.
- Yungul, S., 1945, Some Uses of the Spontaneous Polarization Method: Professional Thesis, California Institute of Technology, Pasadena, 70 p.
- Yungul, S., 1950, Interpretation of Spontaneous Polarization Anomalies Caused by Spherical Orebodies: Geophysics, v. 15, no. 2, p. 237 - 246.
- ZoBell, C.E., 1946, Studies on Redox Potential of Marine Sediments: Bulletin of the American Association of Petroleum Geologists, v. 30, no. 4, p. 477 - 513.